

Development of Microfluidic Devices for Genetic Analysis: Continuous Flow Infrared-mediated PCR (cfIR-PCR) and Microwave Thermal Cycling Systems

---

A Dissertation

Presented to  
the faculty of the School of Engineering and Applied Science  
University of Virginia

---

in partial fulfillment  
of the requirements for the degree

Doctor of Philosophy

by

Kyudam Oh

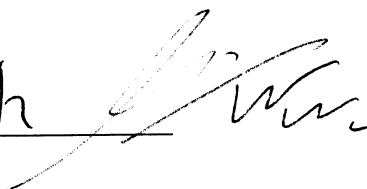
August

2013

APPROVAL SHEET

The dissertation  
is submitted in partial fulfillment of the requirements  
for the degree of  
Doctor of Philosophy

Kyudam Oh  
AUTHOR



The dissertation has been read and approved by the examining committee:

Dr. James P. Landers

---

Advisor

Dr. Roseanne Ford

---

Dr. Giorgio Carta

---

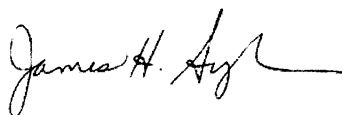
Dr. N. Scott Barker

---

Dr. Gary Koenig, Jr.

---

Accepted for the School of Engineering and Applied Science:



Dean, School of Engineering and Applied Science

August  
2013

## Abstract

The work in this dissertation constitutes four research efforts focused on the development of microfluidic instrumentation and methodology for advanced genetic analysis in polymeric microdevices. Laser ablation has been mainly employed to construct polymeric devices as a result of rapid prototyping and ease of microfabrication. As a part of a genetic analyzer, two types of heating systems were investigated to drive thermocycling in these polymeric microdevices: infrared and microwave, ultimately capable of multiple and high-throughput reactions with portability in DNA analysis. **Chapter 1** introduced the general purpose in the development of microfluidic devices for genetic analysis, especially, describing details of benefits in “Lab on a chip” technologies and microfluidic Polymerase Chain Reaction (PCR) that are directly associated with this work. In **Chapter 2**, the development of continuous flow infrared-mediated PCR (cfIR-PCR) on a single lamp is outlined. An IR-mediated heating system has been utilized in our group to facilitate non-contact PCR inside glass and polymeric microfluidic devices for clinical and forensic applications. However, the number of PCR reactions was limited due to the configuration of our heating system. In present work, the cfIR-PCR system has shown the capability of multi-segmented DNA amplifications from multiple DNA targets that were encapsulated inside emulsion solutions without any cross-contamination, which further proves the feasibility of high-throughput genetic analysis on a single lamp.

As an alternative heating system, a microwave-mediated thermal cycling system is presented in **Chapter 3**. Due to the characteristics of dielectric heating, microwave offers ultrafast thermal cycling of micro and nano-scale reaction solutions in microfluidic devices. Three types of microwave-mediated heating control (*on/off*, *open-loop*, and *proportional voltage*

*controls*) concepts were assessed using polymeric materials to optimize our microwave heating setup. As two major approaches in temperature sensing, a thermocouple (contact sensing) and an IR-pyrometer (non-contact sensing) were utilized to measure temperature in the PCR solution to control thermocycling to accomplish successful DNA amplifications under a microwave field. Additionally, it was demonstrated for PCR applications to be potential use in miniaturized genetic analyzers for Point-of-Care (POC) DNA analysis. In **Chapter 4**, IR-mediated PCR in the single chamber of the polymeric microdevice was shown to achieve the rapid detection of exogenous and evolved genetic materials (DNA/RNA) using degenerate primers. Furthermore, the novel concept of rapid and reliable drug susceptibility testing (DST) for *M. tuberculosis* is then introduced in **Chapter 5**. Standard PCR coupled with hybridization-induced bead aggregation was successfully demonstrated for the detection of PCR amplicons as an advanced alternative of microchip electrophoresis. Finally, summaries and future directions were outlined in **Chapter 6**.

## Table of Contents

Abstract .....	ii
Table of Contents .....	iv
List of Figures .....	viii
List of Tables .....	xi
<b>1. Introduction: Genetic Analysis in Microfluidic Devices .....</b>	<b>1</b>
<b>1.1 General Purpose .....</b>	<b>1</b>
<b>1.2 Micro-Total Analysis Systems (<math>\mu</math>-TAS) and Its Applications .....</b>	<b>4</b>
1.2.1 Microfluidic Literature.....	5
1.2.2 Physics in Microfluidics .....	6
<b>1.3 Polymerase Chain Reaction (PCR) in Microfluidic Devices .....</b>	<b>8</b>
1.3.1 Chemistry and Biology of PCR .....	8
1.3.2 Characteristics of Microchip PCR.....	10
1.3.3 History of Microchip PCR.....	11
1.3.4 Classification of Microchip PCR.....	13
<b>1.4 PCR Heating Systems in Microfluidic Devices.....</b>	<b>14</b>
1.4.1 Contact Heating System.....	14
1.4.2 Non-contact Heating System.....	16
<b>1.5 Temperature Measurement in Microfluidic Devices .....</b>	<b>17</b>
1.5.1 Contact Temperature Measurement .....	17
1.5.2 Non-contact Temperature Measurement .....	19
<b>1.6 Microchip Materials and Fabrication .....</b>	<b>20</b>
1.6.1 Silicon and Glass .....	20
1.6.2 Polymers .....	21
<b>1.7 Surface Passivation in Microfluidic Devices .....</b>	<b>23</b>
<b>1.8 Other Microfluidic PCR Approaches.....</b>	<b>25</b>
1.8.1 Reverse Transcriptase-PCR in Microchips .....	25
1.8.2 Real-time PCR (qPCR) in Microchips.....	27
1.8.3 Droplet PCR in Microchips.....	27
1.8.4 Isothermal and Convection Driven PCR in Microchips.....	28

1.9	Fully Integrated Genetic Analyzer and Recent Trends in Microfluidic PCR .....	28
1.10	Concluding Remarks .....	31
1.11	References .....	32
2.	Continuous Flow Infrared-mediated PCR (cfIR-PCR) System .....	42
2.1	Introduction .....	42
2.1.1	Benefits of Microchip PCR .....	42
2.1.2	Static versus Continuous Flow PCR in Microfluidic Devices .....	42
2.1.3	Continuous Flow Infrared-mediated PCR (cfIR-PCR) .....	44
2.2	Materials and Methods .....	45
2.2.1	cfIR-PCR Instrument .....	45
2.2.2	Microchip Fabrication .....	45
2.2.3	Thermal Gradient Measurement .....	47
2.2.4	Thermal Modeling of the cfIR-PCR Microdevice .....	48
2.2.5	Microchip PCR Protocols .....	49
2.3	Results and Discussion .....	52
2.3.1	Microchip Fabrication .....	52
2.3.2	Establishment of a Thermal Gradient and Measuring Temperatures .....	54
2.3.3	Design Concept of the cfIR-PCR Microdevice .....	53
2.3.4	DNA Amplifications via Thermal Gradient Matching .....	60
2.3.5	Demonstration of Effect of Flow Rates on PCR Efficiency .....	62
2.3.6	Thermal Modeling and Consideration of PCR Efficiency .....	64
2.3.7	Surface Passivation and Emulsion cfIR-PCR .....	68
2.3.8	Genomic DNA Amplification via Continuous Segmented Flows .....	71
2.4	Conclusions .....	75
2.5	References .....	76
3.	Microwave-mediated Thermal Cycling System .....	81
3.1	Introduction .....	81
3.1.1	Applications of Microwave Heating Systems and Characteristics .....	81
3.1.2	Previous Endeavors in Microwave PCR .....	83
3.1.3	Temperature Measurement Methods in Microfluidic Devices .....	85
3.1.4	Non-contact Temperature Measurement for Microwave-mediated PCR .....	86

<b>3.2</b>	<b>Materials and Methods</b>	87
3.2.1	Temperature Control Systems and Configurations	87
3.2.2	Microchip Fabrication and Design	90
3.2.3	Transmission Line and Network Analyzer	92
3.2.4	Pyrometer Calibration	93
3.2.5	PCR Protocol and Microchip PCR	94
<b>3.3</b>	<b>Results and Discussion</b>	95
3.3.1	Polymeric Microdevices for Microwave-mediated Heating System	95
3.3.2	Shifted Transmission Line for Non-contact Temperature Sensing	96
3.3.3	Thermal Modeling of the PCR Solution in the PCR Chamber with a Shifted Transmission Line	97
3.3.4	Microwave Heating Experiments	99
3.3.5	Three Types of Temperature Control Methods	102
3.3.6	Non-contact Temperature Measurement via IR-Pyrometer	105
3.3.7	Temperature Control Methods: Thermocouple vs Pyrometer	106
3.3.8	Microwave-mediated DNA Amplifications via Thermocouple	108
3.3.9	Microwave-mediated DNA Amplifications via Pyrometer	109
<b>3.4</b>	<b>Conclusions</b>	111
<b>3.5</b>	<b>References</b>	112
<b>4.</b>	<b>Rapid Detection of Viral Genetic Materials in Microfluidic Devices using Infrared-mediated Heating System and Degenerate Primers</b>	115
<b>4.1</b>	<b>Introduction</b>	115
4.1.1	Static PCR in Microchips	115
4.1.2	Degenerate Primer-mediated Microchip PCR for Molecular Diagnostics	116
<b>4.2</b>	<b>Materials and Methods</b>	117
4.2.1	Infrared (IR)-mediated Heating System	117
4.2.2	Microchip Fabrication	119
4.2.3	Microchip PCR Protocols	120
<b>4.3</b>	<b>Results and Discussion</b>	122
4.3.1	Microchip Design and Fabrication	122
4.3.2	Preparation of CODHOP-mediated PCR in Microfluidic Devices	123
4.3.3	Air Bubble Formation and Removal Strategies	124
4.3.4	Thermocycling in Engineered Microchip via IR Heating System	126

4.3.5	Comparison of Conventional PCR to Microchip PCR .....	128
<b>4.4</b>	<b>Conclusions</b> .....	130
<b>4.5</b>	<b>References</b> .....	131
<b>5.</b>	<b>Rapid Drug Susceptibility Testing (DST) of <i>Mycobacterium tuberculosis</i> via Standard PCR and Hybridization-induced Bead Aggregation</b> .....	134
<b>5.1</b>	<b>Introduction</b> .....	134
5.1.1	Tuberculosis (TB) and Multidrug-resistant TB (MDR-TB) .....	134
5.1.2	Drug Susceptibility Testing (DST) for Drug Resistant TB .....	134
5.1.3	Standard PCR and Hybridization-induced Bead Aggregation for DST of TB... ..	136
<b>5.2</b>	<b>Materials and Methods</b> .....	137
5.2.1	Reagents and Clinical TB Samples .....	137
5.2.2	Standard PCR Protocols.....	138
5.2.3	Microwell Fabrication and Assay Instruments .....	139
5.2.4	Magnetic Particle Modification .....	139
5.2.5	Hybridization-induced Bead Aggregation Assay and Image Processing.....	140
<b>5.3</b>	<b>Results and Discussion</b> .....	141
5.3.1	Optimization of Standard PCR for DST of TB .....	141
5.3.2	Standard PCR Amplifications and Analysis from Clinical Samples .....	144
5.3.3	Hybridization-induced Bead Aggregation for Serially Diluted PCR Products and Clinical Isolates .....	146
<b>5.4</b>	<b>Conclusions</b> .....	149
<b>5.5</b>	<b>References</b> .....	150
<b>6.</b>	<b>Conclusions and Future Directions</b> .....	152
<b>6.1</b>	<b>Overview Conclusions</b> .....	152
<b>6.2</b>	<b>Future Directions</b> .....	156
6.2.1	cfIR-PCR System.....	156
6.2.2	Microwave-mediated Thermal Cycling System .....	157
<b>6.3</b>	<b>Summation</b> .....	158
<b>6.4</b>	<b>References</b> .....	159

## List of Figures

### Chapter 1

1.1	Schematic in the general concept of developing microfluidic devices for genetic analysis....	4
1.2	Two trends of exponential growth in microfluidics research. ....	5
1.3	Physical characteristics in micro-channels and chambers. ....	7
1.4	Schematic of the Polymerase Chain Reaction (PCR) amplification.....	9
1.5	Miniaturized PCR instruments.....	13
1.6	Contact heating system for microchip PCR applications. ....	15
1.7	Non-contact heating system for microchip PCR applications .....	17
1.8	Two types of temperature measurement methods in microfluidic devices.....	18
1.9	Microfabrications of glass and polymeric devices.....	21
1.10	SEM images of laser ablated surfaces on the PMMA layer .....	23
1.11	Different types of PCR approaches in microfluidic devices.....	26
1.12	Fully integrated microdevices for genotyping in Mathies and Landers groups.....	29
1.13	High-throughput genetic analyzers .....	30

### Chapter 2

2.1	Microfabrication of multi-layered polymeric microdevices .....	46
2.2	Apparatus and determination of the thermal gradient established by infrared (IR)-mediated heating.....	55
2.3	Definition of temperature zones and design of the continuous-flow PCR (cfPCR) microdevice.....	57
2.4	Temperature matching between the cfIR-PCR and TM microdevices via IR-camera .....	61
2.5	cfIR-PCR amplification in the 29-loop microdevice .....	63
2.6	One piece of a loop (segment) for 3D thermal modeling of Computational Fluid Dynamics (CFD). ....	64
2.7	Meshed structure and thermal gradient images in fluidic channels of the cfIR-PCR microdevice.....	65
2.8	Plot describing temperature differences between inlet (A) and outlet (B) of two consecutive denature zones at various flow rates ranging from 0 to 10 $\mu\text{L}/\text{min}$ .....	66
2.9	Relative PCR efficiency at four different BSA concentrations in the 29-loop cfIR-PCR microdevice.....	68
2.10	The oil-surfactant mixed with the PCR sample for emulsion cfIR-PCR.....	70
2.11	Genomic DNA amplifications using different concentrations of the DNA template and BSA in the 43-loop cfIR-PCR microdevice .....	71
2.12	Emulsion cfIR-PCR in the 43-loop microdevice .....	72
2.13	cfIR-PCR via segmented plug flows.....	73

### Chapter 3

3.1	Dielectric heating in the microfluidic PCR chamber.....	82
3.2	Microwave-mediated thermal cycling system.....	88
3.3	Two additional temperature control systems.....	89
3.4	Six layered microdevice used in this research.....	90
3.5	Fabrication procedures of polymeric microdevices.....	91
3.6	Optimization of a matching network (transmission line) using the network analyzer.....	93
3.7	Matching network spectrums of three microchips that have shifted transmission lines generated by the network analyzer.....	97
3.8	Thermal modeling of temperature distributions in the microchamber with a shifted transmission line.....	98
3.9	Microwave heating in the polymeric PCR chamber to demonstrate microwave effect into a type-t thermocouple.....	100
3.10	Maximum rates of microwave heating and natural cooling in our microwave setup.....	101
3.11	Temperature profiles via two temperature control methods in the 125 nL PCR chamber of the PeT microchip.....	103
3.12	Temperature profiles via <i>proportional voltage control</i> in the polymeric (PMMA) microdevice.....	104
3.13	Pyrometer calibration with a thermocouple (reference temperature).....	105
3.14	Temperature profiles driven by a thermocouple and a pyrometer.....	107
3.15	Thermocouple-controlled DNA amplifications.....	109
3.16	Pyrometer-controlled DNA amplifications.....	110
3.17	Thermal modeling of the half PCR chamber in the PMMA microchip and following DNA amplifications.....	111

### Chapter 4

4.1	Schematic of the rapid detection of Human Herpesvirus 4 (HHV-4) using degenerate primers (CODEHOP).....	117
4.2	Infrared (IR)-mediated heating system.....	118
4.2	Drawing and picture for side and top views of the PMMA microchip.....	119
4.4	Rapid thermal bonding of polymeric microdevices.....	120
4.5	Procedure of IR-mediated PCR in the polymeric microdevice.....	121
4.6	Temperature profile of IR-mediated PCR in the polymeric microdevice.....	127
4.7	Overlaid electropherograms of DNA amplifications in different PCR volumes ranging from 5 $\mu$ L to 1 $\mu$ L in the conventional thermocycler.....	128
4.8	Overlaid electropherograms of DNA amplifications from two different concentrations of DNA templates (1 pg and 2 pg) in the microdevice.....	129

## **Chapter 5**

5.1	Schematic of rapid TB drug susceptibility testing (DST) using standard PCR and hybridization-induced bead aggregation.....	136
5.2	qPCR curve of D29 phage amplifications from TB samples.....	141
5.3	Overlaid electropherograms from 25, 30 and 40 cycles of standard PCR.....	142
5.4	Overlaid electropherograms of conventional PCR products from clinical isolates.....	144
5.5	Hybridization-induced bead aggregation was conducted using serially diluted PCR samples .....	147
5.6	Hybridization-induced bead aggregation using D29 PCR amplicons from TB samples.....	148

## **Chapter 6**

6.1	PMMA-based droplet generation kit. ....	157
-----	---	-----

## List of Tables

### Chapter 1

1.1	Single Nucleotide Polymorphism (SNP) in human chromosomes. ....	2
1.2	History of microchip PCR .....	12
1.3	Physical characteristics of several polymeric materials.....	22
1.4	Passivation approaches for microchip PCR.....	25

### Chapter 2

2.1	Material properties in CFD simulation. ....	49
2.2	Primer information used in this research. ....	50
2.3	Experimental dwell times in the PCR functional zones of the 29-loop microdevice at various flow rates ranging from 2 $\mu\text{L}/\text{min}$ to 9 $\mu\text{L}/\text{min}$ . ....	59
2.4	Experimental dwell times in the PCR functional zones of the 43-loop microdevice at 2 $\mu\text{L}/\text{min}$ . ....	60

### Chapter 5

5.1	Information of couples of primer sequences for D29 amplifications. ....	138
5.2	Accuracy of standard PCR in analysis of microchip electrophoresis.....	146

## 1. Introduction: Genetic Analysis in Microfluidic Devices

### 1.1 General Purpose

After the completion of the Human Genomic Project (HGP) in 2003 (draft sequences of the human genome were released in 2001<sup>1,2</sup>), the information of the human genome has been accessible for scientists and engineers to intensively study the structure and function of the human genome that consists of around 23,000 genes as well as functional and repeated sequences. No two individuals have the same genome (including identical twins when epigenetics are considered), and complex variations of the human genome that include polymorphisms among individuals, populations, and races have been discovered. Genetic differences between individuals have been shown to explain many phenotypical variations, as well as inherited disease. A recent review of primary literature reported that over 5 % of variations in human genomic sequences were generated from Single Nucleotide Polymorphism (SNP) in human chromosomes (**Table 1**)<sup>3</sup>. Furthermore, it has been found that these large numbers of variances in the human genome are closely linked to phenotypic changes that can cause physiological changes or diseases such as cancers<sup>4</sup>, diabetes<sup>5</sup>, neurodegenerative diseases<sup>6</sup>, and genetic disorders<sup>7</sup>. These types of polymorphisms affect genes functioning for drug metabolism, transporting drugs into the cell, and the drug target itself, which finally present different metabolic responses to each drug and sometimes, lead to malignant effects for each individual<sup>8</sup>. From this reason, the importance of personalized medications has been emerged to prevent sub-optimal treatment of patients. Therefore, the understanding of genetic complexity and the importance of interpretation in the human genome makes the drive towards implementation in an advanced genetic analyzer more intensive than ever.

**Table 1:** Single Nucleotide Polymorphism (SNP) in human chromosomes. A total of SNP are composed of 1,419,190 bp out of 2.7 billions bp that cover over 5 % of the human genome [3].

Chromosome	Length (bp)	All SNPs		TSC SNPs	
		SNPs	kb per SNP	SNPs	kb per SNP
1	214,066,000	129,931	1.65	75,166	2.85
2	222,889,000	103,664	2.15	76,985	2.90
3	186,938,000	93,140	2.01	63,669	2.94
4	169,035,000	84,426	2.00	65,719	2.57
5	170,954,000	117,882	1.45	63,545	2.69
6	165,022,000	96,317	1.71	53,797	3.07
7	149,414,000	71,752	2.08	42,327	3.53
8	125,148,000	57,834	2.16	42,653	2.93
9	107,440,000	62,013	1.73	43,020	2.50
10	127,894,000	61,298	2.09	42,466	3.01
11	129,193,000	84,663	1.53	47,621	2.71
12	125,198,000	59,245	2.11	38,136	3.28
13	93,711,000	53,093	1.77	35,745	2.62
14	89,344,000	44,112	2.03	29,746	3.00
15	73,467,000	37,814	1.94	26,524	2.77
16	74,037,000	38,735	1.91	23,328	3.17
17	73,367,000	34,621	2.12	19,396	3.78
18	73,078,000	45,135	1.62	27,028	2.70
19	56,044,000	25,676	2.18	11,185	5.01
20	63,317,000	29,478	2.15	17,051	3.71
21	33,824,000	20,916	1.62	9,103	3.72
22	33,786,000	28,410	1.19	11,056	3.06
X	131,245,000	34,842	3.77	20,400	6.43
Y	21,753,000	4,193	5.19	1,784	12.19
RefSeq	15,696,674	14,534	1.08		
Totals	2,710,164,000	1,419,190	1.91	887,450	3.05

Most of infectious diseases occurring in human and animal bodies leave proof of existence as DNA/RNA fragments or genomes as well as their antigens and responding antibodies. However, the main hindrances of molecular diagnostics for these diseases are low amounts of genetic materials in their bodily fluids and time consuming diagnostic processes in genetic analysis. Although there are protein (antigen/antibody)-based immunoassays that can rapidly detect many diseases based on phenotypic and proteomic changes, the final confirmation of disease status in an individual should be verified by detecting genomic materials such as DNA/RNA in the bodily fluid<sup>9</sup>. Therefore, developing an advanced genetic analyzer for rapid diagnostics of these genomic materials in the earlier stages of infectious diseases must be a vital point in an attempt to cure individuals and prevent spreading of these infectious diseases in the

world, especially in developing countries, where current diagnostic methods are not feasible due to poor clinical infrastructures and costs of analytical instruments. In addition to the detection of exogenous genetic materials in human bodies, genome-based quality control and risk assessment have greatly improved the ability to quantify food borne and waterborne pathogenic bacteria causing a severe health hazard<sup>10</sup>. Furthermore, after the introduction of DNA fingerprinting or forensic genotyping into the field of forensic science, it has revolutionized the ability for law enforcement to find offenders based on their repeated DNA sequences in the human genome<sup>11</sup>. From these perspectives, molecular diagnostics and DNA profiling are essential technologies to provide pivotal tools for environmental monitoring and human identification in the forensic purpose.

From these reasons of the importance in genetic analysis and several merits over conventional analytical instrumentations, development of rapid, accurate, reliable, and cost-effective genetic analysis technologies, essentially in microfluidic devices, has been broadly studied so that many research groups have reported the development of partially and fully miniaturized and integrated genetic analyzers<sup>12-15</sup>. These microfluidic devices have focused on realizing many advantages of “Lab on a chip” technologies such as miniaturization, integration, and automation in microfluidic devices. The integration of all functional units into a closed and single microfluidic device can completely remove sample handling to prevent sample contamination and loss. Ultimately, this miniaturized microdevice is capable of achieving true “Point-of-Care” (POC) instrumentation beyond the bench top and conventional instruments. From these motivations and trends of developing microfluidic methodologies and instrumentation in advanced genetic analysis, we are creating high performance microfluidic

devices that enable miniaturization of a genetic analyzer with capabilities of portability, multiplex and high-throughput reactions (**Fig. 1**).

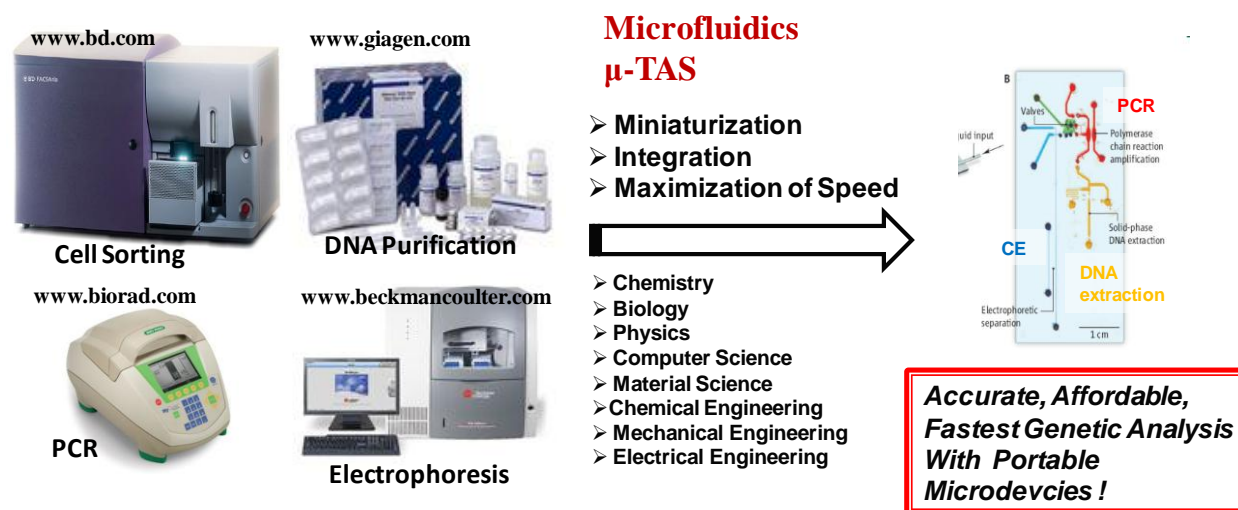


**Figure 1:** Schematic in the general concept of developing microfluidic devices for genetic analysis: the integrated microfluidic device from [12]. DNA extraction (**yellow**), microchip PCR (**red**), and microchip electrophoresis (**blue**) were integrated in a single glass microdevice.

## 1.2 Micro-Total Analysis Systems ( $\mu$ -TAS) and Its Applications

Microfluidic technologies and Micro-Total Analysis Systems ( $\mu$ -TAS)<sup>16</sup> for chemical, biological, medical, and engineering applications have been extensively studied and developed over the past decade, and these efforts have led to exclusive advances in terms of speed, cost, and automation of bio-analytical and bio-technologies. Applications range from simple chemical and biological reactions to complex and multiplexed processes in a single and integrated microfluidic device<sup>17-19</sup>. The first generation of applications using microfluidics technologies was focused on the development of capillary-based microchannel electrophoresis and micro- or nano-scale PCR, especially for clinical and forensic applications. These microdevices increased the sensitivity and decreased the total analysis time to achieve rapid and accurate instrumentation<sup>16,20</sup>. From these initial applications, many research groups have expanded applications of microfluidic

devices in the fields of science and engineering since miniaturization itself has many meaningful advantages. There have been numerous examples where microfluidics has been utilized in the major fields of biotechnology such as protein<sup>21</sup>, cellular and tissue engineering<sup>22</sup>, systems biology<sup>23-25</sup>, drug discovery<sup>26</sup>, and drug delivery<sup>27</sup>.

### 1.2.1 Microfluidic Literature

In order to demonstrate exponential growth of microfluidics research related to biomedical science and engineering, literature search was performed using NCBI (National Center for Biotechnology Information) PubMed from 2000 and 2011 to investigate accumulated numbers of publications including the term *microfluidic* (violet) and *microchip* (orange) (Fig. 2A).

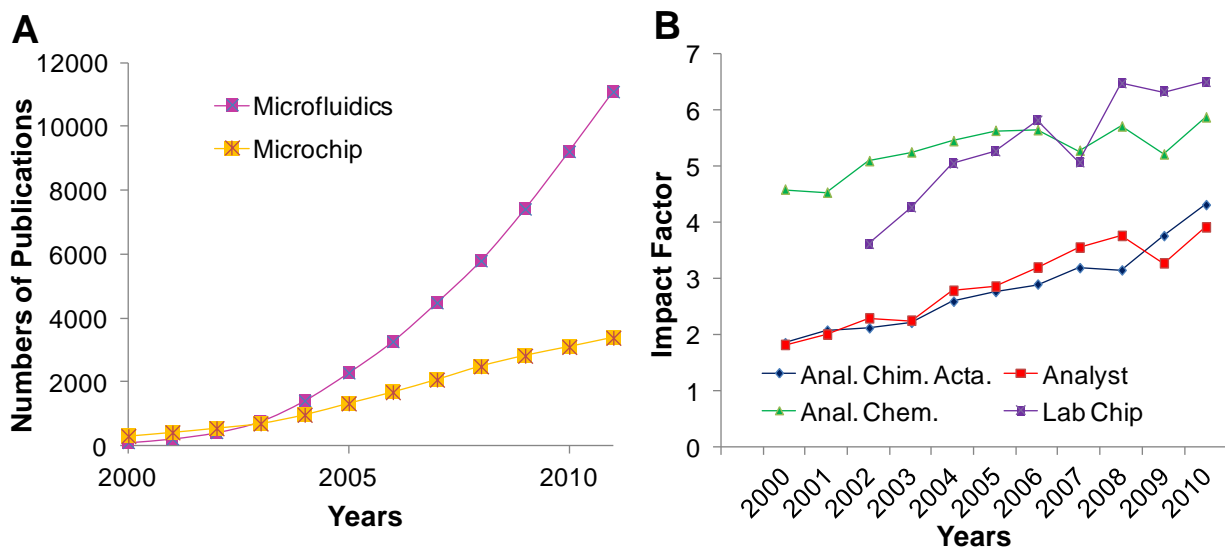


**Figure 2:** Two trends of exponential growth in microfluidics research. (A) Numbers of publication were searched in NCBI PubMed using words “microfluidics or microchip” from 2000 to 2011. (B) Impact factors of the journals related to microfluidics have increased dramatically.

The number of publications related to microfluidic devices or microchips has risen dramatically and it demonstrates that many interdisciplinary fields such as chemistry, biology, physics, biomedical science, and engineering have employed microfluidic technologies to conduct their research. Impact factors (a quantitative method for evaluating a journal; the measurement of frequency for an average article in the journal cited) of journals that ultimately concentrate on microfluidics and microchip studies have continuously increased (**Fig. 2B**). These journals include *Analytica Chimica Acta* (**blue**), *Analytical Chemistry* (**green**), *Analyst* (**red**), and *Lab on a Chip* (**purple**). These collected data have shown that microfluidics technologies have been rapidly growing in the fields of science and engineering, and it will continuously progress as an advanced and essential technology.

### 1.2.2 Physics in Microfluidics

Microfluidic devices are comprised of micron-scale (dimensions on the order of microns) chambers and channels, these small dimensions exhibits unique chemistry and physics<sup>26,28,29</sup>. Although gravity and inertia are dominant factors in the physical world, as a system decreases in the size to a micro-scale world, viscosity, surface tension, and diffusion become important factors. With respect to the main characteristics of flow in a microfluidic device, a micro or nano-scale channel provides low Reynolds numbers due to the small dimension of this microchannel. As an important dimensionless factor, the Reynolds number indicates the relative importance of inertia and viscosity in a fluid system and defines different flow regimes; laminar and turbulence. At low Reynolds numbers ( $< 2100 \sim 2300$ ), the viscous force is dominant to make the flow constant and smooth (**Fig. 3A**). As viscosity produces resistance to shear forces, small Reynolds numbers have a tendency for fluid to flow in a parallel shape as laminar flow.

The laminar flow in the microfluidic device is exploited for several applications such as separation and sorting of chemical and biological reagents and cells. However, two different streams do not mix in the laminar flow regime except through diffusion. In the micro-scale world, laminar flow is dominant to makes diffusion much important for mixing and moving solutes. In addition, the complete mixing of several reagents in laminar flow becomes complicated inside a nano or micro-scale of the chamber and the channel. From this reason, several groups had reported novel mixing systems to effectively and rapidly mix several reagents inside a microfluidic device<sup>30-32</sup>.

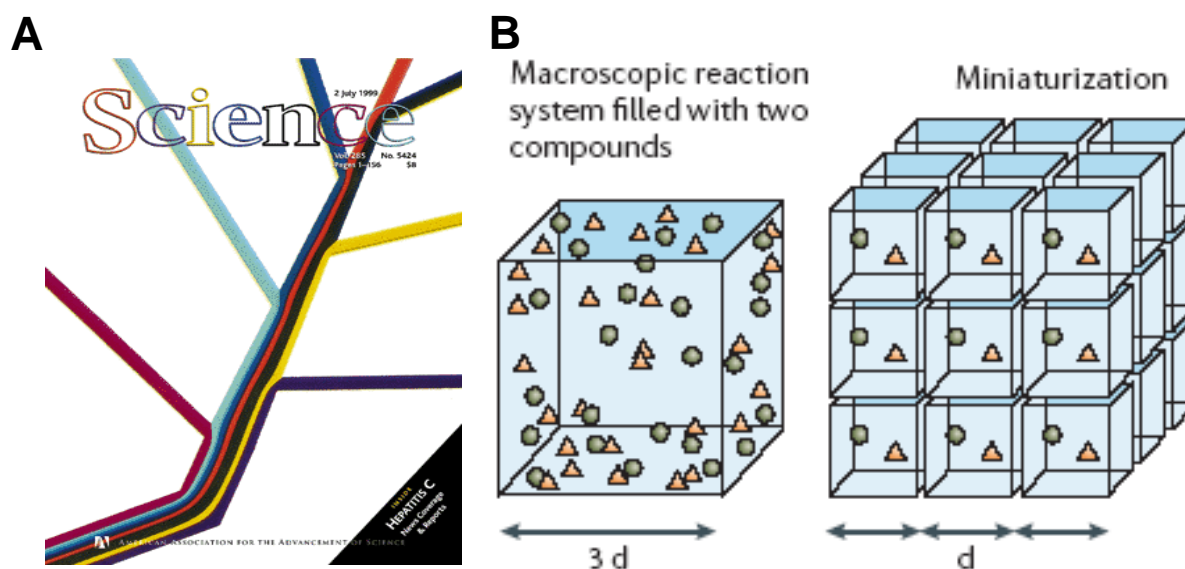


**Figure 3:** Physical characteristics in micro-channels and chambers. (A) Low Reynolds number generates laminar flow that creates only diffusion driven mixing in a microfluidic channel (journal cover of *Science* issued in 2 July 1999). (B) Miniaturization of macroscopic system provides a high surface area to volume ratio that improves heat and mass transfer, and makes important parameter control easier and precisely regulated. Massive parallelization of reactions can be achieved [26].

One characteristic in a micro-scale system is a significant increase in a surface area to volume ratio that improves the rates of mass and heat transfer in micro-scale systems and makes a system rapidly homogenous for temperature and solutes, simply due to a short distance (**Fig.**

**3B).** The miniaturization of a reaction volume is closely related to the ability to achieve multiple reactions for serial and parallel analysis in a single microdevice<sup>26</sup>. However, the increased surface area compared to a reaction volume makes us consider the interaction between reaction reagents and surface walls of channels or chambers. Intensive studies of material and surface chemistry are required to generate a reaction-friendly surface and prevent the adsorption of reaction reagents or cells into this large surface area compared to a small volume.

### 1.3 Polymerase Chain Reaction (PCR) in Microfluidic Devices

#### 1.3.1 Chemistry and Biology of PCR

The invention of the PCR in 1986 by Mullis *et al.*<sup>33</sup> has been revolutionary to the fields of biochemistry, biology, medicine, and engineering that deal with genetic materials such as DNA and RNA. Simply, the PCR is a three-step enzyme-based chemical reaction that allows any nucleic acid fragment to be exponentially multiplied in vitro (**Fig. 4**). At the beginning of this process, double stranded DNA is completely denatured (i.e. DNA strands are separated into a single strand) at the 90 – 96 °C, in what is termed, *denature step*. After denature, a pair of sequence specific primers is annealed at positions flanking the region of denatured single-stranded DNA, to be amplified in what is termed, *anneal step*. Lastly, DNA polymerase recognizes the end of the primer set and extends these regions to synthesize complementary DNA sequences; *extension step* (**Fig. 4A**). Through repeated iteration of three-step processes, the initial copy number of template DNA is exponentially amplified to generate up to a billion copies of the DNA products (**Fig. 4B**). In the first generation of PCR, the Klenow fragment of *E.coli* DNA polymerase was used for the extension process. But, high denature temperature (90 – 96 °C) inactivated DNA polymerase within a short time. After the introduction of DNA

polymerase (*Taq* polymerase) of Thermophilic bacterium (*Thermus aquaticus*) in PCR<sup>34</sup>, PCR process had been automated. *Taq* polymerase shows high thermal stability that eliminates the requirement of an enzyme adding step in each cycle without denaturing thermo-stable DNA polymerase.

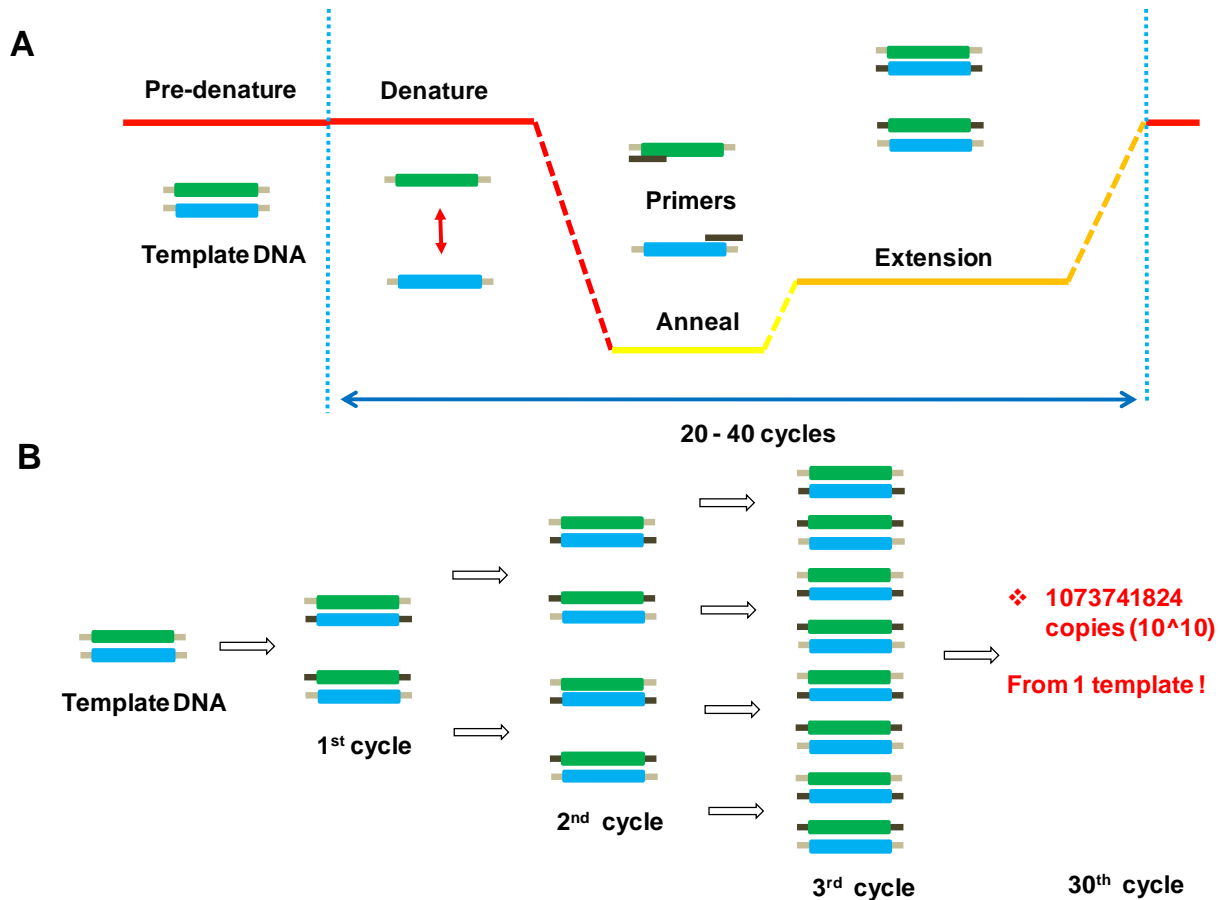


**Figure 4:** Schematic of the Polymerase Chain Reaction (PCR) amplification. (A) PCR three steps; denature, anneal, and extension with pre-denature and final extension steps. (B) Exponential amplifications indicated that  $10^{10}$  ( $10^{10}$ ) copies of DNA can be amplified from only a single copy of DNA via 30 cycles of repeated thermal cycling.

The denature and anneal steps are fast processes dictated by DNA molecular dynamics, and these steps occur during temperature transition periods. However, the extension step is limited by the activity of DNA polymerase that shows the limited numbers of bases incorporated into the DNA strand per second, depending on types of DNA polymerases<sup>35</sup>. In a microfluidic PCR system, the durations of denature and anneal steps can be significantly reduced by up to

several seconds versus conventional thermocyclers because of rapid heat transfer in decreased fluid volume. Furthermore, recently, many companies have introduced engineered DNA polymerases that have heat-stable characteristics, fast polymerase activities, no activity at low temperature to prevent non-specific amplifications at the early stage of PCR amplification. Now, rapid PCR can be finished within several minutes inside microfluidic devices<sup>36,37</sup>.

### *1.3.2 Characteristics of Microchip PCR*

Microchip PCR has been intensively studied to make the unprecedented impact in the microfluidic community because it has great potential, numbers of applications, especially for clinical<sup>38</sup> and forensic applications<sup>11</sup>, and many advantages over conventional instruments<sup>39-41</sup>. First of all, from miniaturization, a total reaction time in PCR amplification significantly decreases because it increases temperature transition times (ramp rates for heating and cooling). It is mainly in consequence of 1) improved heat transfer inside a micro-chamber and channel, and 2) decreased thermal mass of the heater and microchip material. The conventional thermal cycler utilizes a metal heat block as a heating source and the large thermal mass of this block restricts fast thermal cycling in this system. The ramp rate of this thermal cycler was achieved around 1 - 2 °C/s and it takes 1 – 3 hours for the complete amplification of target DNA, depending on the specific reaction used. Secondly, fairly small volumes of the PCR solution such as nano- or pico-liters are able to be processed on a microchip and it causes the reduced consumption of reagents up to several hundred or thousand folds, which can yield considerable savings in reagent costs. Achieving multiple reactions in parallel reactions on the conventional thermal cycler is limited as a result of a large volume of the PCR sample (from 25 µL to 100 µL per one reaction). However, large numbers of parallel amplifications in a single microdevice

(lower than 1 – 2  $\mu\text{L}$  per one reaction in a microchip) can be conducted to achieve multiplex and multiple genetic testing. Consequently miniaturization, which provides clear advantages with micro- and nano-scales of volumes, is capable of achieving portability of PCR instrumentation and its integration with other upstream and downstream functional units.

### 1.3.3 History of Microchip PCR

The first emergence of microfluidic technologies had been reported in the mid to late 1970's for developing a miniaturized silicon chip of gas chromatography system at Stanford University<sup>42</sup> and ink-jet printer at IBM<sup>43</sup>. These were initial approaches using miniaturized microchips. However, Manz *et al.* introduced the real concept of Micro-Total Analysis Systems ( $\mu$ -TAS) as a novel system that could reduce sample usage and increase separation efficiency due to the decreased physical scales of experimental conditions inside the microchip in 1990<sup>16</sup>. With the introduction of  $\mu$ -TAS, Manz *et al.* reported a capillary electrophoresis (CE) microchip in 1992<sup>20</sup> and Northrup *et al.* first developed a microfluidic PCR device in 1993<sup>44</sup> that described a silicon wafer-based static PCR (published in *Anal. Chem.* in 1998<sup>45</sup>). Wilding *et al.* demonstrated the first approach of surface passivation for the microchip PCR in the decreased volume of the PCR reaction using hybrid glass/silicon in 1994<sup>46</sup>. Wooley *et al.* reported that the silicon wafer-based PCR reactor and glass capillary electrophoresis were coupled to build up the first integrated microfluidic device of PCR and CE in the microchip in 1996<sup>47</sup>. Kopp *et al.* introduced the continuous flow format of microchip PCR in 1998<sup>48</sup> and it described that analysis time of PCR amplification was not limited by an instrument and limited by PCR itself. It was mainly because they could decrease reaction time as much as they could just by changing the flow rate. In our group (Dr. Landers group), Oda *et al.* reported infrared(IR)-mediated PCR to

show simple DNA amplification inside an electrophoretic glass-like microchamber in 1998<sup>49</sup> and Huhmer *et al.* reported the effectiveness of the IR-mediated heating system on capillary and microchip devices for PCR applications<sup>50</sup>. Giordano *et al.* reported the development of a polyimide microdevice on the IR-mediated heating system<sup>51</sup>. But it was not useful due to the incapability of integration with microchip electrophoresis (optical issue). Rapid DNA amplification from the human genome was reported using 35 cycles of PCR in the glass microfluidic device, showing fast ramping rates as a result of the thermal conductivity of glass that was around ten times higher than polymeric materials. Additionally, Giordano *et al.* demonstrated that surface passivation on the glass surface by silanization improved PCR amplification, sometimes, combined with other passivation reagents such as BSA<sup>52</sup>. Easley *et al.* reported a fully integrated genetic analysis platform on the glass microdevice in 2006, which made all functional units such as DNA extraction, PCR amplification, and DNA electrophoresis integrated in a single integrated microdevice<sup>12</sup>. The brief history of microchip PCR is outlined in

**Table 2.**

**Table 2:** History of microchip PCR

Year	Achievement
<b>1975 - 80</b>	Gas chromatography system in the miniaturized silicon chip at Stanford (Terry <i>et al.</i> 1979) [42] and ink-jet printer at IBM (Bassous <i>et al.</i> 1977) [43]
<b>1986</b>	PCR invented by Mullis (Mullis <i>et al.</i> 1986) [33]
<b>1990</b>	Concept of Micro-Total Analysis Systems (Manz <i>et al.</i> 1990) [16]
<b>1992</b>	Microchip capillary electrophoresis (CE) (Manz <i>et al.</i> 1992) [20]
<b>1993</b>	Microchip PCR (Northrup <i>et al.</i> 1993) [45]
<b>1996</b>	PCR-CE integrated microdevices (Wooley <i>et al.</i> 1996) [47]
<b>1998</b>	Continuous flow PCR (Kopp <i>et al.</i> 1998) [48]
<b>1998</b>	Infrared-mediated PCR (Oda <i>et al.</i> 1998) [49]
<b>2006</b>	Fully integrated genetic analysis microchip (Easley <i>et al.</i> 2006) [12]

### 1.3.4 Classification of Microchip PCR

When we classify microchip PCR based on the type of the PCR vessel, there are two major types of microchip PCR, a static<sup>53</sup> and continuous flow PCR (cf-PCR) (dynamic)<sup>48</sup> platforms. In the static format (**Fig. 5A**), a non-contact method using a lamp allowed for achieving rapid PCR reactions with fast ramp rates, and selective heating of the PCR solution<sup>51,53,54</sup>; Giordano *et al.* had shown that indirect radiation using a lamp could achieve ultra-fast DNA amplification within 240 seconds<sup>51</sup>. However, multiple and higher throughput reactions on the static format could be confined by the size and the focal spot of the heating system (lamps)<sup>55</sup>. In addition, multiplex or multiple PCR amplifications inside the static chambered vessel are limited by the optimization of anneal temperatures of multiple primers<sup>56</sup>. The reaction speed is further restricted by types of heating lamps and microchip materials, and designs of the microchamber and the microchip<sup>57</sup>.

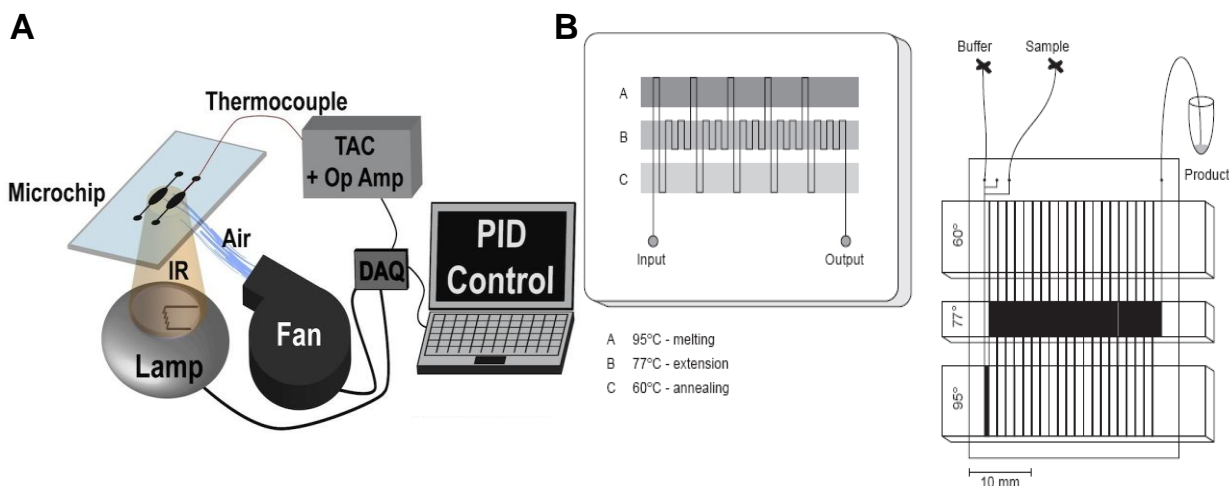


**Figure 5:** Miniaturized PCR instruments. (A) Non-contact infrared-mediated heating system (Dr. Landers lab). (B) Contact heating system for continuous flow PCR on three distinct heat blocks [48].

The first approach of continuous flow PCR (cf-PCR) in a microfluidic device was demonstrated in  $\mu$ -TAS community in 1998 (**Fig. 5B**)<sup>48</sup> and many groups further studied this

format using modified designs of microdevices<sup>58,59</sup>, advanced heaters to improve heating and miniaturization<sup>60,61</sup> as well as different types of PCR amplifications such as reverse-transcriptase PCR<sup>58</sup>, real-time PCR<sup>62</sup>, and droplet PCR<sup>63</sup>. As the main advantage of this heating system, the continuous flow format provides a heating configuration to realize multiple and multiplex reactions via segmented flows and droplet microfluidics<sup>64</sup>. In addition, the PCR speed is extremely improved just by increasing the flow rate and modifying a microchip design<sup>59,60</sup>. However, miniaturization and integration of heaters are critical drawbacks of cf-PCR since it has three different heaters located nearly each other, which causes a lateral heat transfer to prevent precise temperature control within the small microdevice. As results of these critical disadvantages, a simple heating concept using the thermal gradient established by a single contact heater has been introduced by several groups<sup>61,65</sup>. Nonetheless, the modification of this thermal gradient for changing anneal temperature, miniaturization, and integration with other functional units had not been further described as a consequence of using the contact heating approach.

## 1.4 PCR Heating Systems in Microfluidic Devices

### 1.4.1 Contact Heating System

According to previous studies, PCR heating systems are classified as a non-contact (**Fig. 6**) and a contact (**Fig. 7**) approach. They have several advantage and disadvantages, depending on the configuration of heating systems (static or continuous flow, single or multiple heaters), types of microfluidic devices (glass or polymers) and PCR approaches (single or multiple reactions). Two major types of contact heating methods have been utilized for conducting microchip PCR; the metal heat block including Peltier heater<sup>48,58,63,66</sup> and thin film resistive

heater<sup>13,60,61,67-72,73</sup>. A conventional thermal cycler is constructed using the metal heat block where a polypropylene PCR tube is positioned to directly contact this heating source to perform thermal cycling. However, as I emphasized, the large thermal mass of this heat block limits fast heating and cooling decreased up to 1 – 2 °C/sec. In addition to the Peltier-based heat block, several thin film heaters have been commonly used as a heating source for two formats, static and dynamic (continuous flow) PCR platforms. This thin film converts electrical energy to thermal heating for thermal cycling of micro- or nano-scale PCR (**Fig. 6A**) and there are several types of thin film heaters reported such as platinum<sup>67-72</sup> and Al<sup>13,73</sup>. Usually, the thin film (platinum) and temperature sensor were directly fabricated into the thin resistance heater (**Fig. 6B**). However, the actual temperature of the PCR solution was not measured by the temperature sensor since it was usually placed outside the PCR solution in the microchamber<sup>74</sup>.

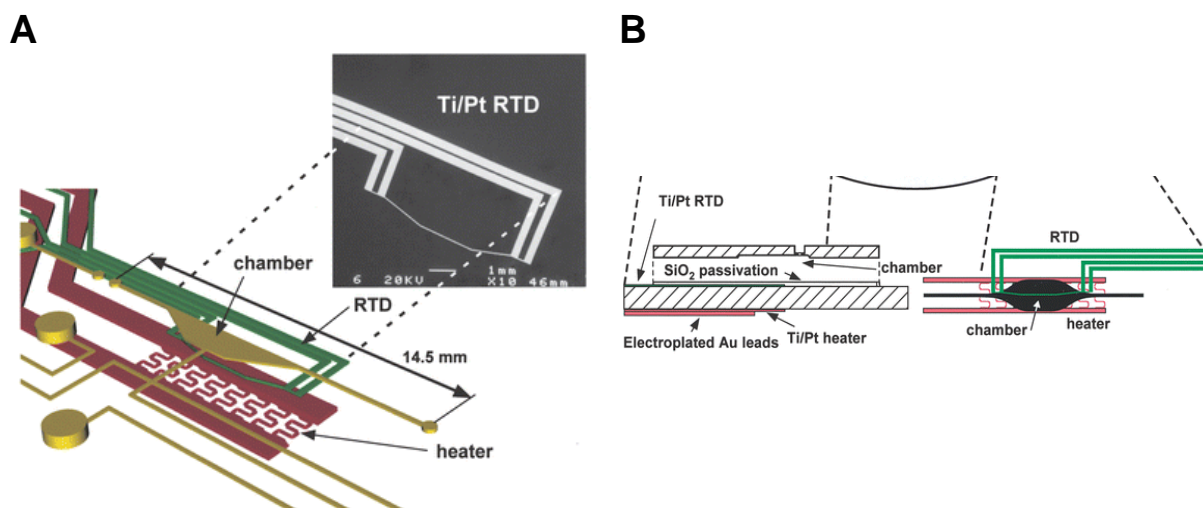


**Figure 6:** Contact heating system for microchip PCR applications [47]. (A) Contact heating system used in Mathies group, which consists of the PCR chamber, resistive temperature detector (RTD), and heater. *Inset:* SEM indicating a close-up view of the RTD structure. (B) Schematic of the microfabricated heater and RTD; the cross-section of the microchip PCR area in microfluidic devices. The PCR chamber is positioned between two glass layers and RTD, and heater was located on the bottom layer of glass.

#### 1.4.2 Non-contact Heating System

As a non-contact heating approach, an IR-mediated heating system was first reported in our group (Dr. Landers group) in 1998 using a single and inexpensive tungsten lamp<sup>49</sup>. A non-contact heating approach can eliminate the thermal mass of the heater and only the thermal mass of the reaction solution should be considered for heating by reason of selective IR-mediated heating of the PCR solution<sup>54</sup>; longer wavelength than visible light, infrared heats object directly without any loss of energy through their environments and there is only heat loss through conduction from the PCR solution to the microchip material. Additionally, our group has shown successful microchip IR-PCR applications using different materials such as glass<sup>12,52</sup> and polymeric materials<sup>51,57,75</sup>. The initial approach for the IR-heating system was conducted by a tungsten lamp with an enforced cooling fan that could increase heating and cooling ramp rates up to 20 °C/s<sup>49</sup>. For forensic applications, as slow and stable heating should be critical to achieve multiplex PCR in a static format of the microdevice, microchip PCR was performed using a halogen lamp (less intensive than a tungsten lamp), which completed STP amplifications with decreased analysis time up to 30 – 40 minutes from 2- 3 hours<sup>57,75</sup>. As another IR-heating system, other groups have reported that a laser-mediated noncontact heating system showed fast ramp rates compared to lamp and contact heating systems (**Fig. 7**)<sup>76,77</sup>. Theoretically, as laser emits narrow ranges of the wavelength for heating the PCR solution, it offers more selective heating than a lamp radiation and increases ramp rates. In addition, several microwave-mediated heating systems have been reported for rapid thermocycling targeted for PCR applications<sup>78-82</sup>. Microwave selectively heats the PCR solution having different dielectric constants with heating the PCR solution much faster than other types of heating systems. As the electromagnetic radiation, both of non-contact heating approaches such as microwave and infrared have longer

wavelength and lower frequencies than visual light and this radiation energy is selectively absorbed into the PCR sample and it dramatically improves temperature transition time to achieve ultra-fast thermocycling.

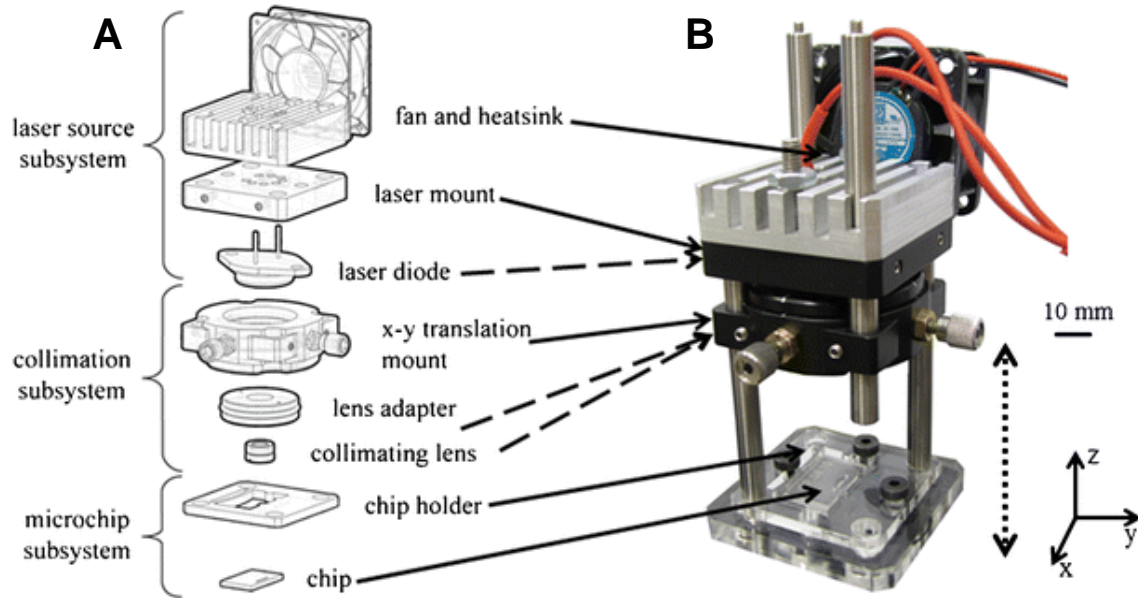


**Figure 7:** Non-contact heating system for microchip PCR applications [76]. (A) Overview diagram of the laser thermocycling system describing the laser source subsystem (*top*), collimation subsystem (*middle*), and microchip subsystem (*bottom*). (B) Assembly of a laser-mediated heating system.

## 1.5 Temperature Measurement in Microfluidic Devices

### 1.5.1 Contact Temperature Measurement

The precise control and measurement of temperature inside a microfluidic device should be critical factors for successful microchip PCR. There have been several methods to accurately measure temperature inside microfluidic devices. As other classifications I mentioned, temperature measurement can be classified as a contact and non-contact method (**Fig. 8**). As a prototype contact measurement of temperature, a thermocouple has been employed in microfluidic devices (**Fig. 8A**) because of several merits such as low cost, simplicity, robustness,

compact size, and temperature range<sup>83</sup>. Although a thermocouple measures the actual value from the reaction solution via directly touching this solution, the appropriate surface coating of a thermocouple is crucial to minimize the adsorption of PCR reagents and temperature measurement can be affected by the radiation of infrared heating and microwave, which is able to disrupt accurate temperature measurement via a thermocouple. Additionally, the thermocouple is located or integrated inside the heater instead of touching the PCR sample and it can generate temperature difference between the PCR chamber and the heater (**Fig. 6B**). Sometimes, another dummy microchamber is required for measuring the actual temperature of the PCR chamber to avoid reagent adsorption on the thermocouple (**Fig. 8A**)<sup>54</sup>.

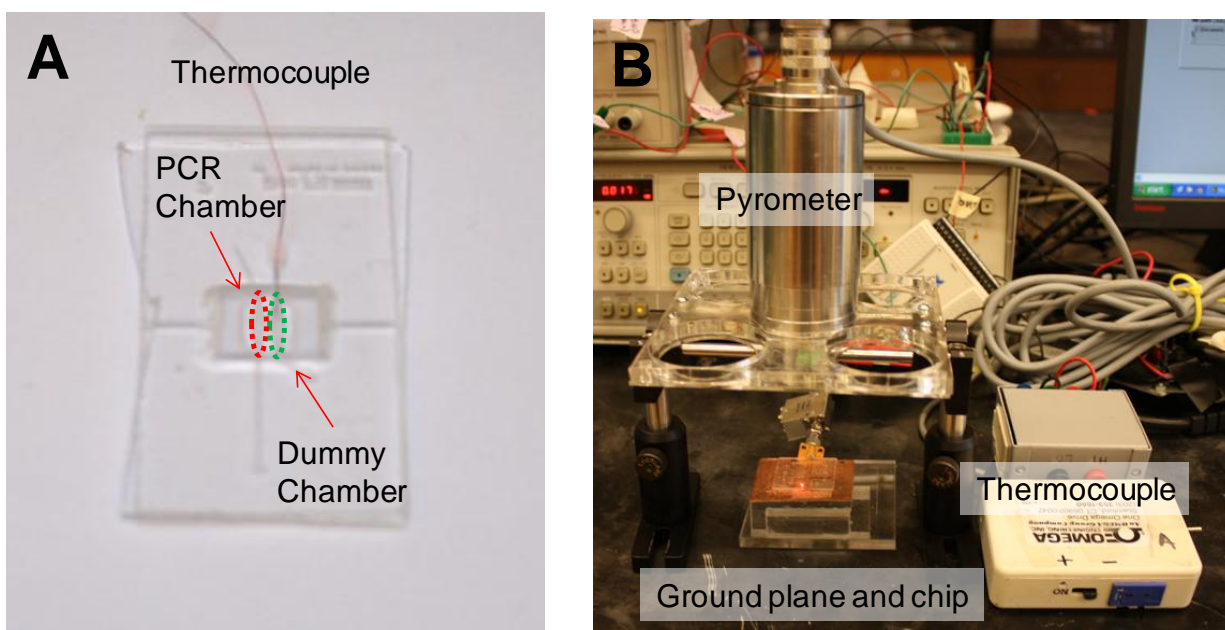


**Figure 8:** Two types of temperature measurement methods in microfluidic devices. (A) Contact temperature measurement using a thermocouple that is placed in the reference microchamber [54]. (B) Non-contact temperature measurement using a pyrometer that senses temperature on the top of the microfluidic device [53].

### 1.5.2 *Non-contact Temperature Measurement*

IR thermometry such as a pyrometer<sup>53</sup> and IR-camera<sup>84</sup> have been used to measure temperature referring to the radiation emitted by target objects at a certain distance. An infrared pyrometer is able to measure only one spot at the fixed distance from this pyrometer and the distance to the spot size ratio is an important factor to measure precise temperature (**Fig. 8B**). As several advantages, a non-contact approach completely removes physical contact of the PCR sample without the thermocouple and placement of the thermocouple into microchips. So, the non-contact approach completely eliminates the cross-contamination caused by contact temperature probes. Measuring right temperature on a moving object can be conveniently conducted by the non-contact method.

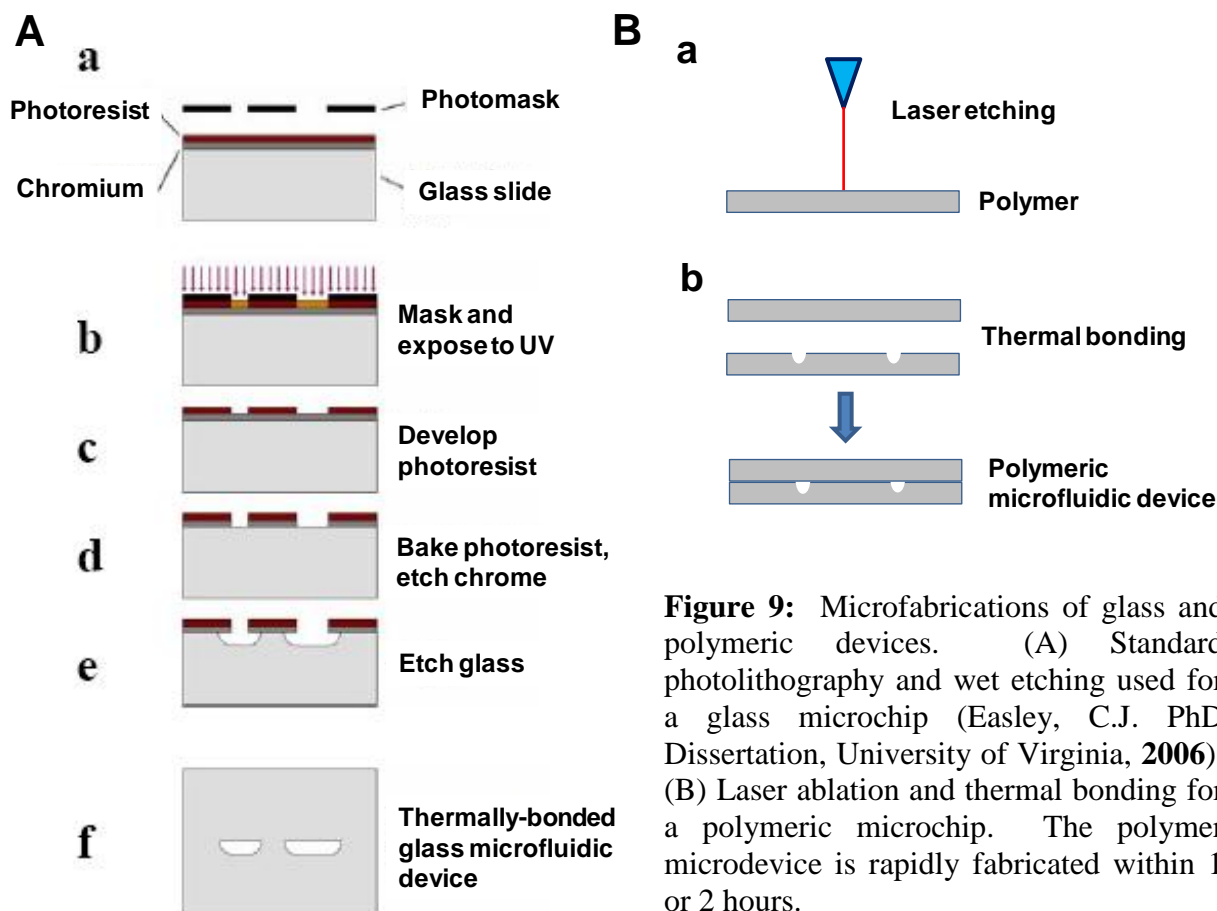
However, emissivity on the surface of a microdevice should be carefully considered to sense correct temperature via IR thermometry. Emissivity describes the ratio emitting the capability of the object to blackbody at the same temperature, emphasizing the radiation emitting and absorbing capability of the object material. The main difficulty of IR thermometry is that all object materials have different emissivity values that are further affected by the distance and angle between the object and the pyrometer, and surface roughness and thickness of microchip materials. Owing to high emissivity values, non-metallic materials such as glass and polymers, common materials for microchip fabrication, are good materials for using IR-thermometry comparing with a metal surface<sup>83</sup>.

## 1.6 Microchip Material and Fabrication

### 1.6.1 Silicon and Glass

Choosing a proper material and fabrication method for developing new microfluidic devices should be a vital point for successful microfluidics research. Especially for microchip PCR applications, these are important steps to be carefully considered before starting research. As the first generation material, silicon has been employed to be microfabricated for PCR applications<sup>47,67,85,86</sup>. The silicon material shows several merits such as superior thermal conductivity, strong chemical resistance, and stability at higher temperature, and a well established fabrication method by semiconductor industry. However, it has several drawbacks such as optical opacity, the high cost of fabrication procedure, and the difficulty of integration with other materials. In addition, the fabrication process is complicated and labor-intensive, and highly specialized skills, micromachining instrument, and clean room facilities are required.

As a microchip material, a glass material has been fabricated in many groups (including our group) for microchip PCR applications<sup>12,13,48,53,58,61,62,74,87-90</sup>. The fabrication process for the glass material consists of standard photolithography, wet etching (HF), and thermal bonding (640 °C, 8 hours)<sup>12</sup> (**Fig. 9A**). Photolithography is a prototype process for microfabrication, usually used for fabrication of silicon/glass materials. It transfers a pattern designed via commercialized drawing software such as AutoCAD or CorelDraw on the mask into a photoresist glass plate using UV light and the pattern transferred on the microchip is chemically etched by liquid chemicals, hydrofluoric acid (HF), to generate the precise depth of channels and chambers. The glass material is optically transparent, biocompatible, and easily integrated with other functional units. However, it is not disposable and requires a dangerous cleaning procedure (using a piranha solution) and a time-consuming fabrication step.



### 1.6.2 Polymers

As alternatives to microchip materials, polymers have been studied and developed due to several advantages such as low cost, easy fabrication, disposability, biocompatibility, optical transprence in visible/UV region, simple fabrication and bonding causing fast prototyping, easiness to transfer manufacturing into large-scale production (embossing and injection molding), and lack of cross-contamination via disposability<sup>30,91-96</sup>. Many polymeric materials as thermoplastics such as polycarbonate (PC)<sup>60,97</sup>, poly(methyl-methacrylate) (PMMA)<sup>55,57,75,98</sup>, polyimide (PI)<sup>51</sup>, polyester (PET)<sup>99</sup>, SU-8<sup>100</sup>, and poly(cyclic olefin)<sup>101</sup> and elastomers as PDMS<sup>102,103</sup>, have been successfully employed for PCR applications. **Table 3** describes physical

properties of well-known polymers to be considered for microfabrication and its applications. The polymeric material consists of macromolecules with a high molecular weight. Above glass transition temperature ( $T_g$ ), it acquires flexibility ready to be molded into its own shape (**Fig. 9B**). As flexibility of applications and rapid prototyping of manufacturing are important criteria for microchip fabrication, the polymer material is the best material fitting into these criteria. After choosing one polymer, the appropriate selection of fabrication methods such as hot embossing<sup>104</sup>, injection molding<sup>105</sup>, soft-lithography (PDMS)<sup>106</sup>, laser ablation<sup>55,57,66,75,107</sup>, and micro-milling<sup>76</sup> should be carefully considered to achieve successful applications in the polymeric microdevice.

**Table 3 :** Physical characteristics of several polymeric materials [30, 91-96].

	<b>PMMA</b>	<b>PC</b>	<b>PET</b>	<b>PI</b>	<b>PDMS</b>	<b>Glass</b>
Glass transition temp ( $T_g$ ) ( $^{\circ}\text{C}$ )	106	150	67 -81	285	N/A	N/A
Thermal conductivity (W/mK)	0.186	0.21	0.15 – 0.24	0.2	0.17 – 0.3	1.1
Transmission of visible light (%)	92	89	90 - 80	87	91	92-97
Melting temperature ( $^{\circ}\text{C}$ )	142	335	280	388	219	< 1000
Density (g/cm <sup>3</sup> )	1.18	1.21	1.35	1.4	0.965	2.0 -3.0
MW of Unit	100	254	192	N/A	74.1	N/A
Specific Heat Capacity (J mol <sup>-1</sup> $^{\circ}\text{C}^{-1}$ )	127.9	279.8	206	115.0	111.5	0.5-0.8
Water absorption (%)	0.3–0.6	0.12–0.34	0.1-0.3	0.32	N/A	N/A
Solvent resistance	Good	Good	Excellent	Good	N/A	Good
Acid/base resistance	Good	Good	Excellent	Good	N/A	Good

After the introduction of photo-ablation for the construction of microdevices in 1997<sup>108</sup>, direct etching and cutting methods via laser have been broadly used for many applications in polymeric microdevices. The laser ablation is a photo-thermal process that transfers photons into

polymer materials and increase temperature around this region to cause thermal decomposition of polymers, we called, a photo-fragmentation. Variable width and depth of the microchannel on plastic materials are fabricated by adjusting its power and transition speed of laser. The user-designed patterns (created in a variety of computer-aided design software such as CorelDraw, AUTOCAD, and Illustrator) can be transferred into a laser ablation machine to cut these patterns on sheets of polymers. As drawbacks, the surface roughness (**Fig. 10**) and bulges on the edge of laser-ablated areas restrict microfabrication and its applications. As an example, these rough surfaces provide nucleation sites of formation of air bubbles in microfluidic devices and these bubbles are further expanded to prevent microchip PCR<sup>57</sup>. Nonetheless, a laser ablated approach still has important advantage to rapidly generate polymeric microdevices for many applications.

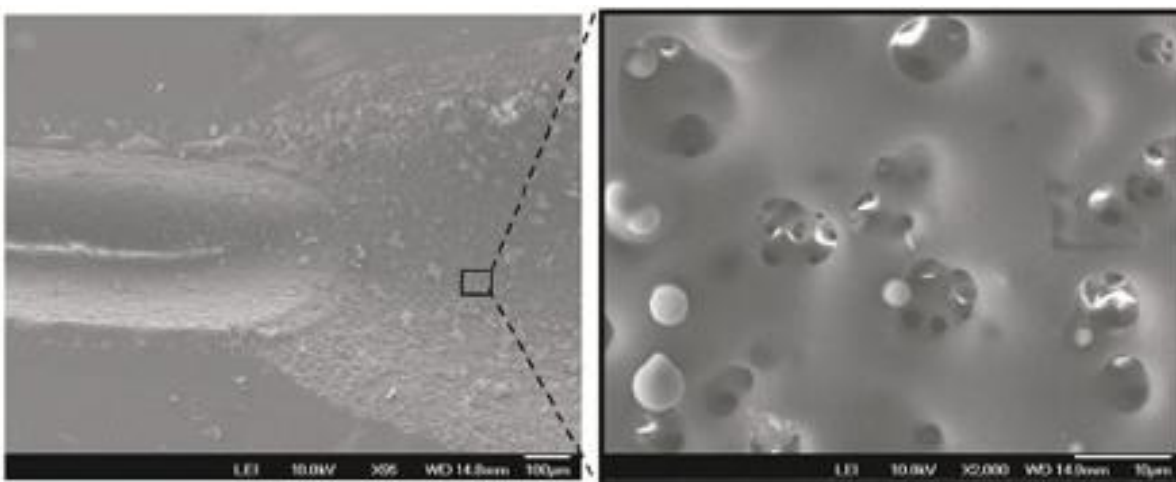


**Figure 10:** SEM images of laser ablated surfaces on the PMMA layer. Surface of PMMA after laser ablation. *Inset:* close view of this surface having many pores. Two images were adapted from [57].

### 1.7 Surface Passivation in Microfluidic Devices

The physical characteristics of a micro-scale channel and chamber provide relatively a large surface area to volume ratio where reagents permanently contact microchip materials and

this contact causes the adsorption of chemical reagents into the surface of these materials. Therefore, it increases the significance of surface chemistry in the microfluidic device<sup>109,110</sup>. In addition, inhibitory chemical or biological reagents that are derived from microchip materials or from PCR reagents decrease PCR efficiency in the microdevice. Therefore, physical characteristics of the microchip and surface chemistry should be thoroughly evaluated to find out proper passivation strategies and investigate biocompatibility of microchip materials and PCR additives before performing microchip PCR. With respect to a continuous format of PCR, syringes and tubes for dealing with the PCR solution should be deliberately chosen to decrease the adsorption of PCR reagents while injecting the PCR solution<sup>111</sup>. Furthermore, different geometry and architecture of the PCR chamber provide the increase or decrease of the surface area to volume ratio up to several folds. Consequently, depending on the geometry and architecture of the microchip, these ratios should be carefully assessed with material properties and PCR reagents to figure out optimal passivation strategies.

There have been two major types of passivation methods for microchip PCR; static<sup>52</sup> and dynamic<sup>112</sup>. The static passivation is a method for inner surface coating of the microchip before starting PCR using PCR compatible reagents. For a example, chemical silanization has been successfully used to make the glass surface PCR-friendly before adding PCR reagents into the PCR chamber<sup>52</sup>. The dynamic passivation refers to a passivation method that add PCR compatible reagents directly into the PCR mixture, and passivation occurs when the PCR solution is injected into the PCR channel and chamber<sup>111</sup>. Therefore, inhibitory effects or biocompatibility of passivation reagents for PCR amplification should be precisely investigated before conducting microchip PCR. The globular shape of proteins such as BSA<sup>52,87,88</sup> and polymers such as PEG and PVP, and Tween 20 have been broadly utilized for dynamic

passivation in microchip PCR<sup>48,51,57,112</sup>. BSA is a common protein that prevents the adsorption of important proteins and enzymes into a vessel and a microchip<sup>113</sup>. However, very high surface area to volume ratio in the small PCR chamber of polymeric microdevices required different passivation reagents such as polymers instead of BSA<sup>51,57</sup>.

**Table 4:** Passivation approaches in microchip PCR.

Chip Materials	PCR Chamber Types	PCR chamber Sizes or Forms	Passivation Methods (Types)	References
Glass	Static	600 nL	Silanization (Sigmacoat) 0.1 µg/µL BSA (Static/Dynamic)	[12]
PDMS	Static	1.9 µL	Parylene coating (Static)	[103]
PMMA	Static	600 nL	0.4 % PEG <sub>10,000</sub> (Dynamic)	[57]
PI	Static	1.7 µL	0.75 % PEG <sub>8,000</sub> (Dynamic)	[51]
PC	Continuous flow	20 loops	0.1 µg/µL BSA (Dynamic)	[60]
PMMA	Continuous flow	20 – 40 loops	1 to 0.1 µg/µL BSA (Dynamic)	[58]
Glass	Continuous flow	20 – 40 loops	Silanization Triton X-100, Tween-20, polyvinyl pyrrolidone (PVP), BSA (Static/Dynamic)	[48]

## 1.8 Other Microfluidic PCR Approaches

### 1.8.1 Reverse Transcriptase-PCR in Microchips

In addition to the standard PCR method, reverse-transcriptase PCR (RT-PCR)<sup>58</sup>, real-time PCR (quantitative PCR; qPCR)<sup>114</sup>, and droplet PCR<sup>115</sup> have been performed in microfluidic devices (**Fig. 11**). For reverse-transcriptase PCR, one additional step such as a reverse transcriptase reaction, which converts RNA into cDNA as the PCR template, is added into the

standard PCR cycle. For the purpose of diagnostics of viral RNA<sup>56</sup> or determination of the level of gene expression from the amount of expressed mRNA<sup>116</sup>, reverse-transcriptase PCR should be required. Hagan *et al.* reported that when conducting reverse transcriptase-PCR in a microfluidic device, the time for a reverse-transcriptase reaction could decrease up to several minutes or seconds at optimal temperature<sup>117</sup>. Furthermore, in order to increase the number of reactions, nano or pico-liter sizes of droplets have been successfully adapted to achieve rapid RT-PCR in microfluidic devices<sup>58,118</sup> (**Fig. 11A**).

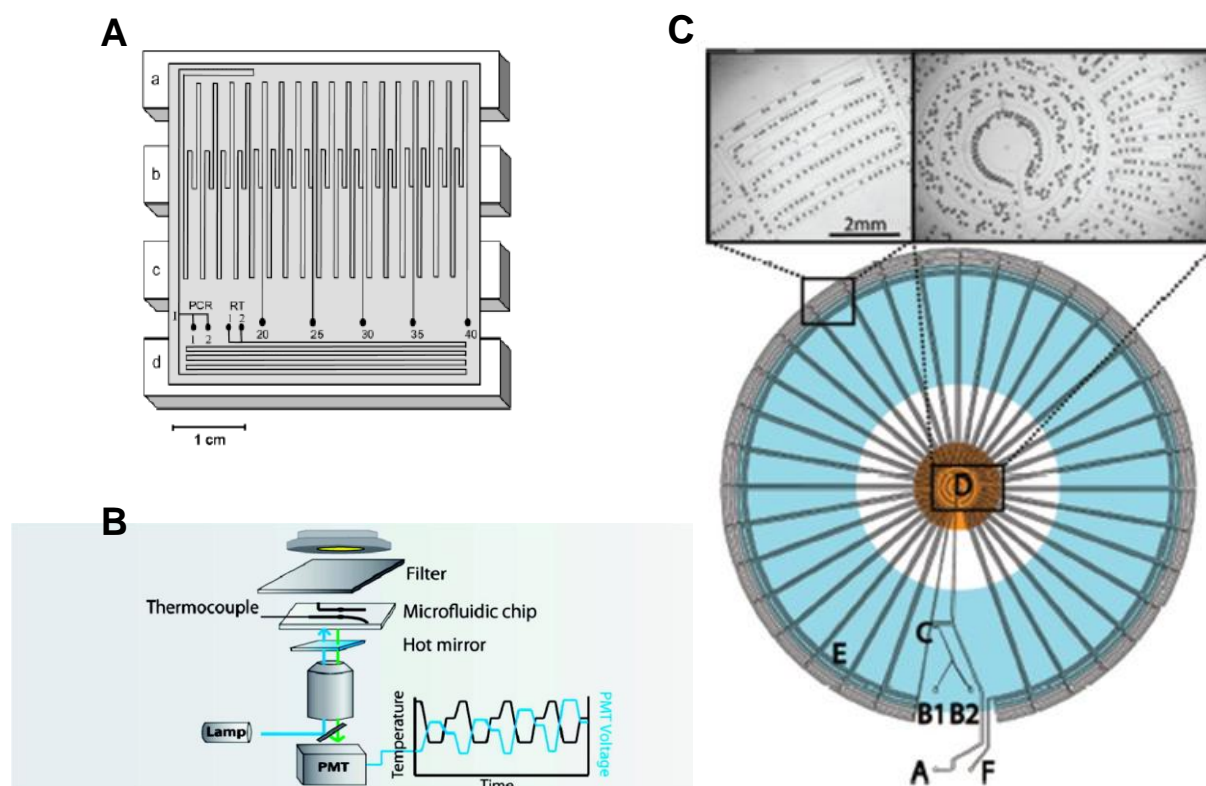


**Figure 11:** Different types of PCR approaches in microfluidic devices. (A) Reverse – transcriptase PCR (RT-PCR) in the continuous flow PCR (cf-PCR) format [118]. (B) Real-time IR-PCR in the glass microdevice [121]. (C) Droplet PCR on the circular shape of heater [63].

### 1.8.2 Real-time PCR (qPCR) in Microchips

Since the introduction of real-time PCR (qPCR) in 1996<sup>119,120</sup>, it has been an important research tool for studying molecular biology and molecular diagnostics. In a real-time process of PCR, PCR amplification is monitored via incorporation of DNA intercalating dyes<sup>121</sup> into double-stranded DNA that are used for the quantification of amounts of amplified double-stranded DNA, as reaction goes. Although the advance of qPCR instrumentation has improved the speed and sensitivity, a conventional qPCR thermal cycler with plastic PCR tubes still has several drawbacks such as non-specific amplifications (false positive signal), lengthy analysis time (compared to microchip PCR), and usage of large amounts of samples and costly reagents. Yu *et al.* recently reported that qPCR on the microfluidic device is able to reduce reaction times up to several times than standard qPCR achieved (**Fig. 11B**)<sup>121</sup>.

### 1.8.3 Droplet PCR in Microchips

Single cell analysis and droplet technology have been combined to conduct multiple and higher throughput reactions in the microfluidic device. Immiscible droplets in the oil phase can compartmentalize biological reactions in the aqueous solution that increases the number of reactions within the compact area. These droplets are rapidly generated and further analyzed within a small microfluidic device with the encapsulation of a single cell into aqueous solutions inside oils. As a result of these merits in droplet technologies, several groups have successfully reported droplet approaches for PCR applications<sup>63,64,115,122-127</sup> (**Fig. 11C**).

#### 1.8.4 Isothermal and Convection Driven PCR in Microchips

One of ways to eliminate thermal cycling in PCR amplification is isothermal DNA amplification and Vincent *et al.* first conducted Helicase-dependent DNA amplifications to detect genetic materials of pathogens from human samples using *E.coli* Urdu Helicase<sup>128</sup>. As the isothermal approach could simplify a PCR heating system by deleting thermal cycling, the miniaturization of the PCR instrument should be more realistic. Marutis *et al.* demonstrated the isothermal DNA amplification of a single DNA template inside droplets that showed the capability of a high-throughput genetic analysis without thermocycling<sup>129</sup>.

As another unique heating system, the static thermal gradient inside the confined PCR chamber area was used to generate buoyancy forces (temperature-induced density differences generate natural convective-induced flow) for convective flow of the PCR mixture. This flow made the PCR solution run through this thermal gradient to conduct convective driven PCR amplification. In this convectively driven PCR system, each temperature zone, cycling time, and residence time were controlled by reactor geometry and the built thermal gradient. Furthermore, a microfluidic pumping system was not required to achieve thermal cycling since convection could drive the PCR fluid flowing through microdevices<sup>130,131</sup>.

### 1.9 Fully Integrated Genetic Analyzer and Recent Trends in Microfluidic PCR

The ultimate goal of microfluidic PCR is to develop integrated microfluidic systems for high-performance genetic analysis. All functional steps for genetic analysis, consisting of cell lysis, DNA extraction, PCR amplification, and electrophoresis, have been partially and fully integrated in a single microfluidic device and these partial and full integrations of these

functional units have been successfully demonstrated by several groups<sup>12,13,132,133</sup>. **Figure 12A** described the characteristics of the fully integrated microfluidic genetic analyzer reported by another (Mathies) group. As another fully integrated genetic analyzer, the integration of DNA extraction, PCR amplifications, and electrophoresis were first reported in our (Dr. Landers) group (**Fig. 12B**).

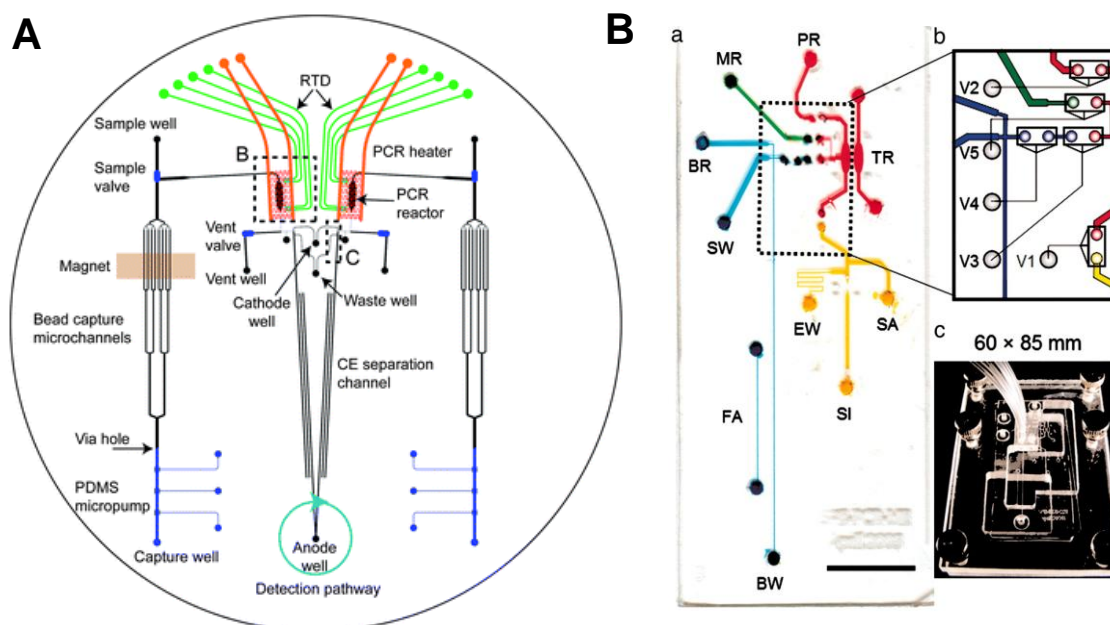


**Figure 12:** Fully integrated microdevices for genotyping in Mathies and Landers groups. (A) DNA template purification, PCR, post-PCR cleanup, inline injection and CE separation can be performed in one microfluidic device [74]. (B) Images of the MGA device [12]. (a) DNA extraction zone (yellow), PCR zone (red), injection zone (green), and separation zone (blue) are connected through a network of channels and vias. (b) Schematic of flow control region. Valves are shown as open rectangles. (c) Device loaded into the manifold.

The recent trends in a micro or nano-scale PCR focus on improving abilities to conduct thousands and millions of multiplex reactions and miniaturize the analytical instrument to achieve integration of all functional units into a single microfluidic device. As recent trends in microchip PCR, I would like to say achieving 1) portability for Point-of-Care (POC) diagnostics

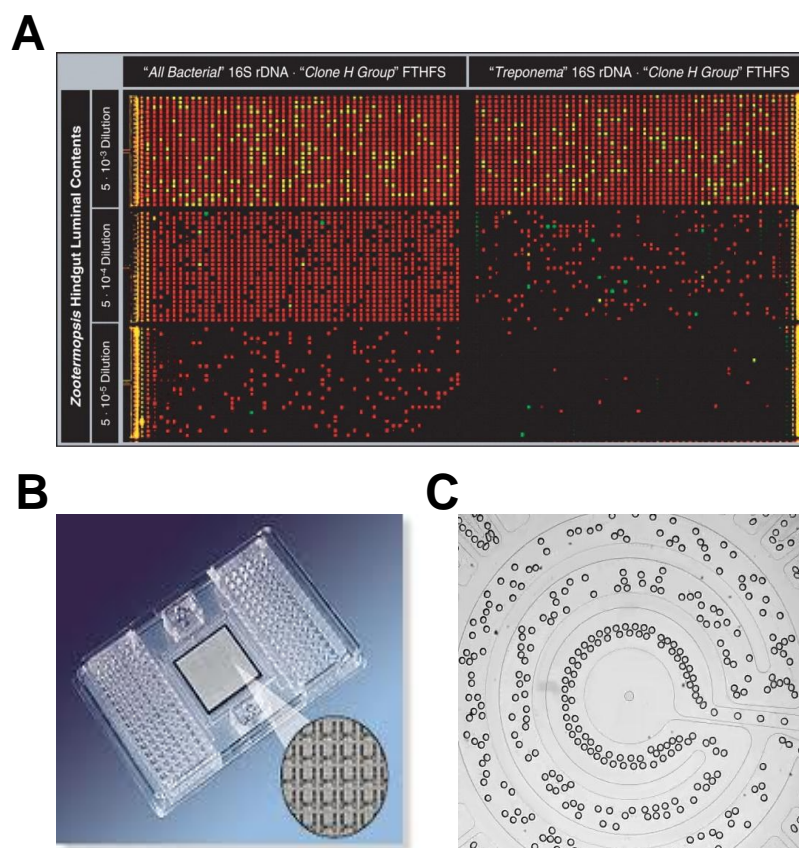


**Figure 13:** High-throughput genetic analyzers. (A) Multiplex microfluidic digital PCR on the microarray using a trapped single bacteria [143]. (B) Commercialized high-throughput qPCR on the microarray [from Fluidigm, Inc.]. (C) Droplet PCR providing multiple compartmentalizations to achieve a high-throughput manner [63].

in DNA analysis and 2) high-throughput genetic analysis using a droplet-based platform or digital PCR system. Accomplishment of portability and high-throughput manners in genetic analysis<sup>134,135</sup> should be our general goal to develop a real POC system that can realize “*a diagnostic test performed near the patient without needing clinical lab*”<sup>136</sup>. This microdevice is able to be brought outside the laboratory and conduct rapid genetic testing for clinical, forensic, and other applications<sup>38</sup>. Furthermore, in consideration of the diagnostic purpose of PCR applications, the existence of genetic materials (or verification of amplified PCR products) is only result for the detection of exogenous DNA and mutations. This simple concept of digital

PCR<sup>118,137</sup> is easily employed in microfluidic PCR without analysis of the size of DNA. Droplet microfluidics platforms have been miniaturized and integrated for the automation of digital PCR<sup>122,143</sup>. Using size-controllable aqueous droplets in immiscible phases, droplet PCR has been studied in many groups<sup>77,123,125-127,138-141</sup>, which have led to promising progress in high-throughput genetic analysis and single cell analysis. From a small volume of each droplet, DNA amplifications from a single copy DNA template and single cell have been reported for a single cell analysis<sup>142,143</sup>. In the future, these trends in microchip PCR will be accomplished inside the integrated microfluidic device (**Fig. 13**).

### 1.10 Concluding Remarks

Developing a microfluidic device for advanced genetic analysis, capable of portability and high-throughput manner, must be a pivotal goal in the  $\mu$ -TAS community. During my Ph.D. study, I have researched continuous flow infrared-mediated PCR (cfIR-PCR) and microwave-mediated thermal cycling systems to achieve these requirements in the microfluidic devices. The thesis in my Ph.D. studies has been directly driven toward the development of microfluidic devices for advanced genetic analysis. Especially two heating systems, infrared (**Chapter 2 and 4**) and microwave (**Chapter 3**), were demonstrated in details to achieve advanced microchip PCR. The initial development of continuous flow PCR on the IR-mediated system (cfIR-PCR) was included in the second chapter (**Chapter 2**) to show the feasibility of implementation of the cfIR-PCR system for multiple and high-throughput genetic analysis. In the third chapter (**Chapter 3**), as one of the alternative heating sources to miniaturize a PCR system, a microwave-assisted system was reported for developing a rapid and portable genetic analyzer. Using this microwave heating setup, several types of heating control methods such as *on/off*,

*open-loop*, and *proportional voltage controls* were tested on our setup. Additionally, two temperature measurement methods, a thermocouple (contact) and a pyrometer (non-contact), have been shown to amplify target DNA from our microwave setup. In the fourth chapter (**Chapter 4**), microfluidic PCR in the static PCR vessel was described with our previous IR-mediated system. In this study, the detection of the respiratory virus (Epstein Barr virus) using degenerate primers (CDC) had been conducted in Dr. Forest lab in Summer 2011 while performing Biotechnology Training Program (BTP) externship. This research allowed me to understand the general concept and method of single chambered microchip PCR on our IR-mediated heating system. Several microfabrication methods and several techniques for the construction of microchips had been learned in this group. In the fifth chapter (**Chapter 5**), I briefly wrote about the process in the development of a new drug susceptibility testing (DST) assay using standard PCR and hybridization induced bead aggregation. This detection method has potential for primary substitutes of gel electrophoresis and fluorescent detection method in genetic analysis.

## 1.11 References

- (1) Lander, E. S.; Linton, L. M.; Birren, B.; Nusbaum, C.; Zody, M. C.; Baldwin, J.; Devon, K.; Dewar, K.; Doyle, M.; FitzHugh, W.; Funke, R.; Gage, D.; Harris, K.; Heaford, A.; Howland, J.; Kann, L.; Lehoczký, J.; LeVine, R.; McEwan, P.; McKernan, K.; Meldrim, J.; Mesirov, J. P.; Miranda, C.; Morris, W.; Naylor, J.; Raymond, C.; Rosetti, M.; Santos, R.; Sheridan, A.; Sougnez, C.; Stange-Thomann, N.; Stojanovic, N.; Subramanian, A.; Wyman, D.; Rogers, J.; Sulston, J.; Ainscough, R.; Beck, S.; Bentley, D.; Burton, J.; Clee, C.; Carter, N.; Coulson, A.; Deadman, R.; Deloukas, P.; Dunham, A.; Dunham, I.; Durbin, R.; French, L.; Grafham, D.; Gregory, S.; Hubbard, T.; Humphray, S.; Hunt, A.; Jones, M.; Lloyd, C.; McMurray, A.; Matthews, L.; Mercer, S.; Milne, S.; Mullikin, J. C.; Mungall, A.; Plumb, R.; Ross, M.; Shownkeen, R.; Sims, S.; Waterston, R. H.; Wilson, R. K.; Hillier, L. W.; McPherson, J. D.; Marra, M. A.; Mardis, E. R.; Fulton, L. A.; Chinwalla, A. T.; Pepin, K. H.; Gish, W. R.; Chissole, S. L.; Wendl, M. C.; Delehaunty, K. D.; Miner, T. L.; Delehaunty, A.; Kramer, J. B.; Cook, L. L.; Fulton, R. S.; Johnson, D. L.; Minx, P. J.; Clifton, S. W.; Hawkins, T.; Branscomb, E.; Predki, P.; Richardson, P.;

- Wenning, S.; Slezak, T.; Doggett, N.; Cheng, J. F.; Olsen, A.; Lucas, S.; Elkin, C.; Uberbacher, E.; Frazier, M. Initial sequencing and analysis of the human genome. *Nature* **2001**, *409*, 860-921.
- (2) Venter, J. C.; Adams, M. D.; Myers, E. W.; Li, P. W.; Mural, R. J.; Sutton, G. G.; Smith, H. O.; Yandell, M.; Evans, C. A.; Holt, R. A.; Gocayne, J. D.; Amanatides, P.; Ballew, R. M.; Huson, D. H.; Wortman, J. R.; Zhang, Q.; Kodira, C. D.; Zheng, X. H.; Chen, L.; Skupski, M.; Subramanian, G.; Thomas, P. D.; Zhang, J.; Gabor Miklos, G. L.; Nelson, C.; Broder, S.; Clark, A. G.; Nadeau, J.; McKusick, V. A.; Zinder, N.; Levine, A. J.; Roberts, R. J.; Simon, M.; Slayman, C.; Hunkapiller, M.; Bolanos, R.; Delcher, A.; Dew, I.; Fasulo, D.; Flanigan, M.; Florea, L.; Halpern, A.; Hannenhalli, S.; Kravitz, S.; Levy, S.; Mobarry, C.; Reinert, K.; Remington, K.; Abu-Threideh, J.; Beasley, E.; Biddick, K.; Bonazzi, V.; Brandon, R.; Cargill, M.; Chandramouliswaran, I.; Charlab, R.; Chaturvedi, K.; Deng, Z.; Di Francesco, V.; Dunn, P.; Eilbeck, K.; Evangelista, C.; Gabrielian, A. E.; Gan, W.; Ge, W.; Gong, F.; Gu, Z.; Guan, P.; Heiman, T. J.; Higgins, M. E.; Ji, R. R.; Ke, Z.; Ketchum, K. A.; Lai, Z.; Lei, Y.; Li, Z.; Li, J.; Liang, Y.; Lin, X.; Lu, F.; Merkulov, G. V.; Milshina, N.; Moore, H. M.; Naik, A. K.; Narayan, V. A.; Neelam, B.; Nusskern, D.; Rusch, D. B.; Salzberg, S.; Shao, W.; Shue, B.; Sun, J.; Wang, Z.; Wang, A.; Wang, X.; Wang, J.; Wei, M.; Wides, R.; Xiao, C.; Yan, C. The sequence of the human genome. *Science* **2001**, *291*, 1304-51.
  - (3) Sachidanandam, R.; Weissman, D.; Schmidt, S. C.; Kakol, J. M.; Stein, L. D.; Marth, G.; Sherry, S.; Mullikin, J. C.; Mortimore, B. J.; Willey, D. L.; Hunt, S. E.; Cole, C. G.; Coggill, P. C.; Rice, C. M.; Ning, Z.; Rogers, J.; Bentley, D. R.; Kwok, P. Y.; Mardis, E. R.; Yeh, R. T.; Schultz, B.; Cook, L.; Davenport, R.; Dante, M.; Fulton, L.; Hillier, L.; Waterston, R. H.; McPherson, J. D.; Gilman, B.; Schaffner, S.; Van Etten, W. J.; Reich, D.; Higgins, J.; Daly, M. J.; Blumenstiel, B.; Baldwin, J.; Stange-Thomann, N.; Zody, M. C.; Linton, L.; Lander, E. S.; Altshuler, D. A map of human genome sequence variation containing 1.42 million single nucleotide polymorphisms. *Nature* **2001**, *409*, 928-33.
  - (4) Whibley, C.; Pharoah, P. D.; Hollstein, M. p53 polymorphisms: cancer implications. *Nat Rev Cancer* **2009**, *9*, 95-107.
  - (5) Sladek, R.; Rocheleau, G.; Rung, J.; Dina, C.; Shen, L.; Serre, D.; Boutin, P.; Vincent, D.; Belisle, A.; Hadjadj, S.; Balkau, B.; Heude, B.; Charpentier, G.; Hudson, T. J.; Montpetit, A.; Pshezhetsky, A. V.; Prentki, M.; Posner, B. I.; Balding, D. J.; Meyre, D.; Polychronakos, C.; Froguel, P. A genome-wide association study identifies novel risk loci for type 2 diabetes. *Nature* **2007**, *445*, 881-5.
  - (6) Breitner, J. C. APOE genotyping and Alzheimer's disease. *Lancet* **1996**, *347*, 1184-5.
  - (7) Check, E. Human genome: patchwork people. *Nature* **2005**, *437*, 1084-6.
  - (8) Evans, W. E.; Johnson, J. A. Pharmacogenomics: the inherited basis for interindividual differences in drug response. *Annu Rev Genomics Hum Genet* **2001**, *2*, 9-39.
  - (9) Yang, S.; Rothman, R. E. PCR-based diagnostics for infectious diseases: uses, limitations, and future applications in acute-care settings. *Lancet Infect Dis* **2004**, *4*, 337-48.
  - (10) Belgrader, P.; Benett, W.; Hadley, D.; Long, G.; Mariella, R., Jr.; Milanovich, F.; Nasarabadi, S.; Nelson, W.; Richards, J.; Stratton, P. Rapid pathogen detection using a microchip PCR array instrument. *Clin Chem* **1998**, *44*, 2191-4.
  - (11) Horsman, K. M.; Bienvenue, J. M.; Blasier, K. R.; Landers, J. P. Forensic DNA analysis on microfluidic devices: a review. *J Forensic Sci* **2007**, *52*, 784-99.

- (12) Easley, C. J.; Karlinsey, J. M.; Bienvenue, J. M.; Legendre, L. A.; Roper, M. G.; Feldman, S. H.; Hughes, M. A.; Hewlett, E. L.; Merkel, T. J.; Ferrance, J. P.; Landers, J. P. A fully integrated microfluidic genetic analysis system with sample-in-answer-out capability. *Proceedings of the National Academy of Sciences of the United States of America* **2006**, *103*, 19272-19277.
- (13) Burns, M. A.; Mastrangelo, C. H.; Sammarco, T. S.; Man, F. P.; Webster, J. R.; Johnsons, B. N.; Foerster, B.; Jones, D.; Fields, Y.; Kaiser, A. R.; Burke, D. T. Microfabricated structures for integrated DNA analysis. *Proc Natl Acad Sci U S A* **1996**, *93*, 5556-61.
- (14) Liu, P.; Mathies, R. A. Integrated microfluidic systems for high-performance genetic analysis. *Trends Biotechnol* **2009**, *27*, 572-81.
- (15) Njoroge, S. K.; Chen, H. W.; Witek, M. A.; Soper, S. A. Integrated microfluidic systems for DNA analysis. *Top Curr Chem*, *304*, 203-60.
- (16) Manz, A.; Graber, N.; Widmer, H. M. Miniaturized Total Chemical-Analysis Systems - a Novel Concept for Chemical Sensing. *Sensors and Actuators B-Chemical* **1990**, *1*, 244-248.
- (17) Reyes, D. R.; Iossifidis, D.; Auroux, P. A.; Manz, A. Micro total analysis systems. 1. Introduction, theory, and technology. *Analytical Chemistry* **2002**, *74*, 2623-2636.
- (18) Auroux, P. A.; Iossifidis, D.; Reyes, D. R.; Manz, A. Micro total analysis systems. 2. Analytical standard operations and applications. *Analytical Chemistry* **2002**, *74*, 2637-2652.
- (19) Whitesides, G. M. The origins and the future of microfluidics. *Nature* **2006**, *442*, 368-373.
- (20) Manz, A.; Harrison, D. J.; Verpoorte, E. M. J.; Fetting, J. C.; Paulus, A.; Ludi, H.; Widmer, H. M. Planar Chips Technology for Miniaturization and Integration of Separation Techniques into Monitoring Systems - Capillary Electrophoresis on a Chip. *Journal of Chromatography* **1992**, *593*, 253-258.
- (21) Joensson, H. N.; Andersson-Svahn, H. Droplet microfluidics--a tool for protein engineering and analysis. *Lab Chip* **2001**, *11*, 4144-7.
- (22) Andersson, H.; van den Berg, A. Microfabrication and microfluidics for tissue engineering: state of the art and future opportunities. *Lab Chip* **2004**, *4*, 98-103.
- (23) Breslauer, D. N.; Lee, P. J.; Lee, L. P. Microfluidics-based systems biology. *Mol Biosyst* **2006**, *2*, 97-112.
- (24) Wang, C. J.; Levchenko, A. Microfluidics technology for systems biology research. *Methods Mol Biol* **2009**, *500*, 203-19.
- (25) Wikswo, J. P.; Prokop, A.; Baudenbacher, F.; Cliffl, D.; Csukas, B.; Velkovsky, M. Engineering challenges of BioNEMS: the integration of microfluidics, micro- and nanodevices, models and external control for systems biology. *IEE Proc Nanobiotechnol* **2006**, *153*, 81-101.
- (26) Dittrich, P. S.; Manz, A. Lab-on-a-chip: microfluidics in drug discovery. *Nat Rev Drug Discov* **2006**, *5*, 210-8.
- (27) Goettsche, T.; Ernst, H.; Messner, S.; Sandmaier, H. Microfluidics: an opportunity for trend-setting drug delivery. *Med Device Technol* **2004**, *15*, 12-5.
- (28) Squires, T. M.; Quake, S. R. Microfluidics: Fluid physics at the nanoliter scale. *Reviews of Modern Physics* **2005**, *77*, 977-1026.
- (29) Beebe, D. J.; Mensing, G. A.; Walker, G. M. Physics and applications of microfluidics in biology. *Annual Review of Biomedical Engineering* **2002**, *4*, 261-286.

- (30) Fiorini, G. S.; Chiu, D. T. Disposable microfluidic devices: fabrication, function, and application. *Biotechniques* **2005**, *38*, 429-46.
- (31) Hessel, V.; Lowe, H.; Schonfeld, F. Micromixers - a review on passive and active mixing principles. *Chemical Engineering Science* **2005**, *60*, 2479-2501.
- (32) Stroock, A. D.; Dertinger, S. K.; Ajdari, A.; Mezic, I.; Stone, H. A.; Whitesides, G. M. Chaotic mixer for microchannels. *Science* **2002**, *295*, 647-51.
- (33) Mullis, K.; Faloona, F.; Scharf, S.; Saiki, R.; Horn, G.; Erlich, H. Specific Enzymatic Amplification of DNA Invitro - the Polymerase Chain-Reaction. *Cold Spring Harbor Symposia on Quantitative Biology* **1986**, *51*, 263-273.
- (34) Saiki, R. K.; Gelfand, D. H.; Stoffel, S.; Scharf, S. J.; Higuchi, R.; Horn, G. T.; Mullis, K. B.; Erlich, H. A. Primer-directed enzymatic amplification of DNA with a thermostable DNA polymerase. *Science* **1988**, *239*, 487-91.
- (35) Wittwer, C. T.; Fillmore, G. C.; Garling, D. J. Minimizing the time required for DNA amplification by efficient heat transfer to small samples. *Anal Biochem* **1990**, *186*, 328-31.
- (36) Neuzil, P.; Zhang, C.; Pipper, J.; Oh, S.; Zhuo, L. Ultra fast miniaturized real-time PCR: 40 cycles in less than six minutes. *Nucleic Acids Res* **2006**, *34*, e77.
- (37) Wheeler, E. K.; Hara, C. A.; Frank, J.; Deotte, J.; Hall, S. B.; Benett, W.; Spadaccini, C.; Beer, N. R. Under-three minute PCR: Probing the limits of fast amplification. *Analyst* **2011**, *136*, 3707-3712.
- (38) Park, S.; Zhang, Y.; Lin, S.; Wang, T. H.; Yang, S. Advances in microfluidic PCR for point-of-care infectious disease diagnostics. *Biotechnol Adv* **2012**, *29*, 830-9.
- (39) Zhang, C.; Xu, J.; Ma, W.; Zheng, W. PCR microfluidic devices for DNA amplification. *Biotechnol Adv* **2006**, *24*, 243-84.
- (40) Roper, M. G.; Easley, C. J.; Landers, J. P. Advances in polymerase chain reaction on microfluidic chips *Anal Chem* **2005**, *77*, 3887-93.
- (41) Zhang, C.; Xing, D. Miniaturized PCR chips for nucleic acid amplification and analysis: latest advances and future trends. *Nucleic Acids Res* **2007**, *35*, 4223-37.
- (42) Terry, S. C.; Jerman, J. H.; Angell, J. B. Gas-Chromatographic Air Analyzer Fabricated on a Silicon-Wafer. *Ieee Transactions on Electron Devices* **1979**, *26*, 1880-1886.
- (43) Bassous, E.; Taub, H. H.; Kuhn, L. Ink Jet Printing Nozzle Arrays Etched in Silicon. *Applied Physics Letters* **1977**, *31*, 135-137.
- (44) Northrup, M. A.; Ching, M. T.; White, R. M.; Watson, R. T. DNA amplification in a microfabricated reaction chamber. In *In transducer 93', Seventh International conference on solid state Sens and Actuators* Yokohama, Japan, 1993, p 924-926.
- (45) Northrup, M. A.; Benett, B.; Hadley, D.; Landre, P.; Lehew, S.; Richards, J.; Stratton, P. A miniature analytical instrument for nucleic acids based on micromachined silicon reaction chambers. *Analytical Chemistry* **1998**, *70*, 918-922.
- (46) Wilding, P.; Shoffner, M. A.; Kricka, L. J. Pcr in a Silicon Microstructure. *Clinical Chemistry* **1994**, *40*, 1815-1818.
- (47) Woolley, A. T.; Northrup, M. A.; Mathies, R. A. Microfabricated integrated DNA analysis systems. *Abstracts of Papers of the American Chemical Society* **1996**, *212*, 155-PHYS.
- (48) Kopp, M. U.; de Mello, A. J.; Manz, A. Chemical amplification: Continuous-flow PCR on a chip. *Science* **1998**, *280*, 1046-1048.

- (49) Oda, R. P.; Strausbauch, M. A.; Huhmer, A. F.; Borson, N.; Jurens, S. R.; Craighead, J.; Wettstein, P. J.; Eckloff, B.; Kline, B.; Landers, J. P. Infrared-mediated thermocycling for ultrafast polymerase chain reaction amplification of DNA. *Anal Chem* **1998**, *70*, 4361-8.
- (50) Huhmer, A. F. R.; Landers, J. P. Noncontact infrared-mediated thermocycling for effective polymerase chain reaction amplification of DNA in nanoliter volumes. *Analytical Chemistry* **2000**, *72*, 5507-5512.
- (51) Giordano, B. C.; Ferrance, J.; Swedberg, S.; Huhmer, A. F. R.; Landers, J. P. Polymerase chain reaction in polymeric microchips: DNA amplification in less than 240 seconds. *Analytical Biochemistry* **2001**, *291*, 124-132.
- (52) Giordano, B. C.; Copeland, E. R.; Landers, J. P. Towards dynamic coating of glass microchip chambers for amplifying DNA via the polymerase chain reaction. *Electrophoresis* **2001**, *22*, 334-340.
- (53) Roper, M. G.; Easley, C. J.; Legendre, L. A.; Humphrey, J. A.; Landers, J. P. Infrared temperature control system for a completely noncontact polymerase chain reaction in microfluidic chips. *Anal Chem* **2007**, *79*, 1294-300.
- (54) Easley, C. J.; Humphrey, J. A. C.; Landers, J. P. Thermal isolation of microchip reaction chambers for rapid non-contact DNA amplification. *Journal of Micromechanics and Microengineering* **2007**, *17*, 1758-1766.
- (55) Lounsbury, J.A., Miranian, D.C., Landers, J.P. A multi-chamber microdevice for simultaneous amplification up to seven individual samples using infrared-mediate PCR. In *Proceedings of the 15th international conference on miniaturized systems for chemistry and life sciences*, Seattle, WA, USA, 2011, p750-752.
- (56) Elnifro, E. M.; Ashshi, A. M.; Cooper, R. J.; Klapper, P. E. Multiplex PCR: Optimization and application in diagnostic virology. *Clinical Microbiology Reviews* **2000**, *13*, 559.
- (57) Lounsbury, J. A.; Poe, B. L.; Do, M.; Landers, J. P. Laser-ablated poly(methyl methacrylate) microdevices for sub-microliter DNA amplification suitable for micro-total analysis systems. *Journal of Micromechanics and Microengineering* **2012**, *22*.
- (58) Obeid, P. J.; Christopoulos, T. K.; Crabtree, H. J.; Backhouse, C. J. Microfabricated device for DNA and RNA amplification by continuous-flow polymerase chain reaction and reverse transcription-polymerase chain reaction with cycle number selection. *Anal Chem* **2003**, *75*, 288-95.
- (59) Li, S.; Fozdar, D. Y.; Ali, M. F.; Li, H.; Shao, D.; Vykoukal, D. M.; Vykoukal, J.; Floriano, P. N.; Olsen, M.; McDevitt, J. T.; Gascoyne, P. R.; Chen, S. A Continuous-Flow Polymerase Chain Reaction Microchip With Regional Velocity Control. *J Microelectromech Syst* **2006**, *15*, 223-236.
- (60) Hashimoto, M.; Chen, P. C.; Mitchell, M. W.; Nikitopoulos, D. E.; Soper, S. A.; Murphy, M. C. Rapid PCR in a continuous flow device. *Lab Chip* **2004**, *4*, 638-45.
- (61) Crews, N.; Wittwer, C.; Gale, B. Continuous-flow thermal gradient PCR. *Biomed Microdevices* **2008**, *10*, 187-95.
- (62) Obeid, P. J.; Christopoulos, T. K. Continuous-flow DNA and RNA amplification chip combined with laser-induced fluorescence detection. *Analytica Chimica Acta* **2003**, *494*, 1-9.
- (63) Schaerli, Y.; Wootton, R. C.; Robinson, T.; Stein, V.; Dunsby, C.; Neil, M. A.; French, P. M.; Demello, A. J.; Abell, C.; Hollfelder, F. Continuous-flow polymerase chain reaction of single-copy DNA in microfluidic microdroplets. *Anal Chem* **2009**, *81*, 302-6.

- (64) Kiss, M. M.; Ortoleva-Donnelly, L.; Beer, N. R.; Warner, J.; Bailey, C. G.; Colston, B. W.; Rothberg, J. M.; Link, D. R.; Leamon, J. H. High-Throughput Quantitative Polymerase Chain Reaction in Picoliter Droplets. *Analytical Chemistry* **2008**, *80*, 8975-8981.
- (65) Wu, W.; Lee, N. Y. Three-dimensional on-chip continuous-flow polymerase chain reaction employing a single heater. *Anal Bioanal Chem* **2011**, *400*, 2053-60.
- (66) Sun, Y.; Satyanarayan, M. V. D.; Nguyen, N. T.; Kwok, Y. C. Continuous flow polymerase chain reaction using a hybrid PMMA-PC microchip with improved heat tolerance. *Sensors and Actuators B-Chemical* **2008**, *130*, 836-841.
- (67) Daniel, J. H.; Iqbal, S.; Millington, R. B.; Moore, D. F.; Lowe, C. R.; Leslie, D. L.; Lee, M. A.; Pearce, M. J. Silicon microchambers for DNA amplification. *Sensors and Actuators a-Physical* **1998**, *71*, 81-88.
- (68) El-Ali, J.; Perch-Nielsen, I. R.; Poulsen, C. R.; Bang, D. D.; Telleman, P.; Wolff, A. Simulation and experimental validation of a SU-8 based PCR thermocycler chip with integrated heaters and temperature sensor. *Sensors and Actuators a-Physical* **2004**, *110*, 3-10.
- (69) Liao, C. S.; Lee, G. B.; Wu, J. J.; Chang, C. C.; Hsieh, T. M.; Huang, F. C.; Luo, C. H. Micromachined polymerase chain reaction system for multiple DNA amplification of upper respiratory tract infectious diseases. *Biosensors & Bioelectronics* **2005**, *20*, 1341-1348.
- (70) Lee, D. S.; Park, S. H.; Yang, H. S.; Chung, K. H.; Yoon, T. H.; Kim, S. J.; Kim, K.; Kim, Y. T. Bulk-micromachined submicroliter-volume PCR chip with very rapid thermal response and low power consumption. *Lab on a Chip* **2004**, *4*, 401-407.
- (71) Lee, D. S.; Wu, M. H.; Ramesh, U.; Lin, C. W.; Lee, T. M.; Chen, P. H. A novel real-time PCR machine with a miniature spectrometer for fluorescence sensing in a micro liter volume glass capillary. *Sensors and Actuators B-Chemical* **2004**, *100*, 401-410.
- (72) Yoon, D. S.; Lee, Y. S.; Lee, Y.; Cho, H. J.; Sung, S. W.; Oh, K. W.; Cha, J.; Lim, G. Precise temperature control and rapid thermal cycling in a micromachined DNA polymerase chain reaction chip. *Journal of Micromechanics and Microengineering* **2002**, *12*, 813-823.
- (73) Rodriguez, I.; Lesaichere, M.; Tie, Y.; Zou, Q. B.; Yu, C.; Singh, J.; Meng, L. T.; Uppili, S.; Li, S. F. Y.; Gopalakrishnakone, P.; Selvanayagam, Z. E. Practical integration of polymerase chain reaction amplification and electrophoretic analysis in microfluidic devices for genetic analysis. *Electrophoresis* **2003**, *24*, 172-178.
- (74) Lagally, E. T.; Emrich, C. A.; Mathies, R. A. Fully integrated PCR-capillary electrophoresis microsystem for DNA analysis. *Lab on a Chip* **2001**, *1*, 102-107.
- (75) Lounsbury, J. A.; Karlsson, A.; Miranian, D. C.; Cronk, S. M.; Nelson, D. A.; Li, J. Y.; Haverstick, D. M.; Kinnon, P.; Saul, D. J.; Landers, J. P. From sample to PCR product in under 45 minutes: a polymeric integrated microdevice for clinical and forensic DNA analysis. *Lab on a Chip* **2013**, *13*, 1384-1393.
- (76) Pak, N.; Saunders, D. C.; Phaneuf, C. R.; Forest, C. R. Plug-and-play, infrared, laser-mediated PCR in a microfluidic chip. *Biomed Microdevices*, *14*, 427-33.
- (77) Kim, H.; Vishniakou, S.; Faris, G. W. Petri dish PCR: laser-heated reactions in nanoliter droplet arrays. *Lab Chip* **2009**, *9*, 1230-5.
- (78) Fermer, C.; Nilsson, P.; Larhed, M. Microwave-assisted high-speed PCR. *Eur J Pharm Sci* **2003**, *18*, 129-32.

- (79) Issadore, D.; Humphry, K. J.; Brown, K. A.; Sandberg, L.; Weitz, D. A.; Westervelt, R. M. Microwave dielectric heating of drops in microfluidic devices. *Lab Chip* **2009**, *9*, 1701-6.
- (80) Orrling, K.; Nilsson, P.; Gullberg, M.; Larhed, M. An efficient method to perform milliliter-scale PCR utilizing highly controlled microwave thermocycling. *Chem Commun (Camb)* **2004**, 790-1.
- (81) Shaw, K. J.; Docker, P. T.; Yelland, J. V.; Dyer, C. E.; Greenman, J.; Greenway, G. M.; Haswell, S. J. Rapid PCR amplification using a microfluidic device with integrated microwave heating and air impingement cooling. *Lab Chip* **2010**, *10*, 1725-8.
- (82) Shah, J. J.; Sundaresan, S. G.; Geist, J.; Reyes, D. R.; Booth, J. C.; Rao, M. V.; Gaitan, M. Microwave dielectric heating of fluids in an integrated microfluidic device. *Journal of Micromechanics and Microengineering* **2007**, *17*, 2224-2230.
- (83) Childs, P. R. N.; Greenwood, J. R.; Long, C. A. Review of temperature measurement. *Review of Scientific Instruments* **2000**, *71*, 2959-2978.
- (84) Yi, P.; Kayani, A. A.; Chrimes, A. F.; Ghorbani, K.; Nahavandi, S.; Kalantar-zadeh, K.; Khoshmanesh, K. Thermal analysis of nanofluids in microfluidics using an infrared camera. *Lab on a Chip* **2012**, *12*, 2520-2525.
- (85) Krishnan, M.; Burke, D. T.; Burns, M. A. Polymerase chain reaction in high surface-to-volume ratio SiO<sub>2</sub> microstructures. *Analytical Chemistry* **2004**, *76*, 6588-6593.
- (86) Schneegass, I.; Brautigam, R.; Kohler, J. M. Miniaturized flow-through PCR with different template types in a silicon chip thermocycler. *Lab on a Chip* **2001**, *1*, 42-49.
- (87) Khandurina, J.; McKnight, T. E.; Jacobson, S. C.; Waters, L. C.; Foote, R. S.; Ramsey, J. M. Integrated system for rapid PCR-based DNA analysis in microfluidic devices. *Analytical Chemistry* **2000**, *72*, 2995-3000.
- (88) Lagally, E. T.; Medintz, I.; Mathies, R. A. Single-molecule DNA amplification and analysis in an integrated microfluidic device. *Analytical Chemistry* **2001**, *73*, 565-570.
- (89) Lagally, E. T.; Simpson, P. C.; Mathies, R. A. Single-molecule DNA amplification and analysis in an integrated microfluidic device. *Sensors and Actuators B-Chemical* **2000**, *63*, 138-146.
- (90) Waters, L. C.; Jacobson, S. C.; Kroutchinina, N.; Khandurina, J.; Foote, R. S.; Ramsey, J. M. Microchip device for cell lysis, multiplex PCR amplification, and electrophoretic sizing. *Analytical Chemistry* **1998**, *70*, 158-162.
- (91) Becker, H.; Gartner, C. Polymer microfabrication technologies for microfluidic systems. *Analytical and Bioanalytical Chemistry* **2008**, *390*, 89-111.
- (92) Becker, H.; Locascio, L. E. Polymer microfluidic devices. *Talanta* **2002**, *56*, 267-287.
- (93) Malek, C. G. K. Laser processing for bio-microfluidics applications (part I). *Analytical and Bioanalytical Chemistry* **2006**, *385*, 1351-1361.
- (94) Malek, C. G. K. Laser processing for bio-microfluidics applications (part II). *Analytical and Bioanalytical Chemistry* **2006**, *385*, 1362-1369.
- (95) Rotting, O.; Ropke, W.; Becker, H.; Gartner, C. Polymer microfabrication technologies. *Microsystem Technologies* **2002**, *8*, 32-36.
- (96) Sun, Y.; Kwok, Y. C. Polymeric microfluidic system for DNA analysis. *Anal Chim Acta* **2006**, *556*, 80-96.
- (97) Liu, R. H.; Yang, J.; Lenigk, R.; Bonanno, J.; Grodzinski, P. Self-contained, fully integrated biochip for sample preparation, polymerase chain reaction amplification, and DNA microarray detection. *Anal Chem* **2004**, *76*, 1824-31.

- (98) Yao, L.; Liu, B.; Chen, T.; Liu, S.; Zuo, T. Micro flow-through PCR in a PMMA chip fabricated by KrF excimer laser. *Biomed Microdevices* **2005**, *7*, 253-7.
- (99) Zou, Q. B.; Miao, Y. B.; Chen, Y.; Sridhar, U.; Chong, C. S.; Chai, T. C.; Tie, Y.; Teh, C. H. L.; Lim, T. M.; Heng, C. Micro-assembled multi-chamber thermal cyclers for low-cost reaction chip thermal multiplexing. *Sensors and Actuators a-Physical* **2002**, *102*, 114-121.
- (100) Tsai, N. C.; Sue, C. Y. SU-8 based continuous-flow RT-PCR bio-chips under high-precision temperature control. *Biosens Bioelectron* **2006**, *22*, 313-7.
- (101) Koh, C. G.; Tan, W.; Zhao, M. Q.; Ricco, A. J.; Fan, Z. H. Integrating polymerase chain reaction, valving, and electrophoresis in a plastic device for bacterial detection. *Anal Chem* **2003**, *75*, 4591-8.
- (102) Quake, S. R.; Scherer, A. From micro- to nanofabrication with soft materials. *Science* **2000**, *290*, 1536-40.
- (103) Shin, Y. S.; Cho, K.; Lim, S. H.; Chung, S.; Park, S. J.; Chung, C.; Han, D. C.; Chang, J. K. PDMS-based micro PCR chip with parylene coating. *Journal of Micromechanics and Microengineering* **2003**, *13*, 768-774.
- (104) Kameoka, J.; Craighead, H. G.; Zhang, H. W.; Henion, J. A polymeric microfluidic chip for CE/MS determination of small molecules. *Analytical Chemistry* **2001**, *73*, 1935-1941.
- (105) Muck, A.; Wang, J.; Jacobs, M.; Chen, G.; Chatrathi, M. P.; V, J.; Vyborny, Z.; Spillman, S. D.; Sridharan, G.; Schoning, M. J. Fabrication of poly(methyl methacrylate) microfluidic chips by atmospheric molding. *Analytical Chemistry* **2004**, *76*, 2290-2297.
- (106) Weibel, D. B.; Whitesides, G. M. Applications of microfluidics in chemical biology. *Current Opinion in Chemical Biology* **2006**, *10*, 584-591.
- (107) Sun, Y.; Kwok, Y. C.; Nguyen, N. T. A circular ferrofluid driven microchip for rapid polymerase chain reaction. *Lab on a Chip* **2007**, *7*, 1012-1017.
- (108) Roberts, M. A.; Rossier, J. S.; Bercier, P.; Girault, H. UV laser machined polymer substrates for the development of microdiagnostic systems. *Analytical Chemistry* **1997**, *69*, 2035-2042.
- (109) Shoffner, M. A.; Cheng, J.; Hvichia, G. E.; Kricka, L. J.; Wilding, P. Chip PCR .1. Surface passivation of microfabricated silicon-glass chips for PCR. *Nucleic Acids Research* **1996**, *24*, 375-379.
- (110) Cheng, J.; Shoffner, M. A.; Hvichia, G. E.; Kricka, L. J.; Wilding, P. Chip PCR. II. Investigation of different PCR amplification systems in microfabricated silicon-glass chips. *Nucleic Acids Res* **1996**, *24*, 380-5.
- (111) Panaro, N. J.; Lou, X. J.; Fortina, P.; Kricka, L. J.; Wilding, P. Surface effects on PCR reactions in multichip microfluidic platforms. *Biomed Microdevices* **2004**, *6*, 75-80.
- (112) Lou, X. J.; Panaro, N. J.; Wilding, P.; Fortina, P.; Kricka, L. J. Increased amplification efficiency of microchip-based PCR by dynamic surface passivation. *Biotechniques* **2004**, *36*, 248.
- (113) Sweryda-Krawiec, B.; Devaraj, H.; Jacob, G.; Hickman, J. J. A new interpretation of serum albumin surface passivation. *Langmuir* **2004**, *20*, 2054-6.
- (114) Neuzil, P.; Zhang, C. Y.; Pipper, J.; Oh, S.; Zhuo, L. Ultra fast miniaturized real-time PCR: 40 cycles in less than six minutes. *Nucleic Acids Research* **2006**, *34*.
- (115) Beer, N. R.; Wheeler, E. K.; Lee-Houghton, L.; Watkins, N.; Nasarabadi, S.; Hebert, N.; Leung, P.; Arnold, D. W.; Bailey, C. G.; Colston, B. W. On-chip single-copy real-time reverse-transcription PCR in isolated picoliter droplets. *Analytical Chemistry* **2008**, *80*, 1854-1858.

- (116) Warren, L.; Bryder, D.; Weissman, I. L.; Quake, S. R. Transcription factor profiling in individual hematopoietic progenitors by digital RT-PCR. *Proceedings of the National Academy of Sciences of the United States of America* **2006**, *103*, 17807-17812.
- (117) Hagan, K. A.; Reedy, C. R.; Uchimoto, M. L.; Basu, D.; Engel, D. A.; Landers, J. P. An integrated, valveless system for microfluidic purification and reverse transcription-PCR amplification of RNA for detection of infectious agents. *Lab Chip* **2010**, *11*, 957-61.
- (118) Heyries, K. A.; Tropini, C.; Vaninsberghe, M.; Doolin, C.; Petriv, O. I.; Singhal, A.; Leung, K.; Hughesman, C. B.; Hansen, C. L. Megapixel digital PCR. *Nat Methods* **2011**, *8*, 649-51.
- (119) Gibson, U. E. M.; Heid, C. A.; Williams, P. M. A novel method for real time quantitative RT PCR. *Genome Research* **1996**, *6*, 995-1001.
- (120) Heid, C. A.; Stevens, J.; Livak, K. J.; Williams, P. M. Real time quantitative PCR. *Genome Research* **1996**, *6*, 986-994.
- (121) Yu, Y. J.; Li, B. W.; Baker, C. A.; Zhang, X. Y.; Roper, M. G. Quantitative Polymerase Chain Reaction Using Infrared Heating on a Microfluidic Chip. *Analytical Chemistry* **2012**, *84*, 2825-2829.
- (122) Hindson, B. J.; Ness, K. D.; Masquelier, D. A.; Belgrader, P.; Heredia, N. J.; Makarewicz, A. J.; Bright, I. J.; Lucero, M. Y.; Hiddessen, A. L.; Legler, T. C.; Kitano, T. K.; Hodel, M. R.; Petersen, J. F.; Wyatt, P. W.; Steenblock, E. R.; Shah, P. H.; Bousse, L. J.; Troup, C. B.; Mellen, J. C.; Wittmann, D. K.; Erndt, N. G.; Cauley, T. H.; Koehler, R. T.; So, A. P.; Dube, S.; Rose, K. A.; Montesclaros, L.; Wang, S.; Stumbo, D. P.; Hodges, S. P.; Romine, S.; Milanovich, F. P.; White, H. E.; Regan, J. F.; Karlin-Neumann, G. A.; Hindson, C. M.; Saxonov, S.; Colston, B. W. High-throughput droplet digital PCR system for absolute quantitation of DNA copy number. *Anal Chem* **2011**, *83*, 8604-10.
- (123) Zhang, H.; Jenkins, G.; Zou, Y.; Zhu, Z.; Yang, C. J. Massively parallel single-molecule and single-cell emulsion reverse transcription polymerase chain reaction using agarose droplet microfluidics. *Anal Chem* **2012**, *84*, 3599-606.
- (124) Beer, N. R.; Hindson, B. J.; Wheeler, E. K.; Hall, S. B.; Rose, K. A.; Kennedy, I. M.; Colston, B. W. On-chip, real-time, single-copy polymerase chain reaction in picoliter droplets. *Analytical Chemistry* **2007**, *79*, 8471-8475.
- (125) Ohashi, T.; Kuyama, H.; Hanafusa, N.; Togawa, Y. A simple device using magnetic transportation for droplet-based PCR. *Biomed Microdevices* **2007**, *9*, 695-702.
- (126) Wang, F.; Burns, M. A. Performance of nanoliter-sized droplet-based microfluidic PCR. *Biomed Microdevices* **2009**.
- (127) Markey, A. L.; Mohr, S.; Day, P. J. High-throughput droplet PCR. *Methods* **2010**, *50*, 277-81.
- (128) Vincent, M.; Xu, Y.; Kong, H. M. Helicase-dependent isothermal DNA amplification. *Embo Reports* **2004**, *5*, 795-800.
- (129) Mazutis, L.; Araghi, A. F.; Miller, O. J.; Baret, J. C.; Frenz, L.; Janoshazi, A.; Taly, V.; Miller, B. J.; Hutchison, J. B.; Link, D.; Griffiths, A. D.; Ryckelynck, M. Droplet-Based Microfluidic Systems for High-Throughput Single DNA Molecule Isothermal Amplification and Analysis. *Analytical Chemistry* **2009**, *81*, 4813-4821.
- (130) Wheeler, E. K.; Benett, W.; Stratton, P.; Richards, J.; Chen, A.; Christian, A.; Ness, K. D.; Ortega, J.; Li, L. G.; Weisgraber, T. H.; Goodson, K. E.; Milanovich, F. Convectively driven polymerase chain reaction thermal cycler. *Analytical Chemistry* **2004**, *76*, 4011-4016.

- (131) Chung, K. H.; Park, S. H.; Choi, Y. H. A palmtop PCR system with a disposable polymer chip operated by the thermosiphon effect. *Lab on a Chip* **2010**, *10*, 202-210.
- (132) Lagally, E. T.; Mathies, R. A. Integrated genetic analysis microsystems. *Journal of Physics D-Applied Physics* **2004**, *37*, R245-R261.
- (133) Njoroge, S. K.; Witek, M. A.; Battle, K. N.; Immethun, V. E.; Hupert, M. L.; Soper, S. A. Integrated continuous flow polymerase chain reaction and micro-capillary electrophoresis system with bioaffinity preconcentration. *Electrophoresis* **2011**, *32*, 3221-3232.
- (134) Takekawa, J. Y.; Iverson, S. A.; Schultz, A. K.; Hill, N. J.; Cardona, C. J.; Boyce, W. M.; Dudley, J. P. Field detection of avian influenza virus in wild birds: evaluation of a portable rRT-PCR system and freeze-dried reagents. *J Virol Methods* **2010**, *166*, 92-7.
- (135) Wang, Z.; Sekulovic, A.; Kutter, J. P.; Bang, D. D.; Wolff, A. Towards a portable microchip system with integrated thermal control and polymer waveguides for real-time PCR. *Electrophoresis* **2006**, *27*, 5051-8.
- (136) Sia, S. K.; Kricka, L. J. Microfluidics and point-of-care testing. *Lab Chip* **2008**, *8*, 1982-3.
- (137) Vogelstein, B.; Kinzler, K. W. Digital PCR. *Proc Natl Acad Sci U S A* **1999**, *96*, 9236-41.
- (138) Walsh, E. E.; Falsey, A. R.; Swinburne, I. A.; Formica, M. A. Reverse transcription polymerase chain reaction (RT-PCR) for diagnosis of respiratory syncytial virus infection in adults: use of a single-tube "hanging droplet" nested PCR. *J Med Virol* **2001**, *63*, 259-63.
- (139) Leng, X.; Zhang, W.; Wang, C.; Cui, L.; Yang, C. J. Agarose droplet microfluidics for highly parallel and efficient single molecule emulsion PCR. *Lab Chip* **2010**, *10*, 2841-3.
- (140) Zhang, Y.; Zhu, Y.; Yao, B.; Fang, Q. Nanolitre droplet array for real time reverse transcription polymerase chain reaction. *Lab Chip* **2011**, *11*, 1545-9.
- (141) Zhang, W. Y.; Zhang, W.; Liu, Z.; Li, C.; Zhu, Z.; Yang, C. J. Highly parallel single-molecule amplification approach based on agarose droplet polymerase chain reaction for efficient and cost-effective aptamer selection. *Anal Chem* **2012**, *84*, 350-5.
- (142) Zare, R. N.; Kim, S. Microfluidic platforms for single-cell analysis. *Annu Rev Biomed Eng* **2010**, *12*, 187-201.
- (143) Ottesen, E.A.; Hong, J.W.; Quake S.R.; Leadbetter, J.R. Microfluidic Digital PCR Enables Multigene Analysis of Individual Environmental Bacteria. *Science* **2006**, *5801*, 1464-7.

## 2. Continuous Flow Infrared-mediated PCR (cfIR-PCR) System

### 2.1 Introduction

#### 2.1.1 *Benefits of Microchip PCR*

As a key component of genetic testing, the polymerase chain reaction (PCR)<sup>1</sup> has been adapted into microfluidic devices as it holds great potential for clinical<sup>2-4</sup> and forensic applications<sup>5</sup>, as well as food testing and environmental monitoring<sup>6-8</sup>. Micro- and nanoscale PCR devices provide several benefits over their macroscale counterparts, including reduction of analysis time<sup>9</sup> and reagent consumption<sup>10</sup>, portability and integration with other functional units<sup>11,12</sup>, and disposability, preventing cross-contamination<sup>13</sup>. Additionally, a single microdevice is able to process large numbers of parallel amplifications, simultaneously, for fast, accurate, and reliable genetic testing<sup>14,15</sup>. With the progress in microfluidic PCR, other considerations for developing a microfluidic device such as microfabrication techniques, material and surface chemistry, thermal and fluidic control, nucleic acid detection, miniaturization, and integration of functional units have significantly progressed, making unprecedented impacts on the  $\mu$ -TAS community<sup>16</sup>.

#### 2.1.2 *Static versus Continuous Flow PCR in Microfluidic Devices*

There have been two major types of microfluidic PCR approaches, static and continuous flow PCR (cf-PCR) (dynamic) platforms. In a static PCR format, the PCR sample is positioned in the confined PCR vessel surrounded by etched microchip materials and PCR amplification occurs by temperature controls of heating sources such as a lamp/laser and film heater. Our group has developed an infrared (IR)-mediated heating system<sup>17</sup> to facilitate PCR within glass<sup>18</sup> and polymeric microfluidic devices<sup>9,19</sup>. This non-contact heating method uses a single lamp to

provide fast heating and cooling rates and, therefore, rapid thermal cycling, completing PCR in as little as 240 seconds<sup>9</sup>. However, the size of the focal spot of the lamp limits the number of reaction chambers for static PCR microdevices<sup>20</sup> and the speed of PCR could be further restricted by the architecture of microchamber and microchip, types of lamps, and microchip materials itself<sup>19</sup>.

For continuous-flow PCR, the PCR solution in the microdevice is flowed into and out of thermally distinct zones, undergoing thermocycling in the process, which can realize a time-space conversion concept of PCR amplification<sup>21</sup>. These temperature zones have been established using resistive thin film heaters<sup>22,23</sup> or external heat blocks and Peltier-based heaters<sup>15,21,24-26</sup>. Furthermore, many groups have evaluated different designs and heating systems<sup>27,28</sup>, different materials, such as polymers<sup>24</sup>, thermal simulations of heat transfer<sup>22,28,29</sup>, integration with other DNA analysis methods<sup>30</sup>, and droplet platforms<sup>10,15</sup>. Longer microchannels in distinct heating zones implement high-throughput continuous reactions using multiple segmented flows<sup>14,27</sup> or individual droplets having multiplex distinct reactions<sup>10,15,31</sup>. Fast reactions can be achieved by increasing flow rates, as long as it does not restrict heat transfer between the PCR sample and microchip (i.e., reduce PCR efficiency)<sup>22</sup>.

Most approaches require multiple heat sources and direct contact with the microchip, which can cause lateral heat transfer among three distinct heaters, increasing the footprint of the PCR instrument. Additionally, the control of three distinct heaters greatly increases the complexity of the system. Although several groups have used a single heat block or rod and moved the sample away from it<sup>32,33</sup>, through a naturally established thermal gradient, changing thermal gradients to obtain different annealing temperatures for different PCR samples, easy control of heater, and miniaturization have not been described as a result of the contact heating

manner. In addition, there have been several unique heating sources such as air<sup>34</sup>, laser<sup>35,36</sup>, and microwave<sup>37-40</sup>, and different heating configurations such as convective flow<sup>41,42</sup>, ferrofluid driven PCR<sup>43</sup>, and a single contact heater<sup>23,33</sup> to conduct PCR on the microfluidic device. Nonetheless, the number of a PCR sample in one microchip and the speed of PCR amplification were partially limited in these systems, and miniaturization should be still a drawback of the contact heating source. From these perspectives, we conceived a novel idea for a continuous flow PCR system via the non-contact IR heating system previously developed in our laboratory.

### 2.1.3 Continuous Flow Infrared-mediated PCR (cfIR-PCR)

In present work, we report the first development of continuous flow infrared-mediated PCR (cfIR-PCR) in a polymeric microdevice. In our setup, the continuous illumination of a single lamp for the duration of the run establishes a thermal gradient from the focal spot outward. PCR sample flows in a circular 20 to 40-loop poly(methyl-methacrylate) (PMMA) microdevice, moving into and out of different temperature zones. The number of loops can be adjusted to accommodate a wide variety of PCR protocols from those for plasmids and viruses for pathogen detection to complex human genomes for forensic applications. A 29-loop microdevice was used to successfully and rapidly amplify a 520 bp fragment of  $\lambda$ -phage DNA to characterize (or assess/validate) our cfIR-PCR instrument, while a 43-loop microdevice was used to successfully conduct consecutive PCR amplifications through three segmented flows from the human targets  $\beta$ -globin and TPOX locus, and  $\lambda$ -phage DNA without any detectable amount of cross-contamination. Our cfIR-PCR system can be further miniaturized and integrated in small microdevices to achieve portability and higher throughput reactions.

## 2.2 Materials and Methods

### 2.2.1 *cfIR-PCR Instrument*

The cfIR-PCR setup was assembled and modified from previous IR-mediated heating system<sup>44</sup>. Three stainless steel pillars were inserted through the PCR PMMA stage where an adjustable table was located to easily change the distance between the microchip and a halogen lamp (L6409-G, International Light Technologies, Peabody, MA, USA). The lamp was closely attached beneath the PCR stage and precisely under the center of the circular region to offer intensive and broad range of heating to establish linear and desired thermal gradient for PCR applications. A miniature type-t thermocouple (Model T240C, Physitemp Instruments, Inc., Clifton, NJ, USA) for maintaining a certain thermal gradient on the polymeric microdevice was connected into the omega box controlled via DAQ card and LabVIEW (National Instruments, Austin, TX, USA) installed computer embedded with PID algorithm. All components of the stage made from PMMA were precisely cut and prepared by 10.6  $\mu\text{m}$  CO<sub>2</sub> laser ablation system (VersaLaser 3.50, Universal Laser Systems, Inc, Scottsdale, AZ, USA) and assembled on the previous IR-mediated heating system.

### 2.2.2 *Microchip Fabrication*

Three-layered architectures (top plate – fluidic layer – bottom plate) of microfluidic devices used in this research were designed using CorelDraw software (Corel, Mountain view, CA, USA) and these designs were transferred into the CO<sub>2</sub> laser system for laser ablation. The polymeric material, PMMA, was chosen to construct our cfIR-PCR microdevice that is a three-layered PMMA microfluidic device consisting of top plate (PMMA 1.5 mm; McMaster-Carr, Aurora, OH, USA), fluidic layer (PMMA 0.2 mm; Astra Products, Baldwin, NY, USA), and

bottom plate (PMMA 1.5 mm). Instead of etching on the surface of thick PMMA, cutting through a thin PMMA sheet was chosen to make the precise and smooth channel and chamber after bonding procedure. The standard etching condition for PMMA were selected as vector cut using 60% (1.5 mm PMMA) and 40% (200  $\mu$ m PMMA) powers at 2% and 30% speed respectively, considering thickness of PMMA, surface smoothness, and bulges on the side of the cutting area. Vector cut through 200  $\mu$ m PMMA generated 250 - 270  $\mu$ m of the wide microchannel with 200  $\mu$ m of the depth (the height of PMMA sheet) (**Fig. 1**). The 1.5 mm thick top and bottom layers of PMMA were selected to improve temperature holds in the PCR solution and generate a linear thermal gradient that is suitable for designing the cfIR-PCR microdevice.

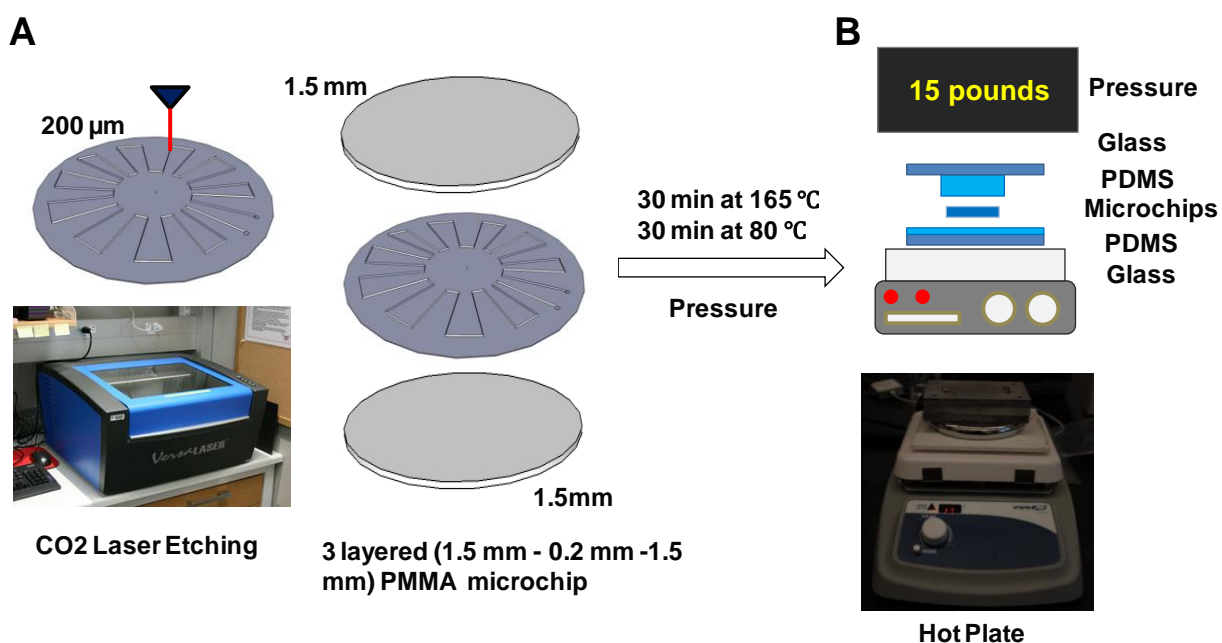


**Figure 1:** Microfabrication of multi-layered polymeric microdevices. (A) Laser ablation of cutting through a thin PMMA (200  $\mu$ m). (B) Thermal bonding on the hot plate [20].

The etched fluidic layer, top and bottom layers of PMMA sheets were completely cleaned by distilled water, and all surfaces of three layers were blown and dried with compressed air to remove residual particles. Bonding procedure was performed with 15 pounds of weight on the hot plate with two pieces of glass plates where aligned multi-layered microdevices were placed

as following the previous bonding procedure<sup>45</sup>. The three-layered PMMA microdevice was heated to reach the glass transition temperature of PMMA at 165 °C with 30 minute holding and cooled to anneal the bonded microdevice at 80 °C for 30 minutes. After thermal bonding, the fluidic channel was completely filled and flowed through with distilled and sterile water for a leaking test and wetting of microchannel before cfIR-PCR. 10-32 Nanoports TM (Upchurch Scientific, Bristol, CT, USA) was attached on the inlet of the cfIR-PCR microdevice using 5-min epoxy (Devcom, Danvers, MA, USA) where Teflon tubing (1.0 mm of the inner diameter; Iris Technologies, Olathe, KS, USA) was inserted to flow a PCR solution.

### 2.2.3 Thermal Gradient Measurement

In order to measure a spatial thermal gradient of the multi-layered microchip at steady-state in temperature distribution, a temperature measurement (TM) microchip, which was a three-layered PMMA as the cfIR-PCR microdevice, was fabricated to measure temperature of the PCR buffer inside the microchannel. The TM microchip contains 1.2 µL of six microchambers (from 1<sup>st</sup> to 6<sup>th</sup> chamber) in 8 directions (from A to H) to generate a total of 48 microchambers and a thermal gradient was measured with several thermocouples simultaneously. The reference thermocouple placed in the reference microchamber (the first microchamber in the first row) was monitored to maintain temperature at 95 °C with multiple thermocouples in other microchambers to get a thermal gradient on the microdevice. The reference thermocouple with the inlet and outlet were completely sealed by a biocompatible adhesive tape (Adhesive Research, Inc., Glen Rock, PA, USA). All temperatures except the reference temperature were recorded using Amprobe multi-thermometer (TMD90A, Amprobe, Everett, WA, USA) with thermocouples until temperature was stabilized. The reference thermocouple was connected into

DAQ card controlled by a LabVIEW programmed computer, was maintained around 95 – 98 °C by PID feedback-controlled lamp duty cycle to get a constant thermal gradient across the microchip. In order to obtain averaged temperature in each microchamber, temperature monitoring and recording were conducted at least three times. Furthermore, IR-camera (i-50, FLIR System, Wilsonville, Oregon, USA) was employed to take a thermal image while performing cfIR-PCR at 14 cm of distance between the IR-camera and the microchip. The thermal image of the TM microchip measured by the IR-camera was compared to the thermal image of the cfIR-PCR microdevice to match two thermal distributions while conducting cfIR-PCR and the maximum temperature displayed on the TM microchip was compared with that of cfIR-PCR microdevice. The lamp was fixed to heat the center of the microchip and it offered even thermal distribution across the microchip. The PCR solution was continuously pumped through the cfIR-PCR microdevice via a syringe pump (Aladdin-1000, World Precision Instrument, Sarasoto, FL, USA). Flow rates controlled by the syringe pump were exploited to determine the dwell time of the PCR solution in three distinct PCR zones.

#### 2.2.4 Thermal Modeling of the cfIR-PCR Microdevice

The simulations were carried out using commercial Computational Fluid Dynamics (CFD) package ANSYS® CFX, release 14.0 (ANSYS, Canonsburg, PA, USA) that employed a hybrid finite-volume/finite-element approach for discretizing the Navier Stokes equations. The equations are then solved by a fully-implicit fully-coupled multigrid solver<sup>46</sup>. The circular cfIR-PCR microfluidic device is comprised of 29 periodic loops in the fluidic layers, herein called a segment. In each segment, the flow enters A region in the denature zone and exists B region through the next denature region. In this CFD, the CAD model of a segment was considered as

the unit of our computational model. The segment was modeled as a solid using the properties of PMMA. A microchannel was cut through a thin PMMA (200  $\mu\text{m}$ ) sheet for water (PCR buffer) in the fluidic layer of the segment to be flowed through. Temperature distributions that were obtained experimentally by the IR-camera were imposed on the bottom and top surface of the PMMA segment. Periodic boundary condition (temperature) was applied on the side walls of the segment. The given volumetric flow rate and temperature was applied on the inlet where the flow comes into the channel in region A, and atmospheric pressure was set on the outlet where the flow comes out of the channel in region B. The rest of exterior boundaries were set to be convective boundary condition (Robin condition) where the amount of convective heat transfer was equal to that of conductive heat transfer at the boundary. A convective heat transfer coefficient of  $10 \frac{\text{W}}{\text{m}^2\text{K}}$  and room temperature of  $T_0 = 20^\circ\text{C}$  were assumed throughout the simulation. The physical properties used in this thermal modeling are listed in **Table 1**.

**Table 1:** Material properties in CFD simulation.

	Specific heat capacity (J/kgK)	Density (Kg/m <sup>3</sup> )	Thermal conductivity (W/mK)	Dynamic viscosity (Kg/ms)
Water	4181.7	997	0.6069	0.0008899
PMMA	1466	1185	0.2085	N/A

### 2.2.5 Microchip PCR Protocols

For cfIR-PCR amplification in the 29-loop microdevice, a 520 bp region of the  $\lambda$ -phage genome was chosen as the target. The primer sequences used in this work were described in **Table 2**. The preparation of the PCR solution for cfIR-PCR follows the normal PCR recipe as the final concentrations; 1 x PCR buffer,  $\text{MgCl}_2$  (3 mM), dNTP mixture (0.2 mM), forward and

**Table 2:** Primer information used in this research.

Gene target	T <sub>m</sub> (°C)	Sequence	Size
λ- phage DNA (520 bp)			
Forward	64.7	5'- GATGAGTTCGTGTCCGTACAACTGG – 3'	25 bp
Reverse	70.8	5'- GGTTATCGAAATCAGCCACAGCGCC – 3'	25 bp
Human TPOX locus (77 bp)			
Forward	60.8	5' – CGGGAAGGGAACAGGAGTAAG – 3'	21 bp
Reverse	62.1	5' – CCAATCCCAGGTCTTCTGAACA – 3'	21 bp
Human β-globin (389 bp)			
Forward	67.5	5' – ACAGCATCAGGAGTGGACAGATCCC-3'	25 bp
Reverse	69.7	5' – AGCCAGGGCTGGGCATAAAAGTCA– 3'	24 bp

reverse primers (4  $\mu$ L) (**Table 2**), *Taq* polymerase (0.2 U/ $\mu$ L), template  $\lambda$ -phage genomic DNA (4 ng/ $\mu$ L), and BSA (from 0.1 to 2 mg/mL), and a total of 50  $\mu$ L PCR cocktail for one reaction; the final BSA concentration varied considering the efficiency of cfIR-PCR and 1 mg/mL of BSA concentration was used for 29-loop cfIR-PCR. Deionized water generated with a Nanopure unit (Barnstead, Dubuque, IA, USA) was used in all experiments. After the preparation of the PCR sample, a total volume of the sample (50  $\mu$ L) was taken into Teflon tubing via the syringe following a mineral oil (Sigma-Aldrich, St. Louis, MO, USA) as a pushing reagent. 50  $\mu$ L PCR solution passed through the microdevice was collected and made ten fractions (5  $\mu$ L per one aliquot) to show the pattern of DNA amplification based on the time scales. The PCR solution was pumped at different flow rates ranging from 2  $\mu$ L/min to 9  $\mu$ L/min; in the work, 2  $\mu$ L/min, 3  $\mu$ L/min, 4.5  $\mu$ L/min, 6  $\mu$ L/min, 7.5  $\mu$ L/min, and 9  $\mu$ L/min were tested in the 29-loop cfIR-PCR microdevice. At the beginning of injection into the cfIR-PCR microdevice, the PCR sample experienced the pre-denature zone for 2 minutes to completely denature double-stranded DNA and started thermocycling on the thermal gradient. After finishing 29 cycles of thermocycling, reagents passed through the final extension region to be collected as 5  $\mu$ L fraction from the outlet and 10 samples (10 x 5  $\mu$ L) were collected using pipetting and evaluated (separated and detected)

by Agilent 2100 Bioanalyzer (Agilent Technologies, Inc., Santa Clara, CA, USA), the commercialized microchip electrophoresis instrument. The same PCR recipe used in cfIR-PCR in the PCR cocktail was employed for preparation of a positive sample on the conventional thermocycler (Mycycler<sup>tm</sup> Thermal Cycler, Bio-Rad, Hercules, CA, USA). The standard PCR cycle for  $\lambda$ -phage DNA amplification was pre-denature at 95 °C for 2 minutes, [denature at 95 °C for 30 seconds, anneal and extension at 68 °C for 30 seconds] x 29, and final extension at 72 °C for 2 minutes.

For emulsion cfIR-PCR amplification in the 43 loop microdevice, a 389 bp region of beta-globin and a 77 bp region of TPOX from the human genome, and 520 bp region of the  $\lambda$ -phage genome were chosen as the targets. The preparation of the PCR solution for cfIR-PCR follows the normal PCR recipe as the final concentrations; 1 x PCR buffer, MgCl<sub>2</sub> (3 mM), dNTP mixture (0.2 mM), forward and reverse primers (4  $\mu$ L) (**Table 2**), *Taq* polymerase, template  $\lambda$ -phage genomic DNA (from 1 to 10 pg/ $\mu$ L) and human genomic DNA (from 4 to 40 ng/ $\mu$ L), and BSA (0.1 mg/mL) for cfIR-PCR to prepare certain amounts of PCR cocktails (from 5  $\mu$ L to 10  $\mu$ L) to be mixed with emulsion (from 10  $\mu$ L to 20  $\mu$ L). The oil-surfactant mixture was prepared following previous procedure<sup>70</sup>; a mixture of the surfactants, Span 80 4.5 % (v/v) (TCI America, Portland, OR, USA), Tween 20 0.4 % (v/v) (Sigma-Aldrich, St. Louis, Missouri, USA), and Triton X-100 0.05 % (v/v) (Acros Organics, NJ, USA) were added into the mineral oil (Sigma-Aldrich, St. Louis, Missouri, USA). The PCR solution was added into this oil-surfactant mixture and small sizes of droplets were generated via pipetting that led to the physical breakdown of the PCR solution into emulsion; 5  $\mu$ L (10  $\mu$ L for dilution experiments) of the PCR cocktail mixed with 10  $\mu$ L (20  $\mu$ L for dilution experiments) of the oil-surfactant mixture to generate 1 to 2 ratio of the PCR cocktail to the oil-surfactant mixture. The image of emulsion

was taken by microscope (AX10, ZEISS, Oberkochen, German). The emulsion PCR sample following by the mineral oil was injected via the syringe pump to push the emulsion PCR solution to perform emulsion cfIR-PCR. After collecting the emulsion PCR sample from the outlet, it was completely spun down to isolate the PCR sample from the emulsion. Lastly, DNA amplification in the PCR sample was evaluated (separated and detected) by Agilent 2100 Bioanalyzer. The same PCR recipe used in cfIR-PCR was employed for preparation of a positive sample on the conventional thermocycler. The standard PCR cycle for the human genomic amplification was pre-denature at 95 °C for 2 minutes, [denature at 95 °C for 30 seconds, anneal at 60 °C for 30 seconds, and extension at 68 °C for 30 seconds] x 43, and final extension at 72 °C for 2 minutes. The PCR products from all positive samples were evaluated (separated and detected) by Agilent 2100 Bioanalyzer.

## 2.3 Results and Discussion

### 2.3.1 *Microchip Fabrication*

To achieve our concept of continuous flow infrared-mediated PCR (cfIR-PCR), a polymeric material, PMMA, was chosen due to rapid fabrication and a relatively low price, because the difficulties of fast prototyping and microchip production were the main drawbacks of other conventional materials such as glass and silicon<sup>47-50</sup>. The laser-based micromachining using CO<sub>2</sub> laser, which is a relatively economical way to fabricate polymers compared to other laser ablation methods, has been successfully employed to ablate a well-characterized polymeric material, PMMA<sup>51-53</sup>. The high absorbance of infrared with low thermal diffusivity in PMMA causes fast heating around cutting area and the rapid decomposition of PMMA into volatile monomer MMA makes the surface edge smoother, which makes it suitable for the construction

of any channel and chamber<sup>51</sup>. For these clear reasons, PMMA is a good polymeric material for laser ablation in addition to injection molding<sup>54</sup>, hot embossing<sup>55</sup>, computer aided micro-milling methods<sup>36</sup>, and chemical solvent bonding<sup>56</sup>. In order to engrave features into the fluidic layer, the optimal combination of laser power, translation speed, and ablation pulse density (PPI; the number of pulses per inch), and laser focusing (distance between laser lenses and chip material) have been experimentally determined to get desired features of the microchannel such as depth, width, and surface roughness, as well as decreased amounts of bulges; bulges should be minimized to improve thermal bonding. In the first step of experimental optimization, the PPI value was set as a default value, 1000 PPI, and only power and translational speed were adjusted to find the optimal set values. All features in the microchip were fabricated by the cut through of a thin PMMA sheet to generate a very precise and smooth channel surrounded by the PMMA surface that was manufactured by the company, and any additional step for smoothing the channel surface was not further required. Laser power is closely related to the depth of engraving with the transition speed. However, width slightly increased with laser power up to 250 - 270  $\mu\text{m}$ . Therefore, direct cut through could generate 250 – 270  $\mu\text{m}$  width of the microchannel and the height of the microchannel was determined via the thickness of a thin PMMA sheet. The direct surface etching with CO<sub>2</sub> laser on a polymer sheet generated a rough surface, generating a significant pitted surface. This pitted surface prevented smooth flow of the PCR solution and trapped air bubbles that could provide nucleation sites inside hole-like structures<sup>19</sup>. Additionally, the inverted triangle shape generated by laser surface etching could be completely collapsed or distorted by high pressure bonding.

Bonding temperature and pressure are adjustable to make optimal bonding for any application: by increasing pressure, temperature can be reduced. Although too much weight

ensures strong bonding, it is able to collapse microchannels and completely stop the PCR solution flowing. Too low weights caused leakages around bonding areas<sup>57</sup>. As our cfIR-PCR microdevice has a longer microchannel, inappropriate bonding of three layered PMMA sheets could lead to leakage of the PCR solution and eventually cfIR-PCR amplification was prohibited. This bonding procedure should be the simplest way to bond any PMMA microdevice within two hours and it could assist us to rapidly prepare different designs of microdevices to optimize our concept of cfIR-PCR. After bonding, the Nanoport was attached on the inlet of the microchip to efficiently pump a reaction sample through the cfIR-PCR microdevice without any leakage. Before starting cfIR-PCR, distilled water was run through the microchannel to check any leakage and completely wetting the microchannel; without wetting of the microchannel before cfIR-PCR, it reduced PCR efficiency.

### 2.3.2 *Establishment of a Thermal Gradient and Measuring Temperatures*

Controlling and monitoring temperature in a microfluidic device is very essential to achieve successful PCR in the microfluidic device due to the critical dependence of PCR amplification on temperature of each functional zone. In present work, a thermal gradient was established across the three layered PMMA TM microchip (1.5 mm top – 0.2 mm fluidic channel – 1.5 mm bottom) by holding temperature in the reference microchamber at 95 °C via feedback control of lamp duty cycle (**Fig. 2A**). The actual thermal gradient on the cfIR-PCR microdevice was presumed with the thermal gradient on the TM microdevice. The circular thermal gradient in the IR-camera image of the TM microdevice (**Fig. 2B**) was round enough to conduct thermal gradient PCR in the polymeric microdevice.

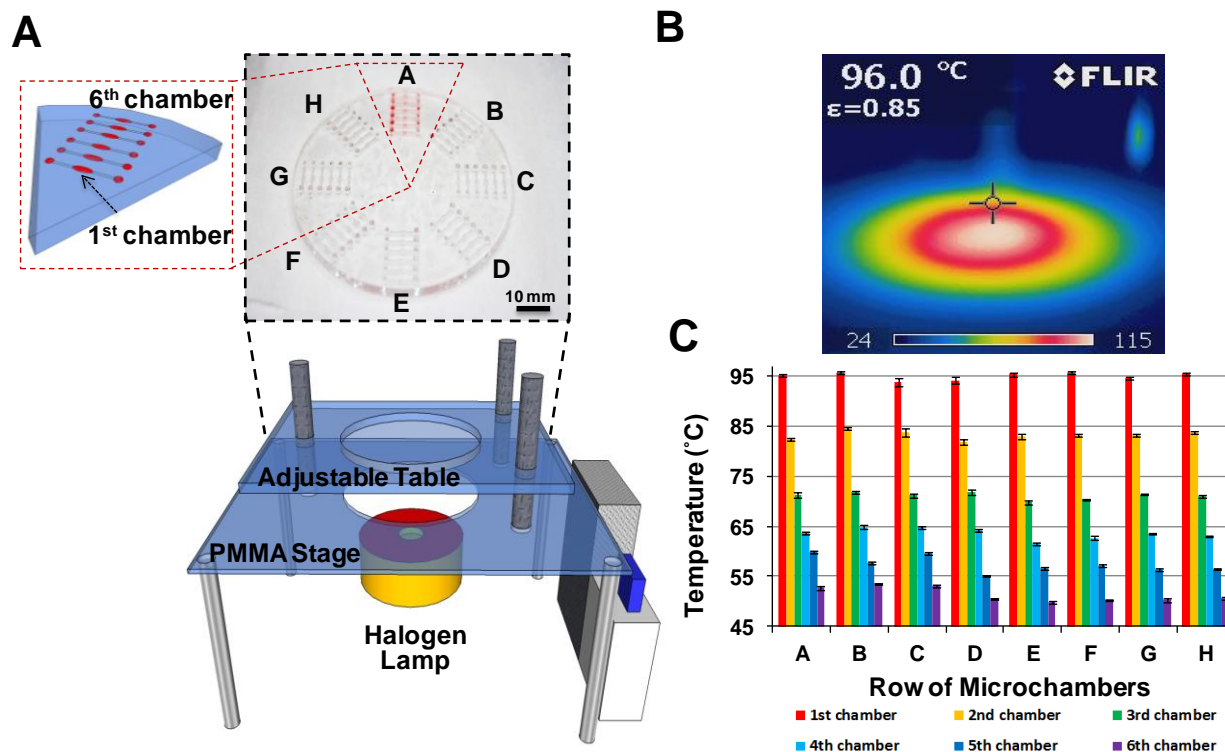


**Figure 2:** Apparatus and determination of the thermal gradient established by infrared (IR)-mediated heating. (A) The system consists of a PMMA stage and halogen lamp that is PID controlled by an in-house LabVIEW program. *Inset:* Temperature Measurement (TM) microchip, which has 6 microchambers per row and 8 rows in 8 directions, for a total of 48 microchambers, is centered above the halogen bulb on an adjustable stage. (B) Thermal image of the TM microchip taken with a IR-camera while heating, showing the established thermal gradient. (C) 2D bar graph of the averaged temperature (measured three times at steady state) in each chamber of the TM microchip, showing the difference in temperature at different locations on the microchip (error bars represent  $n=3$ ).

In order to establish a 2D bar graph (**Fig. 2C**) of averaged temperature across the TM microchip, all temperatures from the 48 microchambers were measured three times to calculate the mean value with the standard deviation, from 1<sup>st</sup> chamber to 6<sup>th</sup> chamber in 8 rows from A to H. As temperature distribution on the circular microdevice was not perfectly symmetry, averaged temperatures were exploited to get the averaged thermal gradient as a 2D bar graph. Additionally, these mean temperatures from 8 microchambers in the same row (from A to H), which are positioned in the circular isothermal region, were further averaged to generate a

thermal gradient as a 2D plot (**Fig. 3A**). This plot illustrated the distance from the center of the microchip versus mean temperature and defined functional zones for three PCR steps. The spatial thermal gradient in this plot at steady state was determined to be  $\sim 4$  °C/mm, permitting a thermal gradient from 95 - 96°C at the center of the microchip to approximately 51 - 52°C at the edge. Actual averaged temperatures (with standard deviations) at distances were 95.1 degree ( $\pm 0.7$ ) at 15 mm, 83.3 degree ( $\pm 0.8$ ) at 17.5 mm, 71.1 degree ( $\pm 0.7$ ) at 20 mm, 63.5 degree ( $\pm 1.1$ ) at 22.5 mm, 57.4 degree ( $\pm 1.6$ ) at 25 mm, and 51.4 degree ( $\pm 1.5$ ) at 27.5 mm. This 2D plot was used to design 29 and 43 loops of cfIR-PCR microchips. As one of characteristics in this plot, temperatures in the 8 microchambers were maintained within a standard deviation of  $\pm 0.7$  to  $\pm 1.4$  from the first row chamber to the 6<sup>th</sup> (last) row chamber. As the reference thermocouple was inserted near the center of the microchip (at 15 mm), the halogen lamp heated intensively around the circular center region, and heat was transferred through the center area to the edge, the standard deviation might increase from the center ( $\pm 0.7$ ) to the edge ( $\pm 1.4$ ).

### 2.3.3 Design Concept of the cfIR-PCR Microdevice

Our design in the cfIR-PCR microdevice has been mainly focused on proving a new concept of continuous flow PCR using a single lamp to achieve fast thermocycling where one cycle could be finished at least within one minute. The cfIR-PCR microdevice was designed from the 2D plot of the thermal gradient measured by the TM microdevice. A thick PMMA (top 1.5 mm and bottom 1.5 mm) maintained a linear thermal gradient enough to generate a broad range of temperature distribution within the microdevice from 95 °C at the center to 52 °C at the edge and 1.5 mm of two PMMA layers (top and bottom layers) insulate the PCR solution to maintain uniformity of temperature as a result of physical properties of PMMA such as low

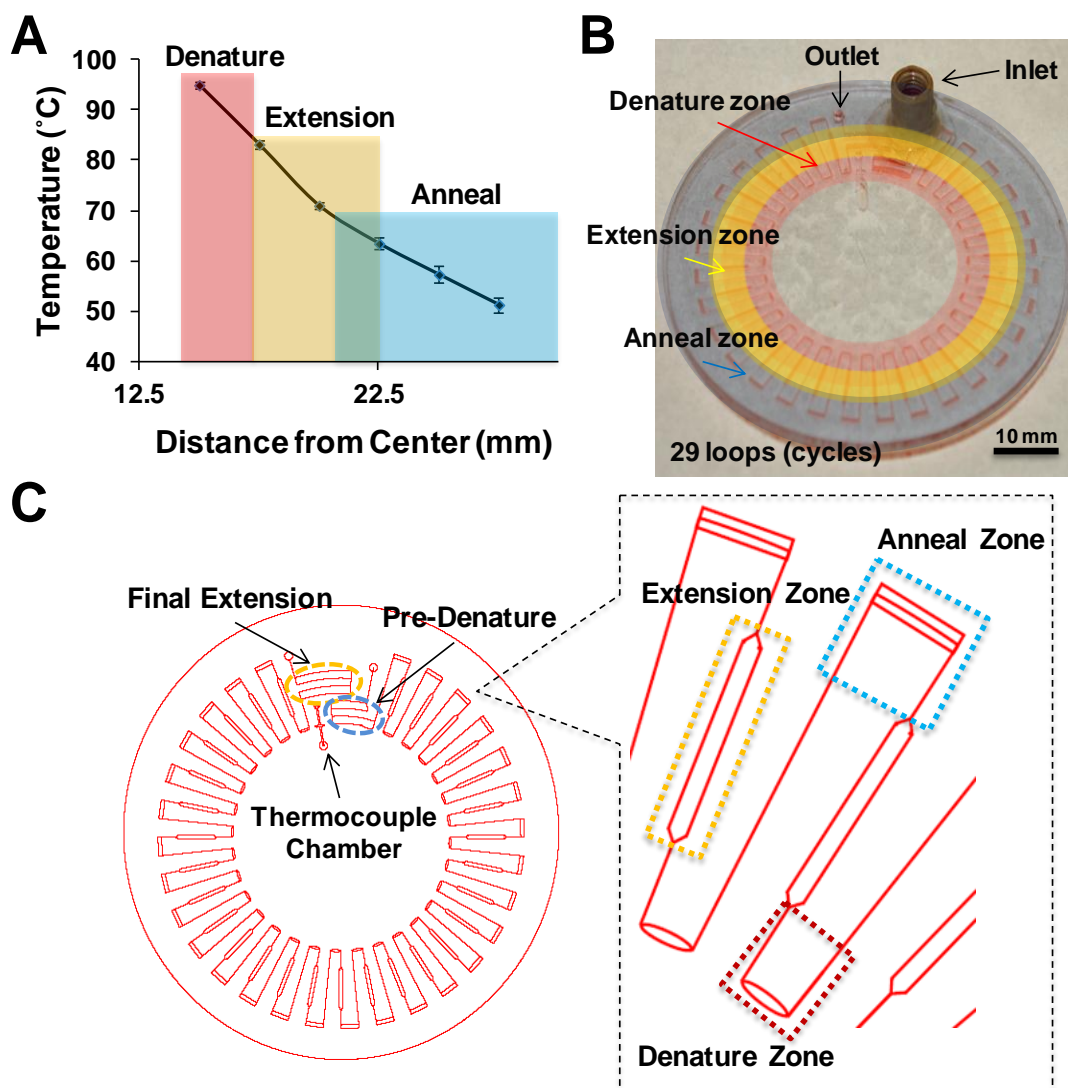


**Figure 3:** Definition of temperature zones and design of the continuous flow infrared-mediated PCR (cfIR-PCR) microdevice. (A) Plot of distance from the center of the microchip versus temperature, showing a decrease in temperature with increasing distance. The functional zones for each of the three steps required for PCR are highlighted by the colored boxes (error bars represent  $n=8$ ). (B) Photograph of the 3-layered PMMA microdevice for cfIR-PCR, highlighting the location of the denature (red), extension (yellow), and anneal (blue) zones. The three layers consist of top and bottom layers (1.5 mm PMMA) and fluidic layer (0.2 mm PMMA). The microchannels are filled with red dye for visualization. (C) Schematic of the cfIR-PCR microchip showing the loops for thermal cycling and location of the thermocouple chamber. *Inset:* Close-up view of two of the 29 loops showing where each functional zone is defined and the calculated volumes in those zones.

thermal conductivity and high heat capacity. Laser ablation around closely located microchannels in a polymeric sheet caused heat dissipation through the nearest area and it

distorted nearly located microchannels around denaturation region. As a difficulty in microfabrication, the denaturation zone was engraved at 15 mm away from the center.

While information about an averaged thermal gradient from the 2D plot on the TM microchip was exploited to conceive cfIR-PCR amplification on the circular polymeric microdevice (**Fig. 3A**), several important criteria for each functional zone (denature, anneal, and extension) were carefully conceived to design our cfIR-PCR microdevice (**Fig. 3B**). For the denaturation zone, reaching a high denaturing temperature around 90 to 96 °C at least for several seconds should be critical for double-stranded DNA to be fully separated. For anneal, maintaining at the fixed anneal temperature for stable annealing of a couple of primers should be important, and for extension, the actual dwell time of PCR amplification should be enough to synthesize a certain length of the DNA strand from the complementary part of DNA. In addition, an optimal time for each zone was studied from previous studies and reference papers<sup>21-23,43</sup>. The bottleneck of PCR is enzyme kinetics instead of anneal and denaturation steps that could take only several seconds to finish, if instrument can achieve rapid thermal transition and heat transfer<sup>58</sup>. Therefore, the extension zone was considered for the PCR solution to travel more to maintain the dwell time ratio of denature: anneal: extension areas as 1 : 1.5 ~ 2 : 2. In order to make different regional velocities on target areas and achieve the optimal dwell time ratio in each functional zone, the widths of anneal and extension zones increased to ensure stable anneal temperature and extension duration. The anneal zone was located at 10 mm away from the denaturation zone and it was vertically expanded in the isothermal region. The extension zone was located at 2.5 mm to 7.5 mm from the denaturation zone and it was horizontally expanded across the thermal gradient region. In order to increase PCR efficiency further, two additional zones such as pre-denature (from 2.5 mm to 0 mm) and final extension (from 2.5 mm to 7.5 mm)

were added to ensure complete denaturation of template DNA for accessibility of PCR primers at the first stage of PCR amplification and complete extension of all complementary DNA strands at the final stage of PCR (**Fig. 3C**). The number of loops defined the cycle number and the length of loops could be adjusted to provide a fixed temperature for anneal. For initial DNA amplification, the loop length was 10 mm that offered anneal temperature at 57 °C. 29 loops of the cfIR-PCR microchip (**Fig. 3B**) was designed to carry out simple cfIR-PCR from  $\lambda$ -genomic DNA for the characterization of our setup and 43 loops of the cfIR-PCR microchip was designed for human genomic DNA amplification.

After fabrication of the cfIR-PCR microdevice, *actual (experimental) dwell times* for three PCR zones were experimentally acquired (**Table 3**). The *actual dwell time* represents a time measurement of diluted dyes passing through each functional zone. Multiple measurement of the *actual dwell time* in all microchannels engraved in every direction were conducted, because the cutting width generated by laser ablation was altered based on the cutting direction and it generated regional and chip-to-chip differences in *actual dwell time*. Therefore, the deviation mainly resulted from laser cutting patterns and additionally, the misalignment of

**Table 3:** Experimental dwell times in the PCR functional zones of the 29-loop microdevice at various flow rates ranging from 2  $\mu\text{L}/\text{min}$  to 9  $\mu\text{L}/\text{min}$ .

PCR Zone	2 $\mu\text{L}/\text{min}$	3 $\mu\text{L}/\text{min}$	4.5 $\mu\text{L}/\text{min}$	6 $\mu\text{L}/\text{min}$	7.5 $\mu\text{L}/\text{min}$	9 $\mu\text{L}/\text{min}$
Denature (sec)	$7.7 \pm 0.9$	$5.1 \pm 0.5$	$3.6 \pm 0.3$	$3.0 \pm 0.4$	$2.4 \pm 0.2$	$2.1 \pm 0.2$
Anneal (sec)	$13.9 \pm 0.6$	$9.3 \pm 0.7$	$6.1 \pm 0.8$	$5.4 \pm 0.3$	$3.5 \pm 0.2$	$3.1 \pm 0.1$
Extension (sec)	$17.7 \pm 0.5$	$12.4 \pm 0.6$	$8.7 \pm 0.6$	$7.7 \pm 0.5$	$5.0 \pm 0.1$	$4.6 \pm 0.1$
One Cycle (sec)	$46 \pm 2.5$	$31.4 \pm 2.3$	$21.5 \pm 2.0$	$18.2 \pm 1.5$	$12.3 \pm 0.6$	$11.1 \pm 0.5$
29 Cycles (min)	$\sim 22$	$\sim 15$	$\sim 10$	$\sim 9$	$\sim 6$	$\sim 5$

fluidic channels caused by the difficulty in locating the fluidic layer between two top and bottom layers for bonding. From these averaged actual dwell times, the assessment of PCR efficiency was performed at various flow rates such as 2, 3, 4.5, 6, 7.5, and 9  $\mu\text{L}/\text{min}$  in the 29-loop cfIR-PCR microdevice by the comparison of the PCR yields. Furthermore, an optimal rate, 2  $\mu\text{L}/\text{min}$ , was chosen for human genomic DNA amplification on the 43-loop cfIR-PCR microdevice and its dwell times were acquired by the same procedure of the 29 loops (**Table 4**).

**Table 4:** Experimental dwell times in the PCR functional zones of the 43-loop microdevice at 2  $\mu\text{L}/\text{min}$ .

PCR Zone	2 $\mu\text{L}/\text{min}$
Denature (sec)	$7.1 \pm 0.7$
Anneal (sec)	$11.5 \pm 0.7$
Extension (sec)	$17.6 \pm 1.1$
One Cycle (sec)	$42.9 \pm 3.0$
43 Cycles (min)	$\sim 31$

#### 2.3.4 DNA Amplifications via Thermal Gradient Matching

The focus of initial part of the experiment was on the characterization of our new instrument cfIR-PCR system; simply, checking whether cfIR-PCR could be applicable for actual microchip PCR. For verification of thermocycling on the established thermal gradient, a 520 bp  $\lambda$ -DNA fragment was selected for PCR amplification and 50  $\mu\text{L}$  PCR sample was flowed through the microchip and ten fractions out of 50  $\mu\text{L}$  were collected from the outlet. Finally, these fractional samples have been analyzed by Agilent 2100 Bioanalyzer, a commercialized microchip electrophoresis instrument. However, in the earlier stage of the development of cfIR-PCR<sup>59</sup>, effective DNA amplification could not be achieved as a result of the inconsistency in two thermal gradients between the TM and the cfIR-PCR microchips. This mismatched thermal

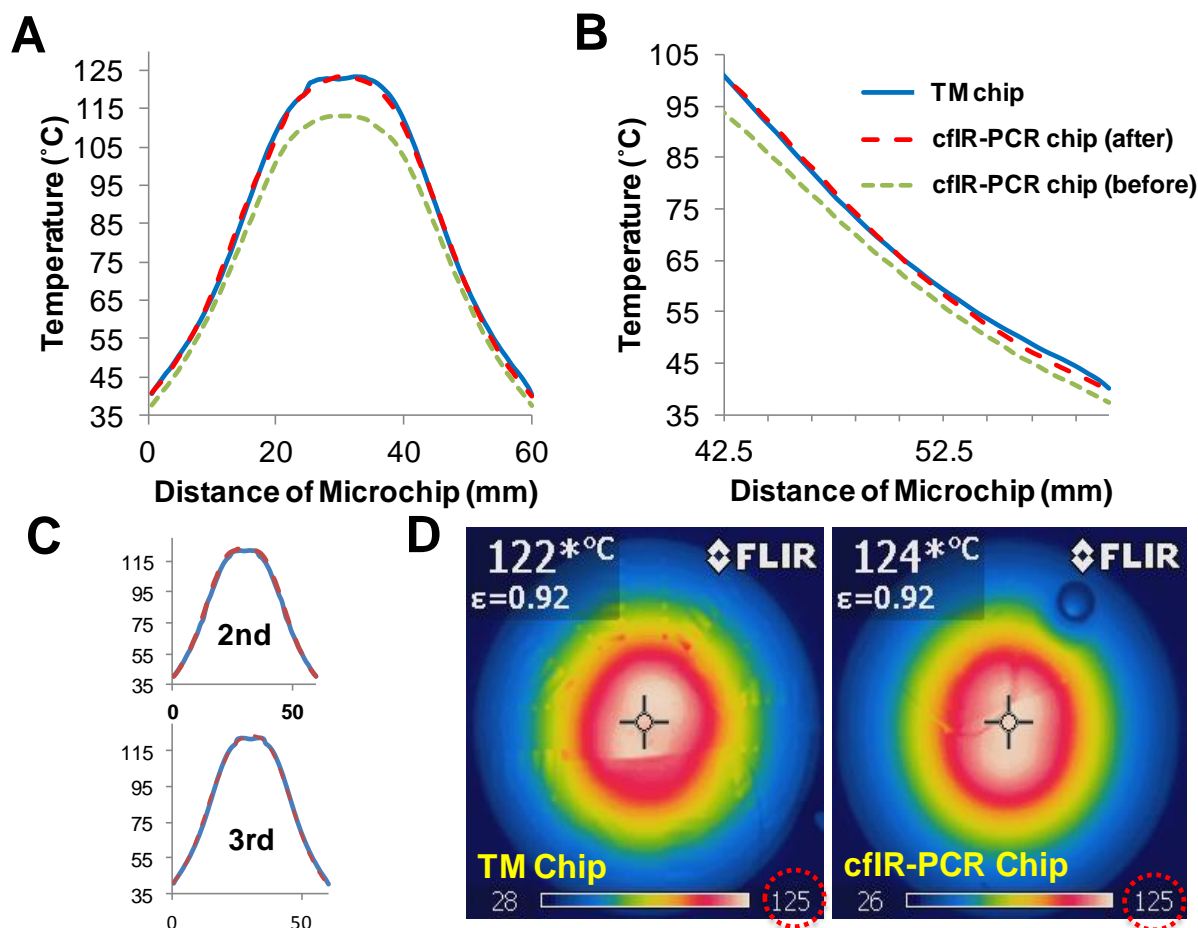


**Figure 4:** Temperature matching between the cfIR-PCR and TM microdevices via IR-camera. (A) 2D plot describing the distance of the microchip versus temperature distribution on two microchips: **Blue**, **green dot**, and **red dot** lines indicated temperature distributions on the TM microchip, the cfIR-PCR microchip before matching, and the cfIR-PCR microchip after matching, respectively. (B) Close-up view of the 2D plot describing temperature gradients on the TM and cfIR-PCR microchips (before and after matching). (C) This comparison was conducted three times to show consistency. (D) Two thermal images matched by IR-camera to show the same thermal gradient (maximum temperature; **red dot circle**) between the TM chip and the cfIR-PCR microchip.

gradient was further improved via matching two thermal images. By comparing the maximum temperatures of two thermal images taken by the IR-camera (**Fig. 4**), the thermal gradient on the cfIR-PCR microdevice was adjusted by the reference thermocouple and the efficiency of cfIR-PCR was improved to acquire DNA amplifications from low copy numbers of template DNA such as the human genome (at least  $\sim 10^2$  or  $10^3$  copies/ $\mu\text{L}$ ). After DNA analysis of 10 fraction

samples in Agilent 2100 Bioanalyzer, multiple overlaid electropherograms were aligned to indicate series of  $\lambda$ -DNA PCR products from ten consecutive fractions as a function of time (seconds) (**Fig. 5A**). DNA amplifications sequentially grew to reach the highest peak and the main reason, we believe, comes from a dynamic passivation process that might gradually occur through microchannels while passing through. Using our setup, we achieved successful DNA amplification of a 520 bp  $\lambda$ -phage fragment and it showed that our heating system could provide an appropriate thermal gradient for thermocycling and consequent PCR amplification.

### 2.3.5 *Demonstration of Effect of Flow Rates on PCR Efficiency*

Regarding cf-PCR, reaction time can be controlled by the flow rate of reagents without any limitation of temperature transition by the PCR instrument itself<sup>21</sup>. In order to assess our instrument, cfIR-PCR was carried out in the 29-loop cfIR-PCR microdevice at different flow rates ranging from 2  $\mu\text{L}/\text{min}$  to 9  $\mu\text{L}/\text{min}$ . These ranges of flow rates offered reaction time from 22 minutes to 5 minutes, which were obtained from actual dwell time experiments (**Table 3**). The yield quality and quantity of cfIR-PCR amplification were comparable to standard PCR on the thermal cycler. From 5  $\mu\text{L}$  of 10 aliquots out of the 50  $\mu\text{L}$  PCR sample, the highest peak (fraction) (**Fig. 5A**) was selected from the each flow rate (2  $\mu\text{L}/\text{min}$ , 3 $\mu\text{L}/\text{min}$ , 4.5 $\mu\text{L}/\text{min}$ , 6 $\mu\text{L}/\text{min}$ , 7.5 $\mu\text{L}/\text{min}$ , and 9 $\mu\text{L}/\text{min}$ ) and these highest peaks were compared with DNA amplifications from a positive control on the conventional thermocycler. As we expected, faster reactions led to fewer DNA amplifications (**Fig. 5B**). Comparing to the amplification time of a positive control, 90 minutes, all DNA amplifications occur within 20 minutes and the minimum reaction time was within 5 minutes, which indicated 4 to 20 times reduction in PCR amplification time, comparing to the conventional counterpart.

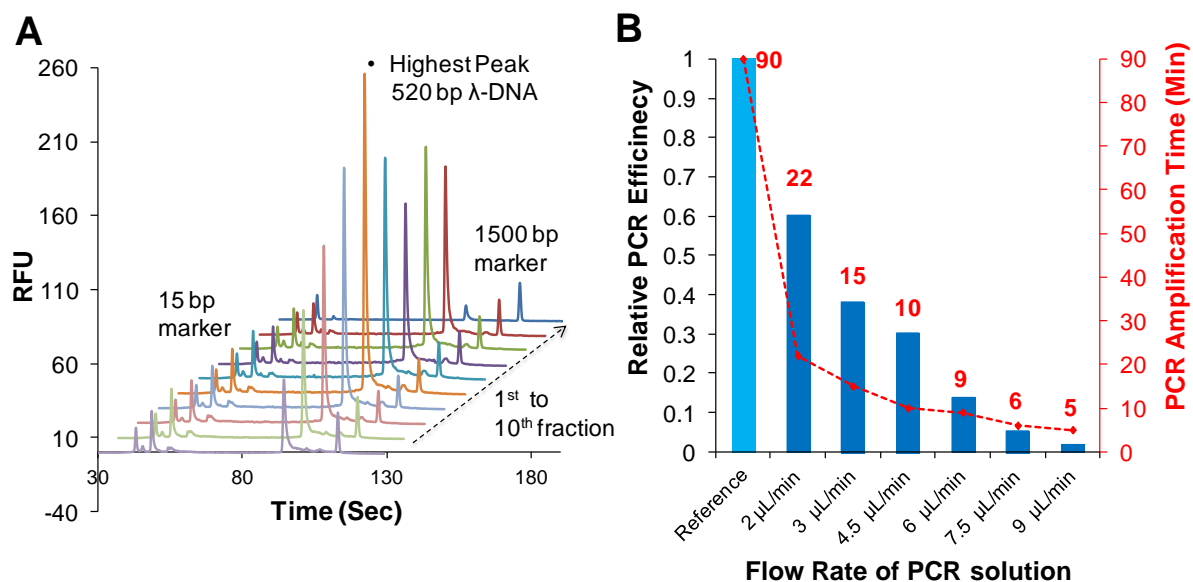


**Figure 5:** cfIR-PCR amplification in the 29-loop microdevice. (A) Electropherogram series of  $\lambda$ -DNA PCR product from 10 consecutive fractions, showing increasing (and eventual plateauing of) product peak heights, demonstrating passivation of the microchannel walls by the PCR mixture as it flows through the device. (B) Relative PCR efficiency and overall PCR time (red) for different flow rates from 2  $\mu\text{L}/\text{min}$  to 9  $\mu\text{L}/\text{min}$ . Relative PCR efficiency was obtained by comparing the highest PCR product the plateau (obtained from the Bioanalyzer data) from each flow rate to conventional tube PCR (set efficiency = 1). “PCR Amplification Time (min)” indicates the actual dwell times at the different flow rates.

The reduced amplification efficiency at flow rates over 7.5  $\mu\text{L}/\text{min}$  might be caused by enzyme kinetics, not having enough times for DNA denaturation and extension. However, fast and engineered *Taq* polymerase could not be used in our setup due to longer pre-denaturation time such as 5 - 10 minutes. Additionally, the low yield of the PCR product over 7.5  $\mu\text{L}/\text{min}$  was as a result of low denaturation temperature that would be caused by fast flow of the PCR solution in the denature, anneal, and extension zones. Furthermore, using serially diluted DNA templates, the minimum template concentration that could be amplified and detectable via Agilent 2100 Bioanalyzer was assessed and it was more than 0.4 ng/ $\mu\text{L}$  in the 29-loop cfIR-PCR

microdevice (data not shown). No peak could describe about lower amplifications than the detection limit of Bioanalyzer or rather than no amplification.

### 2.3.6 Thermal Modeling and Consideration of PCR Efficiency

As previous studies have shown that thermal modeling could effectively assist us to increase the PCR yield in cf-PCR systems<sup>22,28</sup>, heat transfer between the PMMA microchannel and the PCR solution should be considered as the critical factor in successful PCR. In order to assess effective heat transfer at various flow rates, a numerical study using Computational Fluid Dynamics (CFD) was performed to study the effect of volumetric flow rates on the temperature distribution in the fluidic layer of the cfIR-PCR microdevice. From this thermal modeling, it was assumed that we could get a maximum flow rate that should not disrupt the thermal gradient while flowing the PCR solution. This maximum flow rate could be applicable to achieve rapid PCR amplification in our microdevice. Using the ANSYS CFX program, the computational

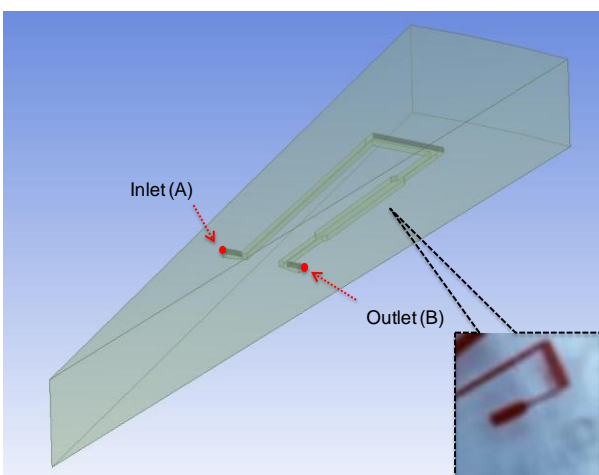


**Figure 6:** One piece of a loop (segment) for 3D thermal modeling of Computational Fluid Dynamics (CFD). *Inset:* a close view of the PCR solution while passing through the microchannel.

simulation was performed using the thermal gradient established on the top and bottom surfaces of the TM microdevice. All modeling was conducted only on one piece of a loop in the cfIR-PCR microdevice and it simplified simulation process (**Fig. 6**). The flow inlet (A point) was chosen at the first entrance of the denaturation zone that was located at the center of the denaturation zone and the outlet (B point) was in the same place

of the next loop in the denature zone. In this study, we focused on finding the temperature difference between A and B points (temperature inconsistency in two denature zones), which should be very critical to conduct efficient DNA amplifications as a result of the complete denaturation of DNA templates in the PCR process. Additionally, as the typical Reynolds number associated with the flow in our model was

$$Re = \frac{\rho U D}{\mu} \sim 0.6 \quad (2.1)$$

In the equation for  $Re$ ,  $U$  is the calculated average velocity inside the channel ( $U = 0.0028 \frac{m}{s}$  for the case with the highest volumetric flow rate of  $10 \mu\text{L/min}$ ),  $D$  is the diameter of the channel ( $D = 0.2 \text{ mm}$ ),  $\rho$  and  $\mu$  are density and dynamic viscosity of the water in **Table 1**, the flow is safely assumed to be laminar and therefore no turbulence model is used. As a result of complexity in the geometry, an unstructured mesh was used to accurately model the segment. **Figure 7** indicates simulated thermal images at three different flow rates (0, 4, and  $10 \mu\text{L/min}$ ) with the meshed structure of one segment (**Fig. 7A**). When the flow of the PCR solution changed from the static state (**Fig. 7B**) to  $4 \mu\text{L/min}$  (**Fig. 7C**), the established thermal gradient in

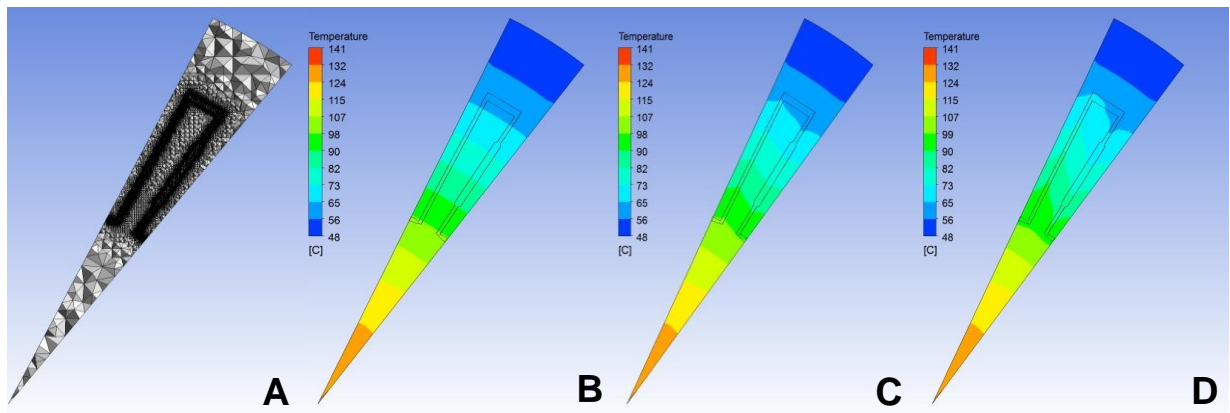


**Figure 7:** Meshed structure and thermal gradient images in fluidic channels of the cfIR-PCR microdevice. (A) Meshed structure of one segment for CFD. (B) Thermal image at the static state. (C) Thermal image at  $4 \mu\text{L/min}$ , and (D) at  $10 \mu\text{L/min}$ .

the PCR solution was slightly moved forward. Finally, the thermal gradient was partially disrupted to presumably prohibit efficient DNA amplification at 10  $\mu\text{L}/\text{min}$  (**Fig. 7D**).

To evaluate the temperature difference between point A and B, and the thermal gradient on the microchip, several simulations were carried out at different flow rates ranging from 0 to 10  $\mu\text{L}/\text{min}$  in multiple segments. Beyond one segment, thermal modeling was expanded to a series of segments on the outlet-inlet temperature difference (to duplicate the scenario where the flow circulates though the circular device as is shown schematically in **Fig. 8**) and it was sufficient to use the calculated outlet temperature for a given volumetric flow rate as the inlet temperature for a new simulation at the same volumetric flow rate. This process was repeated four times to obtain accumulated temperature differences through passing a total number of four

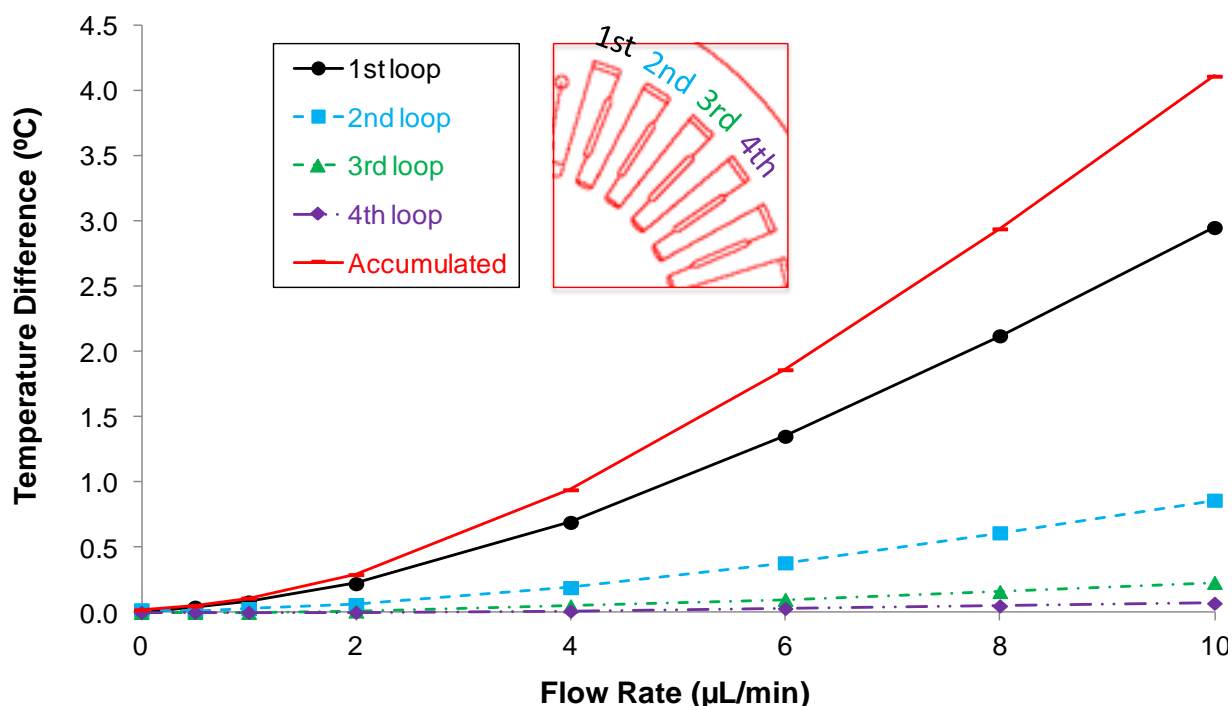


**Figure 8:** Plot describing temperature differences between inlet (A) and outlet (B) of two consecutive denature zones at various flow rates ranging from 0 to 10  $\mu\text{L}/\text{min}$ . After passing consecutive 4 loops of the microdevice, the thermal gradient in the PCR sample is stabilized to reach a fixed thermal gradient in all other loops at all flow rates (up to 10  $\mu\text{L}/\text{min}$ ), which proved that fixed temperature differences could be applied to all other loops after passing 4 loops.

segments. **Figure 8** plot shows the difference between temperatures of the inlet (A) and of the outlet (B) as a function of the volumetric flow rate. As is depicted in this plot (**Fig. 8**), the temperature difference increased monotonically as a function of the volumetric flow rate for a single segment. However, the temperature difference (for each segment) rapidly reduced as the flow circulates through more segments. This observation confirms that heat transfer between the PCR solution and PMMA microchip reaches equilibrium after circulating through approximately 4 segments.

From **figure 8**, we could assume that increased flow rates caused reduced denaturation temperature at the denaturation zone, which might be critical for proper denaturation of the DNA template over 7.5  $\mu\text{L}/\text{min}$ . Furthermore, it was proven by PCR amplifications on the 29-loop microdevice that the efficiency of PCR dramatically reduced from 7.5  $\mu\text{L}/\text{min}$ . However, at 9  $\mu\text{L}/\text{min}$ , the maximum flow rate tested in this study, final stabilized (accumulated) temperature in the denaturation zone after passing four segments was higher than 90 °C that is just 5 degree lower than the standard denature temperature, 95 °C. It should be a suitable temperature for denaturing the DNA template. But, it was not effective or dwell times should be considered together. From **Table 3**, dwell times over 7.5  $\mu\text{L}/\text{min}$  were around 2 -3 seconds. If temperature in the PCR solution was at 90 °C while passing the denaturation zone, the 2 -3 seconds might reduce the PCR efficiency in addition to lower extension times that was around 4 - 5 seconds over 7.5  $\mu\text{L}/\text{min}$ .

### 2.3.7 Surface Passivation and Emulsion cfIR-PCR

The micro-scale of the PCR chamber in microfluidic devices creates a significantly high surface to volume ratio that increases the importance of surface chemistry between PCR reagents and surface material<sup>60</sup>. Several studies have reported that both glass and polymeric microdevices need passivation reagents preventing the absorption of PCR reagents on the surface of the microchannel to improve DNA amplification, although they have different surface properties<sup>9,18,60-62</sup>. The surface area to volume ratio may determine types of a passivation method and amounts of passivation reagents. After the introduction of microchip PCR, many passivation reagents such as BSA<sup>63</sup>, PVP<sup>18</sup>, Tween 20<sup>64</sup>, and PEG<sup>65</sup>, and different passivation approaches (static or dynamic passivation) such as chemical silanization and surface modification have been

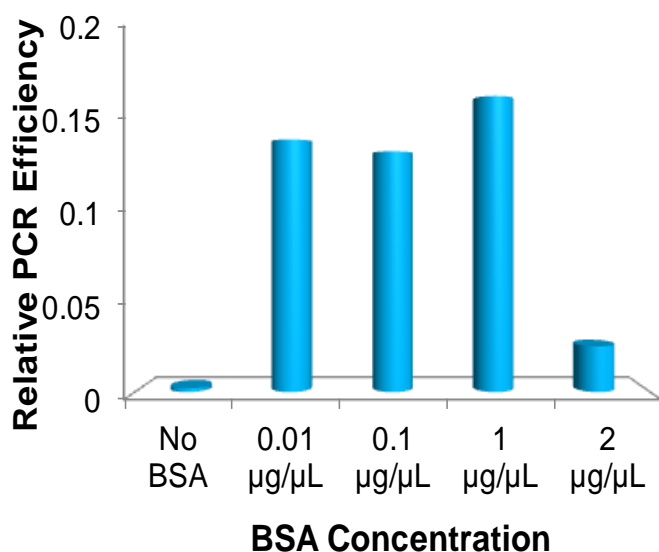


**Figure 9:** Relative PCR efficiency at four different BSA concentrations in the 29-loop cfIR-PCR microdevice. Each PCR efficiency indicates the mean amplification efficiency in each fraction; it was obtained by the summation of PCR product concentrations of 10 fractions at 4.5 µL/min, which was divided by the number of fractions.

studied<sup>18</sup>, sometimes, combination of several approaches to make the PCR chamber PCR friendly in the silicon and glass microfluidic devices<sup>18,66,67</sup>.

Initially, two well-known passivation reagents in microchip PCR, BSA and PEG were tested in the 29-loop cfIR-PCR microdevices using the λ-DNA template. The experiment for optimization of BSA concentrations (from zero to 2 mg/mL) illustrated that the concentration range of BSA should be from 0.1 to 2 mg/mL to obtain

enough DNA amplifications (**Fig. 9**). Therefore, there would be a certain ranges of BSA concentrations that led to effective PCR amplification. However, over or under this range of BSA concentrations, PCR amplification might be inhibited. From this observation, 1 mg/mL of BSA was utilized for DNA amplifications in the 29-loop cfIR-PCR microdevice. In addition, Polyethylene glycol (PEG<sub>10,000</sub>), a common reagent to convert the surface resistant to protein adsorption<sup>19</sup>, was tested as the passivation reagent. However, it could not improve PCR efficiency higher than BSA, and PEG might be effective for having a very high surface-to-volume ratio in the static PCR chamber of polymeric microdevices<sup>18</sup>.

In addition to a passivation issue, certain amounts of air bubbles were generated while the PCR cocktail flowed through a PMMA microchannel. These bubbles usually generated in the denature zone where small bubbles encountered each other to make large air bubbles. Sometimes, these large bubbles disrupted flowing of the PCR solution that influenced PCR efficiency. There have been several approaches to minimizing air bubble formation while conducting microchip PCR for both of static<sup>19,20</sup> and continuous formats<sup>68,69</sup>. Nakayama *et al.*<sup>68</sup> used a mineral oil followed by the PCR sample. This configuration avoided direct contact of the PCR solution to air and condensed oil in the front stabilized flow of the PCR sample. Disruption of stable flow in the PCR solution was the critical inhibitor of PCR amplification. Furthermore, Phaneuf *et al.*<sup>71</sup> have proven that the mineral oil encapsulated PCR samples could improve PCR amplifications in the polymeric microdevice compared to BSA-passivated microchip PCR on the static chamber. Referring to these studies, the emulsion PCR method (**Fig. 10**), which has been introduced to conduct high-throughput PCR and construction of libraries to be screened<sup>70</sup>, was used to solve issues associated with passivation and air bubble formation in present work. So, emulsion PCR was conceived to perform cfIR-PCR in the 43-loop microdevice. The mixture of the PCR

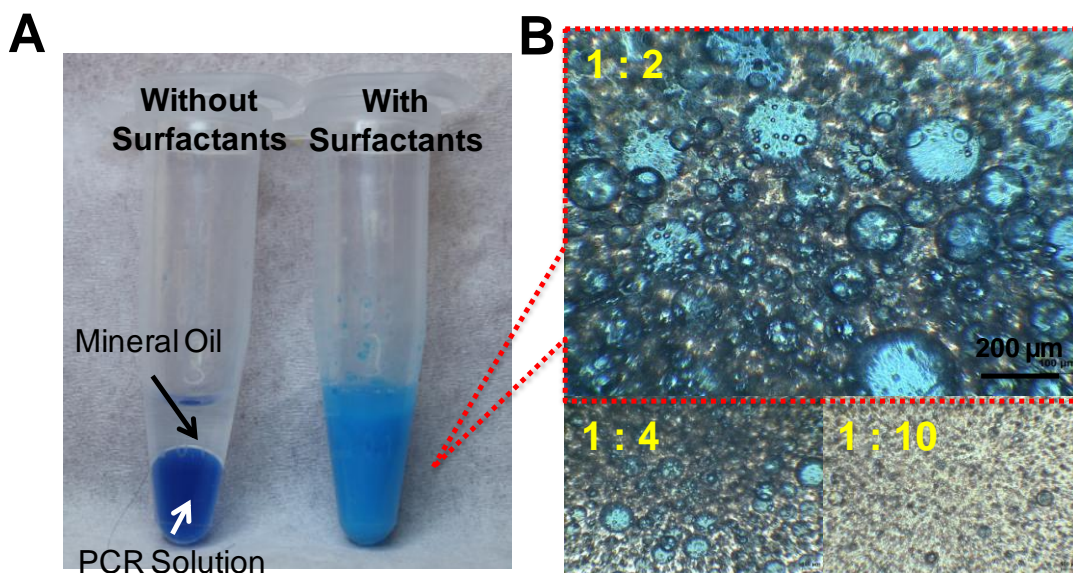


**Figure 10:** The oil-surfactant mixed with the PCR sample for emulsion cfIR-PCR. (A) Comparison between two PCR solutions without (left) and with (right) surfactants (4.5 % (v/v) Span 80, 0.4 % (v/v) Tween 20, and 0.05 % (v/v) Triton X-100) added to the oil-sample mixture and mixed by pipetting [70]. (B) Microscope images of PCR emulsion; the ratio of PCR mixture to the oil-surfactant mixture has been changed from 1 : 2 to 1 : 10. The ratio of 1 : 2 was used for emulsion cfIR-PCR in preset work.

solution with the oil-surfactant mixture as the ratio of 1 : 2 was used to generate large numbers of droplets and this PCR emulsion sample was loaded into the cfIR-PCR microdevice (**Fig. 10A and B**). These encapsulated small droplets (PCR emulsion sample) could be minimized to contact the air and the wall of the microchannel and consequently it removed the passivation problem and the emulsion oil maintained constant flow of the PCR emulsion sample through the microchannel so that the efficiency of PCR improved; small volumes of the PCR sample such as 5 or 10 μL without any oil-surfactant mixture could not produce any PCR amplification from the human genome.

In order to compare PCR efficiency between BSA and emulsion PCR, emulsion cfIR-PCR was conducted using two concentrations of DNA templates (4 ng/μL and 40 ng/μL) with

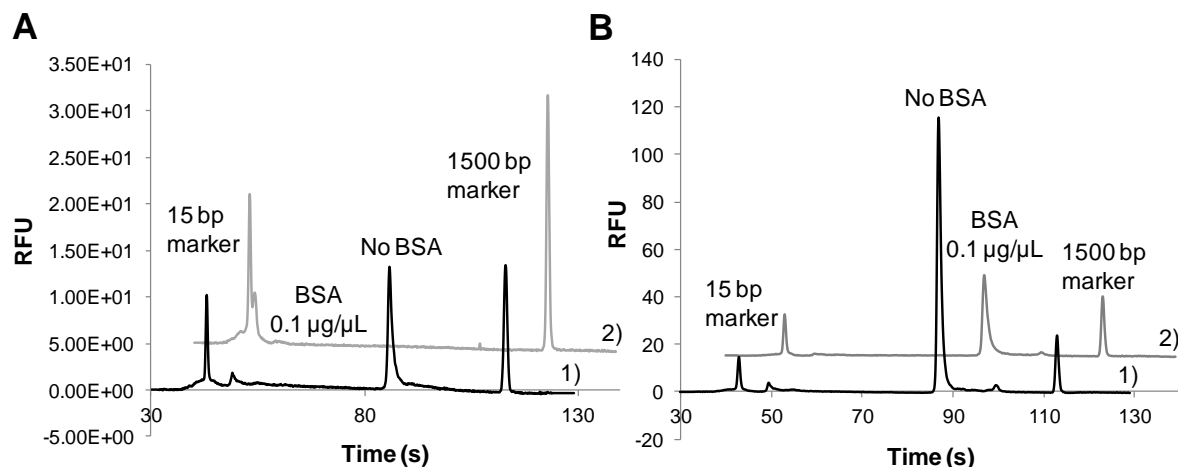


**Figure 11:** Genomic DNA amplifications using different concentrations of the DNA template and BSA in the 43-loop cfIR-PCR microdevice. (A) Overlaid electropherograms show cfIR-PCR amplifications from 4 ng/μL of the DNA template with 1) no BSA and 2) 0.1 μg/μL BSA (B) from 40 ng/μL of DNA with 1) no BSA and 2) 0.1 μg/μL BSA.

and without BSA (**Fig. 11**). The emulsion PCR sample was comprised of 10 μL PCR sample and 20 μL oil-surfactant mixture. These results indicated that emulsion could improve PCR efficiency without adding any passivation reagent and it was slightly better than the BSA passivation approach. Eventually, in our study using the emulsion cfIR-PCR approach, fairly consistent DNA amplifications of a 380 bp DNA segment in the beta-globin gene were accomplished from the human genome.

### 2.3.8 Genomic DNA Amplification via Continuous Segmented Flows

Genomic DNA amplification in microchips needs more accurate temperature control at the earlier stage of amplifications, especially for denaturation. In addition, the high efficiency of PCR or large numbers of cycle should be required, compared to DNA amplification from a high copy numbers of DNA templates. From λ-DNA amplification on the 29-loop cfIR-PCR microdevice, PCR efficiency in our initial setup was calculated and the number of loops was

more added into the design of the cfIR-PCR microdevice to obtain PCR products from low copy numbers of genomic DNA. As one important limitation in our approach, large amounts of loops in the small area of the microchip center around the denaturation region could cause the difficulty of microchip fabrication as a result of the distortion of fluidic layers and misalignment while bonding three layered sheets. Finally, the 43-loop cfIR-PCR microdevice was conceived to carry out cfIR-PCR for genomic DNA amplifications. First of all, a 380 bp of beta-globin fragment was amplified via this 43-loop cfIR-PCR microdevice using our emulsion cfIR-PCR approach. The emulsion (20  $\mu\text{L}$ ) and PCR sample (10  $\mu\text{L}$ ) were completely mixed with pipetting

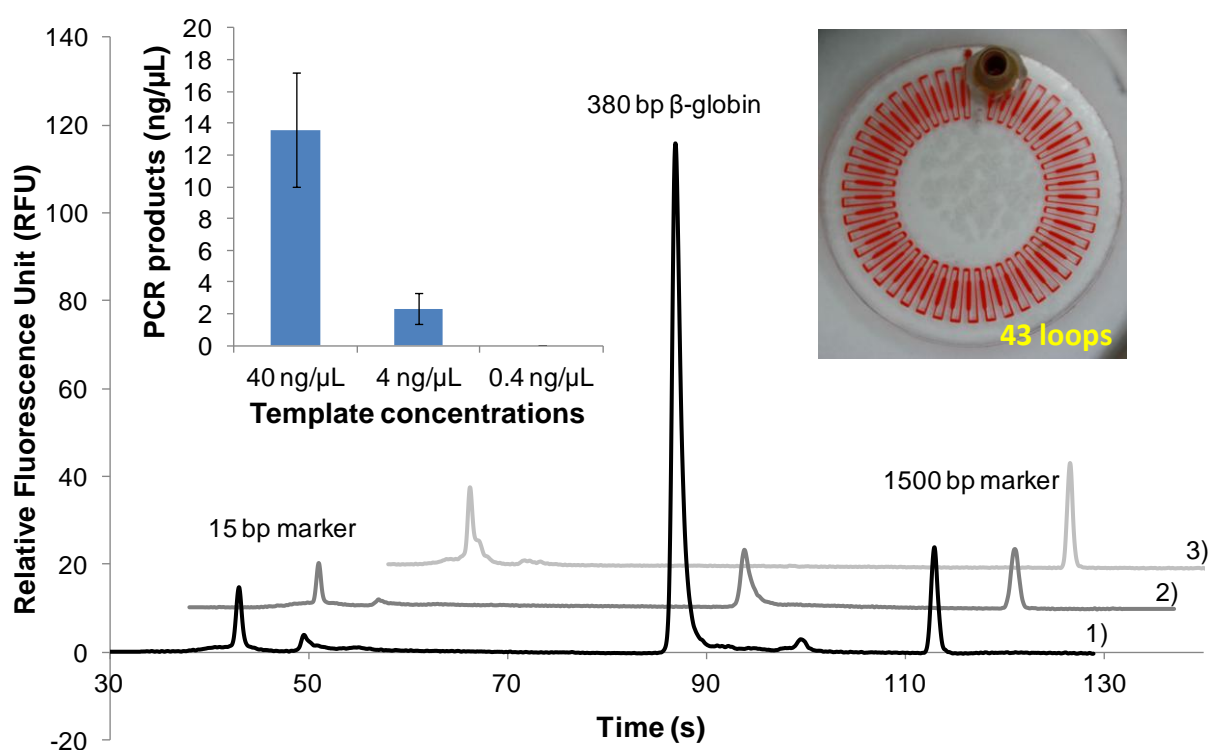


**Figure 12:** Emulsion cfIR-PCR (10  $\mu\text{L}$  PCR sample and 20  $\mu\text{L}$  oil-surfactant mixture) in the 43-loop microdevice. Multiple electropherograms showing successful 3 repeated amplifications of  $\beta$ -globin from different concentrations of human genomic DNA; 1) 40, 2) 4, and 3) 0.4 ng/ $\mu\text{L}$ ) using emulsion mixtures on a 43-loop cfPCR microdevice at 2  $\mu\text{L}/\text{min}$ . *Left inset:* PCR products from different template concentrations and *right inset:* the picture of the 43-loop cfIR-PCR microdevice for DNA amplification from the human genome.

and pumped into the microdevice. Three repeated beta-globin amplifications from different concentrations of templates ranging from 0.4 ng/ $\mu$ L ( $\sim 10^2$  copies/ $\mu$ L) to 40 ng/ $\mu$ L ( $\sim 10^4$  copies/ $\mu$ L) were achieved (**Fig. 12**). The human genomic DNA amplifications from the beta-globin gene has been accomplished within 30 minutes that achieved 4 times reduction in PCR analysis (2 hours to 30 minutes) and at least 4 ng/ $\mu$ L of human genome ( $\sim 10^3$  copies/ $\mu$ L) was required to conduct cfIR-PCR for human genomic amplifications.

In order to show cfIR-PCR via multiple segmented flows, continuous segmented plug

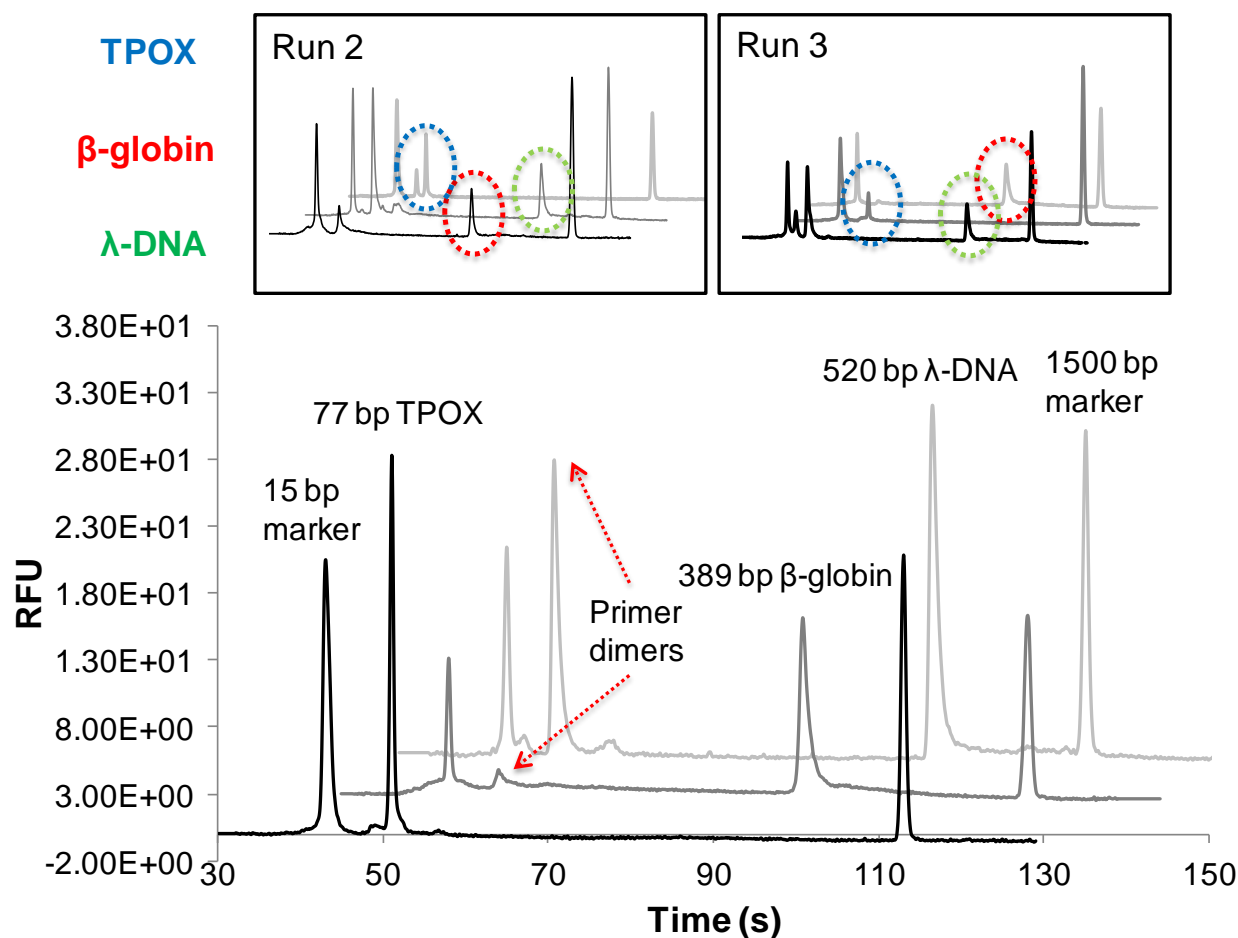


**Figure 13:** cfIR-PCR via segmented plug flows. Segmented flows of three different samples ran through the 43-loop cfIR-PCR microdevice at 2  $\mu$ L/min. The order of three different samples (TPOX locus –  $\beta$ -globin –  $\lambda$ -phage) were alternatively changed to conduct three different replicates. The blue, red, and green circles indicated peaks for TPOX,  $\beta$ -globin, and  $\lambda$ -phage, respectively.

flows were applied for sequential DNA amplifications using three different targets (beta-globin, TPOX locus, and  $\lambda$ -DNA segments) to show the capability of multiple and high-throughput genetic analysis (**Fig. 13**) with droplet technologies. A mixture of the oil-surfactant (10  $\mu$ L) and three different PCR samples (5  $\mu$ L) were mixed and loaded in the form of small segments separated by 5  $\mu$ L of the mineral oil into the cfIR-PCR devices, and these samples were repeatedly exposed to the thermal gradient for cfIR-PCR. Additionally, the order of segmented flows was alternatively changed to repeatedly show three different DNA amplifications. The selected DNA regions from human and  $\lambda$ -genomes were successfully amplified using 5  $\mu$ L PCR mixture at 2  $\mu$ L/min that took 30 minutes to complete cfIR-PCR (**Fig. 13**). The carryover and cross contamination would be minimized by the separation of the mineral oil and the encapsulation into small droplets surrounded by the oil-surfactant mixture. Furthermore, low anneal temperature at 57 °C in the cfIR-PCR microdevice generated different amounts of dimer formations from three PCR products. Especially, the primer sets for the  $\lambda$ -phage segment (at 68 °C) and human beta-globin segment (at 62 °C) produced certain amounts of dimer formations in electropherograms. However, anneal temperature for the primer set of TPOX locus was 58 °C so that any primer dimer was not detectable in the electropherogram. Therefore, the adjustment of primer sequences for multiple-segmented flow PCR should be required to improve PCR efficiency further. From DNA amplifications from segmented flows of PCR samples, we assert that the adequate automated system that can reduce PCR sample volumes more and continuously delivery small volumes of different PCR samples will guarantee a high-throughput manner of multiple segmental or droplet PCR possibly using our concept of cfIR-PCR.

## 2.4 Conclusions

In this study, we are reporting the first approach of continuous flow PCR on the microfluidic devices using a prototypical noncontact heating device "(i.e. an IR lamp)". A single lamp heating could rapidly generate the thermal gradient across the polymeric microdevice and this established thermal gradient was measured and confirmed using two types of temperature measurement methods such as a thermocouple and IR-camera. The PCR solution was continuously flowed on three different PCR regions (denature, anneal, and extension zones) to carry out cfIR-PCR. Consequently, repeated promising DNA amplifications from the  $\lambda$ -phage and human genome were illustrated around 30 minutes, at least 5 minutes from the  $\lambda$ -DNA. The resulting data demonstrated that our thermal gradient should be reasonably measured and controlled to conduct thermal gradient PCR on the polymeric microdevice. Furthermore, segmented flow PCR from three different samples was successfully reported. The emulsion PCR approach was employed to improve PCR efficiency via eliminating microchip passivation and compartmentalize the segments from each sample, which was ultimately utilized to conduct genomic DNA amplifications from a low copy number of DNA templates without any cross-contamination;  $\sim 10^3$  copies/ $\mu\text{L}$  in the template concentration was required to product detectable amounts of DNA amplifications in the 43-loop cfIR-PCR microdevice within 30 minutes. The key elements in the success of rapid cfIR-PCR should be to establish 1) appropriate design of polymeric cfIR-PCR microdevices to improve thermal transfer between a reaction reagent and a microchip material, 2) optimal flow rates to achieve enough heating of the PCR mixture in each PCR zone, and 3) appropriate surface passivation in microfluidic devices. Conclusively, the automation of our cfIR-PCR setup with droplet technologies should have potential for rapid

high-throughput genetic analysis, with encapsulating single cells inside each droplet for single cell analysis.

## 2.5 References

- (1) Mullis, K.; Faloona, F.; Scharf, S.; Saiki, R.; Horn, G.; Erlich, H. Specific Enzymatic Amplification of DNA Invitro - the Polymerase Chain-Reaction. *Cold Spring Harbor Symposia on Quantitative Biology* **1986**, *51*, 263-273.
- (2) Landers, J. P. Molecular diagnostics on electrophoretic microchips. *Anal Chem* **2003**, *75*, 2919-27.
- (3) Verpoorte, S.; Northrup, M. A.; Yager, P.; Quake, S.; Landers, J. Microtechnology in the clinical laboratory: will it solve analytical problems, and when will it make an impact?. *Clin Chem*, *56*, 508-14.
- (4) Park, S.; Zhang, Y.; Lin, S.; Wang, T. H.; Yang, S. Advances in microfluidic PCR for point-of-care infectious disease diagnostics. *Biotechnol Adv* **2011**, *29*, 830-9.
- (5) Horsman, K. M.; Bienvenue, J. M.; Blasier, K. R.; Landers, J. P. Forensic DNA analysis on microfluidic devices: a review. *J Forensic Sci* **2007**, *52*, 784-99.
- (6) Velusamy, V.; Arshak, K.; Korostynska, O.; Oliwa, K.; Adley, C. An overview of foodborne pathogen detection: In the perspective of biosensors. *Biotechnology Advances* **2010**, *28*, 232-254.
- (7) Lazcka, O.; Del Campo, F. J.; Munoz, F. X. Pathogen detection: a perspective of traditional methods and biosensors. *Biosensors & Bioelectronics* **2007**, *22*, 1205-1217.
- (8) Lui, C.; Cady, N. C.; Batt, C. A. Nucleic Acid-based Detection of Bacterial Pathogens Using Integrated Microfluidic Platform Systems. *Sensors* **2009**, *9*, 3713-3744.
- (9) Giordano, B. C.; Ferrance, J.; Swedberg, S.; Huhmer, A. F. R.; Landers, J. P. Polymerase chain reaction in polymeric microchips: DNA amplification in less than 240 seconds. *Analytical Biochemistry* **2001**, *291*, 124-132.
- (10) Beer, N. R.; Hindson, B. J.; Wheeler, E. K.; Hall, S. B.; Rose, K. A.; Kennedy, I. M.; Colston, B. W. On-chip, real-time, single-copy polymerase chain reaction in picoliter droplets. *Analytical Chemistry* **2007**, *79*, 8471-8475.
- (11) Easley, C. J.; Karlinsey, J. M.; Bienvenue, J. M.; Legendre, L. A.; Roper, M. G.; Feldman, S. H.; Hughes, M. A.; Hewlett, E. L.; Merkel, T. J.; Ferrance, J. P.; Landers, J. P. A fully integrated microfluidic genetic analysis system with sample-in-answer-out capability. *Proceedings of the National Academy of Sciences of the United States of America* **2006**, *103*, 19272-19277.
- (12) Liu, P.; Mathies, R. A. Integrated microfluidic systems for high-performance genetic analysis. *Trends Biotechnol* **2009**, *27*, 572-81.
- (13) Fiorini, G. S.; Chiu, D. T. Disposable microfluidic devices: fabrication, function, and application. *Biotechniques* **2005**, *38*, 429-46.
- (14) Curcio, M.; Roeraade, J. Continuous segmented-flow polymerase chain reaction for high-throughput miniaturized DNA amplification. *Anal Chem* **2003**, *75*, 1-7.
- (15) Schaerli, Y.; Wootton, R. C.; Robinson, T.; Stein, V.; Dunsby, C.; Neil, M. A.; French, P. M.; Demello, A. J.; Abell, C.; Hollfelder, F. Continuous-flow polymerase chain reaction of single-copy DNA in microfluidic microdroplets. *Anal Chem* **2009**, *81*, 302-6.

- (16) Roper, M. G.; Easley, C. J.; Landers, J. P. Advances in polymerase chain reaction on microfluidic chips. *Anal Chem* **2005**, *77*, 3887-93.
- (17) Oda, R. P.; Strausbauch, M. A.; Huhmer, A. F.; Borson, N.; Jurens, S. R.; Craighead, J.; Wettstein, P. J.; Eckloff, B.; Kline, B.; Landers, J. P. Infrared-mediated thermocycling for ultrafast polymerase chain reaction amplification of DNA. *Anal Chem* **1998**, *70*, 4361-8.
- (18) Giordano, B. C.; Copeland, E. R.; Landers, J. P. Towards dynamic coating of glass microchip chambers for amplifying DNA via the polymerase chain reaction. *Electrophoresis* **2001**, *22*, 334-340.
- (19) Lounsbury, J. A.; Poe, B. L.; Do, M.; Landers, J. P. Laser-ablated poly(methyl methacrylate) microdevices for sub-microliter DNA amplification suitable for micro-total analysis systems. *Journal of Micromechanics and Microengineering* **2012**, *22*.
- (20) Lounsbury, J. A.; Miranian, D. C.; Landers, J. P. A multi-chamber microdevice for simultaneous amplification up to seven individual samples using infrared-mediated PCR. In *Proceedings of the 15th international conference on miniaturized systems for chemistry and life sciences*, Seattle, WA, USA, **2011**, p 750-752.
- (21) Kopp, M. U.; de Mello, A. J.; Manz, A. Chemical amplification: Continuous-flow PCR on a chip. *Science* **1998**, *280*, 1046-1048.
- (22) Hashimoto, M.; Chen, P. C.; Mitchell, M. W.; Nikitopoulos, D. E.; Soper, S. A.; Murphy, M. C. Rapid PCR in a continuous flow device. *Lab Chip* **2004**, *4*, 638-45.
- (23) Crews, N.; Wittwer, C.; Gale, B. Continuous-flow thermal gradient PCR. *Biomed Microdevices* **2008**, *10*, 187-95.
- (24) Sun, Y.; Satyanarayan, M. V. D.; Nguyen, N. T.; Kwok, Y. C. Continuous flow polymerase chain reaction using a hybrid PMMA-PC microchip with improved heat tolerance. *Sensors and Actuators B-Chemical* **2008**, *130*, 836-841.
- (25) Dorfman, K. D.; Chabert, M.; Codarbox, J. H.; Rousseau, G.; de Cremoux, P.; Viovy, J. L. Contamination-free continuous flow microfluidic polymerase chain reaction for quantitative and clinical applications. *Anal Chem* **2005**, *77*, 3700-4.
- (26) Obeid, P. J.; Christopoulos, T. K.; Crabtree, H. J.; Backhouse, C. J. Microfabricated device for DNA and RNA amplification by continuous-flow polymerase chain reaction and reverse transcription-polymerase chain reaction with cycle number selection. *Anal Chem* **2003**, *75*, 288-95.
- (27) Park, N.; Kim, S.; Hahn, J. H. Cylindrical compact thermal-cycling device for continuous-flow polymerase chain reaction. *Anal Chem* **2003**, *75*, 6029-33.
- (28) Li, S.; Fozdar, D. Y.; Ali, M. F.; Li, H.; Shao, D.; Vykoukal, D. M.; Vykoukal, J.; Floriano, P. N.; Olsen, M.; McDevitt, J. T.; Gascoyne, P. R.; Chen, S. A Continuous-Flow Polymerase Chain Reaction Microchip With Regional Velocity Control. *J Microelectromech Syst* **2006**, *15*, 223-236.
- (29) Chou, C. F.; Changrani, R.; Roberts, P.; Sadler, D.; Burdon, J.; Zenhausern, F.; Lin, S.; Mulholland, A.; Swami, N.; Terbrueggen, R. A miniaturized cyclic PCR device - modeling and experiments. *Microelectronic Engineering* **2002**, *61-2*, 921-925.
- (30) Njoroge, S. K.; Witek, M. A.; Battle, K. N.; Immethun, V. E.; Hupert, M. L.; Soper, S. A. Integrated continuous flow polymerase chain reaction and micro-capillary electrophoresis system with bioaffinity preconcentration. *Electrophoresis* **2011**, *32*, 3221-3232.
- (31) Kiss, M. M.; Ortoleva-Donnelly, L.; Beer, N. R.; Warner, J.; Bailey, C. G.; Colston, B. W.; Rothberg, J. M.; Link, D. R.; Leamon, J. H. High-Throughput Quantitative

- Polymerase Chain Reaction in Picoliter Droplets. *Analytical Chemistry* **2008**, *80*, 8975-8981.
- (32) Crews, N.; Wittwer, C.; Palais, R.; Gale, B. Product differentiation during continuous-flow thermal gradient PCR. *Lab Chip* **2008**, *8*, 919-24.
  - (33) Wu, W.; Lee, N. Y. Three-dimensional on-chip continuous-flow polymerase chain reaction employing a single heater. *Anal Bioanal Chem* **2011**, *400*, 2053-60.
  - (34) Wittwer, C. T.; Fillmore, G. C.; Hillyard, D. R. Automated Polymerase Chain-Reaction in Capillary Tubes with Hot Air. *Nucleic Acids Research* **1989**, *17*, 4353-4357.
  - (35) Kim, H.; Vishniakou, S.; Faris, G. W. Petri dish PCR: laser-heated reactions in nanoliter droplet arrays. *Lab Chip* **2009**, *9*, 1230-5.
  - (36) Pak, N.; Saunders, D. C.; Phaneuf, C. R.; Forest, C. R. Plug-and-play, infrared, laser-mediated PCR in a microfluidic chip. *Biomed Microdevices*, *14*, 427-33.
  - (37) Fermer, C.; Nilsson, P.; Larhed, M. Microwave-assisted high-speed PCR. *Eur J Pharm Sci* **2003**, *18*, 129-32.
  - (38) Shaw, K. J.; Docker, P. T.; Yelland, J. V.; Dyer, C. E.; Greenman, J.; Greenway, G. M.; Haswell, S. J. Rapid PCR amplification using a microfluidic device with integrated microwave heating and air impingement cooling. *Lab Chip* **2010**, *10*, 1725-8.
  - (39) Orrling, K.; Nilsson, P.; Gullberg, M.; Larhed, M. An efficient method to perform milliliter-scale PCR utilizing highly controlled microwave thermocycling. *Chem Commun (Camb)* **2004**, 790-1.
  - (40) Issadore, D.; Humphry, K. J.; Brown, K. A.; Sandberg, L.; Weitz, D. A.; Westervelt, R. M. Microwave dielectric heating of drops in microfluidic devices. *Lab Chip* **2009**, *9*, 1701-6.
  - (41) Wheeler, E. K.; Benett, W.; Stratton, P.; Richards, J.; Chen, A.; Christian, A.; Ness, K. D.; Ortega, J.; Li, L. G.; Weisgraber, T. H.; Goodson, K. E.; Milanovich, F. *Analytical Chemistry* **2004**, *76*, 4011-4016.
  - (42) Chung, K. H.; Park, S. H.; Choi, Y. H. A palmtop PCR system with a disposable polymer chip operated by the thermosiphon effect. *Lab on a Chip* **2010**, *10*, 202-210.
  - (43) Sun, Y.; Kwok, Y. C.; Nguyen, N. T. A circular ferrofluid driven microchip for rapid polymerase chain reaction. *Lab on a Chip* **2007**, *7*, 1012-1017.
  - (44) Leslie, D. C.; Seker, E.; Bazydlo, L. A.; Strachan, B. C.; Landers, J. P. Platinum nanoparticle-facilitated reflective surfaces for non-contact temperature control in microfluidic devices for PCR amplification. *Lab Chip* **2011**, *12*, 127-32.
  - (45) Sun, Y.; Kwok, Y. C.; Nguyen, N. T. Low-pressure, high-temperature thermal bonding of polymeric microfluidic devices and their applications for electrophoretic separation. *Journal of Micromechanics and Microengineering* **2006**, *16*, 1681-1688.
  - (46) Hutchinson, B. R.; Raithby, G. D. A Multigrid Method Based on the Additive Correction Strategy. *Numerical Heat Transfer* **1986**, *9*, 511-537.
  - (47) Sun, Y.; Kwok, Y. C. Polymeric microfluidic system for DNA analysis. *Anal Chim Acta* **2006**, *556*, 80-96.
  - (48) Becker, H.; Locascio, L. E. Polymer microfabrication technologies for microfluidic systems. *Talanta* **2002**, *56*, 267-287.
  - (49) Rotting, O.; Ropke, W.; Becker, H.; Gartner, C. Polymer microfabrication technologies. *Microsystem Technologies* **2002**, *8*, 32-36.
  - (50) Becker, H.; Gartner, C. Polymer microfabrication technologies for microfluidic systems. *Analytical and Bioanalytical Chemistry* **2008**, *390*, 89-111.

- (51) Klank, H.; Kutter, J. P.; Geschke, O. CO<sub>2</sub>-laser micromachining and back-end processing for rapid production of PMMA-based microfluidic systems. *Lab on a Chip* **2002**, 2, 242-246.
- (52) Cheng, J. Y.; Wei, C. W.; Hsu, K. H.; Young, T. H. Direct-write laser micromachining and universal surface modification of PMMA for device development. *Sensors and Actuators B-Chemical* **2004**, 99, 186-196.
- (53) Roberts, M. A.; Rossier, J. S.; Bercier, P.; Girault, H. UV laser machined polymer substrates for the development of microdiagnostic systems. *Analytical Chemistry* **1997**, 69, 2035-2042.
- (54) Muck, A.; Wang, J.; Jacobs, M.; Chen, G.; Chatrathi, M. P.; V, J.; Vyborny, Z.; Spillman, S. D.; Sridharan, G.; Schonung, M. J. Fabrication of poly(methyl methacrylate) microfluidic chips by atmospheric molding. *Analytical Chemistry* **2004**, 76, 2290-2297.
- (55) Kameoka, J.; Craighead, H. G.; Zhang, H. W.; Henion, J. A polymeric microfluidic chip for CE/MS determination of small molecules. *Analytical Chemistry* **2001**, 73, 1935-1941.
- (56) Brown, L.; Koerner, T.; Horton, J. H.; Oleschuk, R. D. Fabrication and characterization of poly(methylmethacrylate) microfluidic devices bonded using surface modifications and solvents. *Lab on a Chip* **2006**, 6, 66-73.
- (57) Tsao, C. W.; DeVoe, D. L. Bonding of thermoplastic polymer microfluidics. *Microfluidics and Nanofluidics* **2009**, 6, 1-16.
- (58) Wittwer, C. T.; Fillmore, G. C.; Garling, D. J. Minimizing the time required for DNA amplification by efficient heat transfer to small samples. *Anal Biochem* **1990**, 186, 328-31.
- (59) Oh, K.; Lounsbury, J. A.; Poe, B. L.; Keshishian, Z.; Landers, J. P. Continuous flow infrared polymerase chain reaction (cfIR-PCR) using an infrared-mediated heating system. In *Proceedings of the 16th international conference on miniaturized systems for chemistry and life sciences* Okinawa, Japan, **2012**, p 1606-1608.
- (60) Lou, X. J.; Panaro, N. J.; Wilding, P.; Fortina, P.; Kricka, L. J. Increased amplification efficiency of microchip-based PCR by dynamic surface passivation. *Biotechniques* **2004**, 36, 248.
- (61) Wilding, P.; Shoffner, M. A.; Cheng, J.; Hvichia, G.; Kricka, L. J. Pcr in a Silicon Microstructure. *Clinical Chemistry* **1995**, 41, 1367-1367.
- (62) Shoffner, M. A.; Cheng, J.; Hvichia, G. E.; Kricka, L. J.; Wilding, P. Chip PCR .1. Surface passivation of microfabricated silicon-glass chips for PCR. *Nucleic Acids Research* **1996**, 24, 375-379.
- (63) Burns, M. A.; Mastrangelo, C. H.; Sammarco, T. S.; Man, F. P.; Webster, J. R.; Johnsons, B. N.; Foerster, B.; Jones, D.; Fields, Y.; Kaiser, A. R.; Burke, D. T. Microfabricated structures for integrated DNA analysis. *Proc Natl Acad Sci U S A* **1996**, 93, 5556-61.
- (64) Sun, K.; Yamaguchi, A.; Ishida, Y.; Matsuo, S.; Misawa, H. A heater-integrated transparent microchannel chip for continuous-flow PCR. *Sensors and Actuators B-Chemical* **2002**, 84, 283-289.
- (65) Yang, J. N.; Liu, Y. J.; Rauch, C. B.; Stevens, R. L.; Liu, R. H.; Lenigk, R.; Grodzinski, P. High sensitivity PCR assay in plastic micro reactors. *Lab on a Chip* **2002**, 2, 179-187.
- (66) Lagally, E. T.; Simpson, P. C.; Mathies, R. A. Monolithic integrated microfluidic DNA amplification and capillary electrophoresis analysis system. *Sensors and Actuators B-Chemical* **2000**, 63, 138-146.

- (67) Lagally, E. T.; Medintz, I.; Mathies, R. A. Single-molecule DNA amplification and analysis in an integrated microfluidic device. *Analytical Chemistry* **2001**, *73*, 565-570.
- (68) Nakayama, T.; Kurosawa, Y.; Furui, S.; Kerman, K.; Kobayashi, M.; Rao, S. R.; Yonezawa, Y.; Nakano, K.; Hino, A.; Yamamura, S.; Takamura, Y.; Tamiya, E. Circumventing air bubbles in microfluidic systems and quantitative continuous-flow PCR applications. *Anal Bioanal Chem* **2006**, *386*, 1327-33.
- (69) Wu, W.; Kang, K. T.; Lee, N. Y. Bubble-free on-chip continuous-flow polymerase chain reaction: concept and application. *Analyst*, *136*, 2287-93.
- (70) Williams, R.; Peisajovich, S. G.; Miller, O. J.; Magdassi, S.; Tawfik, D. S.; Griffiths, A. D. Amplification of complex gene libraries by emulsion PCR. *Nat Methods* **2006**, *3*, 545-50.
- (71) Phaneuf, C. R.; Oh, K.; Pak, N.; Saunders, D. C.; Conrardy, C.; Landers, J. P.; Tong, S.; Forest, C. R., Sensitive, microliter PCR with consensus degenerate primers for Epstein Barr virus amplification. *Biomed Microdevices* *15*, (2), 221-31.

### **3. Microwave-mediated Thermal Cycling System**

#### **3.1 Introduction**

##### *3.1.1 Applications of Microwave Heating Systems and Characteristics*

The initial idea of microwave energy to heat materials that consist of polar molecules was conceived by Raytheon engineer Dr. Percy LeBaron Spencer while conducting a magnetron installation in the radar system of the United Kingdom. From his idea<sup>1</sup>, a microwave oven was first commercialized for the purpose of cooking, named “radarange” in 1947. In addition to food processing<sup>2</sup>, microwave has been utilized for chemical and biological applications, such as organic synthesis<sup>3</sup>, sterilization<sup>4</sup>, and sample extraction<sup>5</sup>, drug discovery (combinatorial organic synthesis)<sup>6</sup>, and cell lysis for DNA isolation<sup>7,8</sup>. There are following merits in microwave heating compared to other types of heating methods. Direct coupling of dielectric energy with a reaction fluid under the microwave field generates much faster heating than thermal conduction, convection, and IR radiation, because it selectively heats target fluids depending on their own dielectric losses. Consequently, it heats the reaction mixture without energy loss for heating vessels or reactor materials, and this feature of microwave dielectric heating produces different types of temperature profiles from other heating systems. With respect to a heating approach in a microfluidic device, a non-contact type of microwave heating decreases the total thermal mass to be heated and cooled, and increases the thermal transition time that is capable of rapid thermal cycling in the microfluidic device<sup>9</sup>. Therefore, microwave heating of micro or nanoscale of reaction fluids inside a micro-bioreactor or microchamber in a microfluidic device provides important benefits for developing thermally controlled microfluidic devices. The importance of advantages in microfluidic research was evidenced above; herein, we have started developing a microwave-mediated heating system for rapid DNA amplification.

Microwave is an electromagnetic wave in a frequency between 0.3 GHz and 300 GHz. When the dielectric materials having permanent or induced dipoles are placed in an oscillating electromagnetic field, it induces the physical rotation of molecular dipoles and generates microwave dielectric heating via pulling, pushing, and collisions of dipoles. The energy generated from induced and intrinsic dipole moments in molecules of materials is dissipated into the surrounding environment as physical heating (**Fig. 1**).

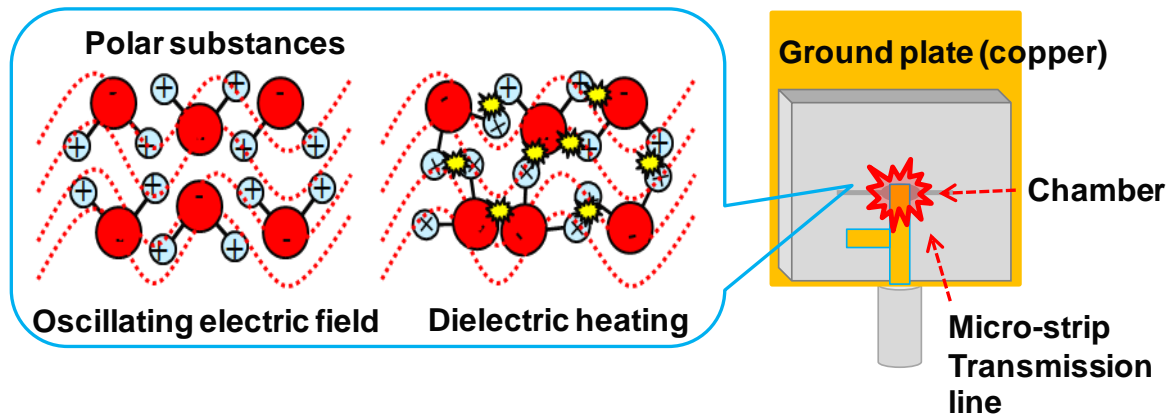


**Figure 1:** Dielectric heating in the microfluidic PCR chamber.

The microwave power,  $P$ , absorbed by a dielectrical material is given by  $P = \omega \epsilon_0 \epsilon'' E^2$ , where the frequency ( $\omega$ ) of the applied electrical field, a constant of the permittivity  $\epsilon_0$ , an imaginary part of the complex permittivity (dielectric loss)  $\epsilon''$ , and electrical field strength  $E$ . The dielectric loss factors are changed based on temperature, their compositions, and microwave frequencies. When ionic salts are added into water, the presence of ions changes water dipole distributions and it affects dielectric heating. Therefore, increased concentrations of salts in the PCR solution can improve heating efficiency, which offers an additional benefit using microwave-mediated heating in a microfluidic device<sup>10</sup>.

### 3.1.2 Previous Endeavors in Microwave PCR

Due to the important benefits from non-contact microwave heating, it has been studied by several groups to conduct rapid thermal cycling for PCR applications. Fermer *et al.* first demonstrated PCR possibility under the microwave field and this study showed that DNA amplifications from bacterial genomic DNA via 25 cycles of thermal cycling were successfully carried out in 100  $\mu$ L of the PCR sample under a single mode microwave cavity<sup>11</sup>. Orrling *et al.* reported that microwave-mediated milliliter-scale (2.5 mL) PCR was conducted to accomplish 33 cycles of real-time PCR<sup>12</sup>. In two studies, the promising proof of a microwave application to PCR was described that increasing the number of the PCR cycle could not denature an enzyme or inhibit PCR amplification. DNA polymerase should be, therefore, intact under the microwave field and heating. Other groups reported several microwave heating systems that had feasibility for PCR applications. Shah *et al.* demonstrated that microwave-mediated heating using a thin film microwave transmission line integrated with a microfluidic channel (PDMS-glass) could heat fluids at various microwave frequencies, and temperature measurement was achieved by a fluorescent detection technique<sup>13</sup>. Issadore *et al.* reported microwave dielectric heating of water drops inside a microfluidic device that integrated a flow-focusing drop maker, drop splitters, and metal electrodes to locally deliver microwave power from an inexpensive, commercially available 3.0 GHz source and amplifier. Temperature inside the drop was measured by a fluorescent dye, and a small volume of a drop boosted the speed of heating and cooling of reagents<sup>14</sup>. However, their heating systems were limited only for heating itself, not showing actual PCR performances. Recently, one of successful DNA amplifications in microfluidic devices under the microwave field has been reported; Shaw *et al.* published a micro-scale microwave PCR using a single-mode cavity, demonstrating the accomplishment of the microchip

PCR with microwave energy and this system showed rapid thermal cycling with parallel DNA amplifications from the human genome<sup>15</sup>. However, although the single-mode cavity is capable of homogeneous heating, the use of such a cavity is not able to achieve direct heating of the PCR solution with low-power, which can further restrict miniaturization of the PCR instrument.

Recently, our group demonstrated that microwave-mediated thermal cycling could be applied for parallel DNA amplifications with an optimally designed matching network. It has been shown for successful PCR amplifications from the  $\lambda$ -phage genome<sup>9</sup>. Ramp rates of microwave-mediated heating revealed possible heating over 60 – 80 °C that could achieve 3 or 4-fold reduction in PCR process time compared to the IR-mediated heating system, if the reaction chamber is small enough. However, temperature was measured and controlled via a type-t of the thermocouple that was directly placed into the PCR vessel to contact the PCR solution. This contact sensing approach is likely to reduce PCR efficiency for following possible reasons. It requires the process of surface passivation to inhibit the adsorption of PCR reagents into the thermocouple or a dummy PCR chamber adjacent to the PCR chamber<sup>16,17,20</sup>. Additionally, direct and localized heating of the PCR solution, which led to non-uniformity of temperature in the PCR vessel, could limit precise temperature measurement. On the top of that, strong prevention of thermal cycling and PCR could occur with the movement of the sample and the formation of air bubbles around the PCR chamber. Sometimes, it impeded the automation of proper thermocycling. Lastly, placing a thermocouple inside a PCR vessel led to a burden of complete sealing in the PCR chamber. Therefore, in present work, IR-thermometry such as a pyrometer<sup>21</sup> or IR-camera<sup>22</sup> has been utilized as an alternative sensing instrument to explore temperature of fluids under the microwave field.

### 3.1.3 *Temperature Measurement Methods in Microfluidic Devices*

The critical dependence of microfluidic DNA amplifications on precise temperature has caused several issues, and the main issue is a serious impediment in exploring thermal property of the PCR sample inside a microdevice due to inappropriate temperature measurement. In order to monitor correct temperature of fluids in microfluidic devices, there have been two types of temperature measurement methods employed, a contact<sup>16,23,24</sup> and a non-contact method<sup>21,22</sup>. As a prototype contact approach, many groups have widely utilized a thermocouple to measure and maintain temperature of a reaction solution to carry out microchip PCR or other reactions. A thermocouple was directly threaded into a heater<sup>25</sup> or a PCR chamber, sometimes, a dummy chamber was needed to measure the actual temperature of the PCR sample<sup>26</sup>. However, temperature measurement was either confined to two dimensional surfaces or elicited an additional problem of surface coating of the thermocouple. Several groups showed that temperature-dependent fluorescent dyes had been used for measuring temperature of fluids<sup>13,27</sup>. However, due to the configuration of our ground plane and transmission line that covered the PCR vessel on the top and bottom, there was a hindrance to measure fluorescent intensity of the PCR solution in this vessel.

As a non-contact temperature measurement method, IR-thermometry such as a pyrometer<sup>21</sup> and IR-camera<sup>22</sup> have been successfully exploited to measure temperature via the radiation emitted by objects of interest at a certain distance in microfluidic devices. An infrared pyrometer measures only temperature of a single location on the surface of the microchip material at a fixed distance from the pyrometer. This measured value can then be converted to actual temperature of fluids in a microfluidic device via calibration of the pyrometer since the pyrometer senses temperature on the surface of the microchip, and its emissivity should be

considered to find precise temperature in the PCR solution. Additionally, it was recently reported that IR-camera was used for measuring surface temperature on a polymeric microchip<sup>22</sup>. Nevertheless, a variety of emissivity on the microchip material should be deliberately evaluated during calibration of these instruments to obtain proper measurement of temperature in reaction fluids.

#### *3.1.4 Non-contact Temperature Measurement for Microwave-mediated PCR*

In present study, a pyrometer as a non-contact temperature sensing instrument has been successfully used for measuring primary temperature of the PCR solution and controlling our IR-heating system<sup>21</sup>. The pyrometer enables us to measure surface temperature of a focal spot on a microdevice without physical contact to the PCR sample, so no influence on the actual reaction. First, it was hypothesized that 1) rapidly established thermal gradient across a thin and polymeric layer (200  $\mu\text{m}$  of thick) would be no or little difference of temperature between the top of a PMMA sheet and the PCR solution and 2) two temperatures reach temperature at steady state fast enough to conduct thermocycling for PCR applications. The thermocouple providing the actual temperature of the PCR sample has been exploited for calibration of the pyrometer. Via calibrating the pyrometer, several factors affecting the emissivity of a thin PMMA, such as the reflectivity and smoothness on the PMMA surface, and the distance and angle between the pyrometer and the microchip surface, were integrated into just one calibration factor applied for pyrometer-mediated temperature control. Furthermore, the main obstacle of temperature measurement under the microwave field is non-uniformity of temperature around the PCR chamber. In order to obviate inaccuracy in temperature sensing via a thermocouple, the pyrometer was calibrated on the heat block with a thermocouple (reference temperature) and

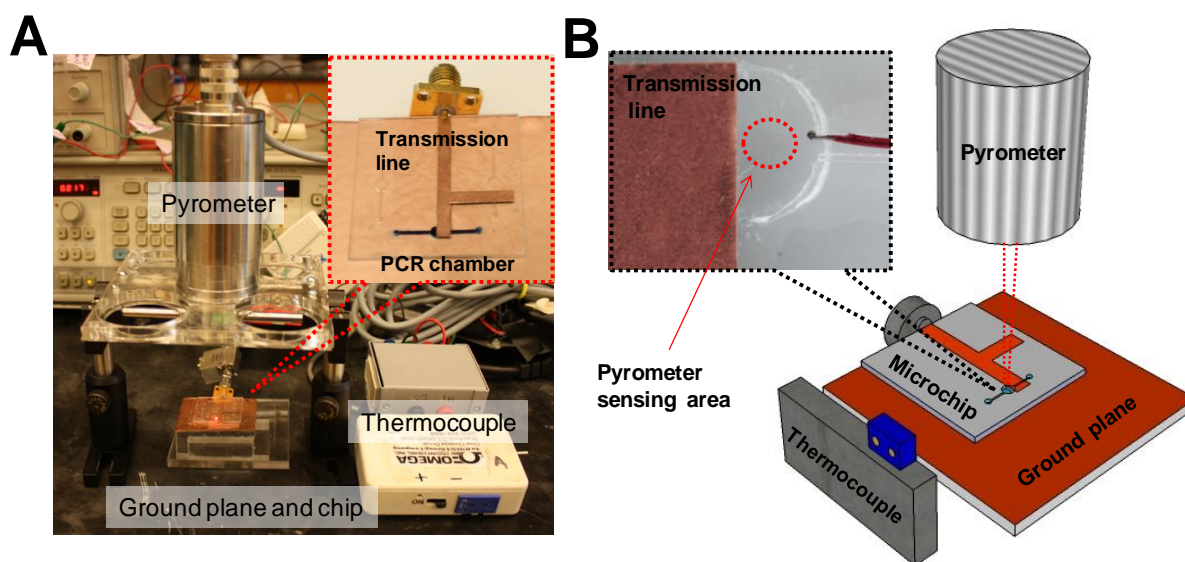
calibration was validated under the microwave field. After calibration, we successfully demonstrated microwave-mediated PCR through the noncontact temperature sensing approach.

## 3.2 Materials and Methods

### 3.2.1 Temperature Control Systems and Configurations

Our microwave heating setup is depicted in **Figure. 2A**. The main difference from previous setup<sup>28</sup> was that a pyrometer (MI-N5-H+, LumaSense technologies, Santa Clara, CA, USA)<sup>21</sup> was installed to measure temperature on the PMMA surface over the PCR chamber after calibrated with a type-t thermocouple (model T240C, Physitemp Instruments, Inc, Clifton, NJ, USA). The location of the thermocouple was placed through the microchannel at the end of the PCR chamber to accurately measure temperature of the PCR sample without microwave influence on the thermocouple (**Fig. 2B**). The distance between the pyrometer and the microchip was adjusted by the size of a laser spot that reached the smallest size at the optimal distance as described in manufacturer's manual. Temperature measured by the thermocouple was exploited to calibrate the pyrometer on a hot plate (PC-420, Corning, Tewksbury, MA, USA). The microwave signal was generated via a conventional sweep oscillator (Agilent Technologies, Inc., Santa Clara, CA, USA) and this signal was further amplified by a 1W amplifier (Mini-circuits) (Hittite Microwave, Chelmsford, MA, USA). An isolator (DiTom Microwave, Inc., Fresno, CA, USA) was installed to prevent possible damage from reflected power of the microchip. The amplifier, the thermocouple with the omega box (a model TAC- 386-T thermocouple-to-analog converter in Omega Engineering, Stamford, CT, USA), and the pyrometer were connected through the national instrument USB-DAQ card board that was regulated via a LabVIEW programmed main computer (National Instruments, Austin, TX, USA). Proportional feedback

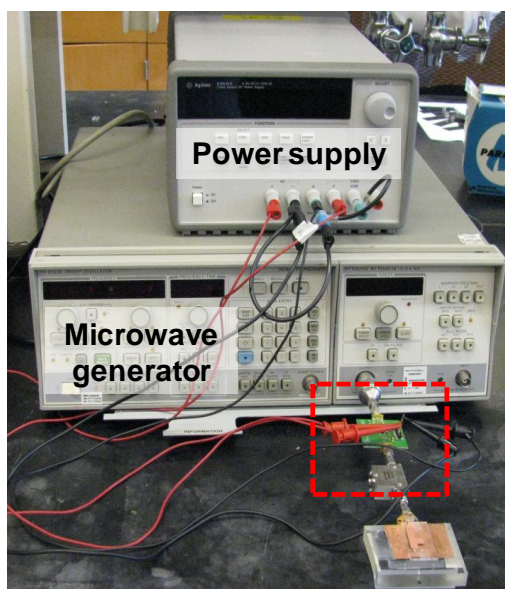
control was programmed in the LabVIEW application to precisely control temperature during temperature transition states. Temperature distribution inside the PCR chamber was simulated using Ansoft ePhysics (ANSYS, Canonsburg, PA, USA) and physical properties of PMMA to demonstrate a prospective thermal gradient in the PCR chamber as thermal modeling.



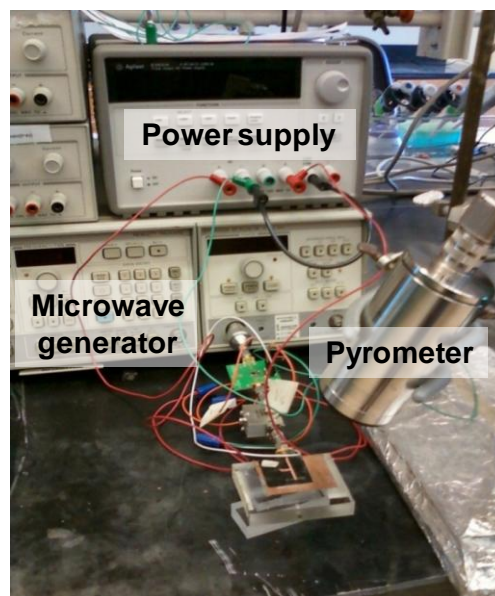
**Figure 2:** Microwave-mediated thermal cycling system. (A) Microwave heating hardware with a noncontact temperature sensing system, a pyrometer. *Inset:* a photograph of a six layered microchip with a shifted transmission line. (B) 3D drawing of a pyrometer-based microwave setup. *Inset:* a close-up view of a thermocouple placed in the PCR vessel.

In addition to *proportional voltage control*, two types of temperature control systems, *on/off control* and *open loop control*, were constructed and tested. In order to build-up *on/off control* system (**Fig. 3A**), the amplifier (connected to a digital part) and the thermocouple (connected to an analog part) were connected through the national instrument USB-DAQ card board regulated via a LabVIEW programmed computer. The power supply to the amplifier were turned on and off to control and maintain temperature as described in our previous lamp control system. A proportional-integral-derivative (PID) feedback control was programmed in LabVIEW applications to precisely control temperature during temperature transition states.

The configuration of *open-loop control* system (**Fig. 3B**) was much simpler than other systems. The power supply was connected into a LabVIEW programmed computer and this power supply was controlled based on three or two input voltage values for PCR thermocycling. After finding the relationship between power and temperature, three or two fixed power values were added into the LabVIEW program to conduct repeated thermocycling without a thermocouple (without any feedback control). In this setup, the pyrometer measured temperature on the surface of the copper transmission line on the top of the PCR microchamber.

**A**

**\* On/off control system**

**B**

**\* Open-loop control system**

**Figure 3:** Two additional temperature control systems for (A) *On/off control*. (B) *Open-loop control*.

### 3.2.2 Microchip Fabrication and Design

A six layered PMMA microdevice (**Fig. 4A**) mainly used in this research was fabricated using CO<sub>2</sub> laser ablation (VersaLaser 350, Universal Laser Systems, Inc., Scottsdale, AZ, USA), thermal bonding procedure for 200  $\mu\text{m}$  thickness of PMMA (Astra product, Baldwin, NY, USA) was followed as previously described in our lab<sup>29,30</sup>. This multi-layered PMMA sheets provide the smooth surface of the microchannel via the surfaces of 2<sup>nd</sup> and 5<sup>th</sup> layers of PMMA sheets. The total volume (1.3  $\mu\text{L}$ ) of the PCR vessel was determined by the diameter of the PCR vessel and the height of the PCR vessel; the height was calculated by the thickness of the PMMA sheet multiplied by the number of the PMMA sheet. Two holes (inlet and outlet) for accessing the PCR chamber were located on the top (first) layer, and the first layer and 6<sup>th</sup> layer have a 2 mm diameter of air pockets over and under the PCR chamber. The third and fourth layers were comprised of two channels and the reaction chamber that led to 400  $\mu\text{m}$  thicknesses (**Fig. 4B**). The layers were cleaned with distilled water and manually aligned with the microscope

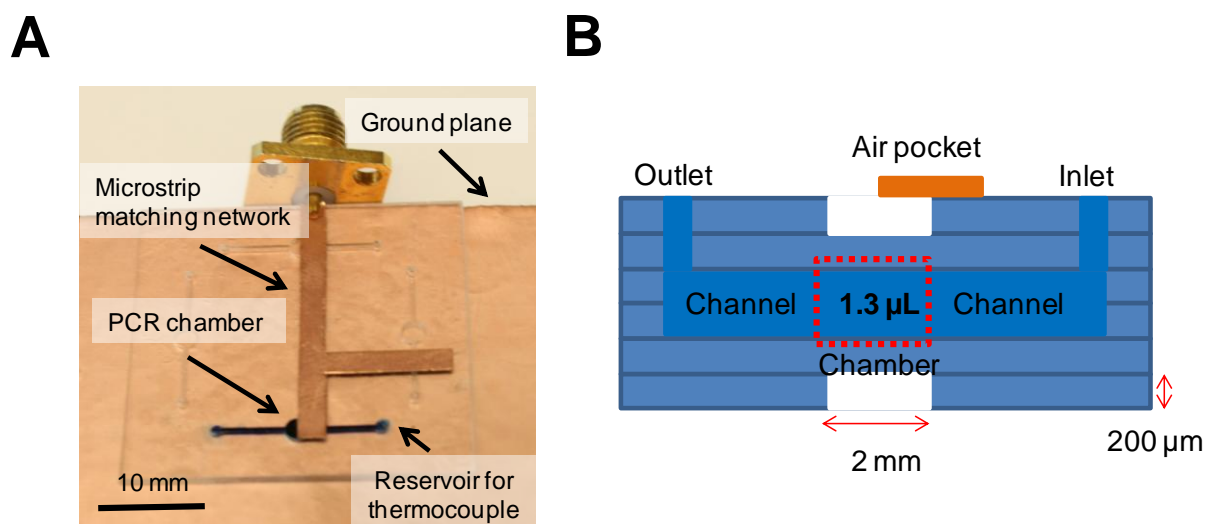


**Figure 4:** Six layered microdevice used in this research. (A) Picture of the polymeric microdevice on the ground plane. Channels were filled with blue dye for contrast. (B) Drawing of a side view of this microdevice.

assistance. Before bonding, all debris from the CO<sub>2</sub> ablation process was blown out by a compressed air. The six-layered PMMA sheets were placed on a laboratory hot plate (PC-420, Corning, Tewksbury, MA, USA), pressurized with 10 pounds, heated to 165°C for 30 min, 80°C for 30 min, and finally cooled down to room temperature to ensure complete annealing of multiple layers<sup>30</sup> (**Fig. 5A**).

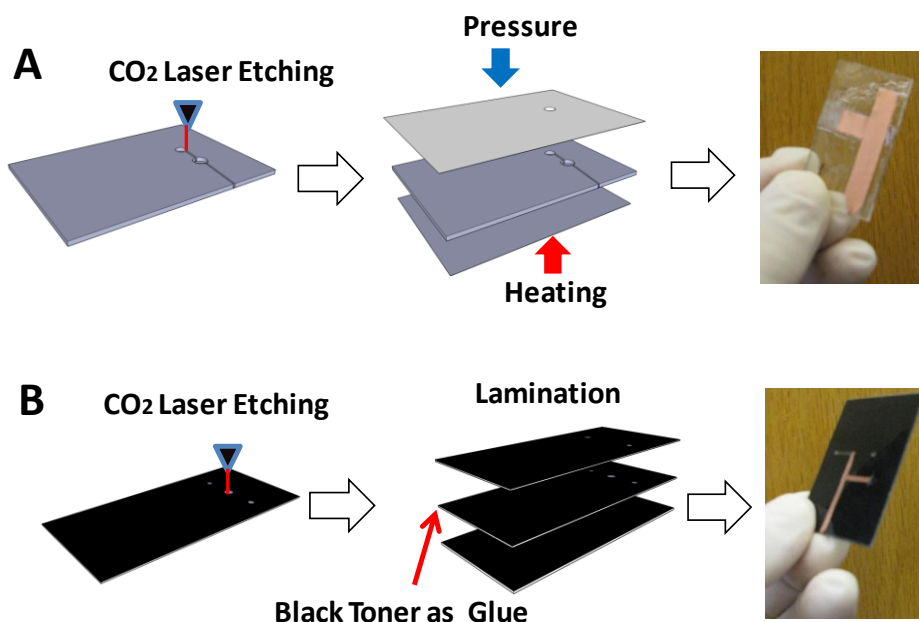


**Figure 5:** Fabrication procedures of polymeric microdevices. (A) Fabrication of the PMMA microdevice via laser ablation and thermal bonding (~ 2 hours). (B) Fabrication of the PeT microdevice via laser ablation and lamination (~ 5 minutes).

A three layered Polyester Toner (PeT) (3M, St. Paul, MN, USA) microdevice used in present work were fabricated using CO<sub>2</sub> laser ablation and lamination<sup>31</sup> as a multilayered structure (**Fig. 5B**). All designs were drawn using CorelDraw 11.0 software. For the purpose of thermal bonding, black tonner was printed on the fluidic layer via laser printer (HP LaserJet 4000, HP, Palo Alto, California, USA), which generated 120  $\mu\text{m}$  thickness of PeT comprising of 110  $\mu\text{m}$  polyester and 10  $\mu\text{m}$  double coating of black toner. The micro-channel and chamber were engraved on the black tonner printer sheet via cut-through of laser ablation. The outlet and inlet

(reservoirs) were generated on the uncoated cover sheet using laser ablation. Three layered PeTs (top layer 110  $\mu\text{m}$ , fluidic toner double coated layer 120  $\mu\text{m}$ , and bottom layer 110  $\mu\text{m}$ ) were aligned and assembled using a standard office laminator at 120 °C. Thermal lamination firmly bonds all PeT sheets by thermal interaction between black toner and uncoated sheets. After construction of the PeT microchip, the total thickness (340  $\mu\text{m}$ ) of the PeT microchip was precisely measured to show no compression of black toner via thermal bonding. The compatibility of the PeT microchip with the PCR reagent was tested using  $\lambda$ -phage DNA amplification<sup>31</sup>.

### 3.2.3 *Transmission Line and Network Analyzer*

The initial microstrip matching network was simulated and designed using an in-house MathCAD (PTC, Needham, MA, USA) model and TX-Line (AWR, El Segundo, CA, USA), based on the information in microchip thickness, material property, and the dimension of the microchip chamber<sup>28</sup>. This design was transferred into 90  $\mu\text{m}$  thick copper tape (36  $\mu\text{m}$  copper and 54  $\mu\text{m}$  adhesive layer; McMaster-Carr, Elmhurst, IL, USA), which was finely cut and attached on the top sheet of a six layered PMMA microdevice. The copper tape completely covered a half of the top PMMA sheet over the PCR chamber to optimally transfer microwave vertically through the PCR vessel. The ground plane consisted of the copper-taped PMMA that was prepared by CO<sub>2</sub> laser ablation and the microchip was firmly placed on the ground plane without any air gap to prevent microwave loss. In order to optimize a matching network (a type of transmission line) on the microchip, a network analyzer was used to monitor a matching network spectrum. After completely filling the PCR vessel with a PCR buffer, the matching network spectrum was monitored and the stub line was trimmed to get minimum reflected power

around -20 dB in 5 – 6 GHz ranges, since the amplifier could amplify microwave that was generated via the microwave generator at the frequency range between 5 and 6 GHz (**Fig. 6**).

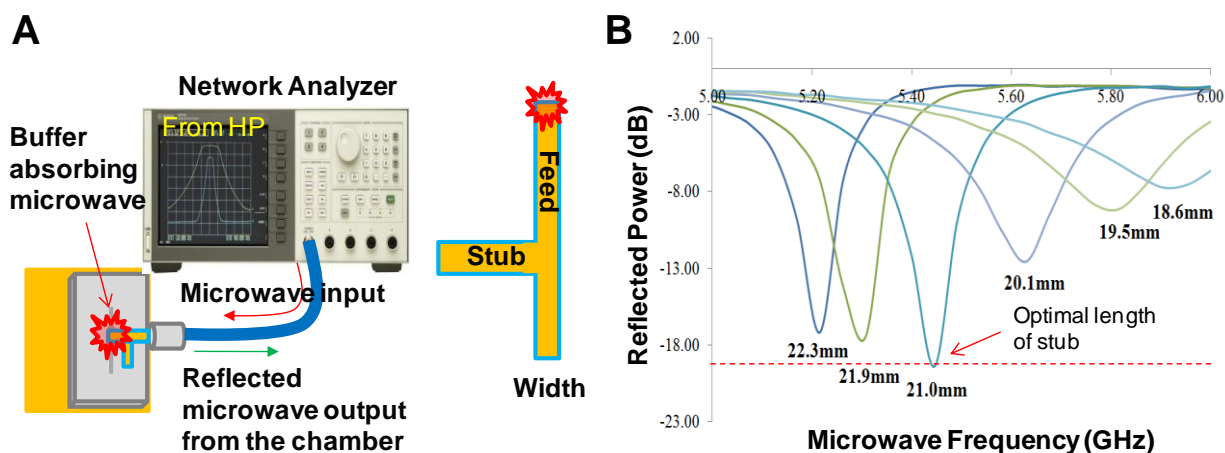


**Figure 6:** Optimization of a matching network (transmission line) using the network analyzer. (A) The PCR buffer filled microchip is connected to the network analyzer to monitor reflection of microwave from the PCR chamber. (B) Matching network spectrum shows the best matching at a certain length of stub.

### 3.2.4 Pyrometer Calibration

Pyrometer calibration for pyrometer driven thermocycling was performed on a laboratory hot plate where the thermocouple-inserted microchip was located after completely filling the PCR chamber with a PCR buffer. The pyrometer was placed over the top of the PCR chamber to measure the temperature of one spot on the microchip, and temperature slowly increased from room temperature to around 100 °C, while monitoring two temperatures with the pyrometer and the thermocouple. The temperature acquired by the pyrometer was calibrated based on the temperature measured by the thermocouple (reference thermocouple). After calibration, two temperatures measured by the pyrometer and the thermocouple were completely validated under the microwave field. Three repeated calibrations were conducted to demonstrate the uncertainty of our calibration method.

### 3.2.5 PCR Protocol and Microchip PCR

A PCR reagent master mix was prepared according to the standard PCR protocol as final concentrations: 1 x PCR buffer,  $\text{MgCl}_2$  (3 mM), dNTP mixture (0.2 mM), forward and reverse primers (4  $\mu\text{L}$ ) (Eurofins Scientific, High Point, NC, USA). Deionized water generated with a Nanopure unit (Barnstead, Dubuque, IA, USA) was used in all experiments. The master mix was combined with 10,000 MW of polyethylene glycol ( $\text{PEG}_{10,000}$ ) (Fisher Scientific, Fairlawn, NJ, USA) to make a final concentration of 0.4% (w/v), BSA (New England Biolabs, Ipswich, MA, USA) to a final concentration of 0.5  $\mu\text{g}/\mu\text{L}$ ,  $\lambda$ -phage genomic DNA (Sigma-Aldrich Corp., St. Louis, MO, USA) as a concentration of template DNA ranging from 0.1  $\text{ng}/\mu\text{L}$  to 10  $\text{ng}/\mu\text{L}$ , and 0.2 U/ $\mu\text{L}$  *Taq* polymerase (Fisher Scientific, Fairlawn, NJ, USA) to complete the reaction solution, then divided a total sample into several aliquots for an individual reaction. The reaction mixture was pipetted into one of the reservoirs that fit the size of a small pipette tip. The PCR solution was injected via pipetting without any pumping system and excess PCR solution at two reservoirs was completely removed. A thermocouple was placed and sealed with a PCR biocompatible adhesive tape (Excel Scientific, Thermal Seal RT, Victorville, CA, USA)<sup>30</sup> on both holes where glues were applied to ensure complete sealing of two holes to prevent any leakage<sup>30,32</sup>. The microchip was positioned on the ground plane and the transmission line was interfaced with the SMA connector. Thermal cycling was controlled by a LabVIEW program or manually adjusted and monitored with the following temperature program: 120 seconds for initial denaturation at 95 °C, then 30 cycles consisted of 15 seconds for denaturation at 95 °C, 15 seconds for anneal at 68 °C, 15 seconds for extension at 72 °C, ending with 120 seconds for final extension at 72 °C; for thermocouple drive DNA amplification, the extension step was

eliminated. PCR products were taken from the microchip using a pipette and analysed on Agilent 2100 Bioanalyzer (Agilent technologies, Inc., Santa Clara, CA, USA).

### 3.3 Results and Discussion

#### 3.3.1 *Polymeric Microdevices for Microwave-mediated Heating System*

All microdevices in this research have been constructed from polymeric materials, PMMA and PeT (**Fig. 5**). A PMMA microdevice consisting of six thin PMMA (200  $\mu\text{m}$ ) sheets have been utilized to conduct microwave PCR. Via CO<sub>2</sub> laser ablation, the PCR chamber was engraved in two sheets (the third and fourth layers of PMMA sheets) that comprised of 1.3  $\mu\text{L}$  of the PCR vessel surrounded by the top and bottom of smooth PMMA sheets. The amount of microwave energy to be transferred can decrease while microwave passes through the polymeric material. Consequently, the thickness of the top PMMA layer on the PCR vessel reduced up to 200  $\mu\text{m}$  to improve heating efficiency. This thin PMMA layer can aid pyrometer temperature sensing, since a thin sheet reaches thermal equilibrium faster than thick one and it was assumed that the temperature of a thin PMMA sheet on the PCR chamber would rapidly reach the same temperature of the PCR solution in the PCR vessel.

Considering low thermal conductivity and high heat capacity of polymeric materials, the polymeric microdevice provides the efficient environment for heating the PCR solution surrounded by a polymer material. However, the copper tape on the top (transmission line) and bottom (ground plane) of the microdevice facilitates rapid cooling of the PCR solution, because the copper has extremely higher thermal conductivity than air and polymers. This configuration of the microchip with the ground plane allowed for rapid heat dissipation and non-uniformity of vertical temperature inside the PCR chamber. In order to solve these issues, two air pockets

were placed on the top and bottom layers of the PMMA microchip as a role of thermal insulator to further improve microwave heating and aid uniform thermal distribution across the PCR vessel.

In addition, easy fabrication and disposability of a polymeric microchip increased turnover time for the optimization of microchip design<sup>33,34</sup>. Complete bonding with high temperature and relative low pressure, which can be easily applied by dumbbell weights, eliminated any leaks around the chamber and channel. The inlet and outlet were completely sealed by PCR adhesive tapes and glues. This sealing approach prevented any leakage and boil burst up to 95 °C and it could ensure improved heating efficiency, stable temperature holds, and reduced amounts of air bubbles. Appropriate thermal bonding and sealing methods would account for the success in stable thermocycling and temperature holds at high temperature<sup>30</sup>.

### 3.3.2 *Shifted Transmission Line for Noncontact Temperature Sensing*

The optimal transmission of microwave energy into nano- and micro-scale PCR-compatible chambers was accomplished using a copper microstrip (a type of transmission line) matching network<sup>9</sup>. The matching network was designed based on the physical properties of microchip materials (PMMA and PeT), and the diameter and height of the PCR chamber via MathCAD model and TX-Line to find an optimal matching network with low amount of power to heat the PCR solution constantly. The transmission line was attached on the microchip surface to cover the top layer of the PCR chamber. Optimization was further tuned or verified via the network analyzer to achieve perfect transfer of microwave with a minimum loss. In present work, in order to effectively utilize non-contact temperature sensing via a pyrometer, the transmission line on the PCR chamber was shifted to uncover a half of the top PMMA sheet over

the PCR chamber where the pyrometer senses temperature, we called, shifted transmission line. While conducting the network analyzer experiment with the microchip having the shifted transmission line, reflected microwave from the PCR solution were measured and it indicated lower than -20 dB; less than -20 dB indicates that 99% of microwave power is transferred into

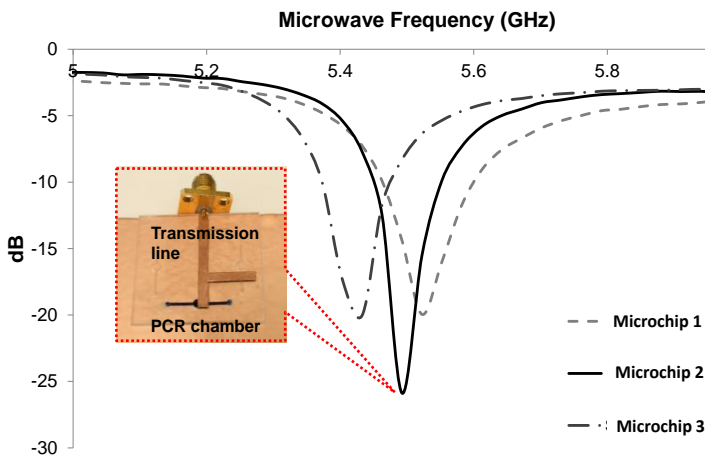


**Figure 7:** Matching network spectrums of three microchips that have shifted transmission lines generated by network analyzer. The optimal frequency would be located around 5.4 and 5.6 GHz.

the PCR vessel for heating the PCR solution. Finally, three randomly chosen microchips were tested on the network analyzer and it demonstrated that the optimization of the transmission line was achieved at the frequency ranging between 5.4 and 5.6 GHz without any trimming process (**Fig. 7**). It indirectly proved that this six layered PMMA

microdevice with a shifted transmission line could perform effective heating for parallel DNA amplifications under our microwave setup.

### 3.3.3 Thermal Modeling of the PCR Solution in the PCR Chamber with a Shifted Transmission Line

The main issue in the pattern of microwave heating was non-uniformity of temperature distribution in the PCR chamber that would be caused by the characteristics of the microwave-mediated heating setup. 1) Our thermal modeling (**Fig. 8**) and 2) measurement of temperature in the PCR solution via a thermocouple showed that non-uniform heat distribution through the

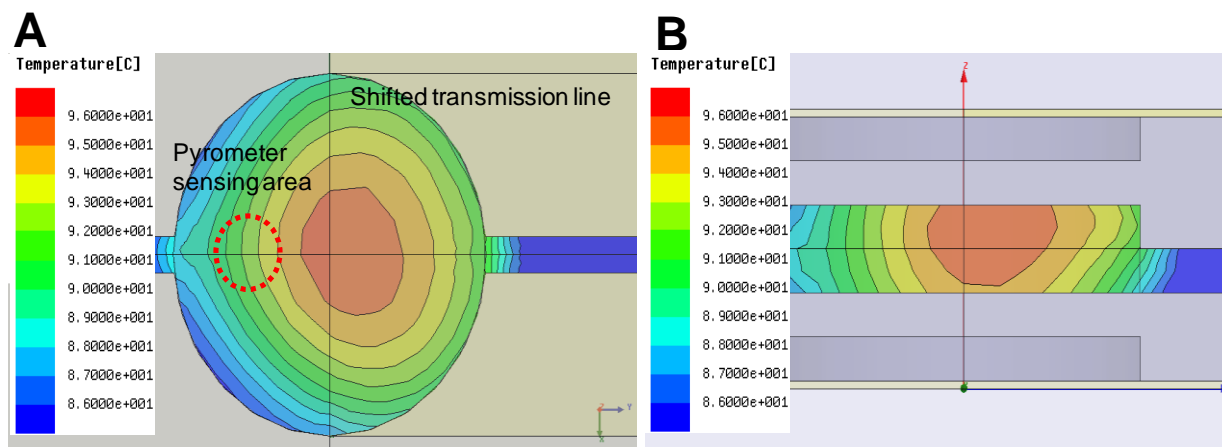


**Figure 8:** Thermal modeling of temperature distributions in the microchamber with a shifted transmission line. (A) Top view of the microchamber and the transmission line shifted to open a half of the microchamber: the **red dot circle** indicated the pyrometer sensing area. (B) Side view of the microchamber.

entire PCR chamber could cause the main problem of PCR thermocycling following inefficient DNA amplification. Additionally, this localized heating raised a chance for failure of proper thermal cycling that is associated with inefficiency PCR while conducting thermal cycling with a thermocouple. Thermal modeling inside the PCR chamber demonstrated a putative thermal gradient in the PCR chamber and indicated that a thermal gradient was established across the entire PCR chamber to reach a maximum temperature at the edge of the transmission line that was attached at the center of PCR chamber (**Fig. 8A**). Although heat transfer through a 1.3  $\mu\text{L}$  volume of liquid in the PCR vessel was extremely fast, continuous and localized microwave heating in the PCR sample and heat dissipation through a polymeric microchip into air might lead to uneven heat distribution in the PCR solution. It could be presumed that this localized microwave heating in the PCR solution and rapid heat dissipation into air would be faster than time to reach equilibrium of temperature inside the PCR chamber (**Fig. 8B**). Although polymeric materials and air pockets on the top and bottom layers of PMMA could improve temperature

holds, the copper tapes from the transmission line and ground plate enhanced heat dissipation through this copper. Therefore, adjusting the configuration and location of air pockets and copper tapes, and redesign of the PCR chamber and microchip must be further studied to obtain homogeneous temperature inside the PCR solution to improve PCR efficiency further.

Instead of measuring a localized portion of the PCR sample using a thermocouple, IR-pyrometer effectively assesses the surface temperature that would indicate the average temperature of the PCR solution after calibration of the pyrometer (**Fig. 8A**). However, the thermocouple only measured one spot of the PCR solution and temperature measurement was dramatically affected by the location of the thermocouple and the existence of air bubbles. This pyrometer-measured average temperature on the PCR chamber area was successfully monitored and utilized to conduct successful microwave PCR to verify the possibility of a non-contact temperature measurement approach. Furthermore, the insertion of the thermocouple into the PCR chamber decreased PCR productivity due to the adsorption of PCR reagents into the thermocouple. This adsorption should be no longer issue with the noncontact temperature measurement.

### 3.3.4 *Microwave Heating Experiments*

Important heating experiments have been performed on our microwave setup to describe the characteristics of microwave heating in a microfluidic device. To prove localized and directly coupling of microwave heating with the PCR solution, a PCR buffer was injected into the PCR chamber, while heating the empty PCR chamber under the microwave field (**Fig. 9**). Furthermore, it demonstrated microwave effect into a type-t thermocouple. At the beginning of heating this empty chamber, microwave could heat microchip materials around 40 – 42 °C once

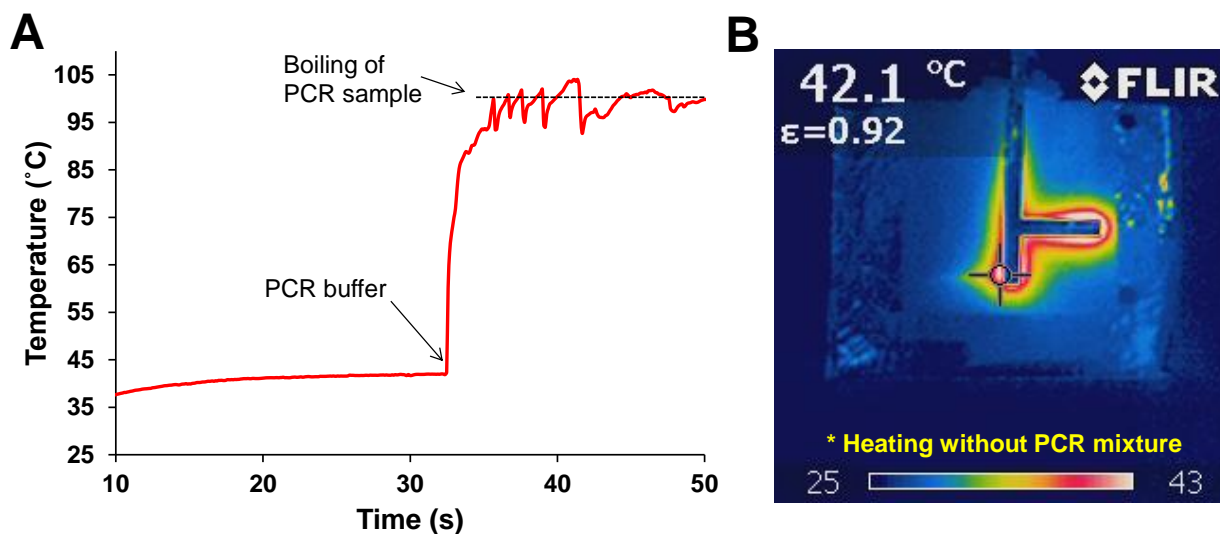


**Figure 9:** Microwave heating in the polymeric PCR chamber to demonstrate microwave effect into a type-t thermocouple. (A) Temperature profile while heating the PCR chamber before and after adding a PCR buffer into the PCR chamber. Boiling of the PCR buffer fluctuated temperature inside the microchamber, which described that boiling occurred around 100 °C. (B) Thermal image of the microchip while heating the empty microchamber. The surface temperature measured by the IR-camera indicated similar temperature measured by the thermocouple.

stabilized and it illustrated that microchip materials could be partially heated by microwave, since a polymeric material has its own dielectric loss (**Fig. 9A**). In addition, temperature values between the thermocouple and the image taken by IR-camera did not significantly vary (**Fig. 9B**) and it emphasized that the microwave field could not disturb thermocouple-based temperature measurement. However, when the PCR buffer was introduced into the PCR chamber, localized microwave heating significantly increased temperature of the PCR buffer up to its boiling point. Temperature fluctuation around the boiling point might be caused by movement of the PCR sample and expansion of air bubbles. Unstable temperature around its boiling point disrupted localized microwave heating and temperature measurement and eventually prevented stable control of microwave heating at high temperature. This heating experiment explained that the characteristics of microwave heating (selective heating of two different materials, intensively

heat PCR buffer, not microchip material) could affect the patterns of microwave heating and natural cooling while thermal cycling conducted. Consequently, the main reason of delayed heating and cooling to reach set temperatures was that additional time was required to heat or cool microchip materials and reach complete equilibrium between the microchip and the PCR buffer.

In addition, using the full power of microwave, the microwave generator was turned on and off to show microwave heating and natural cooling patterns that could show maximum ramp rates on our setup (**Fig. 10**). **Figure 10A** indicated that ramp rates could be achieved up to 35 °C/sec for microwave heating and 16 °C/sec for natural cooling, which could be exploited to boost the speed of microwave-mediated thermocycling faster than IR-mediated heating. Although the copper tape was placed on the top (transmission line) and bottom (ground plane) of

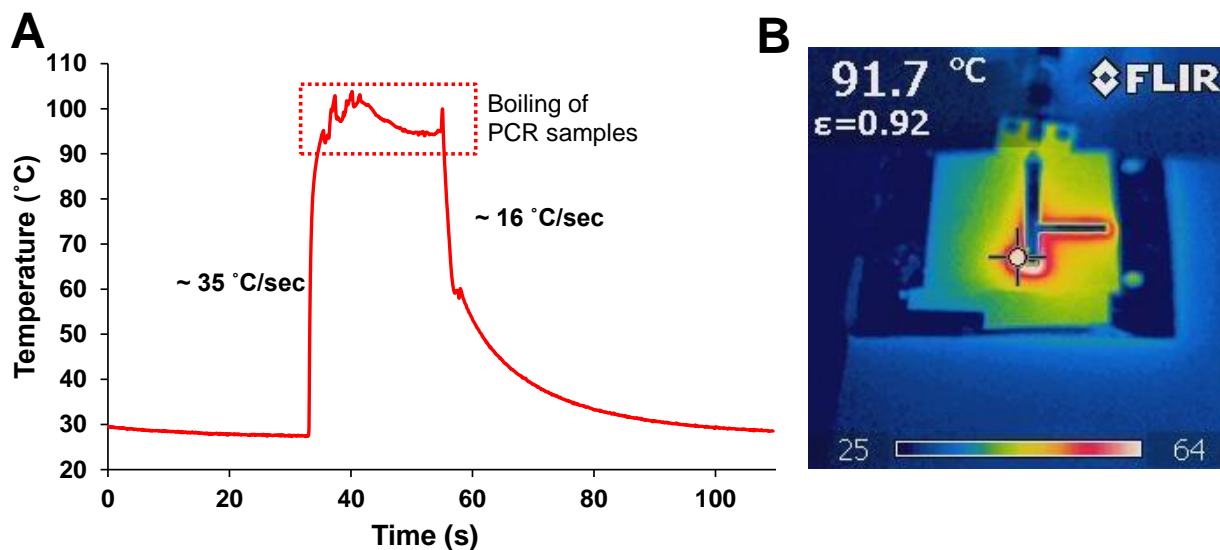


**Figure 10:** Maximum rates of microwave heating and natural cooling in our microwave setup. Manual operation (*on/off control*) for microwave heating and nature cooling of the PCR solution via maximum power. (A) Ramp rates for heating and cooling were 35 °C/sec and 16 °C/sec. (B) Thermal image of the microfluidic device while heating the PCR solution over 95 °C.

the microchip to improve the cooling rate of the PCR buffer, microwave heating was faster than natural cooling. It should be because of direct coupling of microwave energy with the PCR sample. However, natural cooling is able to be further improved using an enforced fan cooling system that has been used in the IR heating system. Additionally, the IR-camera taken thermal image showed that effective heating could be accomplished on a six layered microchip with a shifted transmission line (**Fig. 10B**).

### 3.3.5 Three Types of Temperature Control Methods

Three major types of temperature control methods, *on/off*, *open-loop*, and *proportional voltage controls* were assessed on our microwave heating setup to obtain 30 cycles of thermocycling that could demonstrate possibilities of reliable PCR amplifications on the same microchip; as three types of control methods have their own benefits and drawbacks, the combination of these control methods should be the best way to optimize thermal cycling. *On/off control* is a digital type of a temperature control method by turning on and off the amplifier based on the reference temperature (indicating set points of temperature), which control supply of microwave. When temperature reaches the value higher than a setting value, microwave is not supplied by turning off the power supply into the amplifier. When it reaches lower temperature than a setting value, microwave was on to increase temperature by turning on the power supply into the amplifier. As the full power of microwave was used in this control system instead of controlling the amount of power, the fast ramp rate around 80 °C/sec was acquired during *on/off control* of thermocycling. However, due to the fast ramp rate, temperature profile could not be stably controlled by our PID control system embedded in the LabVIEW program (**Fig. 11A**).

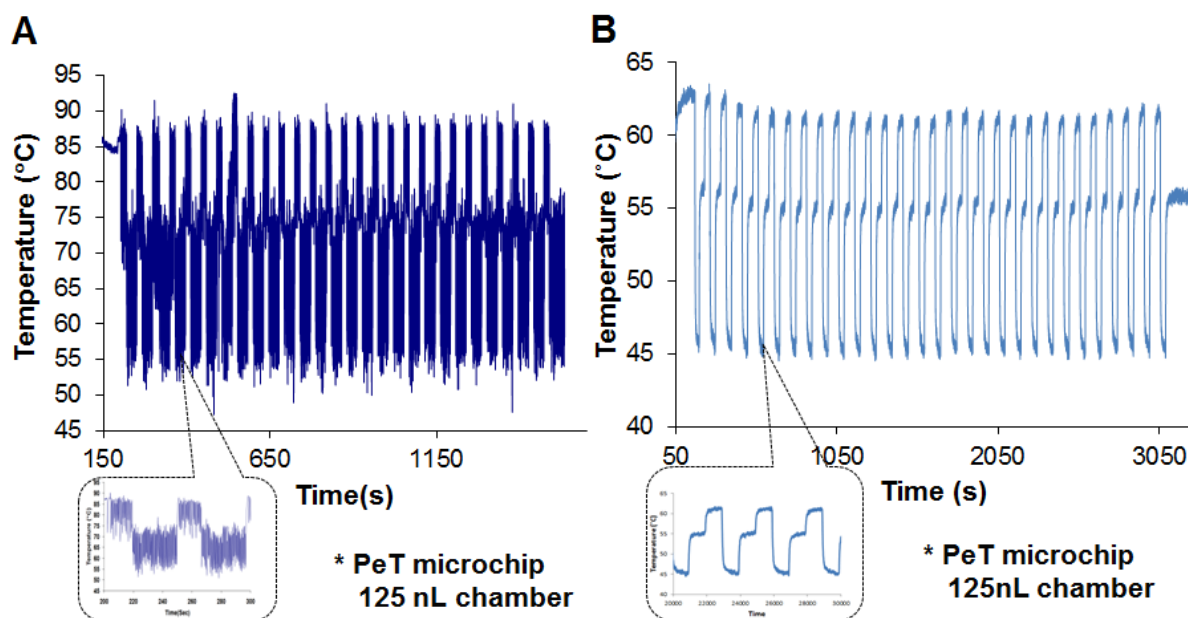


**Figure 11:** Temperature profiles via two temperature control methods in the 125 nL PCR chamber of the PeT microchip. (A) Temperature profile by *on/off control*: 30 cycles (85 °C for 15 seconds and 68 °C for 30 seconds) of temperature profiles indicated rapid temperature transition (~ 80 °C/sec) (B) Temperature profile by *open-loop control*: three voltages, 3, 4, and 5 V were applied for 30 seconds to drive 30 cycles of thermocycling without any feedback control.

The second control method is *open-loop control* without any feedback control. The concept of *open-loop control* (non-feedback control) on our microwave heating system comes from that a certain amount of power heat the same volume of the PCR solution up to precise temperature repeatedly. From the information of microwave power versus temperature inside the PCR vessel, thermocycling could be driven to achieve three (two) step temperature transitions using three (two) designated powers. This approach is an ideal and simple temperature control system to achieve miniaturization of microfluidic PCR instruments, because there is no need to install a temperature control system. However, stable temperature holds could not be obtained at high temperature in our microwave setup. Within around 40 – 70 °C ranges of temperatures, *open-loop control* led to a fairly good temperature profile and holds (**Fig. 11B**). Heating over 90 °C might change the condition of the PCR vessel, because the PeT

microchip has a black toner where the PCR mixture could be absorbed and its volume decreased, which might be very critical for microwave heating and temperature holds. Additionally, air bubbles inside multi-layered polymeric chips might affect microwave heating over 90 °C.

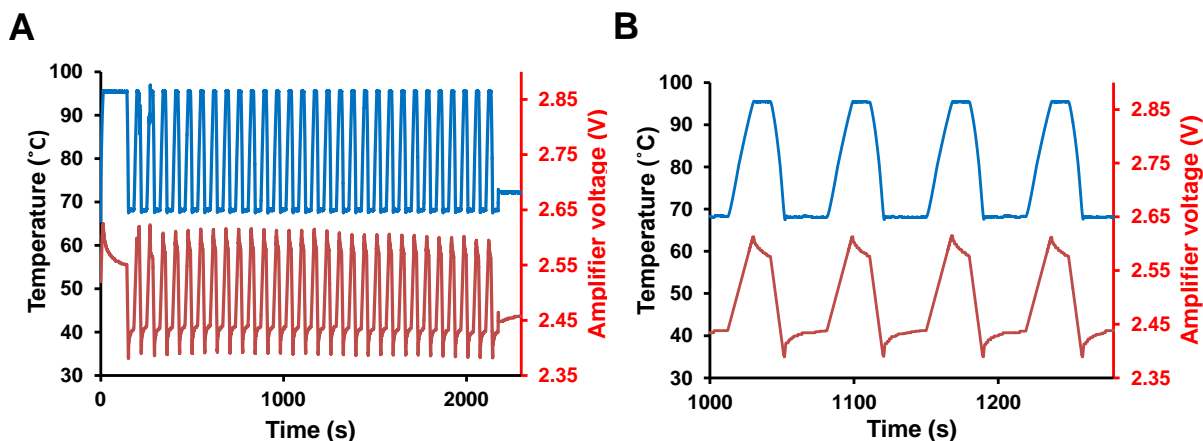


**Figure 12:** Temperature profiles via *proportional voltage control* in the polymeric (PMMA) microdevice. (A) 30 cycles of temperature profile (blue) with amplifier voltage (red): 95 °C for 15 seconds and 68 °C for 15 seconds. (B) Zoom-up of four thermocycling (blue) with amplifier voltage (red). Temperature transition times were obtained as  $\sim \pm 2$  degree/sec.

Lastly, *proportional voltage control* was constructed, which has been used for thermocouple and pyrometer driven thermal cycling systems. This is an analogy type of control method; based on the set points of temperature, power could increase and decrease to reach these set points via the PID controller. Ramp rates were determined by the speeds of increasing and decreasing power. Via this approach, fairly stable temperature holds and 30 cycles have been obtained to produce successful 520 bp  $\lambda$ -DNA amplifications with a thermocouple<sup>28</sup> (Fig. 12). However, the speed of temperature control was much slower than *on/off control*. Consequently, the combination of two types of thermal control methods should achieve fast ramp rates and stable temperature holds; as a theoretical example, when temperature moves to different temperature (from 95 °C to 68 °C and from 72 °C to 95 °C; temperature transition period), *on/off*

*control* digital method can be operated and while holding temperature at each PCR zone, *proportional voltage control* method can be applied. Although *proportional voltage control* is analog-based and it slowly controls temperature, it offers precise temperature control to generate stable temperature holds and decrease overshooting and undershooting while our system operating.

### 3.3.6 Non-contact Temperature Measurement via IR-Pyrometer

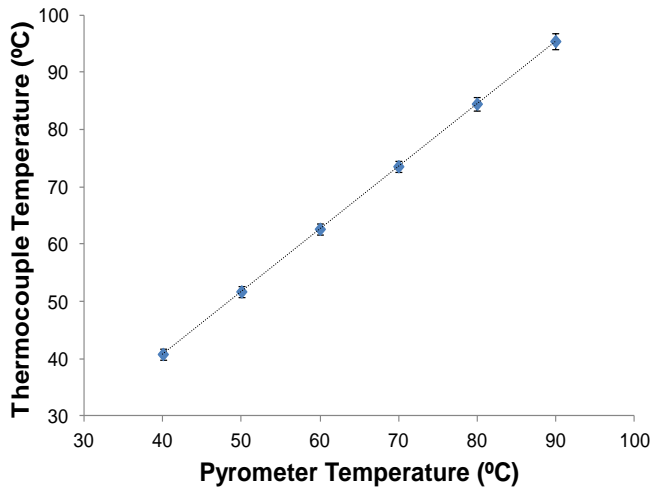


**Figure 13:** Pyrometer calibration with a thermocouple (reference temperature). Repeated calibration data were used to draw the calibration curve with error bars: denature, extension, and anneal temperatures measured by the pyrometer showed temperature with errors;  $95^{\circ}\text{C} \pm 1.54$ ,  $72^{\circ}\text{C} \pm 1.04$ ,  $68^{\circ}\text{C} \pm 0.98$  in a six layered microchip (error bars present  $n=3$ ).

As a non-contact temperature measurement method, a pyrometer can intercept and evaluate the thermal radiation from a glowing object. For IR thermometry, the distance to the spot size ratio should be the important factor to measure correct temperature using a pyrometer. As the critical parameter, the emissivity of a material itself, which can be adjusted by calibration of the pyrometer, is important to drive accurate thermal

cycling. In this study, pyrometer calibration was conducted based on the reference temperature measured by a thermocouple on a heat block (laboratory hot plate). In our previous research<sup>21</sup>, pyrometer calibration was only effective for one microdevice that had been calibrated right before PCR; chip to chip calibration was required. Furthermore, non-uniformity of temperature

in the PCR solution made it hard to achieve the calibration of the pyrometer under the microwave field. In order to simplify the calibration of the pyrometer in this work, it was conducted on the hot plate to calculate the universal emissivity of PMMA that can be applied for the same designed PMMA microchips. In the procedure of calibration, the thermocouple inserted microchip was located on the top of the hot plate to provide reference temperature via a thermocouple and the pyrometer was calibrated based on the temperature measured by this reference thermocouple. Repeated calibrations proved that a single calibration could be effectively utilized for any microdevice and temperature deviation was within  $\pm 1.5$  °C in all functional PCR zones (**Fig. 13**). Using this calibration approach, repeated DNA amplifications have been achieved in our setup that is the first demonstration of microwave-mediated PCR using a noncontact heating approach.

### 3.3.7 Temperature Control Methods; Thermocouple versus Pyrometer

After calibration of the pyrometer, thermocycling was performed by two different temperature sensing approaches; *thermocouple-driven thermocycling* (**Fig. 14A and B**) and *pyrometer-driven thermocycling* (**Fig. 14C and D**). The comparison between two temperature profiles was shown to describe the characteristics of two different temperature measurement methods; thermocouple and pyrometer. In *thermocouple-driven thermocycling* (**Fig. 14A**), temperature was controlled by the thermocouple that drove thermocycling while monitoring temperature by the pyrometer. This thermocouple-based temperature sensing was faster than that by the pyrometer since the thermocouple directly measured actual temperature in the PCR solution. However, pyrometer sensing took time to measure reflected temperature from the PCR solution since thermal equilibrium between the PCR solution and the microchip material was

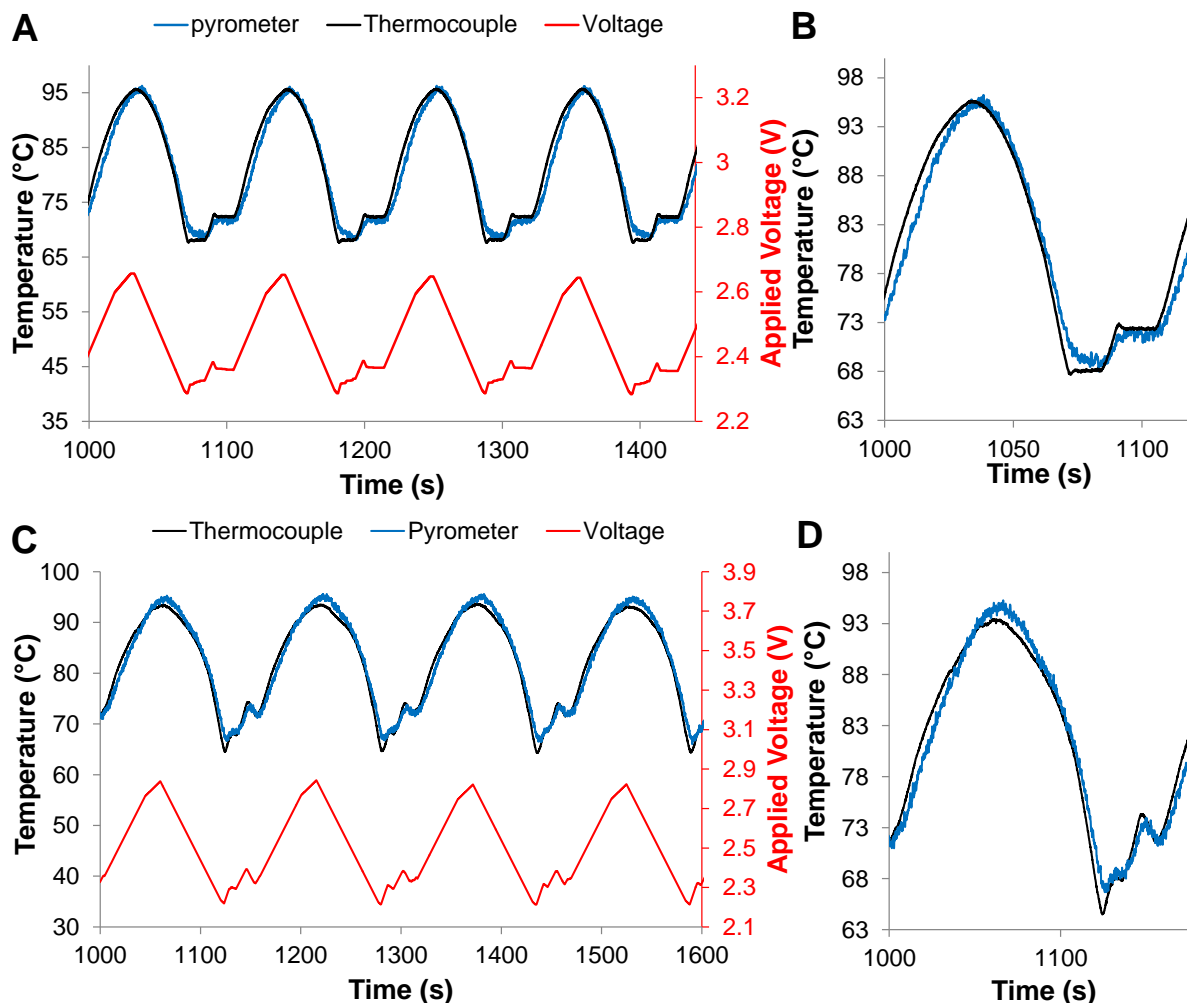


**Figure 14:** Temperature profiles driven by a thermocouple and a pyrometer. Zooms of four thermal cycles and applied voltages from 95 °C to 68 °C and 72 °C with one extended temperature profile. (A) *Thermocouple-driven thermocycling*. The **black** line indicated temperature measured by the thermocouple, **blue** one by the pyrometer, and **red** line shows applied voltage. (B) Close-up view of one thermal cycle via thermocouple-driven control. (C) *Pyrometer-driven thermocycling*. Pyrometer-based temperature sensing is slower than the thermocouple. (D) Close-up view of one thermal cycle via pyrometer-driven control.

obtained within several seconds, which could be described as *lag time*: time difference between the thermocouple and the pyrometer to reach set points of temperatures (**Fig. 14B**). Additionally, selective heating of microwave, to exclude heating of microchip materials, and low thermal conductivity of PMMA further delayed thermal equilibrium on the pyrometer sensing area on the microchip. This characteristic generated lag times in the region of anneal and extension.

For *pyrometer-driven thermocycling* (**Fig. 14C**), it spent more time to finish one cycle than that by the thermocouple due to the *lag time* for the pyrometer to measure the surface temperature of PMMA. Additionally, thermocycling was driven by a slow sensing pyrometer. Therefore, we could say that this *lag time* led to under and over-shooting of temperature in the PCR solution as a result of the time delay of pyrometer sensing following pyrometer driven control. Furthermore, this over and under-shooting of temperature could make temperature in the PCR solution rapidly exceed set points (**Fig. 14D**). Therefore, to achieve ultrafast thermal cycling, it should be carefully considered that pyrometer measurement on a polymeric microdevice can limit temperature sensing as a consequence of this lag time, causing over and under-shooting of temperature in the PCR solution. Furthermore, although the speeds of thermocycling driven by the pyrometer and thermocouple are still slow, these can be further improved to obtain rapid heating and cooling up to 35 °C/sec and 16 °C/sec by adjusting the thermal control software (LabVIEW code controlling software).

### 3.3.8 *Microwave-mediated DNA Amplifications via Thermocouple*

The initial focus in PCR experiments was on amplification of a 520 base pair fragment of the  $\lambda$ -phage genome. PEG and BSA, as passivation reagents, were used to conduct PCR in the six layered PMMA microdevice. To order to assess the efficiency of PCR amplifications in our microdevice and setup, concentrations of DNA templates for PCR varied from 0.1 ng/ $\mu$ L to 10 ng/ $\mu$ L. Resulting electropherograms showed that more than 0.1 ng/ $\mu$ L of  $\lambda$ -phage genomic DNA was required for achieving DNA amplification using our current microchip and heating system (**Fig. 15**). The critical reason for this low efficient-PCR mainly results from non-uniformity of temperature distribution in the PCR vessel and PCR inhibition by the thermocouple. As our

group published before<sup>27</sup>, non-contact pyrometer-based temperature sensing could improve PCR efficiency by preventing direct contact of the PCR solution with the thermocouple. Thermal cycling for thermocouple driven PCR was completed around 35 minutes 2- to 3-fold faster than on the conventional thermal cycler. However, this reaction time was limited by LabVIEW code controlling software instead of heating hardware.

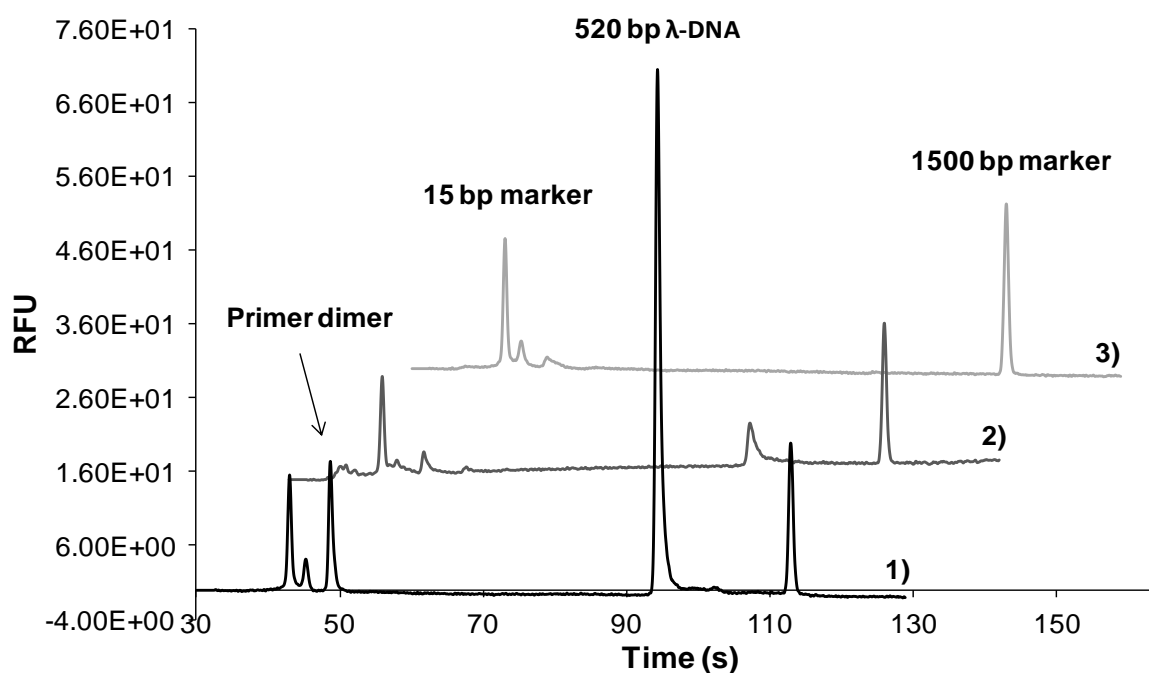


**Figure 15:** Thermocouple-controlled DNA amplifications. Electropherograms shows successful DNA amplifications from a  $\lambda$ -DNA template in a six layered PMMA microchip. Concentration of DNA templates were 1) 10 ng/ $\mu$ L, 2) 1 ng/ $\mu$ L, and 3) 0.1 ng/ $\mu$ L.

### 3.3.9 Microwave-mediated DNA Amplifications via Pyrometer

From our setup and calibration method of a pyrometer, a 520 bp  $\lambda$ -DNA fragment has repeatedly been amplified in our microwave setup and polymeric microdevice (**Fig. 16**). The successful amplifications of target DNA indicated that a pyrometer temperature sensing was fairly enough to conduct thermocycling for PCR amplifications and thermal cycling was

reasonably repeated for proper DNA amplifications from 10 ng/ $\mu$ L of the  $\lambda$ -DNA template. However, there were still drawbacks to be solved. First of all, the efficiency of DNA amplification was lower than our IR heating setup, since we achieved fairly good DNA amplifications on our IR heating setup. Low PCR efficiency should be because of 1) non-uniformity of temperature in the PCR chamber, 2) calibration issue; temperature difference between the actual temperature of the PCR solution and temperature measured by the pyrometer or 3) passivation issues due to a higher surface area to volume ratio from the flat shape of the PCR chamber. Secondly, ramp rates for microwave heating and natural cooling still limit ultrafast thermal cycling on our microwave setup. Improvement of heating rates can be made by

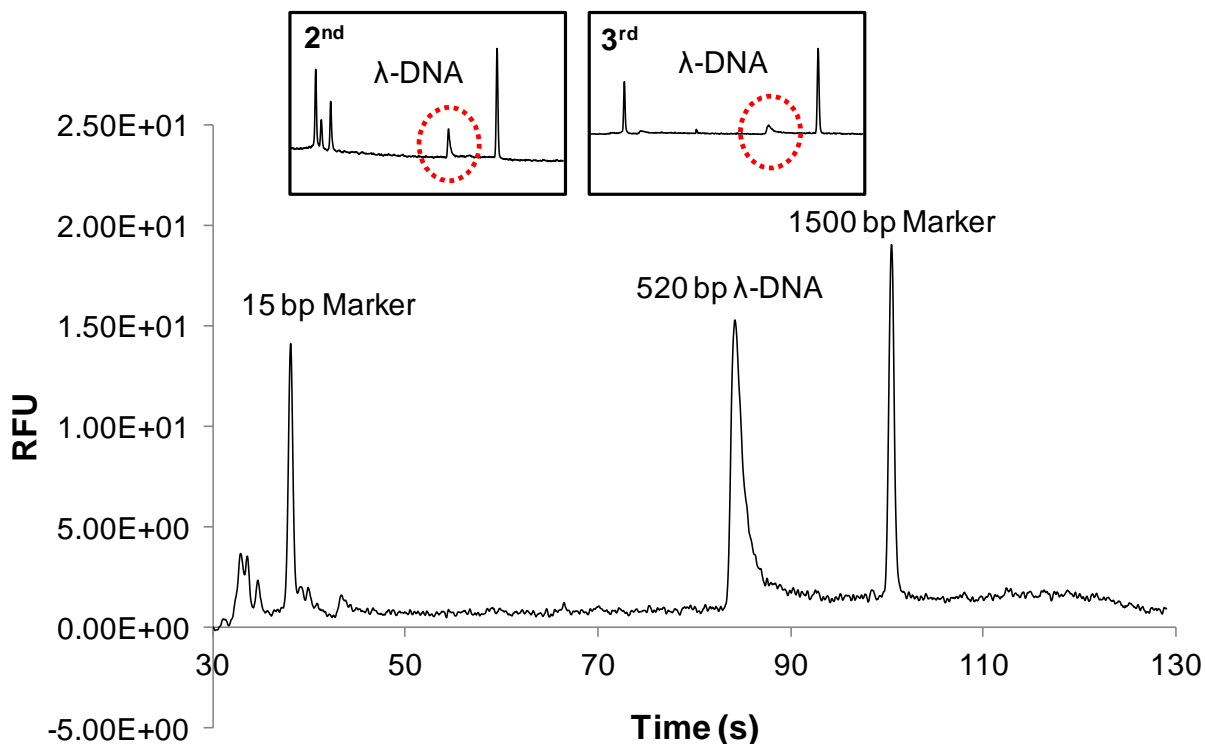


**Figure 16:** Pyrometer-controlled DNA amplifications. Electropherograms show successful DNA amplifications via pyrometer driven thermocycling. 10 ng/ $\mu$ L of  $\lambda$ -DNA template was used to conduct microchip PCR in a six layered PMMA microchip.

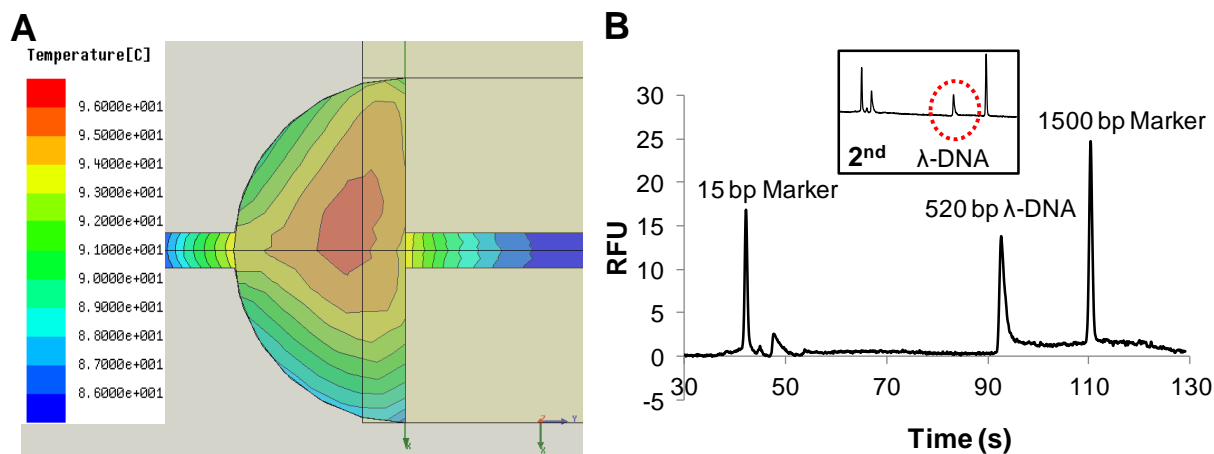


**Figure 17:** Thermal modeling of the half PCR chamber in the PMMA microchip and following DNA amplifications. (A) In order to remove non-uniformity of temperature in the PCR vessel, a half of the vessel under the transmission line was eliminated. (B) Electropherograms shows successful DNA amplifications from the  $\lambda$ -DNA template from the half PCR chamber.

adjusting current LabVIEW code to combine on/off and proportional voltage control. Natural cooling rate can be further enhanced by installation of an enforced fan in our microwave setup.

Furthermore, in order to further improve temperature distribution, a half PCR chamber uncovered by the transmission line was modeled and DNA amplifications were tested using the same PCR recipe and cycles as in a full size of the PCR chamber. Improved temperature distribution was proven by thermal modeling (**Fig. 17A**). However, the efficiency of PCR did not increase (**Fig. 17B**). Alternatives of designs in the PCR chamber, the microchip, and transmission line should be further studied with PCR chemistry such as several passivation strategies to increase microchip PCR yields.

### 3.4 Conclusions

Our successful DNA amplifications prove that rapid microwave heating with parallel DNA amplifications have been achieved utilizing  $\sim 1$  W of microwave power that showed feasibility for developing a portable genetic analyzer. Furthermore, commercially available

components used in the wireless communication industry and an optimized matching network were utilized to efficiently deliver microwave into the microchamber for PCR applications. A well characterized polymeric material, PMMA, has been chosen to construct microdevices using fast, simple microfabrication via CO<sub>2</sub> laser etching. For effective temperature sensing, the pyrometer (IR-thermometry) has successfully been utilized to demonstrate several advantages over thermocouple driven thermocycling such as no surface coating of a thermocouple, complete sealing of the microchamber, and measurement of average temperature around the PCR chamber. Using low-power driven microwave, easy fabrication using polymeric substrates, and temperature monitoring method by a properly calibrated pyrometer system, we demonstrate that the microwave heating system can achieve stable thermocycling that leads to repeated  $\lambda$ -phage DNA amplifications for the purpose of molecular diagnostics and DNA genotyping. Resulting data shows that a minimum detection limit in our setup was between 1 ng/ $\mu$ L to 10 ng/ $\mu$ L in microchip electrophoresis and the optimization of our microdevice and microwave setup should be further needed. This study describes the potential of ultra-fast thermocycling profiles and subsequent DNA amplification using microwave-induced heating that enables the functional integration of microwave-assisted PCR in a portable, low-power genetic analyzer in the future.

### 3.5 References

- (1) Spencer, P. L. Means for treating food stuffs. U.S. Patent 2,605,383, July 29, **1952**.
- (2) Ramaswamy, H.; Vandevoort, F. R. Microwave Applications in Food-Processing. *Canadian Institute of Food Science and Technology Journal-Journal De L Institut Canadien De Science Et Technologie Alimentaires* **1990**, 23, At17-At21.
- (3) Lew, A.; Krutzik, P. O.; Hart, M. E.; Chamberlin, A. R. Increasing rates of reaction: Microwave-assisted organic synthesis for combinatorial chemistry. *Journal of Combinatorial Chemistry* **2002**, 4, 95-105.
- (4) Hume, W. R.; Makinson, O. F. Microwave sterilization. *J Am Dent Assoc* **1986**, 112, 160, 162.

- (5) Marcato, B.; Vianello, M. Microwave-assisted extraction by fast sample preparation for the systematic analysis of additives in polyolefins by high-performance liquid chromatography. *J Chromatogr A* **2000**, *869*, 285-300.
- (6) Santagada, V.; Frecentese, F.; Perissutti, E.; Fiorino, F.; Severino, B.; Caliendo, G. Microwave assisted synthesis: a new technology in drug discovery. *Mini Rev Med Chem* **2009**, *9*, 340-58.
- (7) Goodwin, D. C.; Lee, S. B. Microwave miniprep of total genomic DNA from fungi, plants, protists and animals for PCR. *Biotechniques* **1993**, *15*, 438, 441-2, 444.
- (8) Hultner, M. L.; Cleaver, J. E. A bacterial plasmid DNA miniprep using microwave lysis. *Biotechniques* **1994**, *16*, 990-2, 994.
- (9) Oh, K.; Sklavounos, A. H.; Marchiarullo, D. J.; Barker, N. S.; Landers, J. P. Microwave-assisted polymerase chain reaction (PCR) in disposable microdevices. In *Proceedings of the 15th international conference on miniaturized systems for chemistry and life sciences* Seattle, WA, USA, 2011, p 305-307.
- (10) Tanaka, M.; Sato, M. Microwave heating of water, ice, and saline solution: molecular dynamics study. *J Chem Phys* **2007**, *126*, 034509.
- (11) Fermer, C.; Nilsson, P.; Larhed, M. Microwave-assisted high-speed PCR. *Eur J Pharm Sci* **2003**, *18*, 129-32.
- (12) Orrling, K.; Nilsson, P.; Gullberg, M.; Larhed, M. An efficient method to perform milliliter-scale PCR utilizing highly controlled microwave thermocycling. *Chem Commun (Camb)* **2004**, 790-1.
- (13) Shah, J. J.; Sundaresan, S. G.; Geist, J.; Reyes, D. R.; Booth, J. C.; Rao, M. V.; Gaitan, M. Microwave dielectric heating of fluids in an integrated microfluidic device. *Journal of Micromechanics and Microengineering* **2007**, *17*, 2224-2230.
- (14) Issadore, D.; Humphry, K. J.; Brown, K. A.; Sandberg, L.; Weitz, D. A.; Westervelt, R. M. Microwave dielectric heating of drops in microfluidic devices. *Lab on a Chip* **2009**, *9*, 1701-1706.
- (15) Shaw, K. J.; Docker, P. T.; Yelland, J. V.; Dyer, C. E.; Greenman, J.; Greenway, G. M.; Haswell, S. J. Rapid PCR amplification using a microfluidic device with integrated microwave heating and air impingement cooling. *Lab Chip*, *10*, 1725-8.
- (16) Giordano, B. C.; Ferrance, J.; Swedberg, S.; Huhmer, A. F. R.; Landers, J. P. Polymerase chain reaction in polymeric microchips: DNA amplification in less than 240 seconds. *Analytical Biochemistry* **2001**, *291*, 124-132.
- (17) Easley, C. J.; Karlinsey, J. M.; Landers, J. P. On-chip pressure injection for integration of infrared-mediated DNA amplification with electrophoretic separation. *Lab on a Chip* **2006**, *6*, 601-610.
- (18) Wittwer, C. T.; Fillmore, G. C.; Hillyard, D. R. Automated Polymerase Chain-Reaction in Capillary Tubes with Hot Air. *Nucleic Acids Research* **1989**, *17*, 4353-4357.
- (19) Wittwer, C. T.; Fillmore, G. C.; Garling, D. J. Minimizing the time required for DNA amplification by efficient heat transfer to small samples. *Anal Biochem* **1990**, *186*, 328-31.
- (20) Legendre, L. A.; Bienvenue, J. M.; Roper, M. G.; Ferrance, J. P.; Landers, J. P. A simple, valveless microfluidic sample preparation device for extraction and amplification of DNA from nanoliter-volume samples. *Anal Chem* **2006**, *78*, 1444-51.

- (21) Roper, M. G.; Easley, C. J.; Legendre, L. A.; Humphrey, J. A.; Landers, J. P. Infrared temperature control system for a completely noncontact polymerase chain reaction in microfluidic chips. *Anal Chem* **2007**, *79*, 1294-300.
- (22) Yi, P.; Kayani, A. A.; Chrimes, A. F.; Ghorbani, K.; Nahavandi, S.; Kalantar-zadeh, K.; Khoshmanesh, K. Thermal analysis of nanofluids in microfluidics using an infrared camera. *Lab on a Chip* **2012**, *12*, 2520-2525.
- (23) Giordano, B. C.; Copeland, E. R.; Landers, J. P. Towards dynamic coating of glass microchip chambers for amplifying DNA via the polymerase chain reaction. *Electrophoresis* **2001**, *22*, 334-340.
- (24) Easley, C. J.; Karlinsey, J. M.; Bienvenue, J. M.; Legendre, L. A.; Roper, M. G.; Feldman, S. H.; Hughes, M. A.; Hewlett, E. L.; Merkel, T. J.; Ferrance, J. P.; Landers, J. P. A fully integrated microfluidic genetic analysis system with sample-in-answer-out capability. *Proceedings of the National Academy of Sciences of the United States of America* **2006**, *103*, 19272-19277.
- (25) Lagally, E. T.; Medintz, I.; Mathies, R. A. Single-molecule DNA amplification and analysis in an integrated microfluidic device. *Analytical Chemistry* **2001**, *73*, 565-570.
- (26) Easley, C. J.; Humphrey, J. A. C.; Landers, J. P. Thermal isolation of microchip reaction chambers for rapid non-contact DNA amplification. *Journal of Micromechanics and Microengineering* **2007**, *17*, 1758-1766.
- (27) Issadore, D.; Humphry, K. J.; Brown, K. A.; Sandberg, L.; Weitz, D. A.; Westervelt, R. M. *Lab Chip* **2009**, *9*, 1701-6.
- (28) Marchiarullo, D. J. Development of microfluidic technologies for on-site clinical and forensic analysis, extraction, amplification, separation, and Detection. Ph.D. Thesis, University of Virginia, Charlottesville, VA, **2009**.
- (29) Sun, Y.; Kwok, Y. C.; Nguyen, N. T. Low-pressure, high-temperature thermal bonding of polymeric microfluidic devices and their applications for electrophoretic separation. *Journal of Micromechanics and Microengineering* **2006**, *16*, 1681-1688.
- (30) Lounsbury, J. A.; Poe, B. L.; Do, M.; Landers, J. P. Laser-ablated poly(methyl methacrylate) microdevices for sub-microliter DNA amplification suitable for micro-total analysis systems. *Journal of Micromechanics and Microengineering* **2012**, *22*.
- (31) Duarte, G. R.; Price, C. W.; Augustine, B. H.; Carrilho, E.; Landers, J. P. Dynamic Solid Phase DNA Extraction and PCR Amplification in Polyester-Toner Based Microchip. *Anal Chem*, *83*, 5182-9.
- (32) Pak, N.; Saunders, D. C.; Phaneuf, C. R.; Forest, C. R. Plug-and-play, infrared, laser-mediated PCR in a microfluidic chip. *Biomed Microdevices*, *14*, 427-33.
- (33) Hong, T. F.; Ju, W. J.; Wu, M. C.; Tai, C. H.; Tsai, C. H.; Fu, L. M. Rapid prototyping of PMMA microfluidic chips utilizing a CO<sub>2</sub> laser. *Microfluidics and Nanofluidics* **2010**, *9*, 1125-1133.
- (34) Klank, H.; Kutter, J. P.; Geschke, O. CO<sub>2</sub>-laser micromachining and back-end processing for rapid production of PMMA-based microfluidic systems. *Lab on a Chip* **2002**, *2*, 242-246.

## **4. Rapid Detection of Viral Genetic Materials in Microfluidic Devices using Infrared-mediated Heating System and Degenerate Primers**

### **4.1 Introduction**

#### *4.1.1 Static PCR in Microchips*

During three decades, the Polymerase Chain Reaction (PCR)<sup>1</sup> has stayed as an imperative tool in the field of molecular biology, molecular diagnostics, and forensic science, providing the simple *in vitro* enzyme reaction to exponentially amplify target DNA from many types of specimen. However, conventional PCR is time and reagent consuming since it still requires 1 – 3 hours for one set of reactions and 50  $\mu$ L – 100  $\mu$ L volumes for one reaction. With the advent of “Lab on a chip” technologies<sup>2</sup>, DNA amplification in a microfluidic device, especially a static format on the microfluidic device<sup>3-6</sup>, have been intensively studied in several groups<sup>4,7</sup> in consequence of following reasons. First, a small volume (miniaturization) of the PCR chamber can raise heating and cooling rates by decreasing thermal masses (PCR samples and microchip materials) to be heated and cooled in the glass and polymeric microdevices<sup>8,9</sup>. Secondly, it can accomplish complete reduction of the PCR solution up to nano-liters, sometimes, pico-liter of a droplet size in a continuous flow platform<sup>10</sup>. Additionally, as an essential benefit of miniaturization, integration with other upstream and downstream functional units such as DNA extract and DNA detection methods can be realized on the same microdevice with simple valves and pumps, and ultimately, this fully integrated microfluidic device is capable of improving analysis time and increasing the number of reactions per one device with portability<sup>6</sup>. From these benefits, this present work demonstrates that a static format of the PCR microdevice using an infrared (IR)-mediated heating system is able to detect viral gene segments via sets of degenerate primers.

#### 4.1.2 Degenerate Primer-mediated Microchip PCR for Molecular Diagnostics

In order to achieve multiplex PCR amplifications in a single reaction, the appropriate design of a primer set is very crucial in molecular diagnostics<sup>11</sup>. Furthermore, the set and design of primers can modify PCR protocols and cycles. In case of molecular diagnostics of pathogens such as viruses and bacteria, molecular evolution of genomic DNA and cross-species recombination events, which are continuously accumulated in their genomes, and many types of sub-strains are able to cause the difficulty of the PCR detection using defined numbers of primer sets<sup>12-14</sup>. In order to improve specificity and broaden the sensitivity of PCR-based genetic analysis, *degenerate primers* had been introduced to successfully amplify target DNA from several types of viruses and viral families<sup>15</sup>. Target protein sequences (evolutionarily conserved amino acid motifs in protein family) were used to generate multiply aligned homologous sequences of the target protein family (commonly occurred in its families) and this information was converted to the nucleotide sequences consisting of a pool of primer sets. These sets of *degenerate primers* have been successfully employed for identifying and characterizing homologous sequences of these protein families and new virus sub-strains from clinical samples<sup>16</sup>.

In present work, the target gene (DNA polymerase) of herpes simplex virus (**Fig. 1A**) has been chosen to be amplified and analyzed on the polymeric microfluidic device via degenerate primer strategies following previous achievements in molecular diagnostics on the conventional thermocycler<sup>12</sup>. The herpes simplex viral family has diverged into a variety of sub-strains that can complicate a PCR-based detection due to changes in the primer binding regions, but some partially conserved sequences in the viral genome can be exploited to expand the specificity of a PCR-based assay for the detection of herpes virus DNA. A small library of *degenerate primers*

designed from homologous sequences of highly conserved amino acids (CODEHOP; CONsensus DEgenerate Hybrid Oligonucleotide Primers)<sup>16</sup> were used in a polymeric microdevice to amplify the segment (602 bp) of DNA polymerase gene in the human herpesvirus-4 (HHV-4) genome (**Fig. 1B**). Following successful DNA amplifications from viral DNA templates in the microchip, it reports reduction in PCR time, the reaction volume, and the amounts of DNA templates in microfluidic devices using our IR-mediated PCR system (**Fig. 1C**).

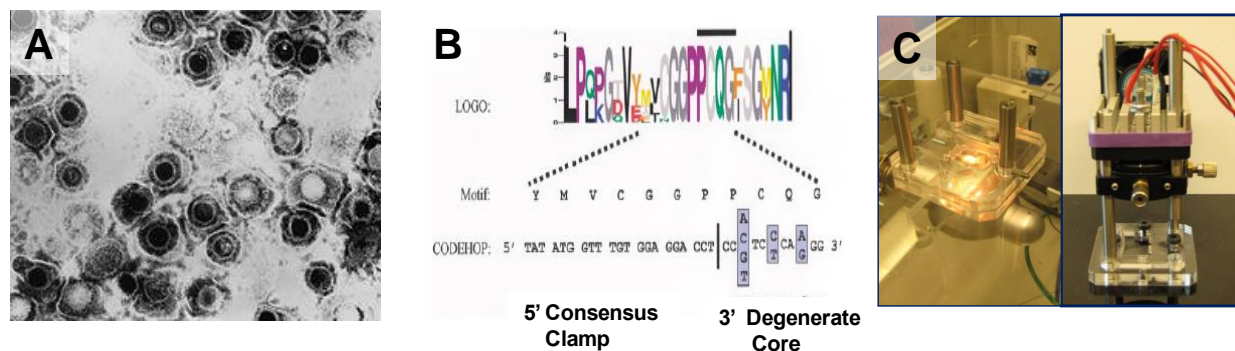


**Figure 1:** Schematic of the rapid detection of Human Herpesvirus 4 (HHV-4) using degenerate primers (CODEHOP). (A) Picture of human crude samples provided by CDC. (B) Schematic of designing CODEHOP. (C) Two types of infrared-mediated heating systems; lamp [6] and laser [30].\* *EBV samples from CDC; plasmid DNA harboring HHV-4 gene, 1 pg/ $\mu$ L ( $1 \times 10^6$  copies/ $\mu$ L).*

## 4.2 Materials and Methods

### 4.2.1 Infrared (IR)-mediated Heating System

Our IR-mediated system (**Fig. 2**) installed with a 50W tungsten lamp (CXR/CXL, General Electric, Fairfield, CT, USA) and an enforced cooling fan (MAGLev motor fan, Sunon Inc., Brea, CA, USA) was used to perform PCR-based molecular diagnostics for the rapid detection of genetic materials. 5/12V power supply (HCBB-75W-A, Power-One, Camarillo, CA,

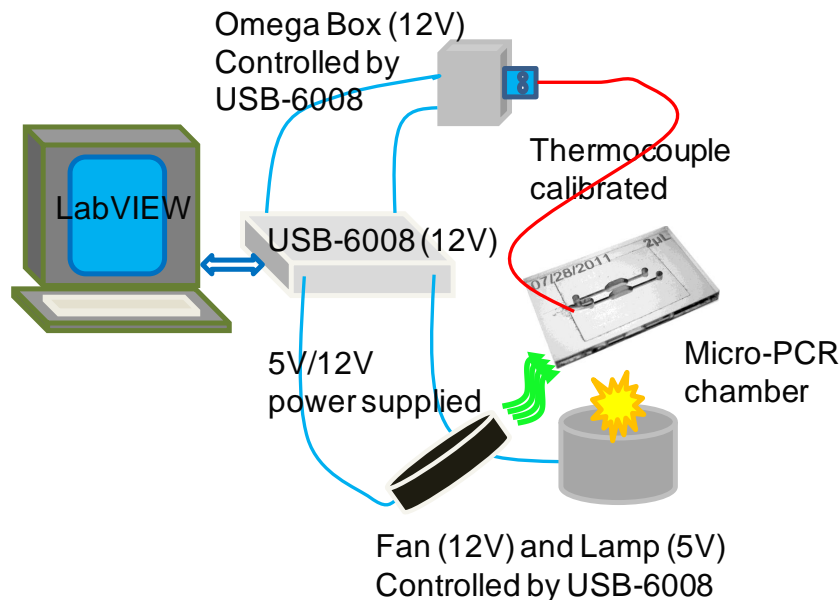


**Figure 2:** Infrared (IR)-mediated heating system [6]. A tungsten lamp for heating and an enforced fan for cooling were employed. This system was controlled via DAQ card (USB-6008) and LabVIEW code. Omega box with a thermocouple was used for temperature measurement. The proportional-integral-derivative (PID) control algorithm was coded in the LabVIEW. 5V/12V power was supplied for each component.

USA) was employed to provide power for these lamp and fan<sup>6</sup>. The temperature control apparatus was built in-house with a USB-6008 data acquisition card that was controlled via a LabVIEW programmed (hardware and software by National Instruments, Austin, TX, USA) computer. The type-t copper-constantan thermocouple (model T240C: Physitemp Instruments, Inc., Clifton, NJ, USA) was connected to a thermocouple-to-analog converter (TAC-386-T, Omega Engineering, Stamford, CT, USA) that amplified and linearized the signal from a thermocouple placed in the microchip<sup>6</sup>. A proportional-integral-derivative (PID) feedback control algorithm was programmed in the LabVIEW to precisely control temperature during temperature transition state. Before conducting microchip PCR, a thermocouple was completely calibrated against a conventional PCR thermocycler. All components were assembled into a portable box that can be delivered to any place<sup>17</sup>.

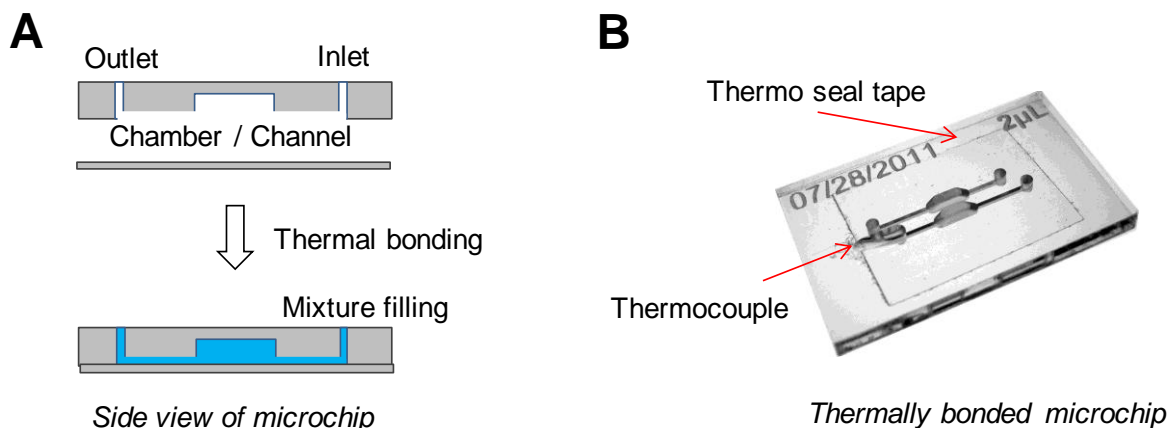


**Figure 3:** Drawing and picture for side and top views of the PMMA microchip. (A) The side view of the microchip illustrated the procedure to make the microchip and fill the PCR chamber with the PCR solution. The computer-aided milling and thermal bonding were utilized for fabrication. (B) The top view of the microchip describes how to effectively seal the microchip after the PCR chamber filled. After a thermocouple inserted, the adhesive thermo seal tape was used to completely seal the PCR chamber.

#### 4.2.2 Microchip Fabrication

The microfluidic device was engineered to optimally conduct PCR in a microscale volume PCR chamber. The dimension of the PCR chamber was 2.3 mm \* 0.5 mm \* 0.75 mm, length \* width \* depth. For the microchip material, PMMA (McMaster-Carr, Elmhurst, IL, USA) was chosen because it was amenable to rapid microfabrication and thermal bonding. All microchips were designed in AutoCAD (AutoDesk, Inc., San Rafael, CA, USA) and fabricated using a 3-axis vertical milling center (Haas Automation, Inc., OM-1A, Oxnard, CA, USA) with miniature end mills (Harvey tool, Rowley, MA, USA) and drill bits (Drill Bit City, Chicago, IL, USA). Other pieces of equipment such as a microchip holder and frame were prepared via CO<sub>2</sub> laser ablation. After milling and laser ablation, the microchip was completely cleaned by ethanol and purified water, and dried by pure nitrogen gas. The bottom of the milled microchip was

thermally bonded by 100  $\mu\text{m}$  of a PMMA film on a hot plate at 165  $^{\circ}\text{C}$  for 30 minutes, and 100 psi pressure following our established bonding procedure<sup>9</sup> (**Fig. 3 and 4**).

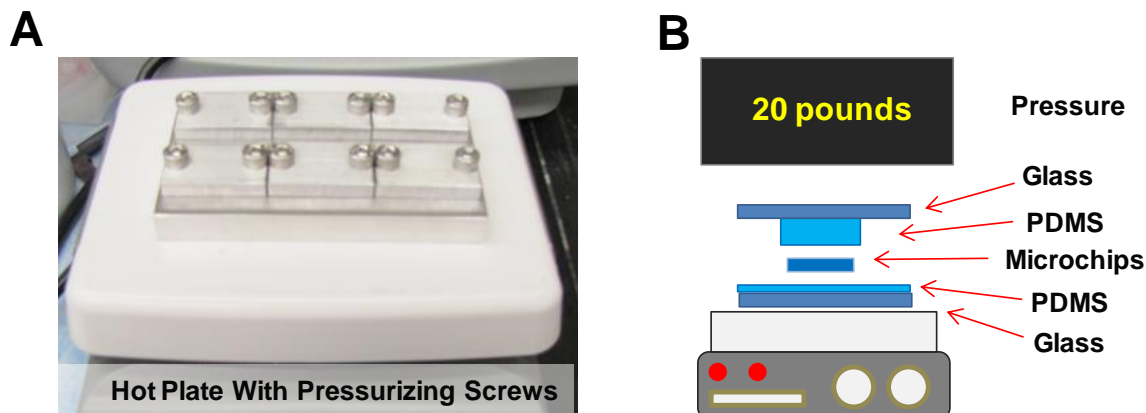


**Figure 4:** Rapid thermal bonding of polymeric microdevices [9]. (A) Laboratory hot plate with pressurizing screws was used for thermal bonding of polymeric microchips. (B) Another approach of the thermal bonding of the polymeric microchip on the hot plate with designated weights.

#### 4.2.3 Microchip PCR Protocols

Template DNA used for microchip PCR was plasmid DNA (pCR®4 TOPO vector, Invitrogen, Grand Island, NY, USA) containing the sequence for the DNA polymerase gene of Epstein-Barr virus (EBV; Human herpesvirus type 4, HHV-4) provided by CDC (Center for Disease Control, Collaborator of Dr. Forest lab at the Georgia Institute of Technology). The PCR solution for the microchip were prepared in 5  $\mu\text{L}$  volume and stored at 4  $^{\circ}\text{C}$  for multiple analyses; 0.5  $\mu\text{L}$  10 x PCR buffer, 0.8  $\mu\text{L}$   $\text{MgCl}_2$  (25 mM), 0.1  $\mu\text{L}$  dNTP mixture (10 mM), 0.1  $\mu\text{L}$  forward and reverse primers (20  $\mu\text{M}$ ), 1.2  $\mu\text{L}$  bovine serum albumin (BSA) (1 mg/mL), and 0.5  $\mu\text{L}$  degenerate primers (50  $\mu\text{M}$ ). The PCR sample was injected into the PCR chamber using a standard pipette tip. The type-t thermocouple was placed into the reference microchamber. Optically transparent and biologically compatible adhesive film (Excel Scientific, Thermal Seal RT, Victorville, CA, USA) was affixed over the inlet and outlet and the hot melt adhesive glue

was applied to the edge of the thermal seal film to ensure complete sealing and prevent any leak from the reservoir where the thermocouple was inserted (**Fig. 5A**). The PCR sample-filled microchip was placed into the microchip holder (**Fig. 5B**) and the adjustable table (**Fig. 5C**) was located over the IR-mediated heating system (**Fig. 5D**). Finally, IR-PCR was conducted on our heating setup.

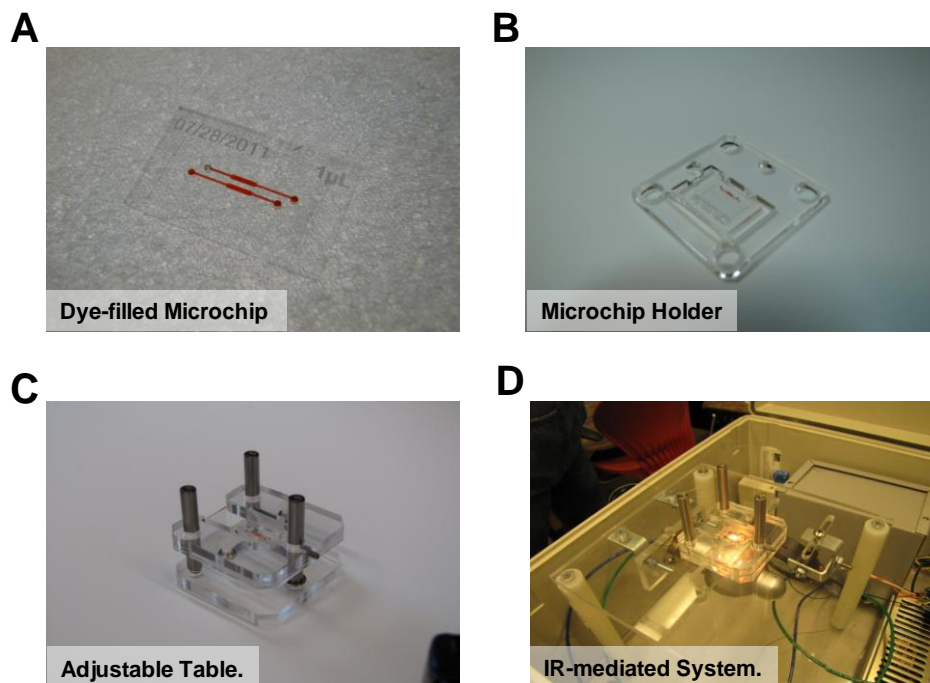


**Figure 5:** Procedure of IR-mediated PCR in the polymeric microdevice. (A) PCR sample was filled into the PCR chamber and a thermocouple was placed into the reference chamber. (B) Microchip was placed on the microchip holder. (C) Microchip holder with the microchip was on the adjustable table. (D) Performing IR-mediated PCR on our setup as described in the previous reference [6].

The same PCR protocol was employed for standard PCR on the conventional thermocycler. The standard PCR cycle optimized by CDC staffs was pre-denature at 94 °C for 2 minutes, [denature at 94 °C for 15 seconds, anneal at 48 °C for 30 seconds, extension at 72 °C for 30 seconds] x 40, and final extension at 72 °C for 7 minutes. The microchip PCR cycle was pre-denature at 95 °C for 1 minute, [denature 93 °C for 5 seconds, anneal at 48 °C for 15 seconds, extension at 72 °C for 15 seconds] x 40, and final extension at 72 °C for 2 minutes. After

conducting microchip PCR, the thermal seal film was carefully peeled away and the PCR sample was taken by a standard pipette tip. The PCR product was evaluated by Agilent 2100 Bioanalyzer (Agilent Technologies, Santa Clara, CA, USA), the commercialized microchip electrophoresis instrument.

## 4.3 Results and Discussion

### 4.3.1 *Microchip Design and Fabrication*

The microfluidic device was effectively engineered to conduct microliter-scale PCR on our IR-mediated heating system. For a microchip material, PMMA was chosen because it was amenable to rapid prototyping and simple thermal bonding<sup>19</sup>. In addition, it is optically transparent, economical, disposable, and relatively compatible with biological reagents. The 0.7 mm diameter of the inlet port allowed for standard pipette tips to press and fit into this reservoir and a PCR solution was easily injected into the PCR vessel with this pipette, obviating any additional pumping. The microchannel connected into the PCR chamber that was narrow enough to prevent molecular diffusion from the PCR chamber and it could lessen the dilution of the PCR product, and large enough to insert the thermocouple (125  $\mu\text{m}$  in diameter) into the reference microchamber. The PCR chamber (2.3 mm \* 0.5 mm \* 0.75 mm, length \* width \* depth) was designed with a high aspect ratio and decrease a surface area to volume ratio. The high aspect ratio of the reaction chamber minimized the surface area (to minimize the adsorption of reagents) and maximized heat transfer into the chamber through the bottom of the device<sup>18</sup>. The IR laser and IR light from the lamp preferentially heat the water; a longer path length was predicted to gather more IR heating from the incident radiation. The thermocouple was experimentally found to inhibit PCR so that it has to be placed in the reference chamber adjacent

to the PCR vessel. Two microchambers (one for PCR and another for temperature reading) were located close enough to experience the same heating from IR-radiation, and thus the reference chamber was used to infer temperature in the PCR solution in the chamber<sup>8</sup>. The prevention of leakage through reservoirs was a very critical step for successful PCR amplification because it caused the PCR solution to flow back through the microchannel while intensively heating the PCR vessel. Complete sealing by the adhesive tape of both reservoirs with thermal glues was effective to inhibit leakage and evaporation through these reservoirs and the thermocouple. Following microchip PCR amplifications, the plastic glue and thermal film were easily peeled away without harming the thermocouple or PCR sample.

#### 4.3.2 *Preparation of CODHOP-mediated PCR in Microfluidic Devices*

In present work, we first demonstrated that CODEHOP-mediated PCR on a polymeric microdevice was exploited for the detection of herpes simplex viruses (Epstein Barr virus). Pools of primers designed for the detection of target viruses were kindly provided by CDC. The optimal anneal temperature at 48 °C was experimentally chosen on the conventional thermocycler by the CDC staffs and the same anneal temperature was employed to show detectable amounts of PCR amplifications in our polymeric microdevices. Too low anneal temperature could generate certain amounts of nonspecific DNA amplifications and too high temperature could not produce any PCR product in microfluidic devices. Additionally, reduced reaction time for a denaturation step from 15 seconds to 5 seconds, an anneal step from 30 seconds to 15 seconds, and an extension step from 30 seconds to 15 seconds were used for microchip PCR and it completely reduced total PCR time from 3 hours to 40 minutes. The ramp rate for heating was ranging from 5.69 °C/s to 6.32 °C/s and cooling to 2.08 °C/s.

All PCR recipes and PCR procedures were optimized based on the previous publications such as 1) CODEHOP-mediated PCR for the detection of herpes simplex virus<sup>12</sup> and 2) IR-mediated microchip PCR<sup>6</sup>. While technically transferring a standard PCR procedure to microchip PCR, concentrations of several PCR reagents were adjusted for the microchip PCR recipe<sup>14</sup>. For CODEHOP-mediated PCR applications in the microchip, higher concentrated primers than the standard PCR approach were used to detect viral sub-strains<sup>13</sup>. The passivation reagent, Bovine Serum Albumin (BSA), was added for dynamic passivation of the microchip surface to counteract the adsorption-mediated loss of PCR reagents<sup>3,4,20-23</sup>. The PCR recipe used in the microchip was tested in the conventional thermocycler to verify successful PCR amplifications from modified recipes where there was no inhibitory effect to ensure our PCR amplifications in the polymeric microchip. The optimized PCR recipe in the microchip was successfully utilized to detect low concentrations (1 and 2 pg of DNA) of target DNA using the polymeric microchip on our IR-mediated heating setup.

#### 4.3.3 *Air Bubble Formation and Removal Strategies*

As I mentioned before, polymeric materials such as PMMA<sup>9</sup>, PC<sup>24</sup>, and PeT<sup>25</sup> for microchip PCR are suitable alternatives instead of silicon/glass materials due to rapid fabrication and simple thermal bonding as well as disposability of microchips and biocompatibility with PCR reagents<sup>26,27</sup>. However, several issues have been reported in static PCR on polymeric microdevices such as imprecise temperature control and measurement, air bubble formation, and passivation<sup>9</sup>. During my time working with Dr. Forest at Georgia Tech, the main subjects were focused on proper passivation of the PCR chamber using appropriate reagents and decrease of air bubble formation inside the PCR chamber. For a passivation issue, BSA, which has intensively

been exploited to passivate the surface of the microchip material, could work well to improve PCR amplifications in polymeric and glass microfluidic devices. However, it was difficult to completely suppress the formation of air bubbles in the PCR chamber. Air bubbles were likely to form along the surface of the PCR chamber, which put away the reaction solution from the PCR chamber into the microchannel and caused complete leakage of the PCR solution. As IR-mediated heating was centered on the small spot around the PCR vessel, this movement of the PCR sample enforced by bubbles could strongly inhibit PCR amplifications via evaporation. Furthermore, the hydrophobicity on the PMMA surface of the PCR chamber and channel increased the chance of air bubble formation and resulting air bubbles made them circular to decrease the surface tension and they moved into the PCR vessel where bubbles had enough space to form large bubbles. If these bubbles were stacked on the tip of the thermocouple in the reference chamber, it could disrupt temperature measurement and consequently inhibited PCR amplifications.

The micro-bubble, which interferes with microchip PCR<sup>28,29</sup>, are able to be generated in many places around the microchamber. First, while thermally bonding multiple sheets of polymers, certain amounts of air bubbles can be trapped between these layers. Heating around air gas-trapped region during the denaturation step induces the formation of air bubbles, which are expanded into the PCR vessel<sup>28</sup>. In order to solve these issues, proper bonding of the polymeric microchip ensures reduction of air bubble formations. Thermal bonding inside the vacuum helps remove all air bubbles in bonded layers. In addition, as laser cutting could not perfectly create the smooth surface on the polymeric material, it caused air trapping around a rough surface while injecting the sample into the PCR vessel<sup>9</sup>. This problem was tackled by polishing the rough surface on the ablated polymer by chemical and physical methods or laser

ablation with defocused laser (smoothing process). The degasification of all PCR reagents or the injection of the PCR solution inside vacuum can decrease the chance to generate air bubbles from samples. Adhesive tapes and manifolds could prevent leakage through the outlet and inlet, and provide enough amount of pressure into the port to suppress expansion of air bubbles<sup>9,30</sup>. The Forest group also conducted PCR inside pressurized boxes where the microchip was located and PCR efficiency was improved. In our group, the manifold has been successfully employed to suppress air bubbles in the PCR chamber and improve PCR efficiency<sup>9</sup>. There are many ways to solve air bubble issues so that it should be carefully considered with types of microchip PCR systems.

#### 4.3.4 *Thermocycling in Engineered Microchip via IR Heating System*

The Forest group reported a laser-mediated system that has 1450 nm infrared laser diode with heat sink and fan, and showed reliable DNA amplifications without feedback control (PID control)<sup>30</sup>, open-loop control. Open-loop control used in their work made instrument is easy to be miniaturized by eliminating a thermal control system. Our group (Dr. Landers group) has reported two types of heating systems for PCR applications; Infrared-mediated heating system<sup>6</sup> and microwave-assisted heating system (**In chapter 3**)<sup>31</sup>. Both systems are non-contact heating methods and they selectively heat a PCR solution much stronger than the microchip material, because lamp radiation is selectively absorbed by two different materials such as a PCR solution and a glass/polymeric microchip, and selective microwave heating depends on different dielectric heating constants of two materials. However, rapid and selective heating caused the difficulty in precise temperature control and measurement. Accurate temperature control on the microfluidic device was a critical step to succeed DNA amplification in a microchip. **Figure 6**

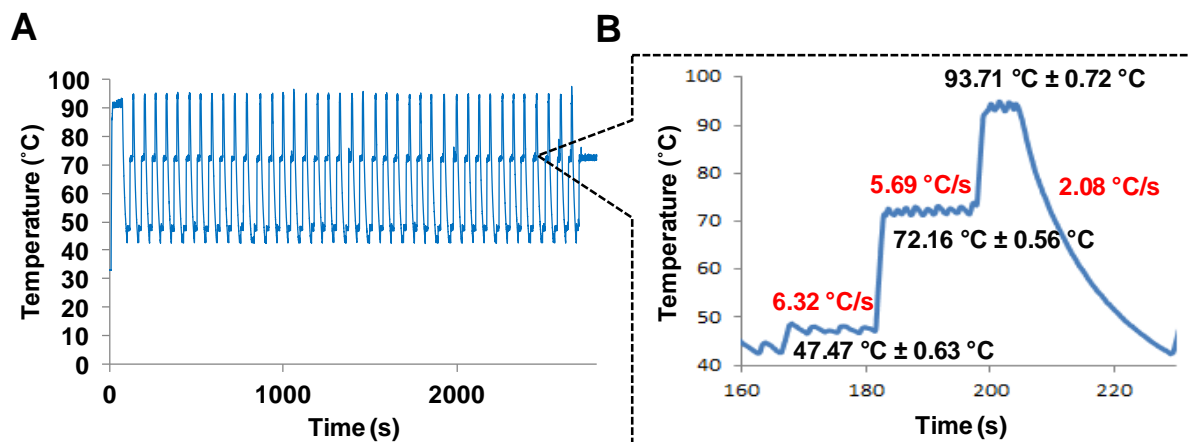


**Figure 6:** Temperature profile of IR-mediated PCR in the polymeric microdevice. (A) 40 cycles of PCR was conducted on our polymeric microchip. (B) The inset indicates ramp rates (heating for 5.69 °C to 6.32 °C/s, and cooling 2.08 °C/s and stable temperature holds (within  $\pm 0.7$  °C) in three different PCR zones.

describes the temperature profile for 40 cycles of PCR that was used for the amplification of target DNA inside the single chambered PMMA microchip. This profile presented rapid thermocycling with stable temperature holds in each PCR zone, because it achieved decreased temperature transition times. The ramp rate for heating was around 5.69 °C/s to 6.32 °C/s and cooling was 2.08 °C/s, which were faster than the conventional thermocycler. Temperature holds in three PCR zones were between  $\pm 0.7$  °C and  $\pm 0.5$  °C and it was stable enough for PCR amplifications at fixed temperatures. The stable temperature hold could provide consistent PCR amplifications. The total analysis time in PCR decreased up to 47 minutes, comparing to 2 - 3 hours on the conventional one. Conclusively using our IR-mediated heating system with a tungsten lamp, we successfully demonstrated the DNA amplification of the 602 bp fragment from the gene of HHV-4 DNA polymerase using total masses of DNA templates ranging from 1 pg to 2 pg (1 pg is a  $10^6$  copies of template DNA by CODEHOP mediated-PCR in a polymeric microdevice).

#### 4.3.5 Comparison of Conventional PCR to Microchip PCR

In order to demonstrate the difficulty of small volume PCR in the conventional setup, several standard PCR amplifications were conducted with reduced PCR volumes ranging from 5  $\mu$ L to 1  $\mu$ L and the same amounts of the DNA template (1 pg of template DNA) used in microchip PCR. **Figure 8** illustrated that PCR yields decreased with the volume of the PCR sample, although DNA concentrations in the same volume of the PCR chamber increased from 0.2 pg/ $\mu$ L to 1 pg/ $\mu$ L: we used the same mass of template DNA in different volumes of the PCR solution. When the PCR volume reached 1  $\mu$ L of the reaction volume, detectable amounts of DNA amplifications had not been analyzed on the microchip electrophoresis (Agilent 2100 Bioanalyzer). The decreased volume of the PCR sample could cause the increment of the surface area to volume ratio and it increased a burden of passivation of the PCR tube.

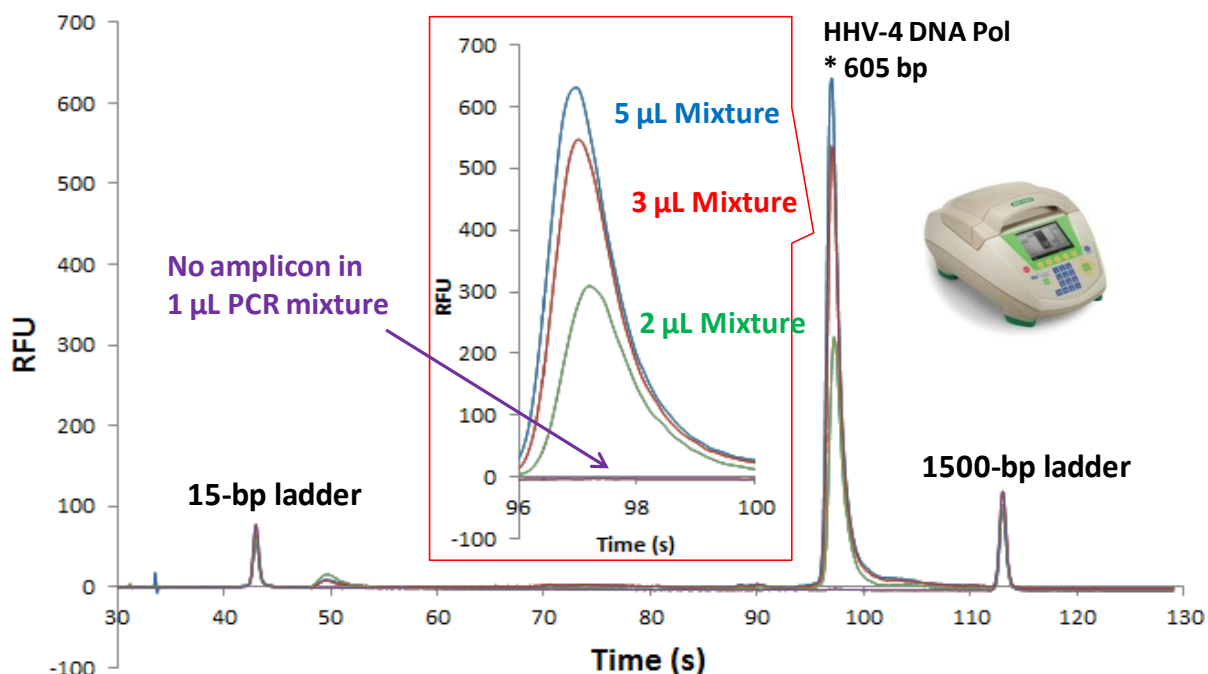


**Figure 7:** Overlaid electropherograms of DNA amplifications in different PCR volumes ranging from 5  $\mu$ L to 1  $\mu$ L in the conventional thermocycler.

Additionally, a small volume sample could be easily evaporated inside the PCR tube, although a mineral oil was placed on the top of the PCR solution to prevent evaporation of the PCR sample. The evaporation of this small volume sample could dramatically change all concentrations of PCR reagents in the microfluidic environment and it might inhibit the PCR amplification in 1  $\mu$ L of the PCR solution on the conventional thermocycler. From these data, we asserted that at least more than a 2  $\mu$ L PCR sample with 1 pg of template DNA should be required for PCR amplification and the small PCR volume lower than 1  $\mu$ L is not suitable on the conventional thermocycler.

As we emphasized, the main drawbacks of a standard PCR procedure are the lengthy analysis time and large volume of the reagent consumption for one reaction (at least 25  $\mu$ L for one sample). Normally, the standard PCR amplification in the conventional thermocycler takes 2 – 3 hours using 50  $\mu$ L to 100  $\mu$ L of volumes in the PCR solution. In the microchip approach,

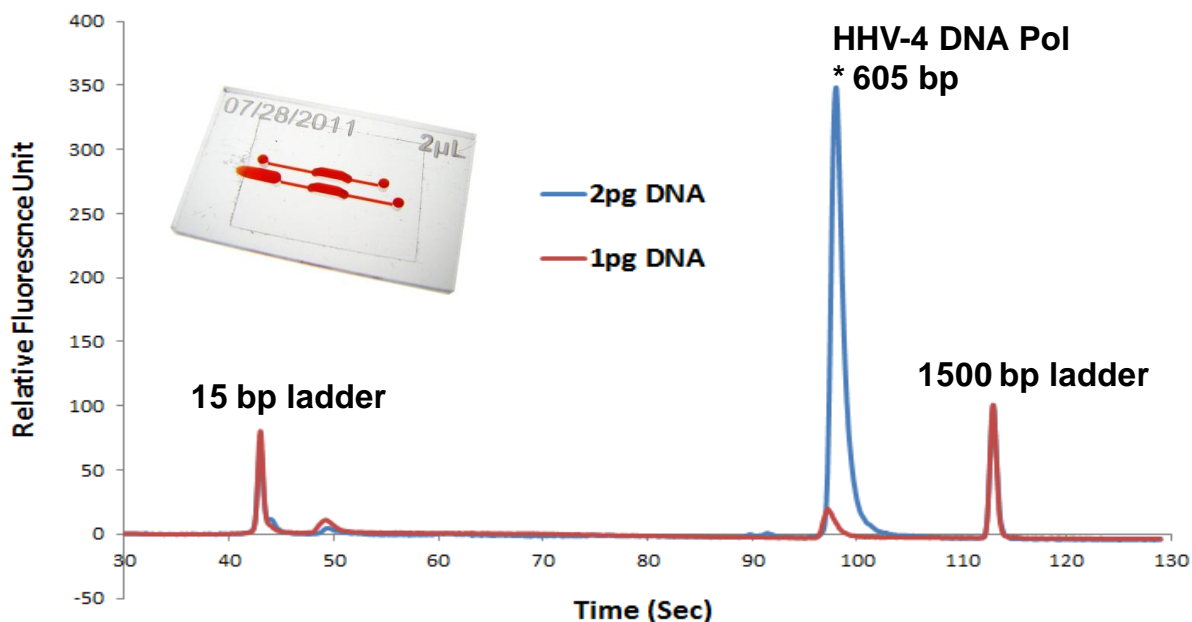


**Figure 8:** Overlaid electropherograms of DNA amplifications from two different concentrations of DNA templates (1 pg and 2 pg) in the microdevice.

the reaction time of PCR amplification and the volume of the PCR sample could extremely be lowered up to several minutes and nano or picoliter volume in the PCR chamber. From these merits, microchip PCR on the polymeric microdevice was successfully conducted in 1  $\mu$ L volume of the microchamber with low amounts of DNA templates (1 pg and 2 pg) and reaction time was completed within 40 minutes and it was three or four time reduction in PCR analysis time comparing to PCR on the thermocycler (**Fig. 8**). Although additional PCR amplifications were carried out with lower amounts of DNA templates than 1 pg of template DNA, any DNA amplification could not be detectable. The main reason might be caused by the large surface area to volume ratio that led to the adsorption of PCR reagents such as *Taq* Polymerase, DNA templates, and other reagents into the PCR vessel or evaporation of the PCR solution through the microchannel. The huge difference of DNA amplification between two template concentrations (1 pg and 2 pg in microfluidic devices) would be caused by this issue, a high surface area to volume ratio in the small volume of the PCR chamber.

#### 4.4 Conclusions

We have demonstrated rapid PCR detection from low amounts (1 and 2 pg) of viral gene in as little as 30 - 40 minutes inside 1  $\mu$ L chambered microchip and temperature ramp rate as high as 8°C/sec was achieved. Analyses were conducted in polymeric microfluidic devices that were fabricated from poly(methyl-methacrylate) (PMMA) via computer-aided milling and CO<sub>2</sub> laser ablation. The material cost for these microfluidic devices is estimated cost to be \$ 0.50 dollars USD per device. This low cost makes these devices potentially disposable and single-use, thereby eliminating carry-over contamination that can complicate molecular diagnostics. Furthermore, the low limit of detection that we have validated is important because very low

copy numbers of viral genomic materials are present in the human bodily fluids, which often have a very low virus titer despite an active infection. Our micro-scale (1  $\mu\text{L}$ ) reaction chamber easily achieved the identification of low amounts of DNA virus genetic materials. This saved time from 3 hours to 40 minutes, reagent consumption from 50  $\mu\text{L}$  to 1  $\mu\text{L}$ , and viral genetic materials from 0.5 - 5 ng to 1 - 2 pg comparing to the conventional counterpart. The heating system was described and characterized, and PCR-based identification of herpes simplex viral DNA was demonstrated with degenerate primers (CODEHOP). Ultimately, our infrared-mediated heating system can be further miniaturized and integrated with other downstream processes to construct fast, accurate, reliable, and portable genetic analyzers in the future.

#### 4.5 References

- (1) Mullis, K.; Faloona, F.; Scharf, S.; Saiki, R.; Horn, G.; Erlich, H. Specific Enzymatic Amplification of DNA In vitro - the Polymerase Chain-Reaction. *Cold Spring Harbor Symposia on Quantitative Biology* **1986**, *51*, 263-273.
- (2) Manz, A.; Graber, N.; Widmer, H. M. Miniaturized Total Chemical-Analysis Systems - a Novel Concept for Chemical Sensing. *Sensors and Actuators B-Chemical* **1990**, *1*, 244-248.
- (3) Northrup, M. A.; Benett, B.; Hadley, D.; Landre, P.; Lehew, S.; Richards, J.; Stratton, P. A miniature analytical instrument for nucleic acids based on micromachined silicon reaction chambers. *Analytical Chemistry* **1998**, *70*, 918-922.
- (4) Oda, R. P.; Strausbauch, M. A.; Huhmer, A. F.; Borson, N.; Jurens, S. R.; Craighead, J.; Wettstein, P. J.; Eckloff, B.; Kline, B.; Landers, J. P. Infrared-mediated thermocycling for ultrafast polymerase chain reaction amplification of DNA. *Anal Chem* **1998**, *70*, 4361-8.
- (5) Giordano, B. C.; Ferrance, J.; Swedberg, S.; Huhmer, A. F. R.; Landers, J. P. Polymerase chain reaction in polymeric microchips: DNA amplification in less than 240 seconds. *Analytical Biochemistry* **2001**, *291*, 124-132.
- (6) Easley, C. J.; Karlinsey, J. M.; Bienvenue, J. M.; Legendre, L. A.; Roper, M. G.; Feldman, S. H.; Hughes, M. A.; Hewlett, E. L.; Merkel, T. J.; Ferrance, J. P.; Landers, J. P. A fully integrated microfluidic genetic analysis system with sample-in-answer-out capability. *Proceedings of the National Academy of Sciences of the United States of America* **2006**, *103*, 19272-19277.
- (7) Lagally, E. T.; Emrich, C. A.; Mathies, R. A. Fully integrated PCR-capillary electrophoresis microsystem for DNA analysis. *Lab on a Chip* **2001**, *1*, 102-107.

- (8) Easley, C. J.; Humphrey, J. A. C.; Landers, J. P. Thermal isolation of microchip reaction chambers for rapid non-contact DNA amplification. *Journal of Micromechanics and Microengineering* **2007**, *17*, 1758-1766.
- (9) Lounsbury, J. A.; Poe, B. L.; Do, M.; Landers, J. P. Laser-ablated poly(methyl methacrylate) microdevices for sub-microliter DNA amplification suitable for micro-total analysis systems. *Journal of Micromechanics and Microengineering* **2012**, *22*.
- (10) Beer, N. R.; Hindson, B. J.; Wheeler, E. K.; Hall, S. B.; Rose, K. A.; Kennedy, I. M.; Colston, B. W. On-chip, real-time, single-copy polymerase chain reaction in picoliter droplets. *Analytical Chemistry* **2007**, *79*, 8471-8475.
- (11) Elnifro, E. M.; Ashshi, A. M.; Cooper, R. J.; Klapper, P. E. Multiplex PCR: Optimization and application in diagnostic virology. *Clinical Microbiology Reviews* **2000**, *13*, 559.
- (12) Rose, T. M. CODEHOP-mediated PCR - a powerful technique for the identification and characterization of viral genomes. *Virology* **2005**, *2*, 20.
- (13) Baines, J. E.; McGovern, R. M.; Persing, D.; Gostout, B. S. Consensus-degenerate hybrid oligonucleotide primers (CODEHOP) for the detection of novel papillomaviruses and their application to esophageal and tonsillar carcinomas. *Journal of Virological Methods* **2005**, *123*, 81-87.
- (14) Staheli, J. P.; Ryan, J. T.; Bruce, A. G.; Boyce, R.; Rose, T. M. Consensus-degenerate hybrid oligonucleotide primers (CODEHOPs) for the detection of novel viruses in non-human primates. *Methods* **2009**, *49*, 32-41.
- (15) Rose, T. M.; Henikoff, J. G.; Henikoff, S. CODEHOP (Consensus-DEgenerate Hybrid Oligonucleotide Primer) PCR primer design. *Nucleic Acids Res* **2003**, *31*, 3763-6.
- (16) Rose, T. M.; Schultz, E. R.; Henikoff, J. G.; Pietrokovski, S.; McCallum, C. M.; Henikoff, S. Consensus-degenerate hybrid oligonucleotide primers for amplification of distantly related sequences. *Nucleic Acids Research* **1998**, *26*, 1628-1635.
- (17) Leslie, D. C.; Seker, E.; Bazydlo, L. A.; Strachan, B. C.; Landers, J. P. Platinum nanoparticle-facilitated reflective surfaces for non-contact temperature control in microfluidic devices for PCR amplification. *Lab Chip* **2011**, *12*, 127-32.
- (18) Phaneuf, C. R.; Pak, N.; Forest, C. R. Modeling radiative heating of liquids in microchip reaction chambers. *Sensors and Actuators a-Physical* **2011**, *167*, 531-536.
- (19) Hong, T. F.; Ju, W. J.; Wu, M. C.; Tai, C. H.; Tsai, C. H.; Fu, L. M. Rapid prototyping of PMMA microfluidic chips utilizing a CO<sub>2</sub> laser. *Microfluidics and Nanofluidics* **2010**, *9*, 1125-1133.
- (20) Sweryda-Krawiec, B.; Devaraj, H.; Jacob, G.; Hickman, J. J. A new interpretation of serum albumin surface passivation. *Langmuir* **2004**, *20*, 2054-6.
- (21) Khandurina, J.; McKnight, T. E.; Jacobson, S. C.; Waters, L. C.; Foote, R. S.; Ramsey, J. M. Integrated system for rapid PCR-based DNA analysis in microfluidic devices. *Analytical Chemistry* **2000**, *72*, 2995-3000.
- (22) Lagally, E. T.; Medintz, I.; Mathies, R. A. Single-molecule DNA amplification and analysis in an integrated microfluidic device. *Analytical Chemistry* **2001**, *73*, 565-570.
- (23) Giordano, B. C.; Copeland, E. R.; Landers, J. P. Towards dynamic coating of glass microchip chambers for amplifying DNA via the polymerase chain reaction. *Electrophoresis* **2001**, *22*, 334-340.
- (24) Sun, Y.; Kwok, Y. C.; Nguyen, N. T. A circular ferrofluid driven microchip for rapid polymerase chain reaction. *Lab on a Chip* **2007**, *7*, 1012-1017.

- (25) Duarte, G. R. M.; Price, C. W.; Augustine, B. H.; Carrilho, E.; Landers, J. P. Dynamic Solid Phase DNA Extraction and PCR Amplification in Polyester-Toner Based Microchip. *Analytical Chemistry* **2011**, *83*, 5182-5189.
- (26) Sun, Y.; Kwok, Y. C. Polymeric microfluidic system for DNA analysis. *Anal Chim Acta* **2006**, *556*, 80-96.
- (27) Tsao, C. W.; DeVoe, D. L. Bonding of thermoplastic polymer microfluidics. *Microfluidics and Nanofluidics* **2009**, *6*, 1-16.
- (28) Liu, H. B.; Gong, H. Q.; Ramalingam, N.; Jiang, Y.; Dai, C. C.; Hui, K. M. Micro air bubble formation and its control during polymerase chain reaction (PCR) in polydimethylsiloxane (PDMS) microreactors. *Journal of Micromechanics and Microengineering* **2007**, *17*, 2055-2064.
- (29) Nakayama, T.; Kurosawa, Y.; Furui, S.; Kerman, K.; Kobayashi, M.; Rao, S. R.; Yonezawa, Y.; Nakano, K.; Hino, A.; Yamamura, S.; Takamura, Y.; Tamiya, E. Circumventing air bubbles in microfluidic systems and quantitative continuous-flow PCR applications. *Analytical and Bioanalytical Chemistry* **2006**, *386*, 1327-1333.
- (30) Pak, N.; Saunders, D. C.; Phaneuf, C. R.; Forest, C. R. Plug-and-play, infrared, laser-mediated PCR in a microfluidic chip. *Biomed Microdevices* **2012**, *14*, 427-33.
- (31) Oh, K.; Sklavounos, A. H.; Marchiarullo, D. J.; Barker, N. S.; Landers, J. P. Microwave-assisted polymerase chain reaction (PCR) in disposable microdevices. In *Proceedings of the 15th international conference on miniaturized systems for chemistry and life sciences* Seattle, WA, USA, **2011**, p 305-307.

## 5. **Rapid Drug Susceptibility Testing (DST) of *Mycobacterium tuberculosis* via Standard PCR and Hybridization-induced Bead Aggregation**

### 5.1 **Introduction**

#### 5.1.1 *Tuberculosis (TB) and Multidrug-resistant TB (MDR-TB)*

Tuberculosis (TB), caused by infection of a bacterium, *Mycobacterium tuberculosis*, presents a worldwide threat, especially in the developing countries, as a result of the fast spread of multidrug-resistant TB (MDR-TB) and lack of advanced analytical infra-structure. MDR-TB can be defined as showing a resistance to at least two the first line antibiotics of TB such as isoniazid (INH) and rifampicin (RIF)<sup>1</sup>. As patients infected by MDR-TB show different resistances to various antibiotics against TB, the rapid determination of drug resistance profiles ensures appropriate therapies and decrease a period of time for patients to be exposed to other people. However, determining drug susceptibility for TB, and thus choosing correct pharmaceuticals for patient treatment, typically takes several weeks of cell-culturing due to slow doubling time of TB<sup>2</sup>. Therefore, developing fast and accurate drug susceptibility testing (DST) for TB is essential to impede its spread in the world<sup>3</sup>. Furthermore, combined with “Lab on a chip” technologies, miniaturization of DST for TB in microfluidic devices can further decrease analysis time and reagent consumption, and increase sensitivity, and ultimately achieve “Point-of-Care” (POC) diagnostics of MDR-TB without any clinical laboratory testing.

#### 5.1.2 *Drug Susceptibility Testing (DST) for Drug Resistant TB*

Two major types of approaches for DST of TB have been studied, genotypical and phenotypical assays. The genotypic assay is a method to find mutations in the critical region of TB genome that provides the information of genetic changes in its genome<sup>4,5</sup>. Generally, drug

resistance in *M. tuberculosis* is generated by mutations causing functional changes of target proteins, which are closely related to target genomic areas of antibiotics metabolism or drug transporting system. However, the final verification and interpretation of these mutations in the target genes and functional regions of its genome in the genotypic assay are required for direct DNA sequencing and multiple or multiplex PCR approaches<sup>1</sup>. In addition to genetics-based assays, phenotypical assays such as luciferase reporter phage assay<sup>6,7</sup>, qPCR assay directly from growing TB<sup>8</sup>, and phage amplified biological assay<sup>9,10</sup> have been reported, and these methods have analyzed the growth status or numbers of live TB in antibiotics-treated media.

Recently, Pholwat *et al.* demonstrated that the qPCR-based DST for TB could amplify the fragment of 16S rRNA gene as target DNA after 3 days incubation in drug-treated media<sup>8</sup>. Furthermore, this group has utilized the D29 mycobacteriophage as an intermediate reagent for rapid diagnostics. In their works<sup>3</sup>, the TB specific bacteriophage, D29 phage, was infected into and replicated inside host TB cells, and their progenies were released into media within one or two days, although in slow growing TB. Lastly the number of phages in antibiotics-treated media was quantified by qPCR, the resulting qPCR curve could represent the status of drug susceptibility for each TB strain from patients (clinical samples). This qPCR based DST for TB using D29 phage has shown 100 % accuracies to several different antibiotics<sup>3</sup>. However, qPCR still requires a real-time fluorescence measuring PCR instrument with costly reagents and it gives rise to limitations of conducting multiple reactions and achieving point-of-care (POC) diagnostics outside clinical laboratory.

### 5.1.3 Standard PCR and Hybridization-induced Bead Aggregation for Drug Susceptibility Testing (DST) of TB

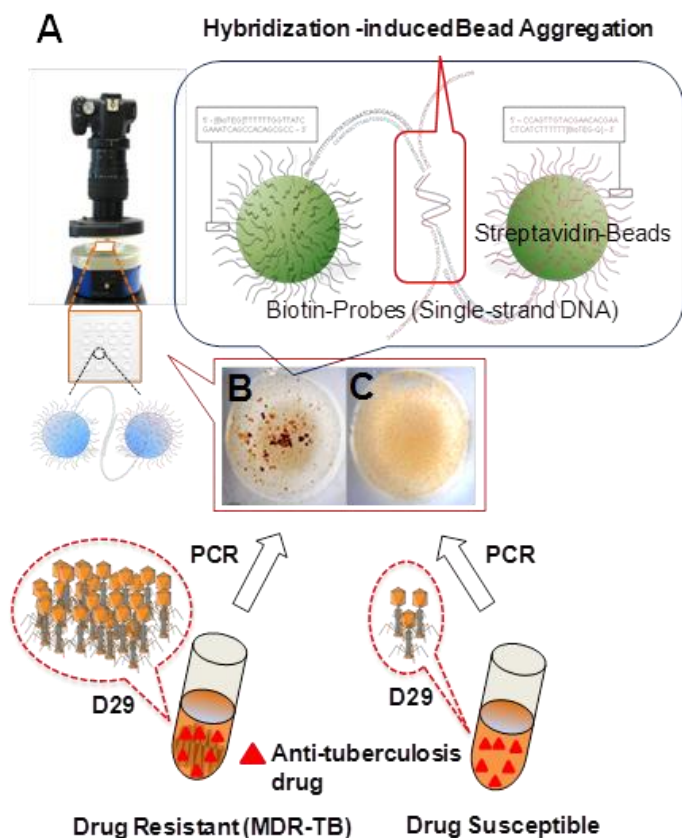


**Figure 1:** Schematic of rapid TB drug susceptibility testing (DST) using standard PCR and hybridization-induced bead aggregation. (A) Mechanical setup and molecular mechanism of hybridization-induced bead aggregation. (B) Multi-particle aggregation induced by PCR products from D29 in MDR-TB media. (C) No aggregation from PCR cocktails without DNA templates.

In order to make the DST assay simpler, faster, and more economical than a phage-based qPCR method, we conceived that a rapid assay could be accomplished via a standard PCR method instead of using a real-time PCR instrument. As the schematic shows (**Fig. 1**), the D29 bacteriophage specifically infects and replicates rapidly only when viable TB is present, allowing for the enumeration of a viable TB (not dead, following drug application) in a sample following incubation. The phage, therefore, will only be in abundance when MDR-TB is present, and thus is the chosen target for PCR.

As the initial assessment in this assay, a cycle controlled PCR method was validated to find drug susceptible and resistant TB samples via the conventional thermal cycler and microchip electrophoresis. Referring to the qPCR curve from D29 infected TB samples<sup>3</sup>, we hypothesized that the amounts of PCR products with different numbers of PCR cycles (three cycles, 25, 30,

and 40 were tested in this study) could be exploited to determine drug susceptibility of TB. From this hypothesis, the number of the PCR cycle was customized on the conventional thermal cycler to detect and analyze the amount of PCR products on microchip electrophoresis. Furthermore, a label free visual detection method has been introduced for the detection of specific DNA sequences using oligonucleotide-spiked magnetic beads through hybridization-induced bead aggregation, which was consequently applied for rapid drug susceptibility testing of TB on a portable microwell.

## 5.2 Materials and Methods

### 5.2.1 Reagents and Clinical TB Samples

Our experiment setup and schematic of rapid TB drug susceptibility testing (DST) were depicted in the **Figure 1A**. A total of 210 clinical isolates of *M. tuberculosis* strains from 35 patients that consist of 10 patients infected by drug susceptible TB and 25 patients by MDR-TB, have been tested for drug susceptibility using standard PCR and hybridization-induced bead aggregation: one patient TB sample was treated by five different antibiotics (five samples generated), two first line and three second line, isoniazid (INH), rifampin (RIF), ethambutol hydrochloride (EMB), amikacin (AMK), and ofloxacin (OFX). One sample was not treated with any drug (one positive sample) ( $35 \text{ patients} * 6 = 210$ ). All samples for the PCR assay were prepared at University of Virginia (UVA) hospital. Totally, 210 clinical samples from 35 patients have been used for testing our assay.

### 5.2.2 Standard PCR Protocols

The PCR recipe has followed the qPCR approach that is recently reported except omitting fluorescent dyes<sup>3</sup>. The preparation of PCR solutions (the final volume was up to 25  $\mu$ L) follows a normal PCR recipe as the final concentration; 1 x PCR buffer,  $MgCl_2$  (3 mM), dNTP mixture (0.2 mM), forward and reverse primers (4  $\mu$ L), *Taq* polymerase (0.2 U/ $\mu$ L) (Fisher, Fair Lawn, NJ, USA), and 5  $\mu$ L of clinical isolates; the same volume of the clinical isolate used in the previous research was utilized in this work. The standard PCR procedure was performed on the conventional thermocycler (Mycycler<sup>TM</sup> Thermal Cycler, Bio-Rad, Hercules, CA, USA). All solutions were prepared in Nanopure water (Barnstead/Thermolyne, Dubuque, IA). The PCR cycling follows initial denaturation at 95 °C for 2 minutes, anneal at 64 °C for 30 seconds for primer set 1 (D29\_F1 and R\_1) and 70 °C for primer set 2 (D29\_F2 and R1) (**Table 1**), and extension at 72 °C for 30 seconds. The number of the PCR cycle has been adjusted from 40 to 25 cycles. The final DNA amplification was evaluated by Agilent Bioanalyzer 2100 (Agilent Technologies, Inc., Santa Clara, CA, USA), the commercialized microchip electrophoresis instrument.

**Table 1:** Information of couples of primer sequences for D29 amplifications.

Primers	Primer Sequences	T <sub>m</sub>
D29_F1	5' – AGCCGATCAGAAGCACGGGC – 3'	67.74 °C
D29_R1	5' – AGCGGCTCTTAGGAGGGGCC – 3'	66.76 °C
D29_F2	5' – AGCCATCCTGTACGGGTTTCC – 3'	63.10 °C
D29_R2	5' – TCTTAGCGAGCCGCCTG – 3'	59.76 °C

\* Red color indicated the set (D29\_R1 and D29\_F2) of primers used in this work.

### 5.2.3 *Microwell Fabrication and Assay Instruments*

Microwells in previous research<sup>11</sup> were used in this work. Each microwell device designed via AutoCAD (Autodesk, San Rafael, CA, USA) has a  $4 \times 4$  matrix of 5-mm-diameter circular wells on a 4-cm square device, which were prepared by cutting through the 1.5-mm-thick PMMA sheet (McMaster-Carr, Santa Fe Springs, CA, USA) via the CO<sub>2</sub> laser ablation (VersaLASER system 3.50, Universal Laser Systems, Scottsdale, AZ, USA). The layer with  $4 \times 4$  matrix of holes was thermally bonded to a blank PMMA piece of the 1.0 mm thickness (Astra product, Baldwin, NY, USA) using established bonding approach in our lab<sup>12</sup>, providing the smooth surface with wells at the bottom. After experiment finished, all microwells were thoroughly cleaned with either 10% bleach or 2 M hydrochloric acid for 5–10 minutes and then rinsed with Nanopure water.

The T1i DSLR camera installed with MP-E 65 mm  $f/2.8$  1–5 $\times$  macro lens (Canon USA Inc., Lake Success, NY, USA) was utilized to take images of the microwells after magnetic bead aggregation. A Thermix Stirrer model 120S magnetic stir plate (Fisher Scientific, Fair Lawn, NJ, USA) was used to apply a rotating magnetic field on the microwell. A heated stir plate model 97042-642 (VWR, Batavia, IL, USA) was employed for bead aggregation experiments at elevated temperature. A Ledu compact desk magnifier lamp (Guy Brown Products, Brentwood, TN, USA) was used without optics to provide lighting while conducting experiments.

### 5.2.4 *Magnetic Particle Modification*

The streptavidin-coated magnetic beads (Dynabeads MyOne Streptavidin C1 beads, Invitrogen, Carlsbad, CA, USA) were spiked with biotinylated oligonucleotides (Eurofins MWG

Operon, Huntsville, AL, USA) following the manufacturer's protocol. The suspension of 200  $\mu\text{L}$  of mixed particles was washed three times using 1 $\times$  binding/washing buffer [5 mM Tris-HCl (pH 7.5), 0.5 mM EDTA, and 1 M NaCl] and incubated with 100  $\mu\text{L}$  of the 1 $\times$  binding/washing buffer and 0.2  $\mu\text{L}$  of 30 mM biotinylated oligonucleotide solution on a rotating rotisserie for 10 minutes (for the purpose of coupling of oligonucleotides with magnetic beads). The magnetic beads were washed three times with 1  $\times$  the binding/washing buffer to completely remove any residual oligonucleotides. Lastly, the beads were resuspended in 500  $\mu\text{L}$  of 1 $\times$  PCR buffer [50 mM KCl, 10 mM Tris-HCl (pH 7.5)].

#### *5.2.5 Hybridization-induced Bead Aggregation Assay and Image Processing*

The hybridization-induced bead aggregation assay was conducted at the room-temperature. First, 17  $\mu\text{L}$  of 1 $\times$  PCR buffer was added to a 5 mm-diameter well, followed by 1  $\mu\text{L}$  of the PCR sample, which were previously amplified from clinical isolates in the conventional thermal cycler. Both of 1  $\times$  PCR buffers and samples were heated at 95  $^{\circ}\text{C}$  before adding into the reaction mixture. The microwell microchip was placed on the vortexer rotated at 500 rpm and a RMF (1000 rpm), which as reversely rotating to the vortexer, was applied to the solution, and lastly, 1  $\mu\text{L}$  of each of detection magnetic beads (1  $\mu\text{L}$  of the 5' modified and 1  $\mu\text{L}$  of the 3' modified oligonucleotides) that have two oligonucleotides displayed on the surface were added into the well. Normally, after 4 minute rotation, the RMF was removed and the vortexer was stopped, and a single picture was taken for each experiment. JPG image files were processed into binary with the gray level threshold set via an isodata algorithm coded in Mathematica<sup>11</sup>. For the HIA, the threshold was set in the saturation channel in HSB (hue-

saturation-brightness) color space with the isodata algorithm. The number of dark pixels (dark area) was normalized and it was compared with the negative control without any DNA template.

## 5.3 Results and Discussion

### 5.3.1 Optimization of Standard PCR for DST of TB

The simple PCR method for drug susceptibility testing (DST) of *M. tuberculosis* (TB) was optimized via standard PCR on the conventional thermal cycler. The PCR protocol followed the previous recipe of real-time PCR without adding a fluorescent dye. A primer set

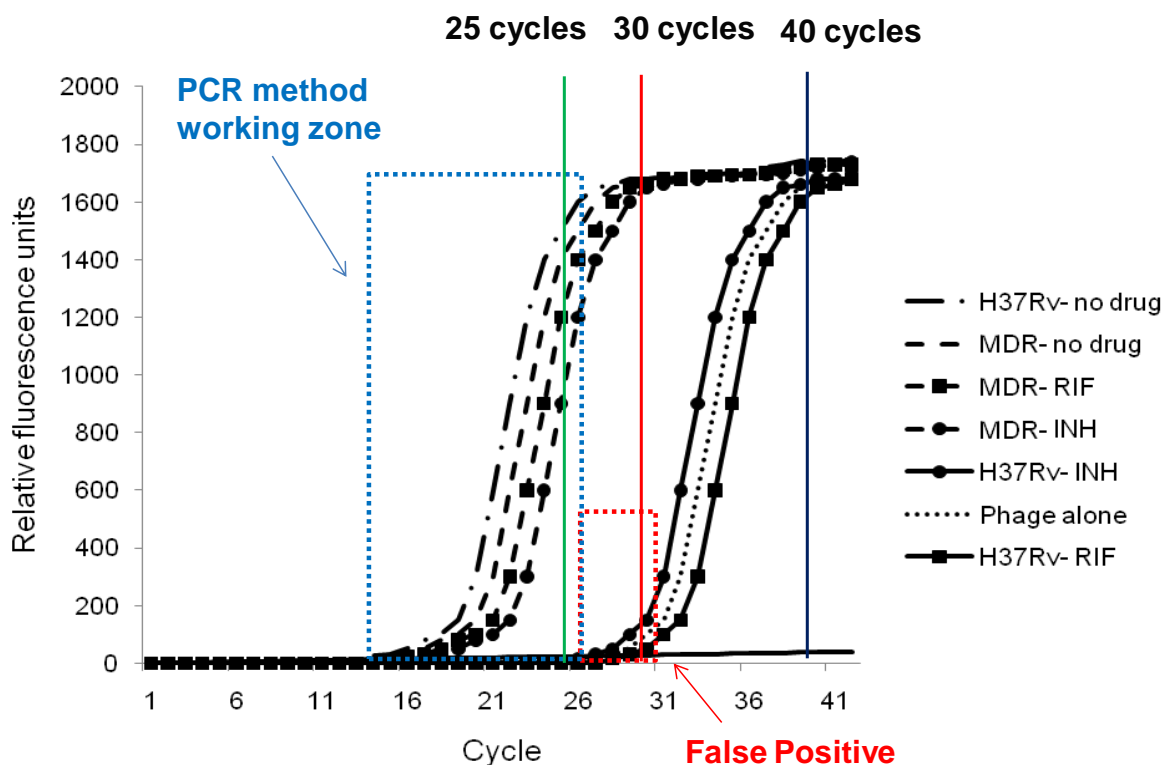


**Figure 2:** qPCR curve of D29 phage amplifications from TB samples. H37Rv (all TB drug susceptible strain) and MDR strains were tested for developing rapid and phage-based DST using real-time PCR. Three different cycles (25, 30, and 40 cycles) were chosen for developing standard PCR assay. 40 cycles of standard PCR generated PCR products from all samples, 30 cycles led to false positive products from negative samples, and 25 cycle completely eliminated PCR products from the negative control.

for amplification of D29 phage fragment was redesigned to be appropriate for the standard PCR method and hybridization-induced bead aggregation assay: the set of oligonucleotides (probes) displayed on the magnetic bead were designed to be complementary to the previous set of primers (D29\_F1 and R1) (**Table 1**). While conducting the bead aggregation assay, the primer-dimer formation generated by the previous primer set could reduce sensitivity in this assay because flank sequences of primer-dimer were bound to oligonucleotides (probes) displayed on the magnetic bead. As the formation of primer-dimer was described as the drawback of this primer set (D29\_F1 and R1) in the publication<sup>8</sup>, a new set of primer was redesigned (to D29\_F2 and R1) to decrease amounts of primer-dimer formation. Conclusively it prevented the formation of primer-dimers from inducing the aggregation of magnetic beads. Before using a new designed primer set (D29\_F2 and R1), it was evaluated by gradually changing anneal temperature to find proper amplification without any formation of primer-dimer and it was decided at 63 °C.

Using a new primer set (D29\_F2 and R1), the number of the PCR cycle has been optimized based on the real-time PCR curve (**Fig. 2**) and following standard PCR experiments

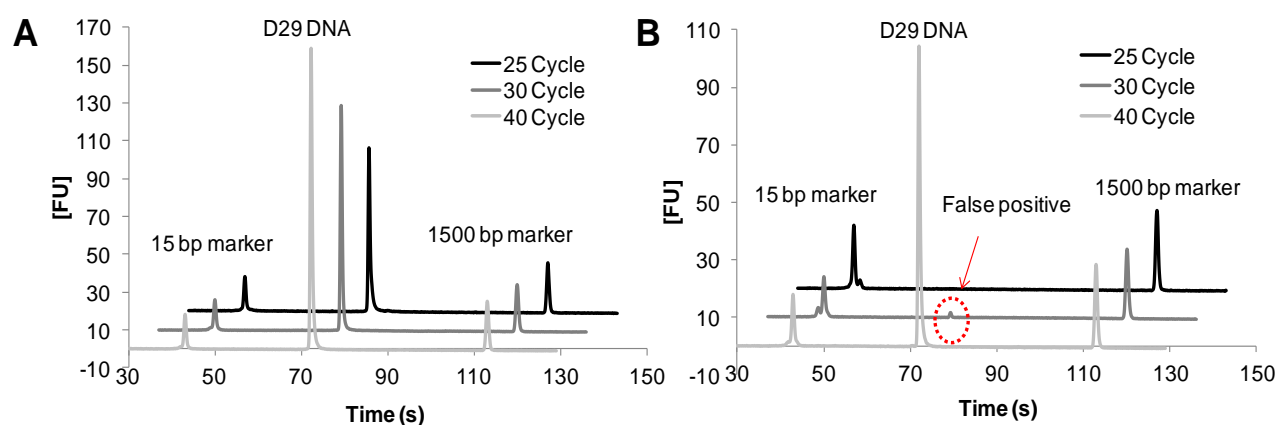


**Figure 3:** Overlaid electropherograms from 25, 30 and 40 cycles of standard PCR. To develop a rapid and simple assay of DST for TB, D29 phage amplifications were conducted by 25, 30, and 40 cycles using from (A) positive (H37Rv without any drug), and (B) negative (phage alone). These PCR products have shown similar patterns of amplifications in the qPCR curve (**Fig. 2**).

(**Fig. 3**). First, three different numbers of PCR cycles, 25, 30, and 40, were assessed to find which cycles could generate discernible DNA amplifications in the conventional thermal cycler from clinical samples. PCR products should be detectable amounts of PCR products from drug resistant TB samples and nothing from drug susceptible TB samples. 40 cycles of PCR was not suitable for a new DST assay because it produced DNA amplifications (higher than 0.1 ng/ $\mu$ L of PCR products) from all samples. In case of 30 cycles, several negative (drug susceptible) samples generated detectable amounts of DNA amplifications that could produce a false positive signal in microchip electrophoresis (2100 Bioanalyzer) (**Fig. 3A and B**). As the detectable amount of the PCR product from a negative sample is highly possible to induce the aggregation of magnetic beads, the number of the PCR cycle further decreased up to 25 cycles and eventually it could not produce any PCR product from a negative (drug susceptible) sample.

In the qPCR curve (**Fig. 2**), “ideal PCR working zone” for the DST assay has been conceived from around 13 to 25 cycles where the positive sample (MDR strains) is able to produce the detectable amounts of DNA amplification in microchip electrophoresis (2100 Bioanalyzer) except a negative control or drug susceptible strains. As PCR efficiencies in both approaches such as conventional and microchip PCR vary, but less or not more than the efficiency in the qPCR curve, 25 cycles of the standard PCR procedure or lower than this, would be the appropriate number of the cycle to get PCR products from clinical samples in the conventional and microchip PCR approaches. Furthermore, the number of the PCR cycle in the qPCR has reduced from 40 to 25 in standard PCR, which achieved ~ 2 time reduction in PCR amplification time.

### 5.3.2 Standard PCR Amplifications and Analysis from Clinical Samples

210 clinical samples of 35 patients were collected from TB cultured media in Dr. Houpt group (our collaborator) at the University of Virginia<sup>3</sup>. All clinical samples were treated with five different types of antibiotics for *M. tuberculosis*; isoniazid (INH), rifampin (RIF), ethambutol hydrochloride (EMB), amikacin (AMK), and ofloxacin (OFX) except one drug untreated sample from each patient (35 samples). These clinical isolates were analyzed via 25 cycles of standard PCR that amplified the D29 segment from each clinical isolate; 210 PCR amplifications were conducted on the thermocycler. **Figure 4** indicates overlaid electropherograms from six clinical isolates (sample 565) from one patient. These

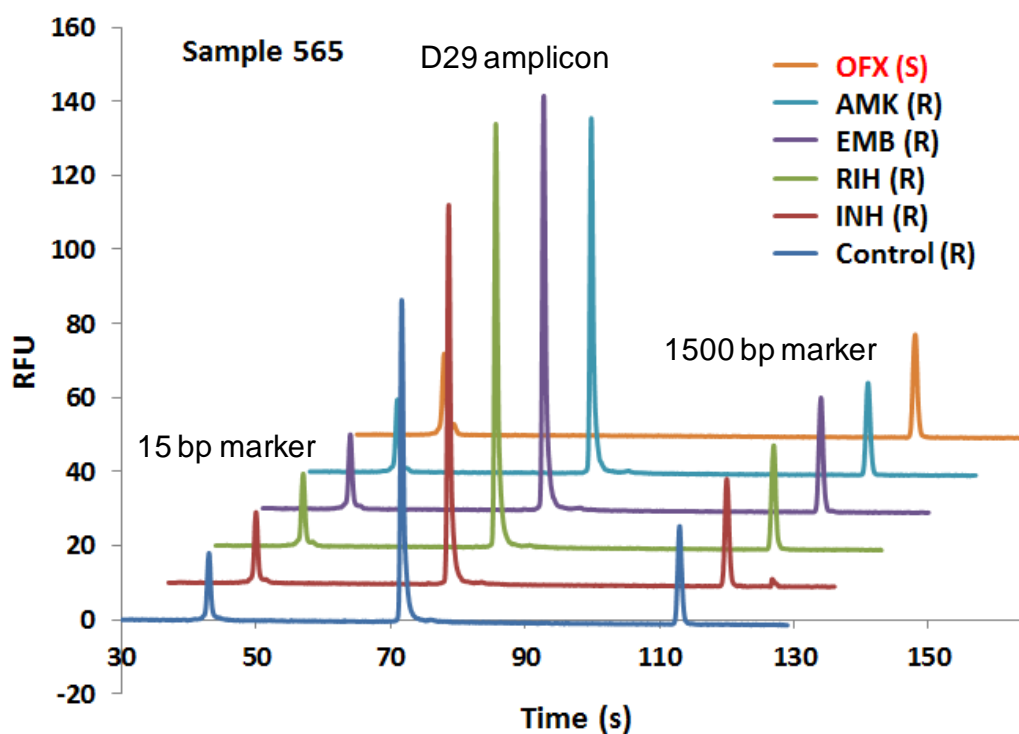


**Figure 4:** Overlaid electropherograms of conventional PCR products from clinical isolates. From clinical isolates, 25 cycles of PCR amplifications were conducted using D29 samples from positive (H37Rv without any drug) and five TB drug treated samples. These clinical isolates (sample 565) have shown drug resistance to two first line and two second line TB antibiotics (INH, RIH, EMB, and AMK) except one second line TB antibiotics (OFX); *R* represents “Resistant” and *S* “Susceptible”.

electropherograms showed drug resistance to four different antibiotics (INH, RIF, EMB, and AMK), however, not to ofloxacin (OFX). This result demonstrated that only drug resistant isolates produced the detectable amounts of PCR products via 25 cycles of PCR and the drug susceptible sample did not show any amplification or amplification might be lower than the limit of detection in microchip electrophoresis. After analyzing all clinical isolates (210 samples from 35 patients treated with five different antibiotics and without any drug) with 25 cycles of standard PCR and microchip electrophoresis (2100 Bioanalyzer), resulting data have been compared to the previous data in the Dr. Houpt group's publication<sup>3</sup>, where they reported their accuracy of the qPCR assay to each TB antibiotics. **Table 2** described that types of antibiotics were used for preparing 35 clinical samples (5 antibiotics) and the numbers and accuracy of errors were generated by 25 cycles of standard PCR for 210 samples. The accuracy of finding drug susceptibility of TB via the standard PCR method following microchip electrophoresis was within the range between 94 % and 100% in drug treated TB isolates; potential errors might result from false positive signals from drug susceptible isolates in drug-treated media. Comparing to the accuracy in the qPCR approach (the D29 phage-based qPCR method offered 100% accuracy to all antibiotics), our simple PCR method showed the accuracy high enough for drug susceptibility testing of TB. However, it is much simpler (without the qPCR instrument), faster (time reduction by decreasing the number of the PCR cycle), and more economical (without fluorescent dyes) than the qPCR method. Ultimately, in our simple and new assay, a real-time PCR step is eliminated and it is able to remove requirement of qPCR instrumentation with fluorescent dyes to simplify drug susceptibility testing of TB.

**Table 2:** Accuracy of standard PCR in analysis of microchip electrophoresis.

Antibiotics	Number of Errors	Accuracy	*Accuracy
Control (w/o drug)	5 errors out of 35	86 %	N/A
Isoniazid (INH)	2 errors out of 35	94 %	100 %
Rifampin (RIF)	2 errors out of 35	94 %	100 %
EMB (Ethambutol)	0 errors out of 35	100 %	100 %
AMK (Amikacin)	2 errors out of 35	94 %	100 %
OFX (Ofloxacin)	2 errors out of 35	94 %	100 %

\* Accuracy of D29 phage-based qPCR approach reported in previous publication [3].

### 5.3.3 Hybridization-induced Bead Aggregation for Serially Diluted PCR Products and Clinical Isolates

Electrophoresis is a time-consuming and instrument limited procedure that requires a fluorescent detection system, limiting portability for DST of TB diagnostics. In order to facilitate dsDNA detection by a simple and robust approach in a microdevice, Hybridization-induced bead aggregation has been introduced in our group<sup>11</sup> and it was illustrated that sequence-specific oligonucleotides (probes) displayed magnetic beads were utilized to show the induced aggregation of magnetic beads from PCR products (dsDNA fragments) under a rotating magnetic field.

First of all, to ensure a hybridization condition, magnetic bead aggregation was characterized and optimized using serially diluted PCR fragments. PCR products from the D29 genome was serially diluted from 1x (7.5 ng/ $\mu$ L of PCR products;  $3 \times 10^{10}$  copies of 250 bp fragments) down to 0.25x ( $0.75 \times 10^{10}$  copies), demonstrating the sensitivity (limit of detection for target PCR products) of this assay. Images of the aggregation of magnetic beads with serially

diluted PCR products from  $\lambda$ -phage genome are shown in **Figure 5** and it demonstrated that the aggregation of magnetic beads reduced with concentrations of PCR products. These aggregations of magnetic beads with dsDNA have been further analyzed by images taken by the

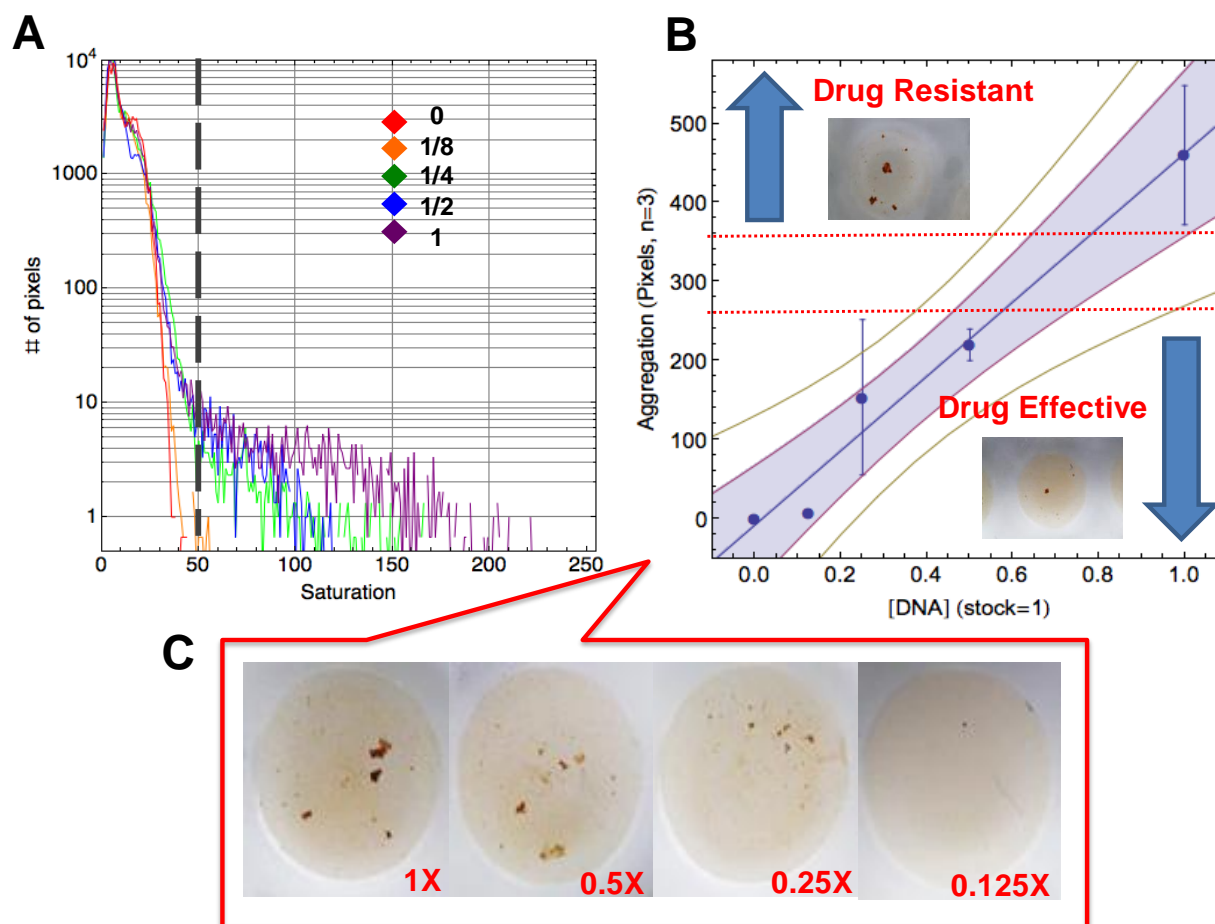


**Figure 5:** Hybridization-induced bead aggregation was conducted using serially diluted PCR samples. (A) Images were analyzed in HSB (Hue-Saturation-Brightness) color space. The saturation histogram of images with 0, 1/8x, 1/4x, 1/2x, and 1x DNA ( $7.5 \text{ ng}/\mu\text{L}$ ;  $3 \times 10^{10}$  copies of fragments/ $\mu\text{L}$ ) were plotted at logarithmic scale, and a threshold (black dashed line) was chosen above which the pixels present the aggregates. (B) The number of pixels with saturation above the threshold represents the extent of aggregation, and is correlated with DNA concentration. (C) Photographs of bead aggregations represented that aggregations decreased with concentrations of PCR amplicons inside the microwell.

camera. As the concentration of DNA gradually increased, the beads started to aggregate, and correspondingly, the number of pixels representing the beads (i.e., % Dark Area) decreased. It explained that the hybridization-induced bead aggregation approach could be utilized for the detection of sequence-specific PCR products, especially, for PCR products from D29 phage, developing DST of TB.

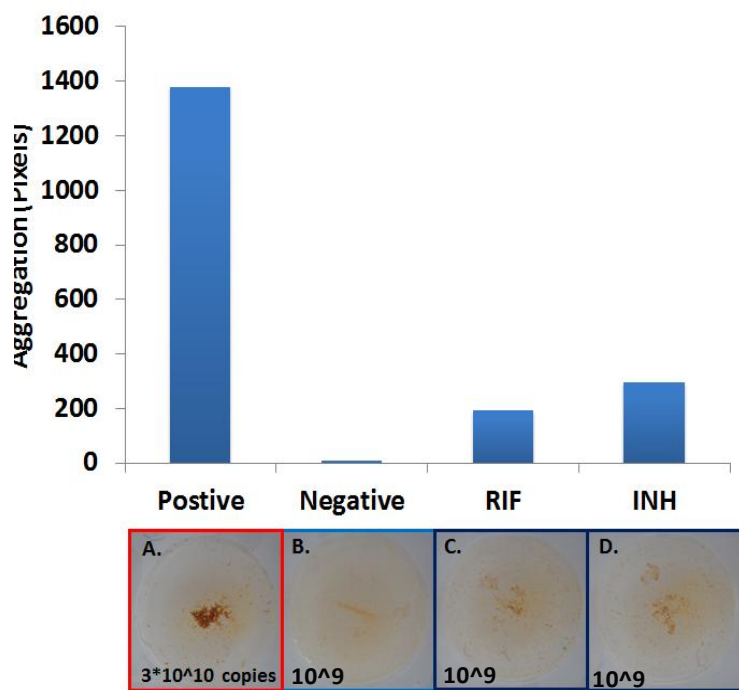


**Figure 6:** HIA for D29 PCR amplicons from TB samples. (A) Positive: H37Rv without any drug. (B) Negative: Phage alone. (C) RIF treated H37Rv. (D) INH treated H37Rv.

To determine the effectiveness of the hybridization-induced bead aggregation method for clinical isolates, three TB samples were treated with either no drug (positive), INH, or RIF, and then incubated with D29 phage. Phage DNA was extracted, amplified with 25 cycles of standard PCR, and detected with the hybridization-induced bead aggregation assay. **Figure 6**

showed that two drug-treated TB samples resulted in significantly less aggregation than the positive control, demonstrating that the TB sample was not drug resistant to INH or RIF; the negative is the phage grown in media without TB cells. This exemplifies the capability of hybridization-induced bead aggregation to determine the presence of either MDR-TB or the correct pharmaceutical to use against a particular TB sample. In present work, we demonstrated that the hybridization-induced bead

approach was successfully employed to develop new drug susceptibility testing (DST) of TB combined with the standard PCR approach we optimized in the previous session. First-line drugs employed to fight TB are isonicotinic hydrazide (INH) and Rifampin (RIF), thus have been chosen to identify possible drug susceptible TB or MDR-TB. Eventually, we showed that hybridization-induced bead aggregation was capable of the detection of amplified D29 PCR fragments from clinical isolates which were treated by the first line antibiotics.

## 5.4 Conclusions

We demonstrate that the D29 phage replicated from viable *M. tuberculosis* in culture media is able to be detected by standard PCR in the conventional thermocycler and the hybridization-induced bead aggregation assay, offering great potential for a simple, rapid, and portable bio-analytical microfluidic approach for determining drug susceptibility of TB. 25 cycles of the standard PCR method targeted for the amplification of D29 fragments was successfully validated to discern viable TB from drug treated media and it resulted in the multidrug resistant determination of TB in less than several hours via quantitative polymerase chain reaction (qPCR); standard PCR within one hour. Additionally, hybridization-induced bead aggregation is successfully demonstrated as a new approach to detect sequence-specific dsDNA from PCR products, which has capability of further decreasing analysis time in DST of TB, since hybridization-induced bead aggregation takes several minutes to induce the aggregation of magnetic beads in a portable microwell.

Consequently, although these improvements in turnaround and ease of assays for drug susceptibility testing of *M. Tuberculosis* have been paradigm shifting, the cost-per-analysis and cumbersome instrumentation required for qPCR remains unrealistic to implement in many

countries, especially without any clinical laboratory. Now, through coupling standard PCR to a label-free method for the detection of sequence-specific dsDNA, clinical isolates from TB patients can be characterized for less than 1 USD, omitting the need for qPCR and achieving Point-of Care (POC) DNA analysis.

## 5.5 References

- (1) Sekiguchi, J.; Miyoshi-Akiyama, T.; Augustynowicz-Kopec, E.; Zwolska, Z.; Kirikae, F.; Toyota, E.; Kobayashi, I.; Morita, K.; Kudo, K.; Kato, S.; Kuratsuji, T.; Mori, T.; Kirikae, T. Detection of multidrug resistance in *Mycobacterium tuberculosis*. *Journal of Clinical Microbiology* **2007**, *45*, 179-192.
- (2) Ardito, F.; Posteraro, B.; Sanguinetti, M.; Zanetti, S.; Fadda, G. Evaluation of BACTEC mycobacteria growth indicator tube (MGIT 960) automated system for drug susceptibility testing of *Mycobacterium tuberculosis*. *Journal of Clinical Microbiology* **2001**, *39*, 4440-4444.
- (3) Pholwat, S.; Ehdaie, B.; Foongladda, S.; Kelly, K.; Houpt, E. Real-time PCR using mycobacteriophage DNA for rapid phenotypic drug susceptibility results for *Mycobacterium tuberculosis*. *J Clin Microbiol* **2011**, *50*, 754-61.
- (4) Said, H. M.; Kock, M. M.; Ismail, N. A.; Baba, K.; Omar, S. V.; Osman, A. G.; Hoosen, A. A.; Ehlers, M. M. Evaluation of the GenoType (R) MTBDRsl assay for susceptibility testing of second-line anti-tuberculosis drugs. *International Journal of Tuberculosis and Lung Disease* **2012**, *16*, 104-109.
- (5) Hillemann, D.; Rusch-Gerdes, S.; Richter, E. Evaluation of the GenoType MTBDRplus assay for rifampin and isoniazid susceptibility testing of *Mycobacterium tuberculosis* strains and clinical specimens. *Journal of Clinical Microbiology* **2007**, *45*, 2635-2640.
- (6) Banaiee, N.; January, V.; Barthus, C.; Lambrick, M.; RoDiti, D.; Behr, M. A.; Jacobs, W. R.; Steyn, L. M. Evaluation of a semi-automated reporter phage assay for susceptibility testing *Myobacterium tuberculosis* isolates in South Africa. *Tuberculosis* **2008**, *88*, 64-68.
- (7) Bardarov, S.; Dou, H.; Eisenach, K.; Banaiee, N.; Ya, S.; Chan, J.; Jacobs, W. R.; Riska, P. F. Detection and drug-susceptibility testing of M-tuberculosis from sputum samples using luciferase reporter phage: comparison with the *Mycobacteria Growth Indicator Tube* (MGIT) system. *Diagnostic Microbiology and Infectious Disease* **2003**, *45*, 53-61.
- (8) Pholwat, S.; Heysell, S.; Stroup, S.; Foongladda, S.; Houpt, E. Rapid First- and Second-Line Drug Susceptibility Assay for *Mycobacterium tuberculosis* Isolates by Use of Quantitative PCR. *Journal of Clinical Microbiology* **2011**, *49*, 69-75.
- (9) McNerney, R.; Kambashi, B. S.; Kinkese, J.; Tembwe, R.; Godfrey-Faussett, P. Fabrication of poly(methyl methacrylate) microfluidic chips by atmospheric molding. *J Clin Microbiol* **2004**, *42*, 2115-20.
- (10) Pai, M.; Kalantri, S.; Pascopella, L.; Riley, L. W.; Reingold, A. L. Bacteriophage-based assays for the rapid detection of rifampicin resistance in *Mycobacterium tuberculosis*: a meta-analysis. *J Infect* **2005**, *51*, 175-87.

- (11) Leslie, D. C.; Li, J.; Strachan, B. C.; Begley, M. R.; Finkler, D.; Bazydlo, L. A.; Barker, N. S.; Haverstick, D. M.; Utz, M.; Landers, J. P. New detection modality for label-free quantification of DNA in biological samples via superparamagnetic bead aggregation. *J Am Chem Soc*, 134, 5689-96.
- (12) Lounsbury, J. A.; Poe, B. L.; Do, M.; Landers, J. P. Laser-ablated poly(methyl methacrylate) microdevices for sub-microliter DNA amplification suitable for micro-total analysis systems. *Journal of Micromechanics and Microengineering* **2012**, 22.

## 6. Conclusions and Future Directions

### 6.1 Overview Conclusions

After the introduction of PCR and the concept of micro-total analysis systems ( $\mu$ -TAS) in 1986<sup>1</sup> and 1990<sup>2</sup>, genetic analysis technology has been extremely fast studied and developed in microfluidic platforms and consequential developments in microfluidic technologies have made unprecedented progress in chemical, biological, and medical applications beyond clinical and forensic applications. In addition, the completion<sup>3,4</sup> and research<sup>5</sup> in the Human Genome Project (HGP) have made the development of advanced genetic analysis technologies invaluable in our community. With the novel concept of “Lab on a Chip”, illustrating that “a laboratory is built on a compact microchip”, great merits from a micro or nano-scale platforms such as miniaturization and integration with other functional units can be achieved in microfluidics-based genetic analyzers that have capabilities of portability and high-throughput reactions<sup>6-8</sup>. From these perspectives, my Ph.D. works have focused on achieving two important characteristics on a microfluidic device, portability and high-throughput capability in advanced genetic analysis; multiple and high-throughput Point-of-Care (POC) DNA analysis.

**Chapter 1** introduced the general purpose in the development of microfluidic devices for genetic analysis with describing micro-total analysis systems ( $\mu$ -TAS). Especially, microfluidic polymerase chain reaction (PCR) has been illustrated from basic chemistry and biology of PCR to integrated genetic analysis in the microfluidic device. In order to demonstrate multiple and high-throughput capability of genetic analysis using an IR-lamp, continuous flow infrared-mediated PCR (cfIR-PCR) (**Chapter 2**) had been conceived on our previous setup, an IR-mediated heating system. In the **Chapter 2**, I mainly described about the process of the development of the cfIR-PCR system that enables conducting multiple PCR using segmented

plug flows in a PMMA microdevice. As a result of the limitation of the number of PCR amplification in a single or multiple chambered PCR microdevice<sup>9</sup>, the continuous format of PCR was attempted on a three layered PMMA microdevice, utilizing the thermal gradient that was rapidly built by a single lamp. The desired thermal gradient measured by the temperature measurement (TM) microchip with several thermocouples was carefully applied on the cfIR-PCR microdevice where the PCR sample ran through to conduct thermocycling. The disposable microdevice of a well-characterized polymeric material, PMMA, boosts the speed of the development and optimization of our concept, cfIR-PCR, due to rapid prototyping and ease of microfabrication. Via our setup and circular polymeric microdevices, DNA amplifications from the  $\lambda$ -phage and the human genome have been accomplished and eventually multiple PCR using segmented plug flows of three distinct PCR samples from the  $\lambda$ -phage genome and human genome have been reported without any carryover via microchip electrophoresis (2100 Bioanalyzer). Especially, emulsion technology has been combined with cfIR-PCR to completely exclude the PCR sample from the wall of the microchannel to solve passivation issues, minimize the cross-contamination from different segmented samples, and decrease the amounts of air bubbles to generate constant flow of the PCR solution. Conclusively, it described the feasibility that if the automation of our cfIR-PCR heating system with droplet technologies is achieved in the future, our cfIR-PCR system is capable of high-throughput genetic analysis on our cfIR-PCR system.

In the **Chapter 3**, a microwave-mediated heating system has been demonstrated to achieve the concept of a portable genetic analyzer. As an alternative approach of the noncontact heating system, the microwave heating system delivers the entire portion of microwave energy to intensively heat nano and micro-liters of the PCR solution surrounded by air pockets and the

polymeric material. The optimized matching network, which was designed by a computer-aided modeling and made from the copper tape, has further effectively transferred microwave into the PCR chamber. Using our microwave heating setup and matching network, we reported rapid microwave heating up to 60 – 80 °C per second with parallel DNA amplifications on the polymeric microdevice<sup>10</sup>. However, the resulting PCR amplification was not efficient mainly due to 1) non-uniformed temperature distribution that was confirmed by a thermocouple and thermal modeling, and 2) inappropriate surface passivation of the PCR chamber and the thermocouple, which should be further studied with different designs of microchips and materials. In order to facilitate microwave heating on a polymeric microdevice, a noncontact temperature measurement method using a IR-pyrometer was utilized to perform thermocycling on the same microdevice. Pyrometer measurement could completely solve the issue for passivation of a thermocouple. The issue of non-uniformity of temperature in the PCR chamber was partially solved by changing the configuration of matching network, we called, a shifted transmission line, which opened a half of the copper tape over the PCR chamber. A temperature measuring spot for pyrometer measurement was located over the top of the PMMA sheet where a half of the PCR chamber was exposed. Before thermocycling, the pyrometer was completely calibrated based on the reference temperature of the thermocouple on the reference heater (hot plate). Finally, our microwave heating with the IR-pyrometer achieved repeated DNA amplifications from  $\lambda$ -genomic DNA that was the first report of microwave-mediated DNA amplifications using a noncontact temperature measurement method.

In the **Chapter 4**, an IR-mediated heating system<sup>7,11</sup>, invented in Dr. Landers lab one decade ago<sup>12</sup>, was demonstrated to achieve rapid, sensitive, and reliable microchip PCR on a polymeric microdevice. This research was a part of my externship in the Biotechnology

Training Program (BTP) at the University of Virginia (UVA). As a target DNA template, the gene of DNA polymerase from herpes simplex virus (Epstein Barr Virus) was selected with CODEHOP degenerate primers<sup>13</sup> that was kindly provided by CDC. In order to realize fast prototyping and ease of productions of a designed microdevice, Poly(methyl methacrylate) (PMMA) was fabricated using a computer-aided milling machine and a CO<sub>2</sub> laser cutter in the Department of Mechanical Engineering at the Georgia Tech. Lastly, comparing to standard PCR on the thermocycler, which inhibited micro-scale PCR (lower than 1  $\mu$ L), the single chambered PCR amplification in the polymeric microdevice was successfully achieved using 1 and 2 pg of template DNA and analyzed in microchip electrophoresis (Agilent 2100 Bioanalyzer). Importantly, analysis time in PCR and the amount volume per one PCR reaction decreased up to 40 minutes from 3 hours and to 1  $\mu$ L from 50  $\mu$ L. This work illustrated the first approach of IR-mediated microfluidic PCR using the CODEHOP primers on the polymeric microdevice.

In the **Chapter 5**, we described that the process of developing rapid and accurate drug susceptibility testing (DST) for *M. Tuberculosis* (TB)<sup>14</sup> using standard PCR following the hybridization-induced bead aggregation method<sup>15</sup>. As a result of a slow growing TB, the screening of multi-drug resistant TBs (MDR-TB) to the first and second line antibiotics has limited appropriate drug treatment of patients (sub-optimal treatment) and eventually increased possibility to spread MDR-TB, especially in the developing countries where advanced bio-analytical instrument and proper cures could not reach. The first optimization was performed for choosing the number of the PCR cycle to classify drug susceptibility of TB to different antibiotics. 210 clinical isolates from TB patients (35 patient samples treated by five different antibiotics to TB) had been analyzed to find the accuracy of our assay to each antibiotics. The resulting data indicated accuracy ranging from 94% to 100%. This accuracy compared to

previous approach supported that reduced numbers of cycles in standard PCR could be applicable for drug susceptibility testing (DST) of TB. In addition, hybridization-induced bead aggregation using sequence-specific oligonucleotide spiked magnetic beads was introduced to detect different quantities of PCR amplicons from two different TB strains, drug resistant or susceptible. Hybridization-induced bead aggregation following standard PCR on the conventional thermocycler has been successfully combined with a D29 phage-based TB cell counting approach for testing drug susceptibility in *M. tuberculosis*. Furthermore, the total analysis time of DST has decreased due to the reduced numbers of the PCR cycle and short analysis time in the hybridization-induced bead aggregation assay, removing qPCR instrumentation.

## **6.2 Future Directions**

### *6.2.1 cfIR-PCR System*

The continuous flow format of microchip PCR using an infrared (IR) heating system (cfIR-PCR) has been first reported in the present work and it has demonstrated a promising progress for developing a high-throughput genetic analyzer, if the automation is achieved with droplet technologies, which was successfully reported in the three layered PMMA microdevice<sup>16</sup>. Furthermore, our system holds many advantages and applications due to the non-contact heating manner using a single lamp such as ease of miniaturization and integration with moving microdevices. However, several additional works need to be achieved in our present system.

First, our cfIR-PCR approach has to be further optimized in order to achieve DNA amplification and detection from very low amounts of the DNA template, which should be more

realistic situation in clinical and forensic fields; DNA amplification from a single copy of DNA template should be obtained within 35 - 40 cycles of thermocycling. Low PCR yields should be solved by 1) re-validating the thermal gradient on the cfIR-PCR microdevice while conducting cfIR-PCR 2) studying passivation of the microchannel with the optimal design of the microchip 3) controlling the flow rate to minimize the disruption of the thermal gradient. Secondly, our cfIR-PCR microchip having a 60 mm in the diameter is still large compared to other PCR microchips. Improving or changing fabrication technologies for constructing the cfIR-PCR microdevice can realize multi-parallel operations of multiple cfIR-PCR in the integrated

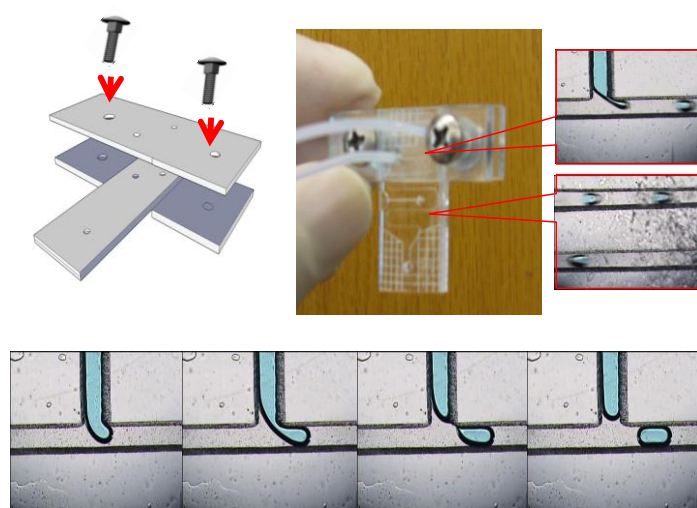


**Figure 1:** PMMA-based droplet generation kit [16].

automation.

microdevice with the automation of the droplet PCR (**Fig. 1**)<sup>16</sup>. Ultimately, the integration with other upstream and downstream processes such as DNA extraction from clinical cells and electrophoresis or qPCR should be required to develop a fully integrated genetic analyzer with the

### 6.2.2 Microwave-mediated Thermal Cycling System

As a noncontact heating approach, microwave heating, compared to thermal conduction and IR radiation, is ideal to achieve ultrafast thermocycling in a microfluidic device. However,

the main problem of microwave heating was derived from the same reason as this advantage is; a direct, intensive, and localized heating of the PCR micro-fluids. It caused localized heating of the PCR solution and generated the thermal gradient in the PCR chamber. In order to further improve microwave heating in the polymeric microdevice, the redesign of the PCR vessel architecture, the relocation of air pockets, and the adjustment of the matching network (a transmission line) should be required to further improve PCR efficiency. In addition, if the sample volume decreases up to nano or pico-liter size of droplets with suitable temperature measurement, ultrafast thermal cycling for PCR applications can be obtained in our setup. Conclusively in order to realize a portable microdevice for advanced genetic analyzer, the fluorescent detection, qPCR, or hybridization-induced bead aggregation through the open PCR chamber should be suitable to minimize the size of the PCR instrument instead of using microchip electrophoresis.

### **6.3 Summation**

During my Ph.D. in Dr. Landers lab, my research goals were directed towards the development of advanced PCR instrumentations, having capabilities of multiple and high-throughput analysis, and portability. Two important characteristics in genetic analysis have been achieved by developing two novel heating systems: continuous flow infrared-mediated PCR (cfIR-PCR) and microwave-mediated thermal cycling systems. There are many studies we still have to finish as future directions and there are many applications we can further explore using two heating systems.

PCR analysis will continuously play important roles as the part of genetic analysis and an essential tool in genetic engineering, if new technologies for advanced genetic detection or amplification methods will not be introduced in the future. For molecular diagnostics and forensic genotyping, a DNA detection method, especially, for very low amounts of DNA such as several copies of fragments, can revolutionize our community and novel DNA detection method must be developed. The hybridization-induced bead aggregation assay in our group, magnetic beads-based DNA detection and label free approach, should be an example of new technologies to advance conventional bio-analytical chemistry further.

#### 6.4 References

- (1) Mullis, K.; Faloona, F.; Scharf, S.; Saiki, R.; Horn, G.; Erlich, H. Specific Enzymatic Amplification of DNA Invitro - the Polymerase Chain-Reaction. *Cold Spring Harbor Symposia on Quantitative Biology* **1986**, *51*, 263-273.
- (2) Manz, A.; Graber, N.; Widmer, H. M. Miniaturized Total Chemical-Analysis Systems - a Novel Concept for Chemical Sensing. *Sensors and Actuators B-Chemical* **1990**, *1*, 244-248.
- (3) Venter, J. C.; Adams, M. D.; Myers, E. W.; Li, P. W.; Mural, R. J.; Sutton, G. G.; Smith, H. O.; Yandell, M.; Evans, C. A.; Holt, R. A.; Gocayne, J. D.; Amanatides, P.; Ballew, R. M.; Huson, D. H.; Wortman, J. R.; Zhang, Q.; Kodira, C. D.; Zheng, X. H.; Chen, L.; Skupski, M.; Subramanian, G.; Thomas, P. D.; Zhang, J.; Gabor Miklos, G. L.; Nelson, C.; Broder, S.; Clark, A. G.; Nadeau, J.; McKusick, V. A.; Zinder, N.; Levine, A. J.; Roberts, R. J.; Simon, M.; Slayman, C.; Hunkapiller, M.; Bolanos, R.; Delcher, A.; Dew, I.; Fasulo, D.; Flanigan, M.; Florea, L.; Halpern, A.; Hannenhalli, S.; Kravitz, S.; Levy, S.; Mobarry, C.; Reinert, K.; Remington, K.; Abu-Threideh, J.; Beasley, E.; Biddick, K.; Bonazzi, V.; Brandon, R.; Cargill, M.; Chandramouliswaran, I.; Charlab, R.; Chaturvedi, K.; Deng, Z.; Di Francesco, V.; Dunn, P.; Eilbeck, K.; Evangelista, C.; Gabrielian, A. E.; Gan, W.; Ge, W.; Gong, F.; Gu, Z.; Guan, P.; Heiman, T. J.; Higgins, M. E.; Ji, R. R.; Ke, Z.; Ketchum, K. A.; Lai, Z.; Lei, Y.; Li, Z.; Li, J.; Liang, Y.; Lin, X.; Lu, F.; Merkulov, G. V.; Milshina, N.; Moore, H. M.; Naik, A. K.; Narayan, V. A.; Neelam, B.; Nusskern, D.; Rusch, D. B.; Salzberg, S.; Shao, W.; Shue, B.; Sun, J.; Wang, Z.; Wang, A.; Wang, X.; Wang, J.; Wei, M.; Wides, R.; Xiao, C.; Yan, C. The sequence of the human genome. *Science* **2001**, *291*, 1304-51.
- (4) Lander, E. S.; Linton, L. M.; Birren, B.; Nusbaum, C.; Zody, M. C.; Baldwin, J.; Devon, K.; Dewar, K.; Doyle, M.; FitzHugh, W.; Funke, R.; Gage, D.; Harris, K.; Heaford, A.;

- Howland, J.; Kann, L.; Lehoczy, J.; LeVine, R.; McEwan, P.; McKernan, K.; Meldrim, J.; Mesirov, J. P.; Miranda, C.; Morris, W.; Naylor, J.; Raymond, C.; Rosetti, M.; Santos, R.; Sheridan, A.; Sougnez, C.; Stange-Thomann, N.; Stojanovic, N.; Subramanian, A.; Wyman, D.; Rogers, J.; Sulston, J.; Ainscough, R.; Beck, S.; Bentley, D.; Burton, J.; Clee, C.; Carter, N.; Coulson, A.; Deadman, R.; Deloukas, P.; Dunham, A.; Dunham, I.; Durbin, R.; French, L.; Grafham, D.; Gregory, S.; Hubbard, T.; Humphray, S.; Hunt, A.; Jones, M.; Lloyd, C.; McMurray, A.; Matthews, L.; Mercer, S.; Milne, S.; Mullikin, J. C.; Mungall, A.; Plumb, R.; Ross, M.; Shownkeen, R.; Sims, S.; Waterston, R. H.; Wilson, R. K.; Hillier, L. W.; McPherson, J. D.; Marra, M. A.; Mardis, E. R.; Fulton, L. A.; Chinwalla, A. T.; Pepin, K. H.; Gish, W. R.; Chisoe, S. L.; Wendl, M. C.; Delehaunty, K. D.; Miner, T. L.; Delehaunty, A.; Kramer, J. B.; Cook, L. L.; Fulton, R. S.; Johnson, D. L.; Minx, P. J.; Clifton, S. W.; Hawkins, T.; Branscomb, E.; Predki, P.; Richardson, P.; Wenning, S.; Slezak, T.; Doggett, N.; Cheng, J. F.; Olsen, A.; Lucas, S.; Elkin, C.; Uberbacher, E.; Frazier, M. Initial sequencing and analysis of the human genome. *Nature* **2001**, *409*, 860-921.
- (5) Sachidanandam, R.; Weissman, D.; Schmidt, S. C.; Kakol, J. M.; Stein, L. D.; Marth, G.; Sherry, S.; Mullikin, J. C.; Mortimore, B. J.; Willey, D. L.; Hunt, S. E.; Cole, C. G.; Coggill, P. C.; Rice, C. M.; Ning, Z.; Rogers, J.; Bentley, D. R.; Kwok, P. Y.; Mardis, E. R.; Yeh, R. T.; Schultz, B.; Cook, L.; Davenport, R.; Dante, M.; Fulton, L.; Hillier, L.; Waterston, R. H.; McPherson, J. D.; Gilman, B.; Schaffner, S.; Van Etten, W. J.; Reich, D.; Higgins, J.; Daly, M. J.; Blumenstiel, B.; Baldwin, J.; Stange-Thomann, N.; Zody, M. C.; Linton, L.; Lander, E. S.; Altshuler, D. A map of human genome sequence variation containing 1.42 million single nucleotide polymorphisms. *Nature* **2001**, *409*, 928-33.
  - (6) Roper, M. G.; Easley, C. J.; Landers, J. P. Advances in polymerase chain reaction on microfluidic chips. *Anal Chem* **2005**, *77*, 3887-93.
  - (7) Easley, C. J.; Karlinsey, J. M.; Bienvenue, J. M.; Legendre, L. A.; Roper, M. G.; Feldman, S. H.; Hughes, M. A.; Hewlett, E. L.; Merkel, T. J.; Ferrance, J. P.; Landers, J. P. A fully integrated microfluidic genetic analysis system with sample-in-answer-out capability. *Proceedings of the National Academy of Sciences of the United States of America* **2006**, *103*, 19272-19277.
  - (8) Horsman, K. M.; Bienvenue, J. M.; Blasier, K. R.; Landers, J. P. Forensic DNA analysis on microfluidic devices: a review. *J Forensic Sci* **2007**, *52*, 784-99.
  - (9) Lounsbury, J. A.; Miranian, D. C.; Landers, J. P. A multi-chamber microdevice for simultaneous amplification up to seven individual samples using infrared-mediated PCR. In *Proceedings of the 15th international conference on miniaturized systems for chemistry and life sciences*, Seattle, WA, USA, **2011**, p 750-752.
  - (10) Oh, K.; Sklavounos, A. H.; Marchiarullo, D. J.; Barker, N. S.; Landers, J. P. Microwave-assisted polymerase chain reaction (PCR) in disposable microdevices. In *Proceedings of the 15th international conference on miniaturized systems for chemistry and life sciences* Seattle, WA, USA, 2011, p 305-307.
  - (11) Leslie, D. C.; Seker, E.; Bazydlo, L. A.; Strachan, B. C.; Landers, J. P. Platinum nanoparticle-facilitated reflective surfaces for non-contact temperature control in microfluidic devices for PCR amplification. *Lab Chip* **2011**, *12*, 127-32.
  - (12) Oda, R. P.; Strausbauch, M. A.; Huhmer, A. F.; Borson, N.; Jurrens, S. R.; Craighead, J.; Wettstein, P. J.; Eckloff, B.; Kline, B.; Landers, J. P. Infrared-mediated thermocycling for ultrafast polymerase chain reaction amplification of DNA. *Anal Chem* **1998**, *70*, 4361-8.

- (13) Rose, T. M.; Henikoff, J. G.; Henikoff, S. CODEHOP (COnsensus-DEgenerate Hybrid Oligonucleotide Primer) PCR primer design. *Nucleic Acids Res* **2003**, *31*, 3763-6.
- (14) Pholwat, S.; Ehdaie, B.; Foongladda, S.; Kelly, K.; Houpt, E. Real-time PCR using mycobacteriophage DNA for rapid phenotypic drug susceptibility results for *Mycobacterium tuberculosis*. *J Clin Microbiol*, *50*, 754-61.
- (15) Leslie, D. C.; Li, J.; Strachan, B. C.; Begley, M. R.; Finkler, D.; Bazydlo, L. A.; Barker, N. S.; Haverstick, D. M.; Utz, M.; Landers, J. P. New detection modality for label-free quantification of DNA in biological samples via superparamagnetic bead aggregation. *J Am Chem Soc*, *134*, 5689-96.
- (16) Oh, K.; Nelson, D. A.; Landers, J. P. Droplet-based polymerase chain reaction (PCR) using infrared-mediated heating system. In *Proceedings of the 15th international conference on miniaturized systems for chemistry and life sciences* Seattle, WA, USA, 2011, p 1680-1682.